TID-7653 (Pt. I)

MASTER

Proceedings of

NUCLEAR PROPULSION CONFERENCE

August 15-17, 1962

NAVAL POSTGRADUATE SCHOOL

MONTEREY, CALIFORNIA

This document is
PUBLICLY RELEASABLE
Hugh Kuiken
Authorizing Official
Date: 8/4/08

United States Atomic Energy Commission
Division of Technical Information

LEGAL NOTICE

This report was prepared as an account of Government sponsored work. Neither the United States, nor the Commission, nor any person acting on behalf of the Commission:

A. Makes any warranty or representation, expressed or implied, with respect to the accuracy, completeness, or usefulness of the information contained in this report, or that the use of any information, apparatus, method, or process disclosed in this report may not infringe privately owned rights; or

B. Assumes any liabilities with respect to the use of, or for damages resulting from the use of any information, apparatus, method, or process disclosed in this report.

As used in the above, "person acting on behalf of the Commission" includes any employee or contractor of the Commission, or employee of such contractor, to the extent that such employee or contractor of the Commission, or employee of such contractor prepares, disseminates, or provides access to, any information pursuant to his employment or contract with the Commission, or his employment with such contractor.

This report has been reproduced directly from the best available copy.

Printed in USA. Price $3.00. Available from the Office of Technical Services, Department of Commerce, Washington 25, D. C.

USAEC Division of Technical Information Extension, Oak Ridge, Tennessee

DISCLAIMER

Portions of this document may be illegible in electronic image products. Images are produced from the best available original document.

TID-7653(Pt.I)
PROPULSION SYSTEMS AND ENERGY CONVERSION

Proceedings of
NUCLEAR PROPULSION
Conference

NAVAL POSTGRADUATE SCHOOL
August 15-17, 1962
MONTEREY, CALIFORNIA

July 1963
DTI Issuance Date

Sponsored by
SPACE NUCLEAR PROPULSION OFFICE, AEC/NASA
AMERICAN ROCKET SOCIETY
AMERICAN NUCLEAR SOCIETY
INSTITUTE OF AEROSPACE SCIENCES

FOREWORD

The papers presented in this volume are the outgrowth of the first national conference on the subject of nuclear propulsion for rockets, ramjets, and space vehicles. The Nuclear Propulsion Conference itself was held at Monterey, California, at the U. S. Naval Postgraduate School, and was jointly sponsored by the American Rocket Society, the Institute of Aerospace Sciences, and the American Nuclear Society; the three largest and most vigorous technical societies concerned with nuclear propulsion.

This volume follows the typical organization of the Conference, though the order of subjects is different here than at Monterey. Included here are many of the good papers submitted, but which were not presented at the Conference because of time limitations. Those presented are grouped first in each section. There is no Index to the volume.

At the beginning of planning, late in 1960, the organizing committee felt that a serious lack of exchange of information was already confusing work in nuclear propulsion and would soon significantly hamper such work. Yet, because of the nature of the work itself, it was obvious that any technical forum supplied by the societies would fail in its goal of exchange of useful information unless the meeting aimed for discussion of work in classified areas. Thus, of necessity and by design, the meeting was organized on an entirely classified basis. It could not have been held at all without the support of the Space Nuclear Propulsion Office of the USAEC/NASA, headed by Mr. Harry B. Finger. His office undertook

the security clearance responsibility for the meeting, and enthusiastically supported the meeting in every other way possible. This Proceedings has been published under the auspices of the SNPO, and was compiled by Mr. William Hanna of that office.

We hope that the Conference served its major purpose; to acquaint the legitimately interested technical community with the real state-of-the-art in existing nuclear propulsion programs. It was noted that most of the papers came from the USAEC National Laboratories, while most of the attendees came from the nuclear and aerospace industries of the country. This is rightly so and emphasizes the premise which initially suggested the meeting: That nuclear propulsion is passing through a vigorous transition state from National Laboratory scale to industrial sized development. Surely, unless such a transition continues, and it is well along in the NERVA and RIFT programs, nuclear propulsion will not be able to fill its proper role in the era of space flight before us.

Altogether, about 215 papers were submitted. The majority of these were classified and required security documentation as well as the careful record-keeping employed to keep track of all papers. Pertinent papers were sent to each Session Chairman, who alone had the responsibility for assembling his session. We owe a debt of gratitude to these gentlemen. The major accounting and distribution job of paper handling was done by Mildred Foglesong of the Los Alamos Scientific

Laboratory. Without her constant attention, careful work, and accurate records the Conference organization could not have functioned. Millie, we thank you. And last, but of utmost importance were the pre-Conference activities of Prof. Frank E. Faulkner of the U. S. Naval Postgraduate School, and the continual efforts of the ARS Meetings Management Staff, particularly Mr. Rod Hohl, in setting up housing, registration, and other necessary arrangements.

Robert W. Bussard

Robert W. Bussard
Program Chairman
Nuclear Propulsion Conference

For the Organizing Committee:

Robert F. Trapp (ANS)
Douglas Aircraft Company

Clare Stanford (IAS)
Nuclear Division, Martin-Marietta Co.

Frank E. Rom (ARS)
Lewis Research Center, NASA

TABLE OF CONTENTS

CRITICAL ASSEMBLY EXPERIMENTS IN SUPPORT OF PROPULSION REACTOR DEVELOPMENT

J. R. Morton III

Lawrence Radiation Laboratory, University of California
Livermore, California

The critical assembly work in support of neutronic calculations for propulsion reactor development has been a continuing program at Livermore. This program includes both graphite and beryllium oxide moderated assemblies fueled with uranium of 93.2% U^{235} content.

The assemblies are constructed of blocks of moderator material 6 inches square with thicknesses of 1/2 inch and one inch. The fuel material is in the form of 0.001- and 0.002-inch-thick foils, which fit into void spaces in the moderator. This simple but flexible type of construction permits study of quasi-homogeneous assemblies with simple geometries and a variety of fuel densities. The uncorrected moderator-to-fuel atomic ratios which have been studied range from 300 to 2340 for the graphite assemblies and from 247 to 7660 for the beryllium oxide assemblies. Except for the BeO-moderated assemblies with moderator-fuel ratios in excess of about 1000, the neutron energy spectra are expected to be substantially epithermal. Because of the great uncertainties in neutron cross sections in the epithermal region, calculations require much experimental data.

Experiments with these multiplying assemblies may be either critical or subcritical. Critical experiments are done chiefly to determine neutron flux distributions under various conditions and to measure resonance absorption integrals by the danger coefficient method. A great many useful measurements have been performed with subcritical assemblies: they include measurements of multiplication of a neutron source and measurement of the prompt decay of a short burst of neutrons within an assembly by the "pulsed neutron technique." The most obvious advantage of the pulsed source method is that it permits fairly direct measurements of large reactivity changes within an assembly.

BeO-moderated assemblies with a moderator-fuel ratio of 247 have been studied during the past several years by means of the pulsed neutron technique. Series of experiments have been performed to evaluate various materials for their neutronic effects upon the operation of a reactor.

Measurements of absorber materials, which might be considered for control poisons, permit the following ordering, in terms of decreasing absorption (based upon 0.25 g/cm^2 surface density): Re, Rh-Ir(80-20%), Cd > In > Hf > Ag > Au > Ta > W > Nb.

Other experiments permit ordering of various materials according to their effectiveness as reflectors. From a comparison in terms of surface density we obtain: BeO > Ni > Hastelloy R-235 > René 41 > T-304 stainless steel > carbon steel > copper and brass. A similar comparison in terms of reflector thickness produces the same general pattern except that beryllium oxide is less effective than nickel, Hastelloy, and René over a considerable range of thickness, and copper and brass are no longer equivalent.

CRITICALITY EXPERIMENTS AND CALCULATIONS FOR HIGH-TEMPERATURE, GRAPHITE-MODERATED ASSEMBLIES WITH SIMPLE GEOMETRY

A. G. Cole and R. G. Finke

Lawrence Radiation Laboratory, University of California
Livermore, California

INTRODUCTION

An important aspect of the design of a Pluto type reactor is the effect of temperature on reactivity. Current designs are based on the results of multigroup diffusion code calculations which do not treat the effect of temperature accurately. The Hot Box[1] experimental facility has been used to provide an experimental basis for normalizing existing machine calculations, and for improving nuclear parameters for future calculations.

EXPERIMENTAL RESULTS

Experiments have been carried out with bare, graphite-moderated/enriched-uranium assemblies over the carbon-to-uranium-235 atomic ratio range, 583:1 to 21,690:1, and with critical temperatures ranging between 46 and 1110°F.

The experimental results are presented in Table I. The C/U-235 ratios are taken from the amount of graphite per lattice unit and the amount of U-235 present in the associated foils; no corrections have been made for foil self-shielding or flux depression. All dimensions are room-temperature measurements, and the heights include 2.5 in. for the contribution of the base layer, low-mass table, and floor. The poison of the neutron source container[2] was present in the center of the assembly for all criticality determinations. The effective density of the graphite includes flow passages and control voids. The graphite has an equivalent boron poison level of 5 ppm. The measured thermal expansion of Hot Box graphite (grade CS-312) in the vertical and horizontal directions is shown in Fig. 1. A fuel element[3] consists of 1-, 2-, or 4-mil oralloy (93.2% U-235) foils encased in an envelope of 2-mil stainless steel, type 347.

BUCKLING TEMPERATURE COEFFICIENTS

Buckling calculations have been done for each assembly as critical at room temperature, and as overstacked to be critical at an elevated temperature (see Table II). These calculations were done using the reported room-temperature measurements and without correcting for the small variation in effective density. The fractional change in buckling divided by the associated change in temperature gives the buckling temperature coefficient for each experiment (Fig. 2). This quantity is dependent on the spread between critical temperatures and to achieve consistency, the calculated coefficients have been corrected to correspond to a median temperature of 500°F. These calculations cannot be considered pertinent to homogeneous systems without making corrections for foil self-shielding.

MACHINE CALCULATIONS

Calculations have been carried out with the one-dimensional, neutron-diffusion code, 9-ZOOM[4] with 18 energy groups. Standard cross sections[5] were used with appropriate group-dependent foil flux disadvantage factors and with graphite absorption cross sections corresponding to 5 ppm boron equivalent. Those experiments having discrete regions differing in fuel concentration or foil spacing were not homogenized in the calculations.

The calculations for assemblies critical at elevated temperatures were carried out with dimensions and densities adjusted for thermal expansion. The energy spectrum of thermal neutrons was adjusted through transfer coefficients based on the free gas moderator model. Standard sets of transfer coefficients correspond to temperatures of 300, 650, and 1000°K. A graphical interpolation has been made for k_{eff} at the critical temperature.

The difference between k_{eff} values calculated for an assembly as critical at room temperature, and as overstacked for a high-temperature experiment, using room-temperature measurements and densities for both, provides a measure of the experimental excess reactivity (at room temperature) to be overcome by elevating the temperature.

Since the effect of elevating the temperature is to decrease reactivity, a calculated k_{eff} for the high-temperature critical assembly lower than that for the room-temperature critical assembly indicates an over-calculation of the temperature effect. The difference between such k_{eff} values, divided by the above experimental reactivity effect, provides a measure of the extent of the over-calculation. Table II presents a summary of these calculations and a calculation of the contribution due to thermal expansion alone. Since this contribution is a small fraction of the experimental temperature effect, the over-calculation must be due to nuclear parameters such as the neglect of Doppler broadening of resonance levels and the inadequacy of the free gas moderator model.

REFERENCES

[1] H. L. Reynolds and C. E. Walter, "HOT BOX, a High-Temperature Critical Facility," UCRL-5483 (1959).

[2] R. Finke, E. Goldberg, H. Reynolds, and G. Grammens, "Summary Report on a High-Temperature BeO Critical Experiment," UCRL-6329 (1961).

[3] C. E. Walter, "A Fuel Element for an Elevated-Temperature Critical Assembly," UCRL-5334 (1958).

[4] S. P. Stone, et al., "9-ZOOM: A One-Dimensional, Multigroup, Neutron Diffusion Theory Reactor Code for the IBM 709," UCRL-5682 (1959).

[5] H. L. Reynolds, "Critical Measurements and Calculations for Enriched-Uranium, Graphite-Moderated Systems," UCRL-5175 (1958).

Table I. Hot Box graphite critical experiments.

Uncorrected C/U^{235}	Reported in Hot Box Note No.	Effective graphite density (g/cm^3)	Base dimensions (ft)	Critical height (in.)	Critical temp (°F)	Max temp reached by assembly (°F)	Note on lattice	Fuel element thickness and spacing	
583	50	1.4642	4 × 4	57.5	72	--	Infinite planes	4-mil at 1 inch	Foil thicknesses (top view)
				59.6	741	763			
				60.6	1039	985			
1,184	49	1.4642	4 × 4	64.8	72	--	Infinite planes	4-mil at 2 inches	4 4 2 2 4
		1.4658	4 × 5	47.5*	72	--	Infinite planes	4-mil at 2 inches	4 4 2 2 4
				50.6	272	272			4 4 2 2 4
				52.6	975	973			4 4 2 2 4
				50.4	72	--	Mixed lattice	4-mil at 2 inches 2-mil at 1 inch	Foil spacing (top view)
2,380	48	1.4731	4 × 5	59.2	72	--	Infinite planes	4-mil at 4 inches	8 8 8 8 8 8
				65.6	940	1005			4 4 4 4 4 4
				69.6	1630**	1208			8 8 8 8 8 8
7,164	30	1.4781	6 × 6	54.8	66	--	Overlap lattice	2-mil at 4 inches	8 8 8 8 8 8
				61.1***	85	--		2-mil at 8 inches	4 4 4 4 4 4
				72.2***	1110	--			8 8 8 8 8 8
8,956	27, 31, 35	1.4781	6 × 6	62.0	50	--	Overlap lattice	2-mil at 5 inches (where 4 above)	
				74.1	880	863		2-mil at 10 inches (where 8 above)	
9,546	35	1.4770	6 × 6	63.3	66	--	Infinite planes	2-mil at 8 inches	
10,760	32	1.4799	6 × 6	71.5	60	--	Overlap lattice	2-mil at 6 inches (where 4 above) 2-mil at 12 inches (where 8 above)	
14,440	42	1.4897	8 × 8	61.5	79	--	Infinite planes	2-mil at 12 inches	Foil spacing (side view)
				61.0	81	--	Broken planes		
				68.8	723	721			
				72.7	1064	1051			- -
16,850	40	1.4897	8 × 8	70.2	72	--	Infinite planes	2-mil at 14 inches	- - -
				68.7	51	--	Broken planes		- -
				83.3	961	992			- - -
21,690	41	1.4919	8 × 10	78.8	46	--	Broken planes	2-mil at 18 inches	- -
				88.8	552	598			

*Calculated value. (Not experimentally verified.)

**Extrapolated from 1208°F.

***Extra stainless steel present.

Table II. Machine calculation results.

C/U^{235}	Room temp k_{eff}	High temperature T_c °F	High temperature k_{eff}	Overstack excess reactivity	Percent over-calculation*	Δk_{eff} thermal expansion only	Δk_{eff} nuclear only	Percent over-calculation nuclear
583	1.0406	741	1.0500	0.00936	-13	0.00266	0.00670	-18
	-	1039	1.0426	.01375	-14	.00413	.00962	-21
1,184	-	272	1.0299	-	-	-	-	-
	-	975	1.0267	.01551	+21	.00321	.01230	+26
	1.0337	868	1.0284	.01686	+31	.00345	.01341	+39
2,380	1.0272	950	1.0121	.03471	+44	.00408	.03063	+50
	-	(1620)	(0.9992)	.05143	+55	.00807	.04336	+65
7,164	1.0197	1110	.9897	.06298	+48	.00420	.05878	+51
8,956	1.0102	880	.9825	.07060	+39	.00334	.06726	+41
9,546	1.0031	-	-	-	-	-	-	-
10,760	1.0051	-	-	-	-	-	-	-
14,440	0.9977	723	.9732	.06249	+39	.00263	.05986	+41
	-	1060	.9652	.08789	+37	.00388	.08401	+39
16,850	0.9916	961	.9608	.08145	+38	.00340	.07805	+39
21,690	0.9800	552	0.9606	0.0463	+42	0.0015	0.0448	+43

*$[k_{eff}$ (room temp) $- k_{eff}$ (high temp)$]/\Delta k_{eff}$ (overstack excess).

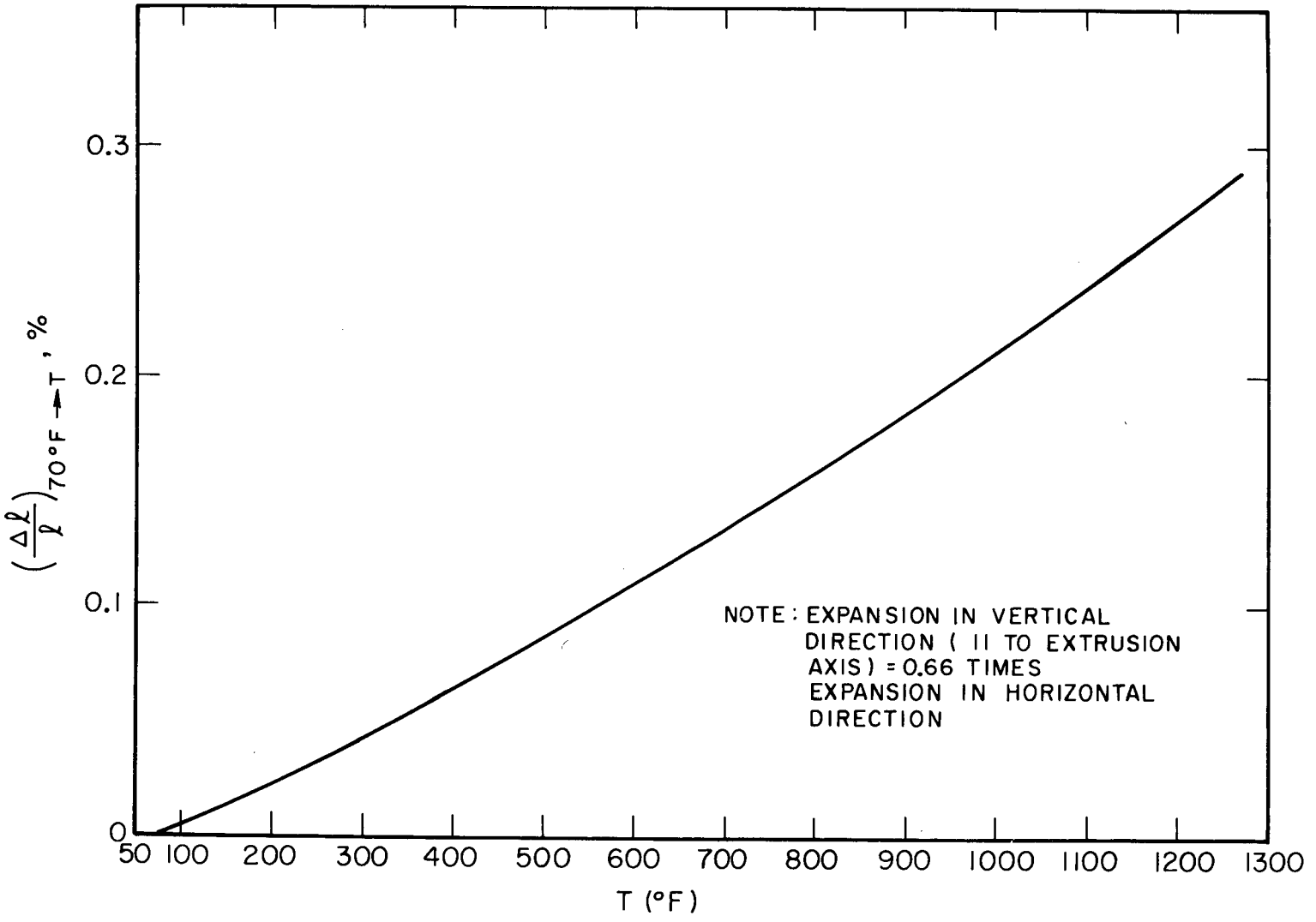

Fig. 1. Linear thermal expansion of Hot Box graphite in horizontal direction (⊥ to extrusion axis) as measured by LRL autographic dilatometer.

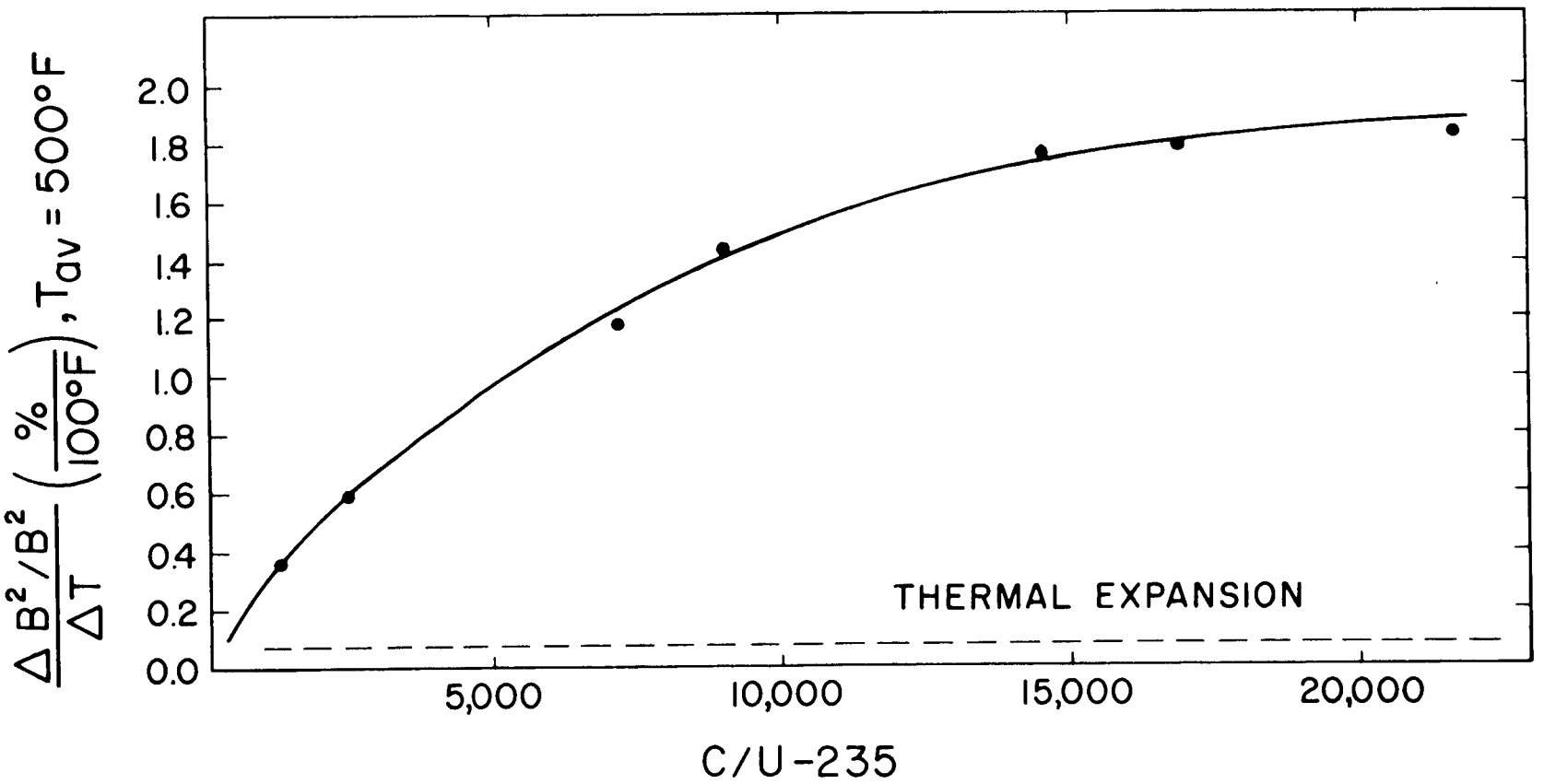

Fig. 2. Buckling temperature coefficient expressed in percent per hundred degrees Fahrenheit and corrected to a mean critical temperature of 500°F.

A DISCUSSION OF THE CORRELATION OF CRITICAL CONDITIONS OF HOMOGENEOUS BARE REACTORS CONTAINING A RESONANCE ABSORBER*

B. Pinkel, G. B. W. Young, and A. Leonard

The RAND Corporation

ABSTRACT

This paper summarizes the results given in RAND Memorandum RM 2940-PR which extends the work reported in RAND Memorandum RM-2280, A Correlation of the Critical Conditions for Homogeneous Bare Reactors, by showing the effect on reactor criticality of a material having strong resonance absorption bands. Whereas current methods for calculating the effect of various materials on the uranium requirement of the reactor involve the use of electronic computers, the simplified method presented in these Memorandums enables calculation to be made rapidly by hand.

This method is intended to facilitate feasibility studies of systems using nuclear reactors by providing engineers with an insight into factors affecting criticality.

SUMMARY AND CONCLUSIONS

This study analyzes a method of correlating the criticality conditions of homogeneous reactors composed of a moderator, a fissile material, and an absorber having high resonance capture bands. The method was illustrated by application to Safonov's 53-group machine analysis of a series of reactors containing H_2O, U^{235}, and U^{238} in various mole ratios.

By utilizing a flux-spectrum parameter it was possible to correlate parameters representing the neutron contribution rates by fission from U^{235} and U^{238} and the neutron capture rates in the several material components of the reactor at criticality for a wide range of H_2O-to-U^{235} and U^{238}-to-U^{235} mole ratios.

An expression was obtained for computing the change in flux spectrum caused by the incorporation of a resonance absorber in the

*This research is sponsored by the United States Air Force under Project RAND. This is an abridgment of RAND Memorandum RM-2940-PR. The views, conclusions, and recommendations expressed herein do not necessarily reflect the official views or policies of the United States Air Force.

reactor. This provided a method of computing the term representing the neutron absorptions in the equation for the reactor buckling. Calculations made for U^{238} by this simplified method agreed well with values obtained from the 53-group machine calculations, thus indicating that the influence on criticality of the introduction of other resonance absorbers can be computed from the information in this paper and a tabulation of cross sections.

SYMBOLS

B buckling, cm^{-1}
E neutron energy, ev
N number of atoms or molecules per unit volume
$(\Phi_{epi}/\Phi_T)^*$ epithermal-flux ratio at $N_x = 0$
$(\Phi_{fast}/\Phi_T)^*$ fast-flux ratio at $N_x = 0$

Subscripts

a absorption
f fission
i group i
m moderator
o thermal-energy parameters (this corresponds to m^{th} group)
r radiative capture
s scatter
T total
t transport
u U^{235}
x additional reactor material

I. INTRODUCTION

The study of Ref. 1 was limited to homogeneous bare reactors containing only uranium and a moderator. In the present study the addition of an absorber containing strong resonance capture bands is considered. The method is illustrated by application to the correlation of the criticality conditions of a reactor containing U^{235}, U^{238}, and H_2O obtained from a 53-group analysis by Safonov.[2] The purpose of this type of correlation is to provide insight into the effect of material parameters on criticality conditions for engineering feasibility evaluations without recourse to electronic computing machines.

II. ANALYSIS

Following the method of Ref. 1 the summation of the m equations of an m group analysis of a reactor based on diffusion theory leads to the following equation:

$$\frac{\lambda_t}{3}\nabla^2\Phi_T + \left[\nu\sum_{i=1}^{m}\Sigma_{fi}\frac{\Phi_i}{\Phi_T} - \sum_{i=1}^{m}\Sigma_{ai}\frac{\Phi_i}{\Phi_T}\right]\Phi_T = 0 \qquad (1)$$

where the total flux is

$$\Phi_T = \sum_{i=1}^{m} \Phi_i \tag{2a}$$

and the average transport mean free path is

$$\lambda_t = \sum_{i=1}^{m} \lambda_{ti} \frac{\Phi_i}{\Phi_T} \tag{2b}$$

Equation (1) may be written in the usual form involving the buckling, B

$$\nabla^2 \Phi_T + B^2 \Phi_T = 0 \tag{3}$$

where

$$\frac{\lambda_t B^2}{3} = \nu \sum_{i=1}^{m} \Sigma_{fi} \frac{\Phi_i}{\Phi_T} - \sum_{i=1}^{m} \Sigma_{ai} \frac{\Phi_i}{\Phi_T} \tag{4}$$

The foregoing equation may be written in terms of the parameters of the reactor components as follows:

$$\frac{\lambda_t B^2}{3N_u} = \sum_{i=1}^{m} (\nu\sigma_{fui} - \sigma_{aui}) \frac{\Phi_i}{\Phi_T} - \sigma_{amo} \frac{N_m}{N_u} \sum_{i=1}^{m} \frac{\sigma_{ami}}{\sigma_{amo}} \frac{\Phi_i}{\Phi_T}$$
$$- \frac{N_x}{N_u} \sum_{i=1}^{m} \sigma_{rxi} \frac{\Phi_i}{\Phi_T} + (\nu_x - 1) \frac{N_x}{N_u} \sum_{i=1}^{m} \sigma_{fxi} \frac{\Phi_i}{\Phi_T} \tag{5}$$

where σ_a = capture cross section.*

The radiative captures in material X will be broken up into two terms, the first representing captures in the vicinity of thermal energies where it will be assumed that the capture cross sections vary as $1/\sqrt{E}$, and the second representing the remainder of the radiative captures in the epithermal and fast regions and hence including the resonance capture range.

Thus

$$\frac{N_x}{N_u} \sum_{i=1}^{m} \sigma_{rxi} \frac{\Phi_i}{\Phi_T} = \sigma_{axo} \frac{N_x}{N_u} \sum_{i=1}^{m} \sqrt{\frac{E_o}{E_i}} \frac{\Phi_i}{\Phi_T} + \frac{N_x}{N_u} \sum_{i=1}^{m-1} \sigma_{rxi} \frac{\Phi_i}{\Phi_T} \tag{6}$$

where E_i is the energy of the i^{th} group.

*In the case of U^{235} it also includes the fission cross section. Where no fissions occur, $\sigma_a = \sigma_r$ and the two terms are used interchangeably.

Because the first term on the right-hand side of Eq. (6) includes some of the captures in the epithermal groups adjacent to the thermal group, this must be considered in the calculation of the last term of the equation, and a reminder of this is introduced in the form of a horizontal bar at the top of the summation sign. Equation (6) serves as the definition of this last term.

Thus Eq. (5) may be written

$$\frac{\lambda_t B^2}{3N_u} = \sum_{i=1}^{m} (\nu\sigma_{fui} - \sigma_{aui})\frac{\Phi_i}{\Phi_T} - \left(\sigma_{amo}\frac{N_m}{N_u} + \sigma_{axo}\frac{N_x}{N_u}\right)F_4(P)$$

$$- \frac{N_x}{N_u}\sum_{i=1}^{m-1} \sigma_{rxi}\frac{\Phi_i}{\Phi_T} + (\nu_x - 1)\frac{N_x}{N_u}\sum_{i=1}^{m} \sigma_{fxi}\frac{\Phi_i}{\Phi_T} \qquad (7)$$

where

$$F_4(P) = \sum_{i=1}^{m} \frac{E_o}{E_i}\frac{\Phi_i}{\Phi_T} \qquad (8)$$

and the assumption is made that the moderator capture cross section likewise varies as $1/\sqrt{E}$. The quantity P is an index of the flux spectrum and will be discussed later.

An attempt will be made to show how each of the terms in Eq. (7) correlates with parameters that describe the composition of the reactor. When B is determined, then the critical size for reactors of a variety of shapes can be determined from Eq. (3).

It was pointed out in Refs. 1 and 3 that nearly the same flux distribution with respect to neutron energy occurs in reactors containing different moderators when the mole ratios are such that they give the same mean energy degradation (by contacts with the moderator) per collision with U^{235}.

The following expression for the flux-spectrum parameter P is derived in Ref. 4.

$$P = \frac{5.2\frac{N_m}{N_u} + 0.25\frac{N_x}{N_u}}{1 + 0.005\frac{N_x}{N_u}} \qquad (9)$$

Figure 1 shows the thermal flux Φ_o/Φ_T plotted against P for a range of values of N_m/N_u and N_x/N_u. A single curve is obtained. For the purpose of displaying other portions of the flux distributions, the following definitions were adopted: of the 53 groups used in Ref. 2, the flux in groups 1 through 4, which covered an energy band from 10^5 to 10^7 ev, was called the fast flux because this energy range substantially covered the birth energies of the neutrons. The remainder of the flux between the fast-flux band and the thermal band was summed and called the epithermal flux.

The contributions of U^{235} to Eqs. (5) and (7) for the buckling parameter are contained in the first term on the right side of these equations and will be designated $F_3(P)$ in conformance with Ref. 1.

$$\sum_{i=1}^{m} (\nu\sigma_{fui} - \sigma_{aui})\frac{\Phi_i}{\Phi_T} = F_3(P) \tag{10}$$

This term represents the neutron contributions by fission of U^{235} and the neutron removal by capture in U^{235}. It is shown in Fig. 2 plotted against P.

The quantity F_4 computed from the flux spectrums obtained from the 53-group analysis, (Ref. 2) and from the cross sections of the moderator are shown in Fig. 3.

Near thermal energies the capture cross section of material X is assumed to vary as $1/\sqrt{E}$. This portion of the capture in X is represented in Eq. (7) by

$$\sigma_{axo}\frac{N_x}{N_u}F_4(P)$$

The function in Fig. 3 is used to compute this term.

The epithermal and fast captures in material X which include the resonance captures are represented in Eq. (7) by the term

$$\frac{N_x}{N_u}\sum_{i=1}^{m-1}\sigma_{rxi}\frac{\Phi_i}{\Phi_T}$$

In deriving an expression for this term from which to obtain correlation parameters it is necessary to take into account the sharp local depressions in flux that are obtained at energies where large resonance-capture cross sections occur. Expressions for these depressed flux levels can be obtained in terms of the flux at the same energy for $N_x = 0$ and a flux depression factor Γ.

$$\Gamma_{xi} = \frac{1 + \frac{N_u\sigma_{aui}}{N_m\sigma_{smi}}}{1 + \frac{N_u\sigma_{aui}}{N_m\sigma_{smi}} + \frac{N_x\sigma_{rxi}}{N_m\sigma_{smi}}} \tag{11}$$

$$(\Phi_i/\Phi_T)^* = g_i(\Phi_{epi}/\Phi_T)^* \tag{12}$$

where g_i varies only slowly with N_m/N_u. Thus

$$\sum_{i=1}^{m-1}\sigma_{rxi}\frac{\Phi_i}{\Phi_T} = \left(\frac{\Phi_{epi}}{\Phi_T}\right)^*\sum_{i=1}^{m-1}\Gamma_{xi}\sigma_{rxi}g_i \tag{13}$$

The value of Γ_{xi} in Eq. (11) depends mainly on the value of $N_x \sigma_{rxi} / N_m \sigma_{smi}$. Thus the summation in Eq. (13) for a given material X and fissile material is a function mainly of $N_x / N_m \sigma_{smi}$, and Eq. (14) can be approximated by

$$\sum_{i=1}^{m-1} \sigma_{rxi} \left(\frac{\Phi_i}{\Phi_T}\right) = \left(\frac{\Phi_{epi}}{\Phi_T}\right)^* F_6 \left(\frac{\sigma_{sm} N_m}{N_x}\right) \qquad (14)$$

Figure 4 shows a plot of F_6 utilizing Eq. 14. The plot in Fig. 4 applies when material X is U^{238}. For other materials Eq. (13) may be used to compute the appropriate F_6 curve.

The term in Eq. (7)

$$\frac{N_x}{N_u}(\nu_x - 1) \sum_{i=1}^{m} \sigma_{fxi} \frac{\Phi_i}{\Phi_T}$$

represents the neutron contribution from material X. For a material X where no fission reactions occur, this term is of course equal to zero.

For U^{238} the above summation contains contributions only from the fast flux in groups having energies above 10^6 ev.

The analysis indicated that the term representing the net neutron contributions by fission of U^{238} could be expressed as follows:

$$\frac{N_x}{N_u}(\nu_x - 1) \sum_{i=1}^{m} \sigma_{fxi} \frac{\Phi_i}{\Phi_T} = \frac{N_x}{N_u} \left(\frac{\Phi_{fast}}{\Phi_T}\right)^* F_7 \left(\bar{\sigma}_{sm} \frac{N_m}{N_x} + \bar{\sigma}_u \frac{N_u}{N_x}\right) \qquad (15)$$

Figure 5 shows a plot for U^{238} of F_7 from Eq. 15 and the data of Ref. 2. Other materials X which fission and contribute neutrons will give rise to different functions for F_7. For those materials that do not contribute neutrons, $F_7 = 0$.

The transport mean free path λ_t is defined by Eq. (2c). It is shown in Fig. 6 plotted against P and N_x/N_u.

The curves in Fig. 7 show the buckling parameter computed from Eq. (7) for values of N_x/N_u of 0, 4, 10, 20, 40, and 60. Also shown in Fig. 7 are points representing the buckling parameters taken directly from Ref. 2. The discrepancy between the points and lines represents the error of the correlation method.

It is of considerable interest to examine whether or not the term which represents the radiative captures in material X in the epithermal and fast-flux ranges, can be accurately computed from Eq. (13) for the present case where X is U^{238}, because the same procedure would allow calculation of this term for other materials from the present information.

The subject term calculated from Eq. (13) is compared with the results of the 53-group machine analysis in Table 1. A detailed description of the method of making the computation is given in Ref. 4.

Table 1

COMPARISON OF EQ. (13) AND REF. 2 VALUES FOR THE RADIATIVE CAPTURE TERM FOR U^{238}

$(N_x/N_u = 40)$

	$\sum_{i=1}^{m-1} \sigma_{rxi} \frac{\Phi_i}{\Phi_T}$	
N_m/N_u	Eq. (13)	Ref. 2
50	.68	.73
200	.91	.91
500	1.01	1.00

It is also of some interest to compare the flux values computed by the relation

$$\Phi_i/\Phi_T = \Gamma_{xi}\, g_i\, (\Phi_{epi}/\Phi_T)^* \qquad (16)$$

with the values taken from the 53-group machine calculation of Ref. 2 for the energy groups in which large resonance captures occur in the U^{238}.

Table 2

COMPARISON OF Φ_i/Φ_T COMPUTED BY EQ. (16) WITH VALUES FROM THE 53-GROUP MACHINE CALCULATIONS OF REF. 2

$(N_x N_u = 40)$

	$\frac{N_m}{N_u} = 50$		$\frac{N_m}{N_u} = 200$		$\frac{N_m}{N_u} = 500$	
i	Eq. (16)	Ref. 2	Eq. (16)	Ref. 2	Eq. (16)	Ref. 2
21	.00141	.001685	.001696	.001803	.001426	.001465
24	.000252	.000280	.000541	.000566	.000690	.000632
29	.000111	.0001218	.000285	.0002945	.000367	.000380
36	.0000105	.00001066	.0000348	.0000349	.0000612	.0000645

REFERENCES

1. Pinkel, B., and G. B. W. Young, A Correlation of the Critical Conditions for Homogeneous Bare Reactors, The RAND Corporation, Memorandum RM-2280, October 29, 1958.
2. Safonov, George, Critical Mixtures of Uranium and 500°F Light Water, The RAND Corporation, Report R-279, January 8, 1955.
3. Pinkel, B., and G. B. W. Young, A Discussion of the Correlation of Critical Conditions for Bare Homgeneous Reactors, The RAND Corporation, Paper P-1713, June 4, 1959.
4. Pinkel, B., G. B. W. Young, and A. Leonard, A Method of Correlating Critical Conditions of Homogeneous Bare Reactors Containing a Resonance Absorber, The RAND Corporation, Memorandum RM 2940-PR, May 1962.

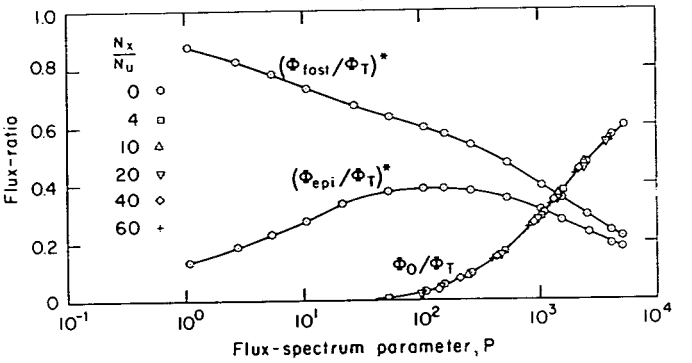

Fig. 1—Variation of flux with P

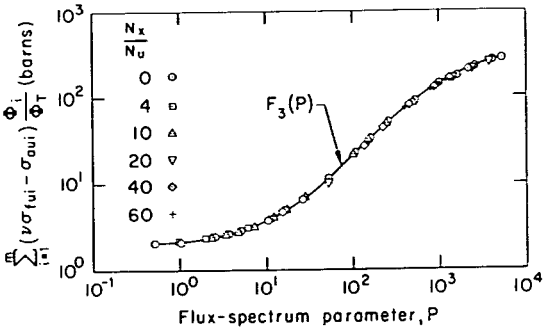

Fig. 2—Term in Eq. 7 for net neutron contributions by U^{235}

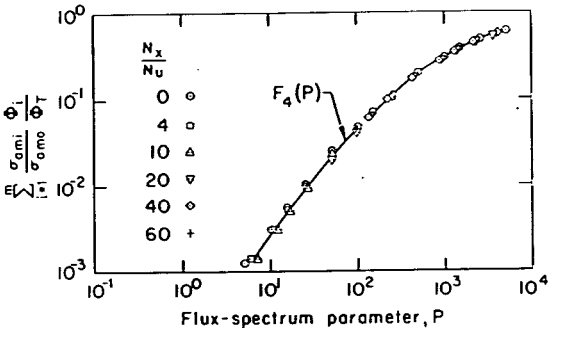

Fig. 3—Portion of terms for $1/\sqrt{E}$ captures in Eq. 7

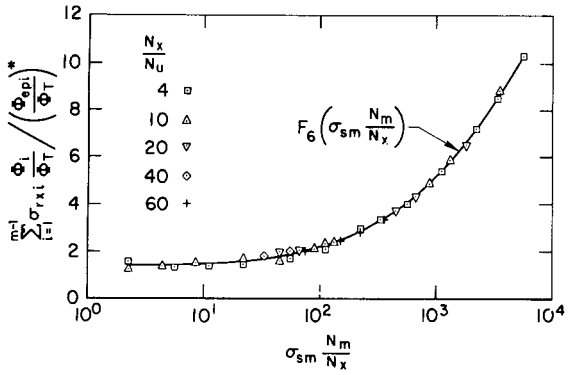

Fig. 4—Portion of the term in Eq.7 for epi and fast captures in U^{238}

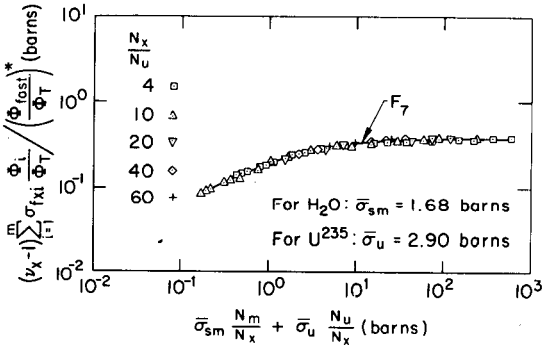

Fig. 5—Contribution of U^{238} fissions in Eq. 7

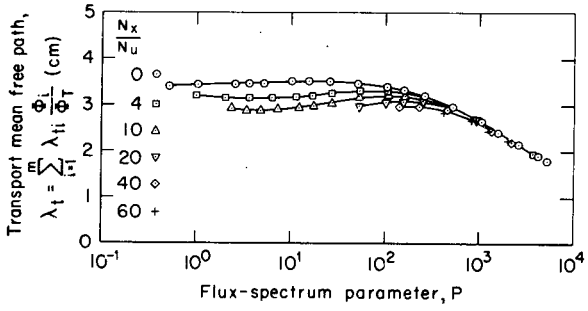

Fig. 6—Transport mean free path

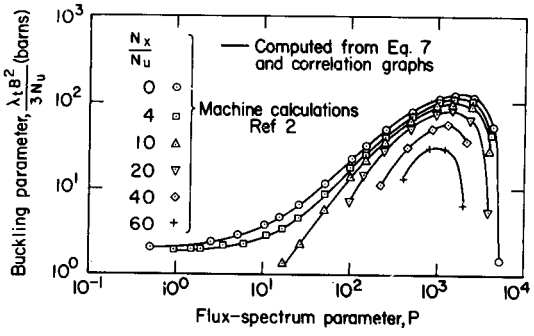

Fig. 7—Comparison of computations from Eq.7 and Ref. 2

NUCLEAR RADIATION TRANSFER AND HEAT DEPOSITION RATES IN LIQUID HYDROGEN

M. O. Burrell

Research Projects Division
George C. Marshall Space Flight Center

One of the most pressing problems in the development of nuclear powered rockets is the accurate determination of the nuclear radiation heating in the rocket fuel and of the radiation transmitted to the payload region. Since liquid hydrogen is a likely fuel for propulsion, the accurate calculation of radiation heat deposition and radiation transfer in liquid hydrogen is mandatory. At the present stage of development, it is desirable to base calculations on simple geometries and discrete energies which are adaptable to future configurations and energy spectra. The calculations in this paper are intended to fulfil this need.

The present calculations utilize Monte Carlo techniques and are for plane slab geometries and right circular cylinders with flat ends. The source (either neutrons or gamma rays) is always monoenergetic. The source for the cylinder is point isotropic and on the axis of the cylinder, while the slab source is plane parallel rays incident at any specified angle. The calculation provides statistical estimates of the transmitted and reflected number current, flux, and energy as well as the heat deposition rate as a function of depth in the hydrogen.

The neutron histories are terminated when their energy is reduced below 1 ev. The location of these terminations is tabulated and averaged over a volume element, thus giving the spatial distribution of the slow neutrons. The average energy of these neutrons is 0.5 ev. This volume distribution of slow neutrons may be representative of the source distribution for the 2.23 Mev gamma rays produced by the hydrogen capture of a neutron. However, the para-hydrogen scattering cross section will decrease below 0.1 ev[1] and this may result in considerable migration of the neutrons. Neutrons lose a large fraction of their energy in a few collisions with protons and scatter only into the forward hemisphere. The neutron energy deposition in a cylinder of liquid hydrogen is a large fraction of the total neutron energy incident on the cylinder. This is expected since the mean free path of a 2-Mev neutron, in liquid hydrogen ($\rho = .07$ gm/cm^3) is about 3.2 inches . Since the neutrons scatter only

[1] Whittemore, W. L., et al, "Differential Neutron Thermalization," General Atomic (Division of General Dynamics), GA-2503, Annual Summary Report, October 1961.

into the forward hemisphere, and because the energy is reduced considerably after a few collisions (on the order of one-half at each scatter), the neutron energy which escapes the cylinder by reflection or transmission is a very small fraction of the incident energy. This is substantiated in the calculations presented in this paper. The foregoing is not true of the gamma rays which have a mean free path about 20 times that of neutrons in hydrogen. Compton scattering is the primary mechanism for energy deposition in the gamma ray energy range of interest. In hydrogen, photoelectric absorption is of no consequence until the gamma's energy is below 0.01 Mev and pair production is certainly negligible under 10 Mev. Because of the low Compton energy absorption cross section below 0.1 Mev, the photon must scatter a very large number of times in order to degrade the energy to 0.01 Mev. From the foregoing, it is expected that an appreciable fraction of the incident gamma ray energy will escape a hydrogen cylinder of feasible dimensions. For example, the energy deposition in a 30-foot diameter hydrogen cylinder of 50-foot length was calculated for a point isotropic source of 2-Mev neutrons and gamma rays on the center line 20 feet from the cylinder. In this case, 97% of the incident neutron energy and 65% of the incident gamma ray energy were transferred to the liquid hydrogen.[1]

[1] Burrell, M. O., "Nuclear Radiation Transfer and Heat Deposition Rates in Liquid Hydrogen," NASA Technical Note D-1115, August 1962.

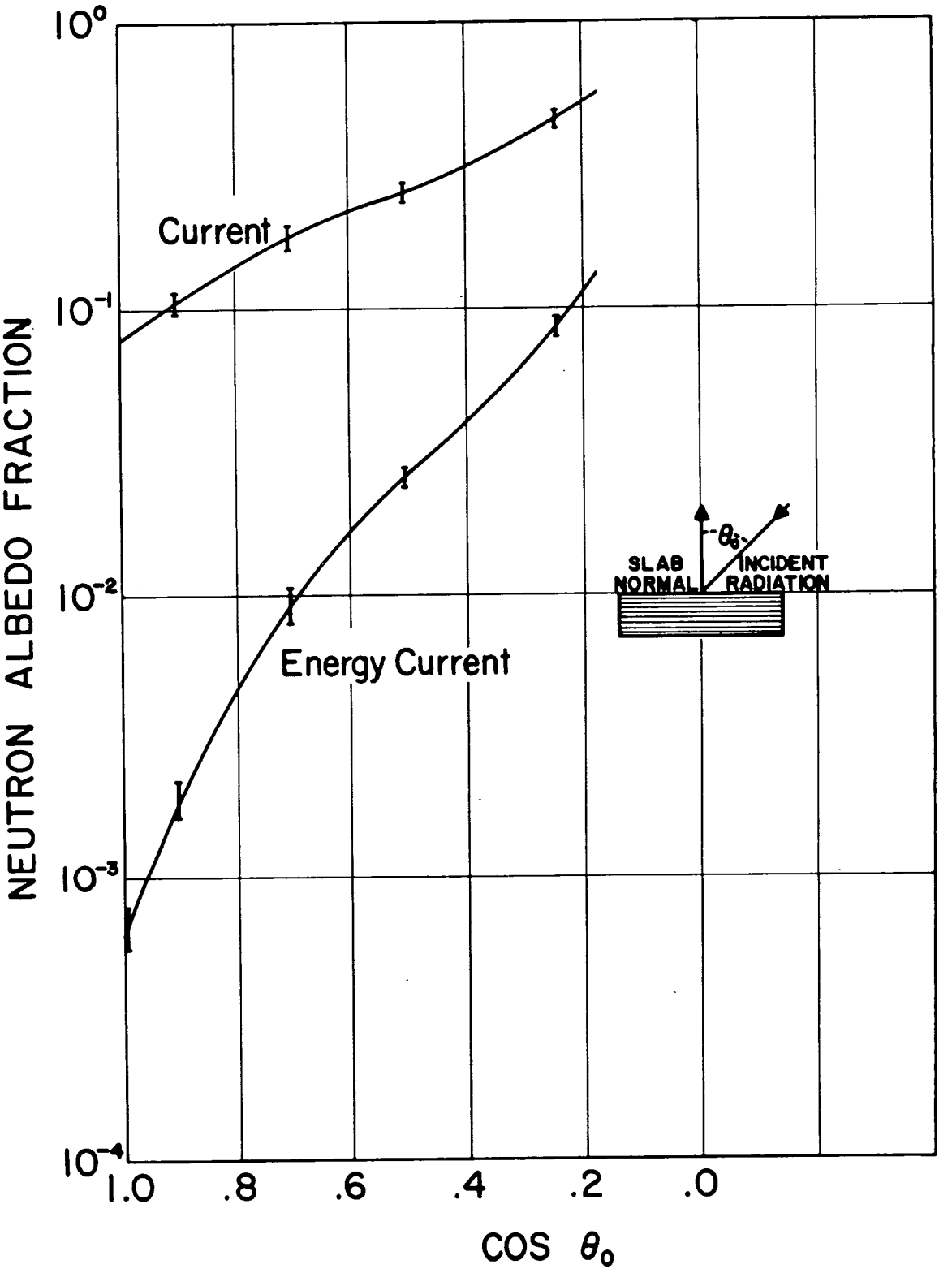

FIG. 1 Neutron Albedo vs. Cos θ_o for E_o = 2 Mev, $E_N = 10^{-6}$ Mev

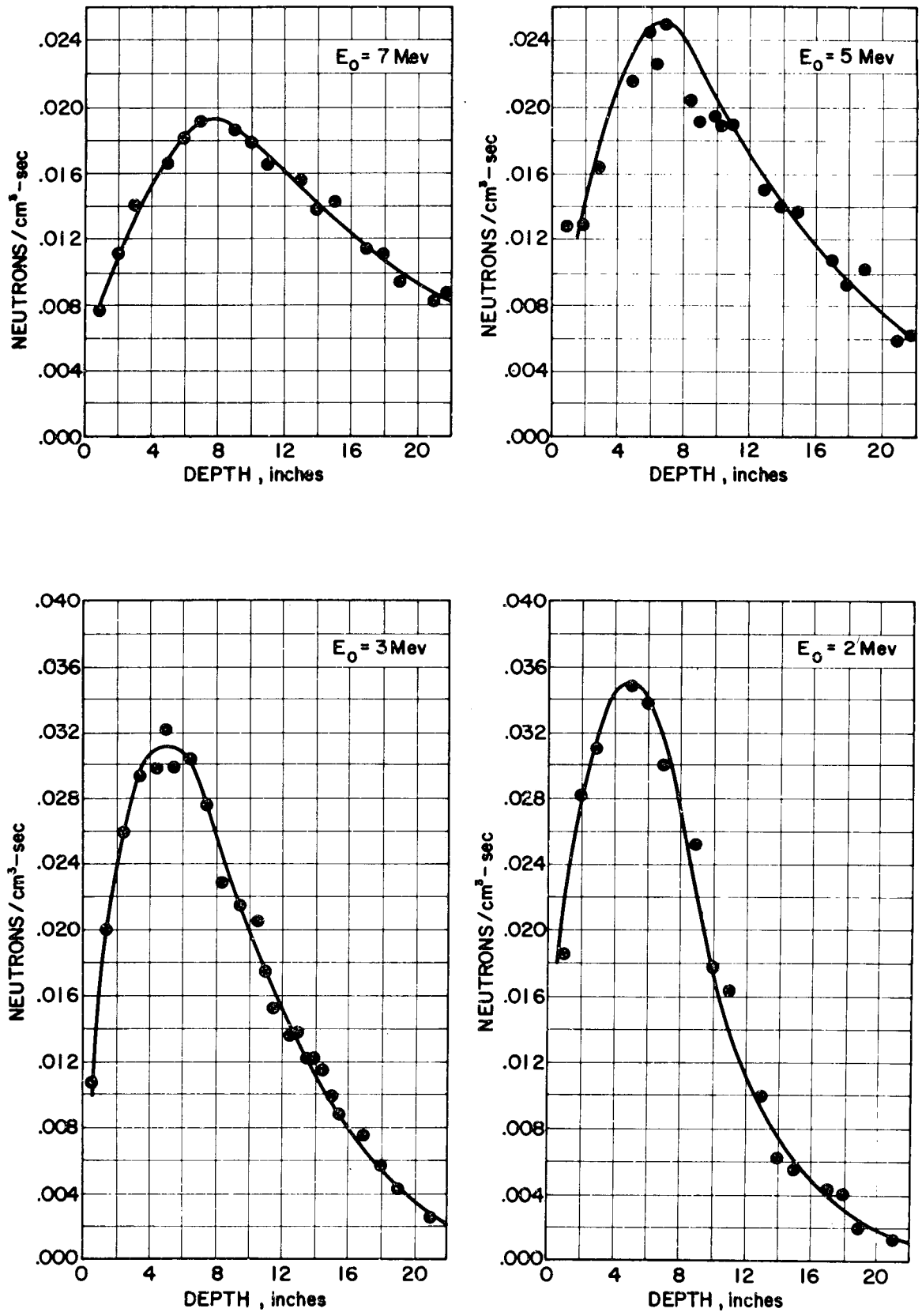

FIG. 2 Spatial Distribution of 0.5 ev Neutrons in Liquid Hydrogen Due to Normal Incident, Monoenergetic Neutrons (1 neutron/cm^2-sec) on Hydrogen Slabs. Incident Energy is given by E_o on graph

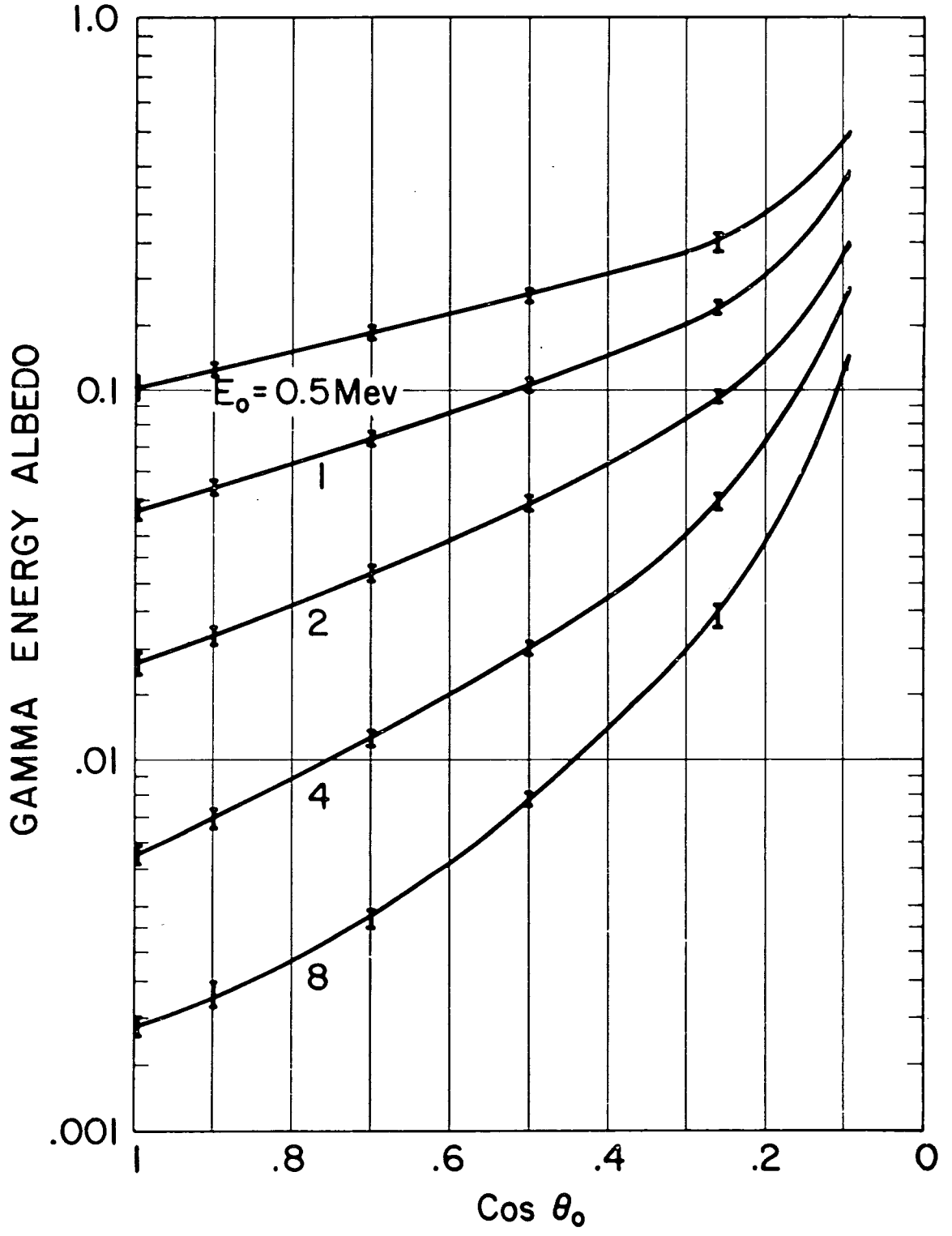

FIG. 3 Gamma Ray Energy Current Albedo Factors Versus Angle of Incidence for Monoenergetic Parallel Rays Incident on Hydrogen Slabs

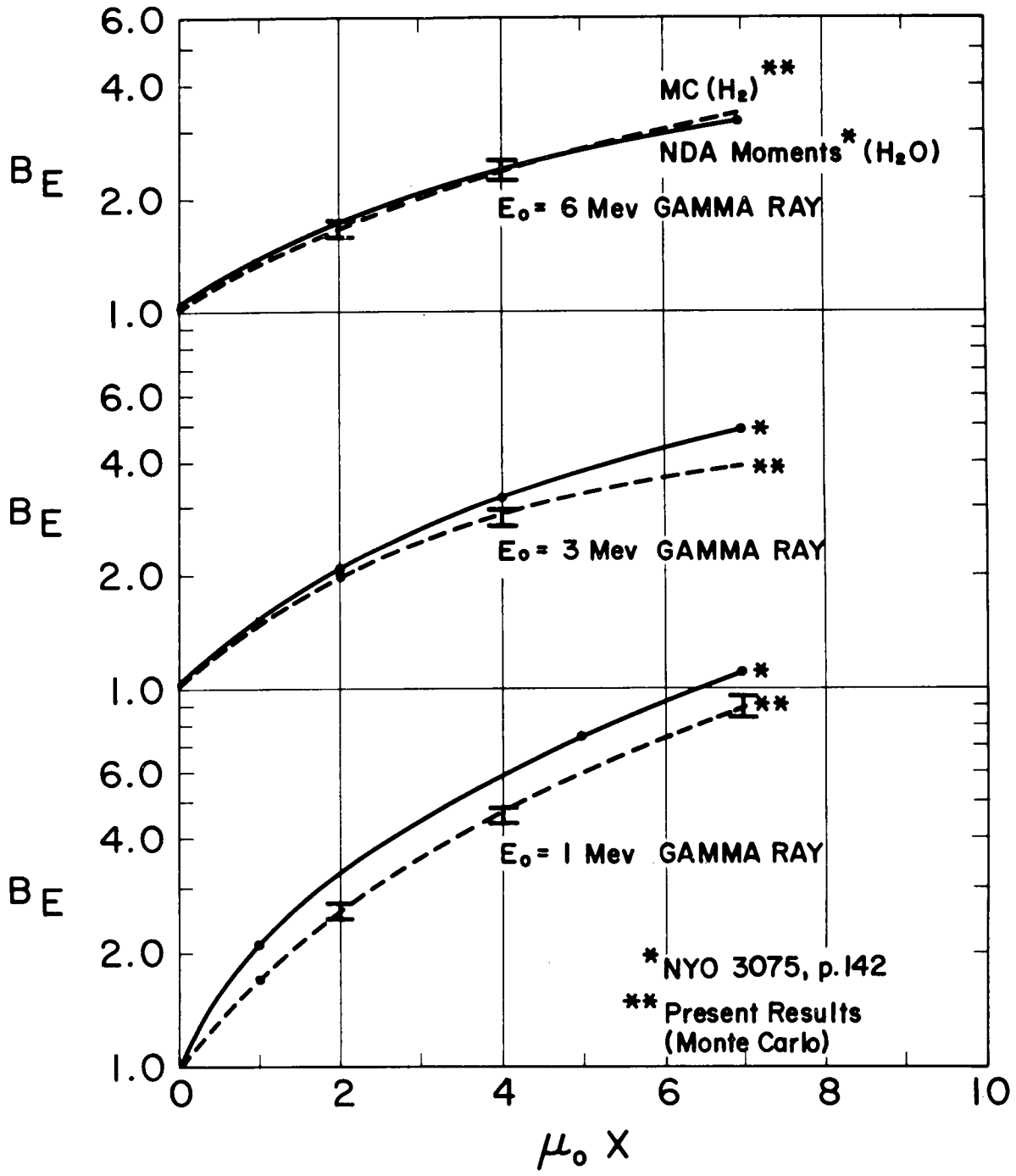

FIG. 4 Energy Flux Buildup Factors vs. Mean Free Paths for Normal Incident Gamma Rays in H_2O and H_2; Plane Monoenergetic Sources. Energies are above 0.025 Mev in Monte Carlo Calculations

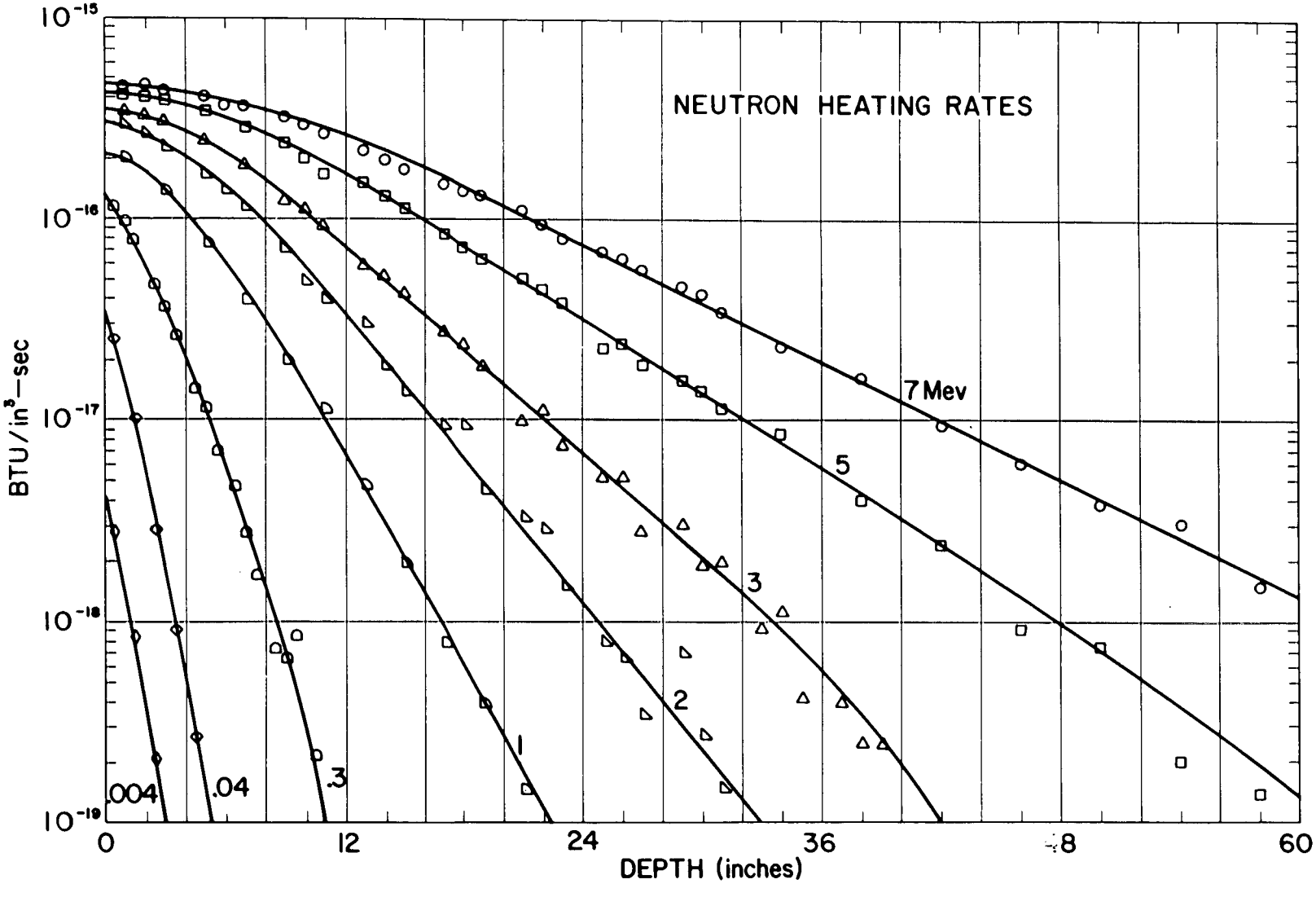

FIG. 5 Heat Deposition vs. Depth in Liquid Hydrogen Slabs for Mono-energetic Neutrons (1 neutron/cm^2 - sec) Incident Normal to the Surface

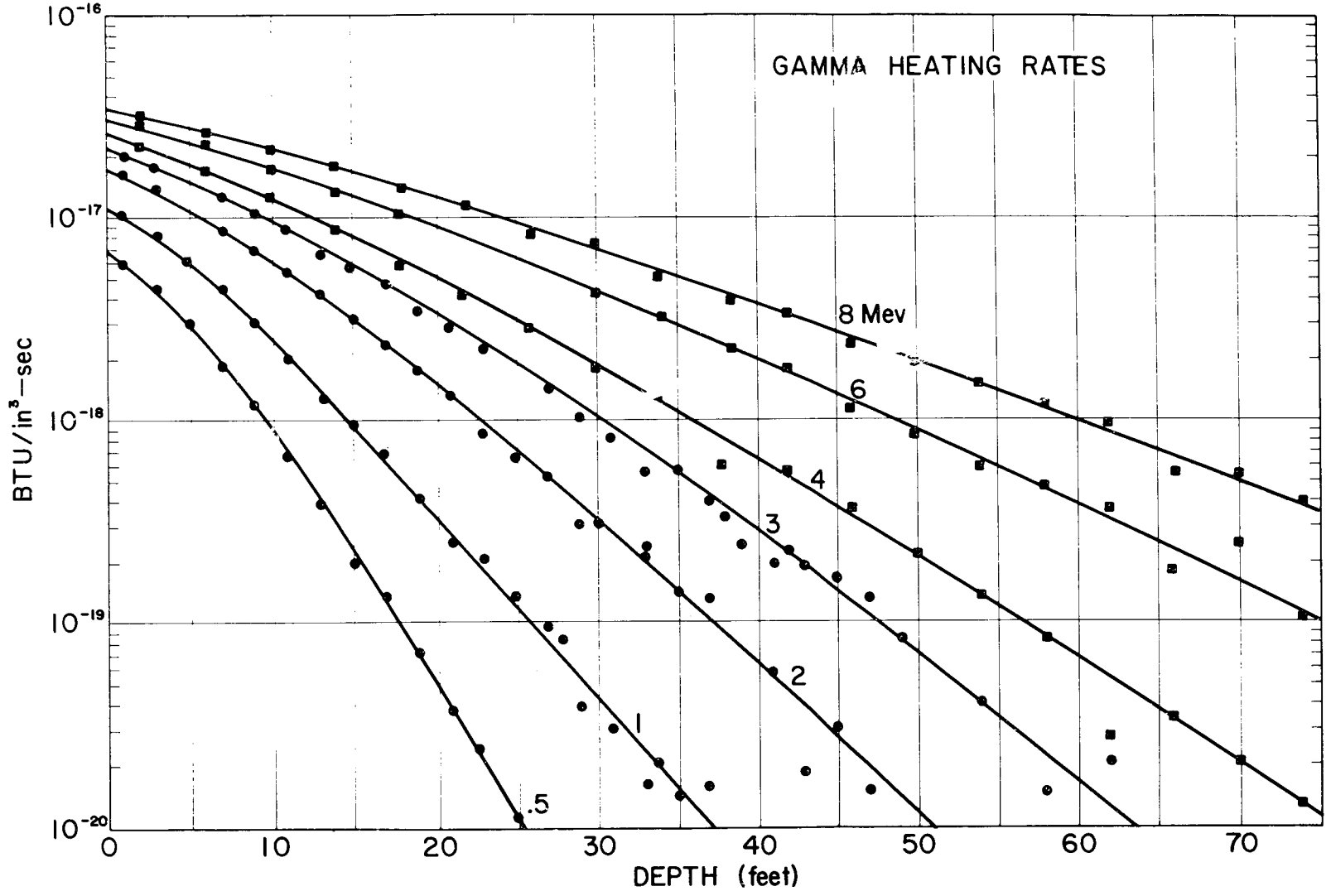

FIG. 6 Heat Deposition vs. Depth in Liquid Hydrogen Slabs for Monoenergetic Gamma Rays (1 photon/cm²-sec) Incident Normal to the Surface

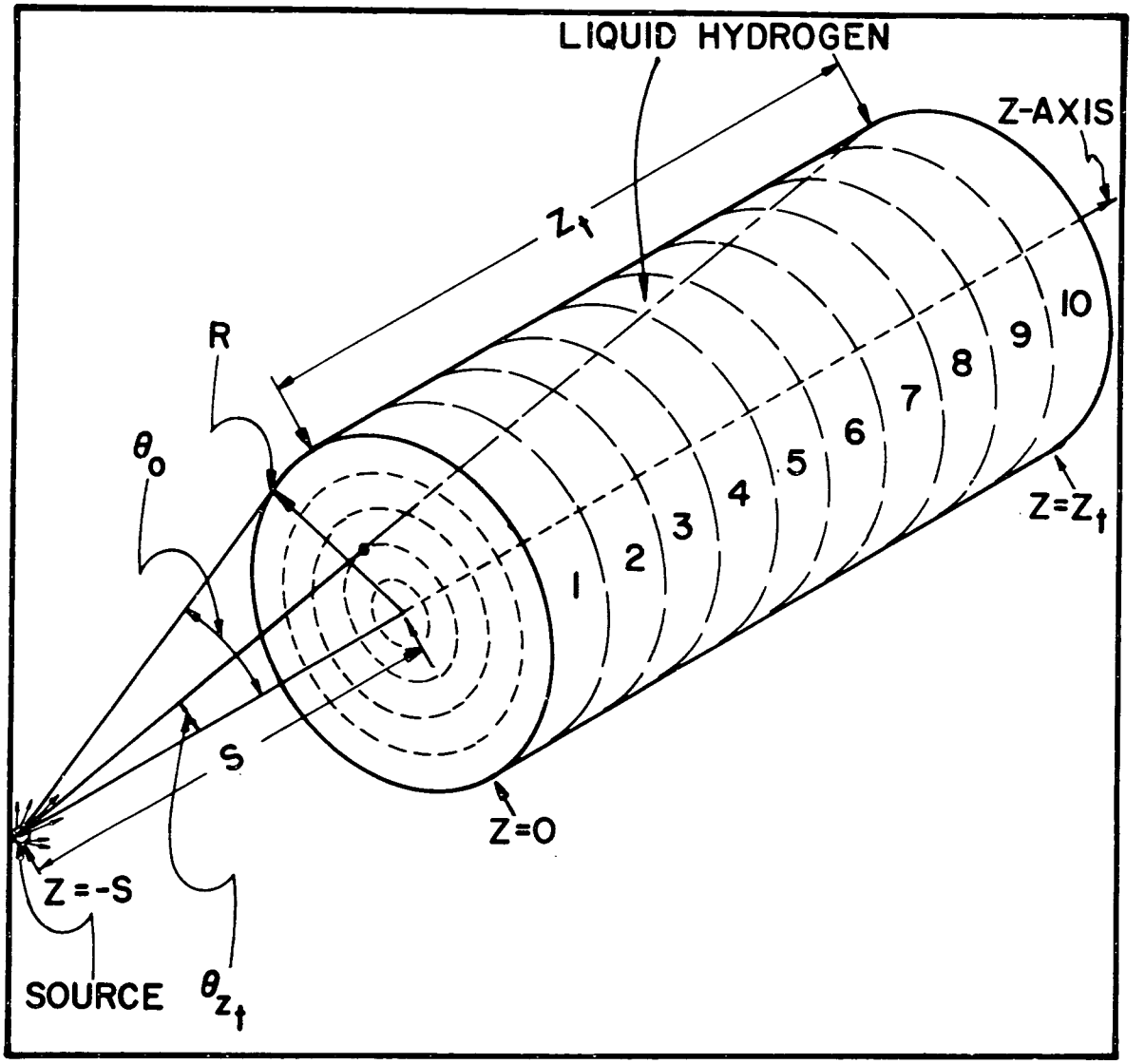

FIG. 7 Source and Geometry Used in the Cylindrical Monte Carlo Calculations

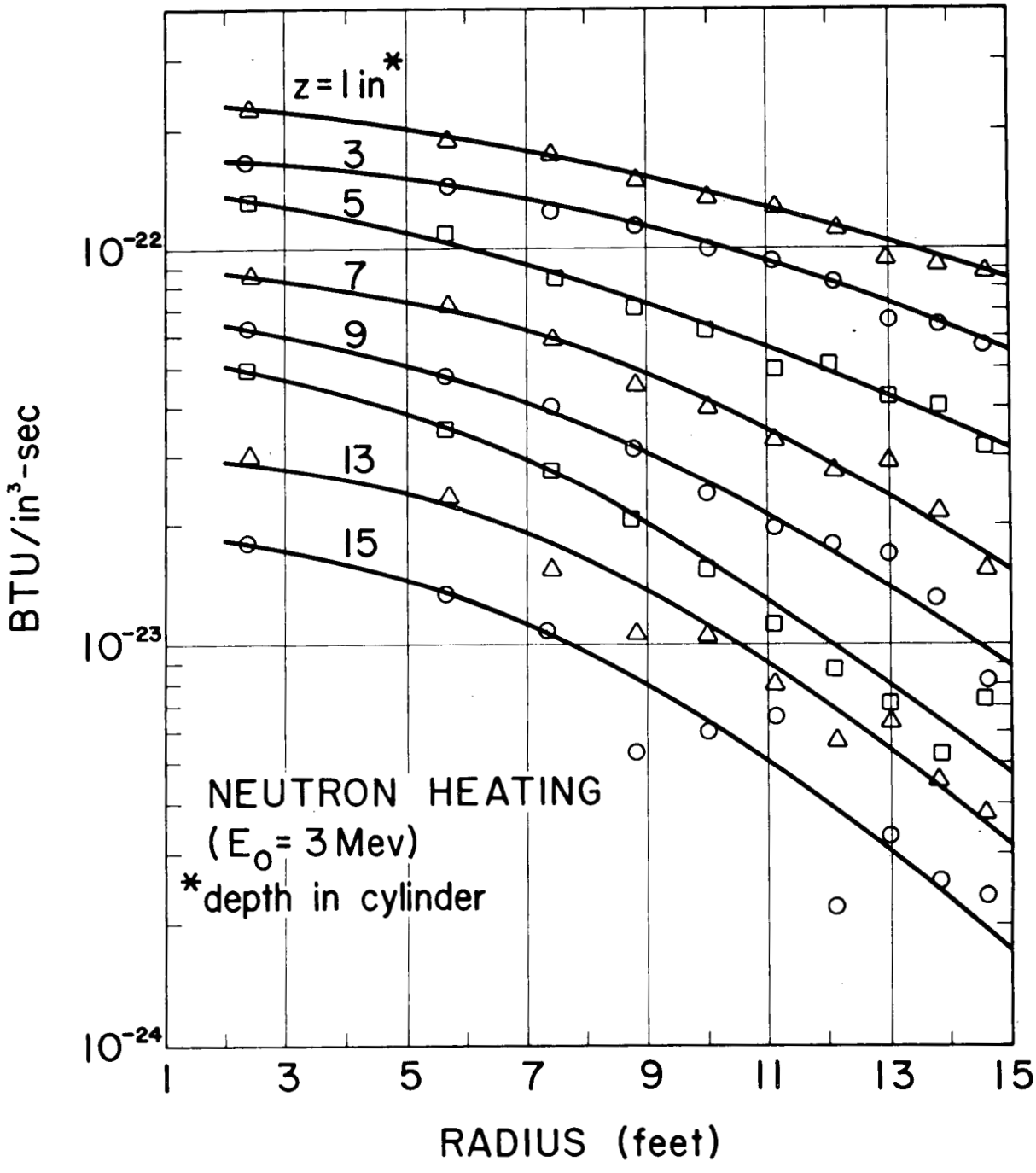

FIG. 8 Neutron Heating Rate (BTU/in^3-sec) in a Liquid Hydrogen Cylinder from a Point Isotropic Source (1 neutron/sec) of 3 Mev Neutrons at a Distance of 11.25 feet from the 30-foot Diameter Cylinder

TABLE I

Neutron Energy Disposition in a 30-Foot Diameter Liquid Hydrogen Cylinder of 5 Mean Free Paths Length.

E_o (Mev)	Separation of Source From Cylinder (Feet)	Solid Angle Fraction of Cylinder	Fraction of Incident Energy Adsorbed In H_2 Cylinder	Fraction of Incident Energy Escaping Sides of Cylinder	Fraction of Incident Energy Escaping Far End of Cylinder	Fraction of Incident Energy Reflected at Near End of Cylinder
1	11.25	0.2	0.970	0.014	0.011	0.007
3	11.25	0.2	0.958	0.026	0.010	0.006
7	11.25	0.2	0.939	0.048	0.009	0.005
1	20	0.1	0.966	0.015	0.016	0.002
3	20	0.1	0.953	0.028	0.015	0.002
7	20	0.1	0.937	0.050	0.011	0.002

TABLE II

Gamma Ray Disposition in a 30-Foot Diameter Liquid Hydrogen Cylinder of 5 Mean Free Paths Length.

Eo (Mev)	Separation of Source From Cylinder (Feet)	Solid Angle Fraction of Cylinder	Fraction of Incident Energy Adsorbed In H2 Cylinder	Fraction of Incident Energy Escaping Sides of Cylinder	Fraction of Incident Energy Escaping Far End of Cylinder	Fraction of Incident Energy Reflected at Near End of Cylinder
1	11.25	0.2	0.658	0.283	.008	.047
3	11.25	0.2	0.600	0.382	.002	.010
6	11.25	0.2	0.509	0.477	.001	.003
1	20	0.1	0.668	0.278	.010	.041
3	20	0.1	0.613	0.372	.004	.008
6	20	0.1	0.537	0.450	.002	.002
2.23	0.03	0.499	0.828	0.102	.002	.060

NEUTRON CONTRIBUTIONS TO LH_2 PROPELLANT HEATING

G. A. Graves and J. R. Streetman
Los Alamos Scientific Laboratory
University of California
Los Alamos, New Mexico

To supplement our previously reported work on gamma rays,[1] a total of 440,000 neutron histories were followed within LH_2 propellant in order to establish the principal features of this source of propellant heating. The calculation also gave the energy distribution of neutrons emerging from various surfaces of the geometry employed and, by recording the locations at which each neutron's energy finally dropped below ten kilovolts, provided important information on the probable distribution of the 2.23 Mev gamma-ray-producing neutron captures.

The geometry (Figure 1) consisted of approximately the first three feet of liquid hydrogen contained in a flat-bottomed conical walled tank placed ten feet from an "equivalent point source" of reactor neutrons.

This source was basically derived from the axial leakage exhibited in the six highest groups of DSN transport calculations on a typical reactor system, but each of these groups were further subdivided for the calculation, so that thirty-eight energy groups were ultimately used to represent an unshielded reactor leakage spectrum over the energy interval from 8 Mev to 17 kev. This spectrum is shown in Figure 2. The total source intensity was adjusted to provide about the same number of neutrons impinging per unit area on the tank bottom as one would expect from a properly oriented, intact reactor centered on the source position - i.e., the "equivalent source" was adjusted to emit $\sim$0.6 neutron per reactor fission, or $\sim 2 \times 10^{19}$ neutrons per second per 1000 MW, with the average energy of these neutrons being $\sim$0.7 Mev.

Two areas of the tank bottom were distinguished, so that the effects of neutrons entering near the tank axis could be separated from those entering its outer portion. This is seen both in Figure 1 and in the more detailed view of the tank geometry presented in Figure 3, which also shows the energy deposition zones employed. A total of 140,000 neutrons were sampled from six different energy regions for each of these two areas; the results of these twelve problems were normalized to 1000 MW of reactor power and so combined and printed that they could be examined individually or in composite. In a similar way, 160,000 additional neutron histories were also run in order to test the effect of spectral modifications in the high energy region, and thus determine the influence of the uncertainties which may exist there.

Elastic scattering was presumed, with isotropy in the center-of-mass system and a scattering cross section identical to the total hydrogen atom cross section. Each history was terminated whenever the neutron's energy dropped below 10 kev.

Figure 4 shows values obtained for the propellant heating from neutrons scattered within the on-axis tank sectors. The relaxation length of this heating is remarkably constant, considering the complex nature of the input spectrum. The attenuation exhibited is almost exactly a factor of ten per foot, or a factor-of-e in ~13 cm, as one can see from the straight line drawn through the curve. The heating at depth appears to rise above that which would be predicted by an extrapolation of this line, though the statistics in this region of low deposition do not yield this inference unambiguously.

A curve of the probable source intensity of "capture gammas" was produced from the distribution of neutron cutoffs obtained in the present calculation. These data, representing neutrons absorbed per cm^3 per second at various depths along the axis of the tank are shown in Figure 5. (In the figure, we have allowed for the absorption of leakage neutrons whose histories were not run in the Monte Carlo calculation, because their initial energies were below 17 kev, by making an appropriate increase in the number of lowest group Monte Carlo cutoffs.) Each cutoff has been presumed to result in a capture event in the immediate neighborhood of the cutoff point. On this basis, 80% of the captures occur in the first four inches of propellant and over 95% occur in the first foot. (Even if the captures should not occur at the cutoff point, experience with other calculations has shown us that further diffusion before capture tends to reduce the maximum value of the capture heating, while little affecting its volume integrated contribution.)

For computer study, the intensity of captures across a section perpendicular to the tank axis was related to the on-axis value through an inverse-square ratio on distance from the reactor center, and these local captures all gave rise to isotropically distributed 2.23 Mev gamma rays. The heating contributions from fourteen such thin-sectioned transverse capture volumes were found at various detector points and summed to produce the values ascribed to this cause in Figure 6.

Figure 6 shows propellant heating input rates to be expected at various depths along the axis of a tank such as this from each radiation cause, and also totals the effects from all the radiation sources. All the data are normalized for a 1000 MW unshielded reactor source. The curve labeled "reactor gammas" is based on calculations which used a reactor point-source model, a ten foot separation, and performed computer integrations of the direct, first-scattered, and buildup heating contributions from each line of a multi-group gamma spectrum representing the axial leakage from a reactor.(1)

Considering all sources, one notes that the present Monte Carlo study on neutron heating extended to an adequate propellant depth, since neutrons produce only ~2% of the heating at the 92 cm level to which the problem was carried.

The high heating rates found near the front of the tank were distributed fairly uniformly over the tank face. It was found that the neutron heating in the center bottom region of the tank is not dependent on tank diameter for diameters greater than about five feet ($R \geq 2.5$ feet), which shows that the present results are likely to apply regardless of the detailed shape of the tank's end.

In spite of the fact that reactor neutrons directly carry only about 20% of the total energy imported to propellant, their contribution near the front face is several times that from reactor gammas. (With a specific heat for LH_2 of $\sim$2.25 cal/gm-^{o}C, the maximum power input shown here would produce a temperature rise rate of $\sim$0.6^{o}R/sec.) Such a high-valued, high-gradient heating source could be coped with readily under many conditions of "potential flow," even without a shield[1], but the greater likelihood of a nearly uncontrolled propellant circulation forces the inclusion of a shield to preclude the possibility of intolerable temperature rises in the propellant.

Further details on the present calculation will be available in a forthcoming Los Alamos Scientific Laboratory report.

(1) Cf. "Radiation Heating in the Liquid Hydrogen Propellant of Nuclear Rockets," G. A. Graves and J. R. Streetman, Transactions of the American Nuclear Society, Vol. 4, No. 1, June 1961.

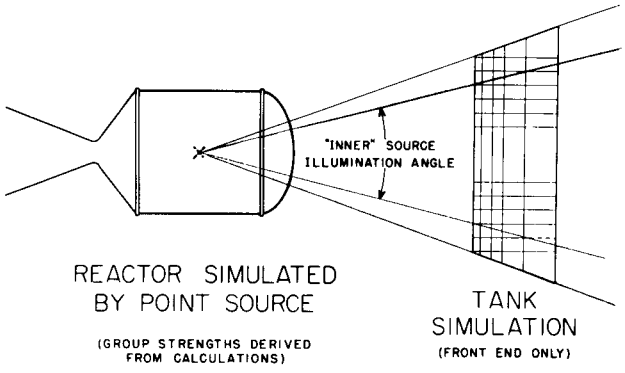

Figure 1. The overall geometry

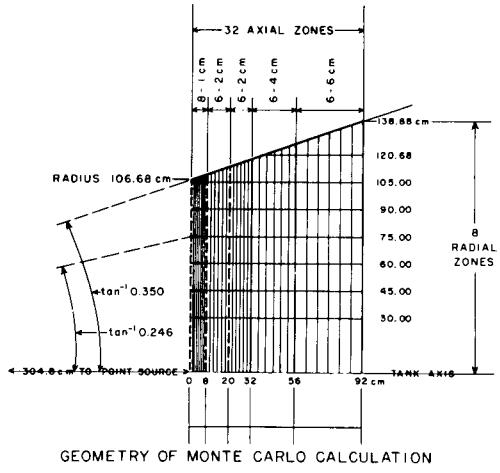

Figure 3. Detailed view of tank geometry

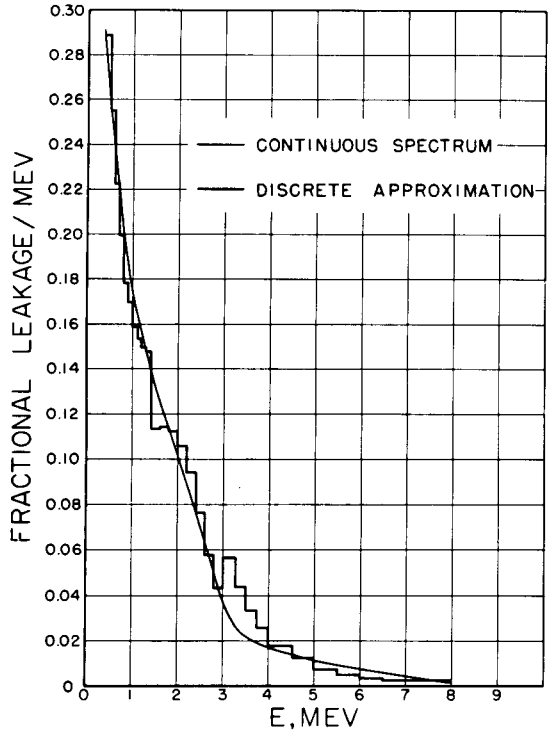

Figure 2. The source spectrum

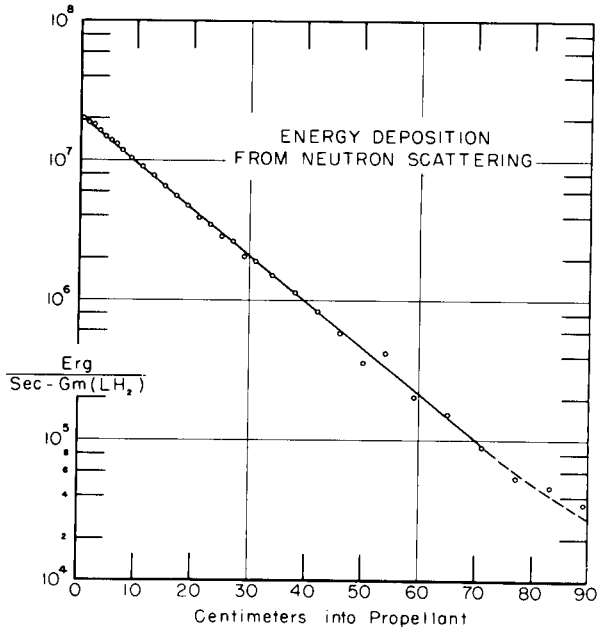

Figure 4. Axial kinetic energy deposition

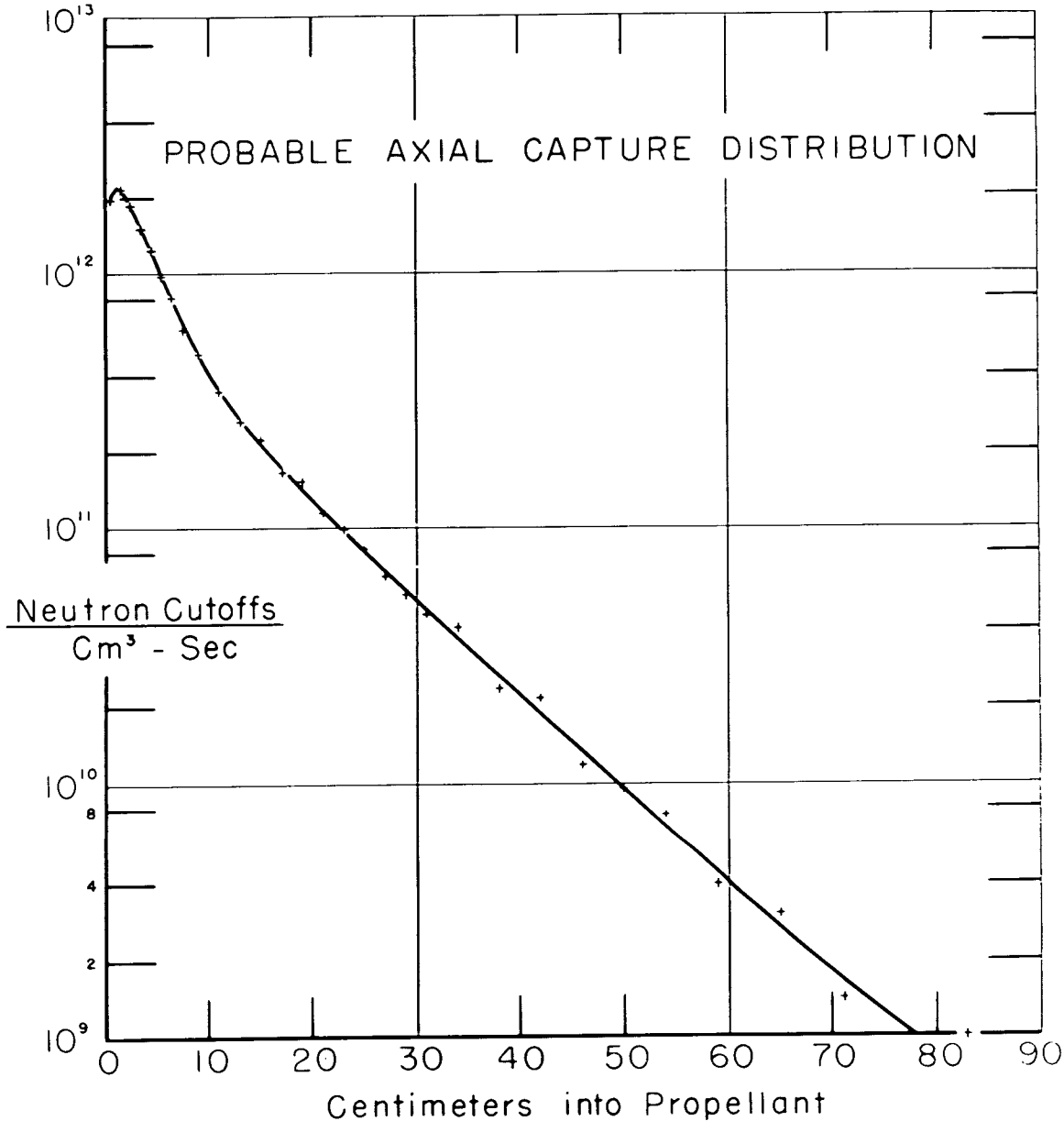

Figure 5. Distribution of cutoffs

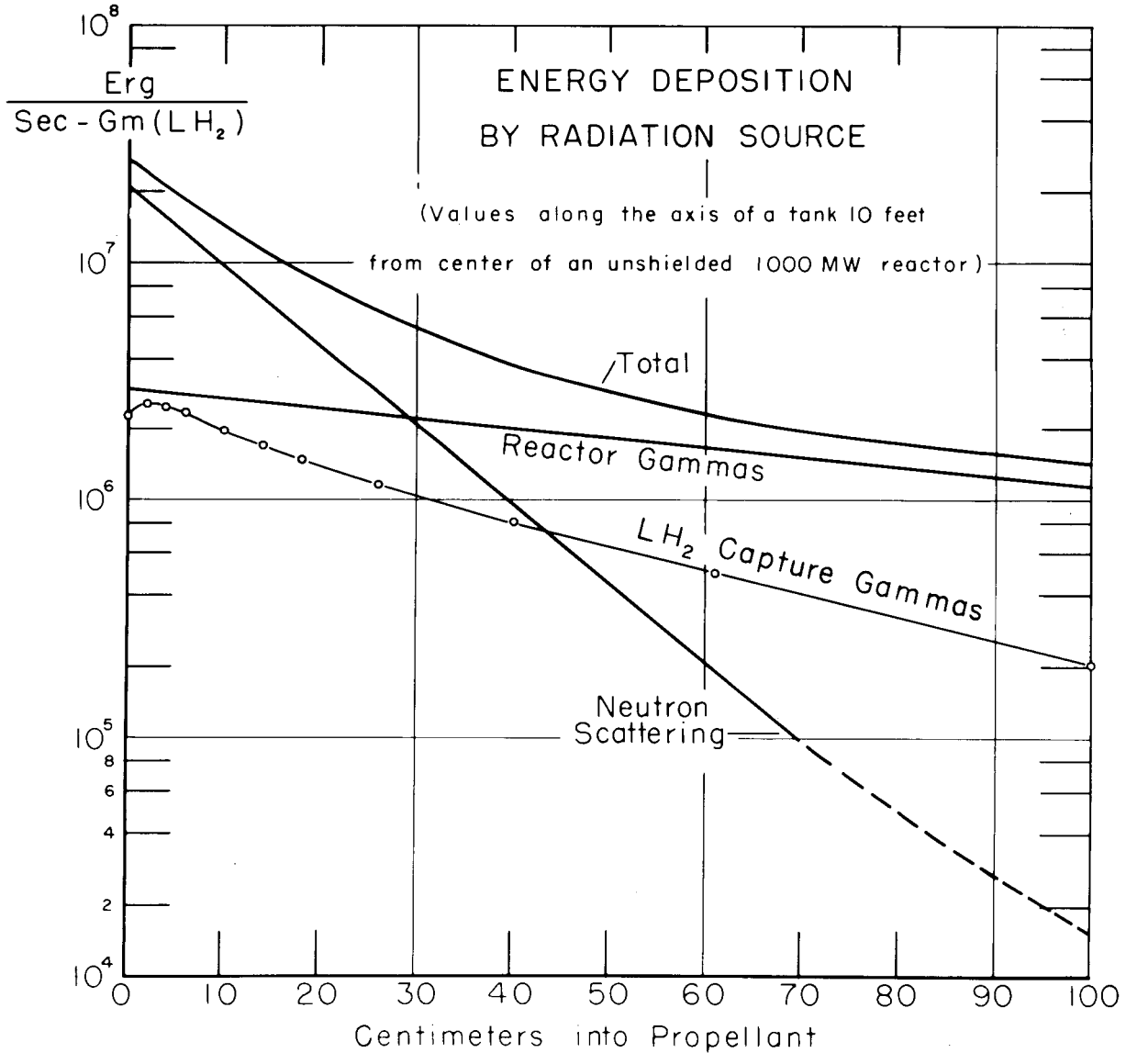

Figure 6. Total energy deposition from all sources

RADIATION-INDUCED MOLECULAR REACTIONS IN LIQUID HYDROGEN

H. G. Carter
General Dynamics, Fort Worth, Texas

I. Introduction

Much consideration is being given to the gross deposition of radiation energy inside the propellant storage systems of nuclear-powered space vehicles. It is customarily assumed that such radiation energy is instantly translated into familiar thermal effects. It would seem, however, that the microscopic processes associated with radiation-heating in liquid hydrogen are worthy of attention. Of particular interest from the standpoint of propellant-shield and pressure-vessel design should be the formation of energy-storing molecular species through which the production of actual thermal energy is temporarily postponed. Consideration of potential energy expelled from a storage system in the form of such species could lead to lower overall design weights, owing to less stringent provisions for shielding, pressure vessel construction, and/or boil-off.

The present objective is to determine whether a significant amount of energy is temporarily stored through the formation of radiation products in liquid hydrogen and whether such products survive in the liquid for a long enough period of time that their mechanical expulsion competes favorably with their return to the H_2 ground state through the liberation of kinetic energy.

That energy storage mechanisms in liquid hydrogen should be looked into is suggested by the general nature of the propellant heating problem. In an important class of cases one has to reckon with radiation-induced heating only while the nuclear power source is in operation and while the propellant is being expelled from the storage tank at a high rate. Furthermore, in foreseeable space vehicles, the fraction of the total volume of propellant which is nearest the radiation source and which therefore absorbs most of the radiation is also nearest the storage exit or pump. Therefore, volume elements of the liquid are exposed to the most intense radiation only shortly before they are expelled, and hopefully, the potential energy created may not have time to dissipate into thermal motion.

It is expected that full-scale propellant tanks for "one-way" vehicles will be completely emptied in around ten minutes. Using a typical tank length of the order of 100 feet and effective energy-flux relaxation length of 3 feet - which is reasonable for mixed neutron and gamma radiation in liquid hydrogen - it is seen that the majority of the molecules affected by radiation are expelled within 20 seconds after being affected. Hence, a 20-second period can be taken as the minimum time for which energy must remain stored in radiation products if energy storage effects are to be significant.

II. Radiation Induced Reactions in Liquid Hydrogen

Energy deposited in liquid hydrogen by neutral radiation is initially transferred to recoil protons or Compton-scattered electrons in the case of neutrons and gamma rays, respectively. The major secondary processes in which the radiation products may participate do not appear to involve the mobility or density of molecules in such a way that reactions due to energetic protons or electrons in the liquid should be much different from those observed in the gas (Ref. 1, 2, 3), e.g., due to α-particles (Ref. 1). It is therefore assumed that the types and proportions of various radiation products are independent of the molecular density as well as of the charged particle type and energy.

According to this assumption, when a charged particle passes through hydrogen, which is normally almost entirely in the H_2 ground state, approximately equal amounts of energy go into the production of H-atom pairs (through the formation of the $^3\Sigma_u$ H_2-state) and into the production of H_2^+ ions. By means of the reactions

$$H_2^+ + H_2 \Longrightarrow H_3^+ + H \quad : \quad H_3^+ + e^- \Longrightarrow 3H \text{ or } H_3^+ + e^- \Rightarrow H_2^* + H$$

the ionization process leads indirectly to further dissociation and excitation.

What might be called the principal events with respect to ionic and dissociative reactions are summarized in Figure 1. The more obscure reactions are omitted and the assumption of exactly one $^3\Sigma_u$ (dissociative) excitation for each H_2 ionization is merely a convenient approximation. The two major branches represent reactions which proceed concurrently (not as optional branches) after the deposition of 33 ev by energetic charged particles. Figure 1 shows that 5 H atoms are formed for every 33 ev deposited. Since the potential energy between pairs of H_2 molecules is 4.73 ev, the energy stored in the production of H atoms is $(\frac{1}{2})$ (5) (4.73), or 36% of the energy deposited. It can be assumed that the energy of the excited H_2 state is of the order of the dissociation energy, so that the energy stored in ionic and dissociative reactions alone comes to about 43%. Most of the remaining 57% of the deposited energy is initially released

in the disintegration of the repulsive molecular configurations. Figure 1 shows the initial H-atom energies.

Considerably more than 43% of the deposited energy will be stored if collisions between energetic H atoms and H_2 molecules are effective at producing the excited H_2 state. The permissable energy levels for an H_2 molecule excited to low states of vibration and rotation in the ground electronic state are described by

$$E_{Jv} = 0.015(\tfrac{1}{2})J(J+1) + 0.533v,$$

where E_{Jv} is the energy in ev of a molecule in its J^{th} rotational state and its v^{th} vibration state. The excitation of an H_2 molecule by an energetic H atom occurs through the formation and decomposition of an H_2-H (or H_3) complex. A contour map of the theoretical potential field (Ref. 4) shows that H atoms with energies of the order of 1 ev should be able to surmount the potential "ridge" and enter the "Basin" corresponding to an H_3 complex in a large fraction of solid collisions. Furthermore, the lifetimes of various H_3 states, which have been calculated by the author, show that energetic complexes hold together long enough for the energy to become well "mixed" among various internal degrees of freedom. Therefore, in H-H_2 collisions which are solid enough to effect appreciable momentum transfer, there should be a high probability of H_2 excitation to levels of 0.533 ev or more.

Exclusive of a small magnetic effect, the para- to ortho-hydrogen conversion ($J=0 \rightarrow J=1$) reaction can only occur through the formation and decomposition of an H_3 complex, which, because of an energy barrier in the H_2-H field (activation energy), requires an H-atom energy of at least 0.30 ev. Little of the deposited energy can be stored in ground state conversion, since the energy imparted to the residual molecule through momentum transfer is much larger than the energy stored (0.015 ev). Thus, although ortho-hydrogen has an extremely long lifetime in the liquid, any significant energy storage depends on the lifetimes of the more robust forms of excited H_2 and upon the lifetimes of unrecombined H atoms.

Whether the energy going into product formation remains stored in non-thermal form for the 20 seconds or so required for the expulsion of the irradiated portion of the liquid depends upon the rate of recombination of H-atoms pairs and the rate of de-excitation of H_2 molecules. Available data on these reactions (see below) show that most recombination and de-excitations occur after the radiation products slow down and go into thermal equilibrium with the liquid.

III. Recombination of H atoms

The number of 3-body collisions per cm^3 per sec is given by $Z = R_A (H)^3$ for H atoms as third bodies and $Z = R_M(H)^2(H_2)$ for H_2 molecules as third bodies. Values (H) and (H_2) are the concentrations of atoms and molecules, respectively. Two sets of theoretical results and two sets of experimental results are available in connection with the recombination coefficients. The theoretical results are mutually inconsistent, as are the experimental results. The four sets of results labeled E-1, E-2, T-1, and T-2 are described as follows:

(E-1) In 1934 Amdur (Ref. 5) measured R_A and R_M using a discharge tube to obtain H atoms. Atoms and molecules

were allowed to pass from the discharge tube into a drift tube, where the energy deposited at a calorimeter-catalyst was measured as a function of distance. Amdur got $R_A = 2.05 \times 10^{16}$ cm^6 mole^{-2} sec^{-1} and $R_M \leq \frac{1}{10} R_A$.

(E-2) In 1934 Steiner (Ref. 6) measured R_A and R_M using an arrangement similar to that of Amdur, except that the H-atom concentration was measured as a function of position by a spectroscopic method. Steiner got $R_M = 1.3 \times 10^{16}$ cm^6 mole^{-2} sec^{-1} and $0 < R_A \leq \frac{1}{10} R_M$.

(T-1) In 1935 Eyring et al (Ref. 7) calculated R_A using the transition state method. This is a quasi-classical approach in which system points corresponding to triples of particles are assumed to move, with equipartioned energy, upon the appropriate potential surface in configuration space. Eyring et al got $R_A = 3.1 \times 10^{15}$ cm^6 mole^{-2} sec^{-1}.

(T-2) In 1951 Bauer (Ref. 8) calculated R_A by an approximate quantum mechanical method. Bauer got $R_A = 10^{-42}$ cm^6 sec^{-1} = 3.6×10^5 cm^6 mole^{-2} sec^{-1}.

The data upon which the results E-1 were based were probably misinterpreted. It is likely that the energy deposition at the calorimeter-catalyst was mainly due to the de-excitation of excited H_2 molecules produced along with the H atoms in the discharge tube. The results T-1 depend strongly upon features of the H_3 potential energy surface in regions where the methods used to obtain the surface are of doubtful validity; moreover, it appears that some of the surface-dependent parameters were chosen to give an R_A within an order of magnitude of the experimental results. The results E_2 only set an upper bound on R_A (the ambiguity arising from the effect of wall recombinations). Therefore, T-2 and E-2 are consistent and involve no obvious sources of error.

Recombination with an H_2 molecule as the third body is thought to involve an activation energy comparable to that for the formation of an H_3 complex (0.30 ev). Therefore, at liquid hydrogen temperature, this type of recombination should be inoperative. On the other hand, theoretical considerations show that R_A for liquid-hydrogen temperature should not differ from R_A for room temperature by more than an order of magnitude.

IV. Recombination During Propellant Expulsion

R_A can be used to estimate the maximum radiation level for which most of the H atoms are expelled (unrecombined) from a propulsion system of interest. The fraction of H atoms which recombines per second at a point where the concentration is (H) can be written $F = R_A(H)^3/(H) = R_A(H)^2$. For $R_A = 1.3 \times 10^{-33}$ cm^6 sec^{-1}, it is seen that F is a very small fraction as long as (H) does not exceed 10^{15} H atoms/cm^3. For $R_A = 10^{-42}$ cm^6 sec^{-1}, the corresponding number is (H) = 10^{20} H atoms/cm^3. Rough estimates of the radiation levels corresponding to these concentrations at the point where the liquid hydrogen is expelled and for reasonable flow rates give 10^{17} ev/cm^2-sec and 10^{22} ev/cm^2-sec, respectively. This would mean, for example, that most H atoms would be expelled for fast-neutron fluxes up to 10^{11} neutrons/cm^2-sec or up to

10^{16} neutrons/cm^2-sec, depending on whether the experimental upper bound on R_A or Bauer's value is correct.

V. Superlastic De-excitation of H_2 Molecules

If the recombination coefficients for H atoms should approach the experimental upper limit given above, the process of de-excitation by energy release to another body ("super-elastic scattering") could have more influence on the energy storing capabilities of liquid hydrogen than recombination, since, in general, H atoms recombine in an excited state. A quantum mechanical treatment of the H_2-H_2 inelastic cross section has been given by Salkoff and Bauer (Ref. 9). The super-elastic cross section and the vibrational relaxation time (mean lifetime), τ, of excited molecules in equilibrium can be related to the inelastic cross section through the principle of detailed balance, according to which the rates of an elementary process and its inverse are equal for equilibrium conditions.

For hydrogen gas at an unspecified low density and for the first excited vibrational level of H_2, Bauer and Salkoff evaluated τ in the range 1000°K to 8000°K. From the values obtained, the density used appears to have been about 10^{18} molecules/cm^3. Their results are well represented by $\tau = 6.41 \times 10^{-11} \exp(115.2T^{-1/3})$ (sec).

Adjusting to the molecular density of liquid hydrogen and making the admittedly Brobdingnagian extrapolation to 20°K, one obtains $\tau \sim 100$ minutes for the lifetime of the excited state. Thus, there are some grounds for believing the lifetimes of H_2 states in the liquid are extremely long.

Even if the extrapolation to 20°K is valid, the value of τ obtained above depends upon the assumption of isolated binary collisions in the liquid. According to a theory of relaxation in liquids by Zqanzig (Ref. 10), this assumption is valid provided the frequency of vibration is much larger than the frequency of collisions experienced by a molecule in the liquid. Owing to the relative stiffness of the H_2 molecule and to the low temperature involved, this criterion is found to be satisfied for liquid hydrogen.

VI. Emission and Absorption of Infrared Rays

If the transmission of electromagnetic energy to the walls of the system is more rapid than the expulsion of the irradiated portion of the liquid, then the energy initially stored in excitation will go into wall-heating, through lattice excitations, regardless of the inefficiency of the H_2 super-elastic process. The rate at which such energy migrates through the liquid is determined by the lifetime against emission, $A(b,a)$, and the mean free path with respect to absorption, $\ell(a,b)$, where the first and second arguments denote the initial and final states, respectively. $A(b,a)$ and $\ell(a,b)$ can be related to the "Einstein coefficient for absorption", $B(a,b)$. The latter quantity can be obtained from analysis of the absorption spectrum produced by a thin sample of the liquid.

A Canadian group (Ref. 11) has measured the infrared absorption spectrum of liquid hydrogen. The data have been used to calculate $B(a,b)$, $A(b,a)$, and $\ell(a,b)$ for various transitions in normal hydrogen. The results are given in Table I.

Table I. Emission and Absorption in Liquid Hydrogen

Line	State a v	J	State b v'	J'	B(a,b) (cm^2/erg-sec)	A(b,a) (sec^{-1})	ℓ(a,b) (cm)
S(0)	0	0	1	2	10.21(2	0.929(-1	0.81
S(1)	0	1	1	3	4.24(2	0.951(-1	0.54
Q(1)	0	1	1	1	9.40(2	3.37(-1	0.51

The product $\ell A(b,a)$ can be regarded as the effective velocity of infrared-ray propagation in the direction of emission. Since it is of the order of 0.1 cm/sec, the migration of infrared-ray energy to the walls of a realistic system is gradual.

VII. Conclusions

The conclusions of the present study are summarized as follows:

(1) At least 43% of the energy deposited by radiation in liquid hydrogen is stored temporarily, mainly through the dissociation of H_2 molecules. A large fraction of the remaining energy may be stored through inelastic collisions between energetic H atoms and molecules in the liquid.

(2) For the flow-rates presently envisioned, most of the H atoms produced by radiation will be expelled for incident energy fluxes up to at least 10^{17} ev/cm^2-sec. Quantum mechanical results are consistent with predominant H-atom expulsion at levels up to 10^{22} ev/cm-sec.

(3) Excited H_2 molecules, which are apt to be formed in significant concentrations by recombination and by H-atom inelastic scattering, may remain excited in the liquid for much longer than the 20 seconds or so required for the expulsion of the irradiated portion of the liquid. Extrapolation of the theoretical relaxation time, while questionable, indicates that the lifetime of the first vibrational level in the liquid is of the order of 100 minutes.

(4) The lifetime of excited H_2 states against emission in the liquid is of the order of seconds; however, the mean-free-path against absorption by re-excitation of the original type of H_2 state is so small that the effective rate of infrared-ray diffusion is much less than 1 cm/sec. Hence, in the event that the partitioning of energy by super-elastic scattering goes slowly, then the walls of the liquid hydrogen tank will not be heated significantly by infrared radiation. The storage of energy in the form of excited H_2 states can be verified experimentally by the observations of infrared rays trapped in the liquid.

It is further concluded that, insofar as radiation heating of the propellant has a significant influence on the design of a nuclear-powered vehicle, further investigations into the rates of radiation-induced molecular reactions are warranted and that any experimental data obtained on the radiation heating of liquid hydrogen should be interpreted in the light of possible delays in the equipartition of energy stored in radiation products.

REFERENCES

1. Eyring, H., Hirschfelder, J. O., and Taylor, H. S., "The Theoretical Treatment of Chemical Reactions Produced by Ionization Processes: Part 1." Journal of Chemical Physics 4 (1936), 479-491.

2. Murray, R. L., "Mass-Spectroscopic Study of Ionic Reactions in Hydrogen." Journal of Applied Physics 23 (1952), 6-11.

3. Ortenburger, I. B., Hertzberg, M., and Ogg, R. A., Jr., "Secondary Reactions in a Gas Discharge." Journal of Chemical Physics 33 (1960), 579-583.

4. Hirschfelder, J., Eyring, H., and Topley, B., "Reactions Involving Hydrogen Molecules and Atoms." Journal of Chemical Physics 4 (1936), 170-177.

5. Amdur, I., "The Recombination of Hydrogen Atoms II. Relative Recombination Rates of Atomic Hydrogen and Atomic Deuterium." Journal of the American Chemical Society 57 (1935), 856-858.

6. Steiner, W., "The Recombination of Hydrogen Atoms." Transactions of the Faraday Society 31 (1935), 623-636.

7. Eyring, H., Gershinowitz, H., and Sun, C. E., "The Absolute Rate of Homogeneous Atomic Reactions." Journal of Chemical Physics 3 (1935), 786-796.

8. Bauer, E., "Dissociation of Hydrogen Molecules by Vibrational Excitation and Three-Body Recombination Coefficients." Physical Review 84 (1951), 315-32.

9. Salkoff, M., and Bauer, E., "Excitation of Molecular Vibration on Collision." Journal of Chemical Physics 29 (1958), 26-31.

10. Zwanzig, R., "Theory of Vibrational Relaxation in Liquids." Journal of Chemical Physics 34 (1960), 1931-1935.

11. Allin, E. J., Hare, W. F. J., and MacDonald, R. E., "Infrared Absorption of Liquid and Solid Hydrogen." Physical Review 98 (1955), 554-555.

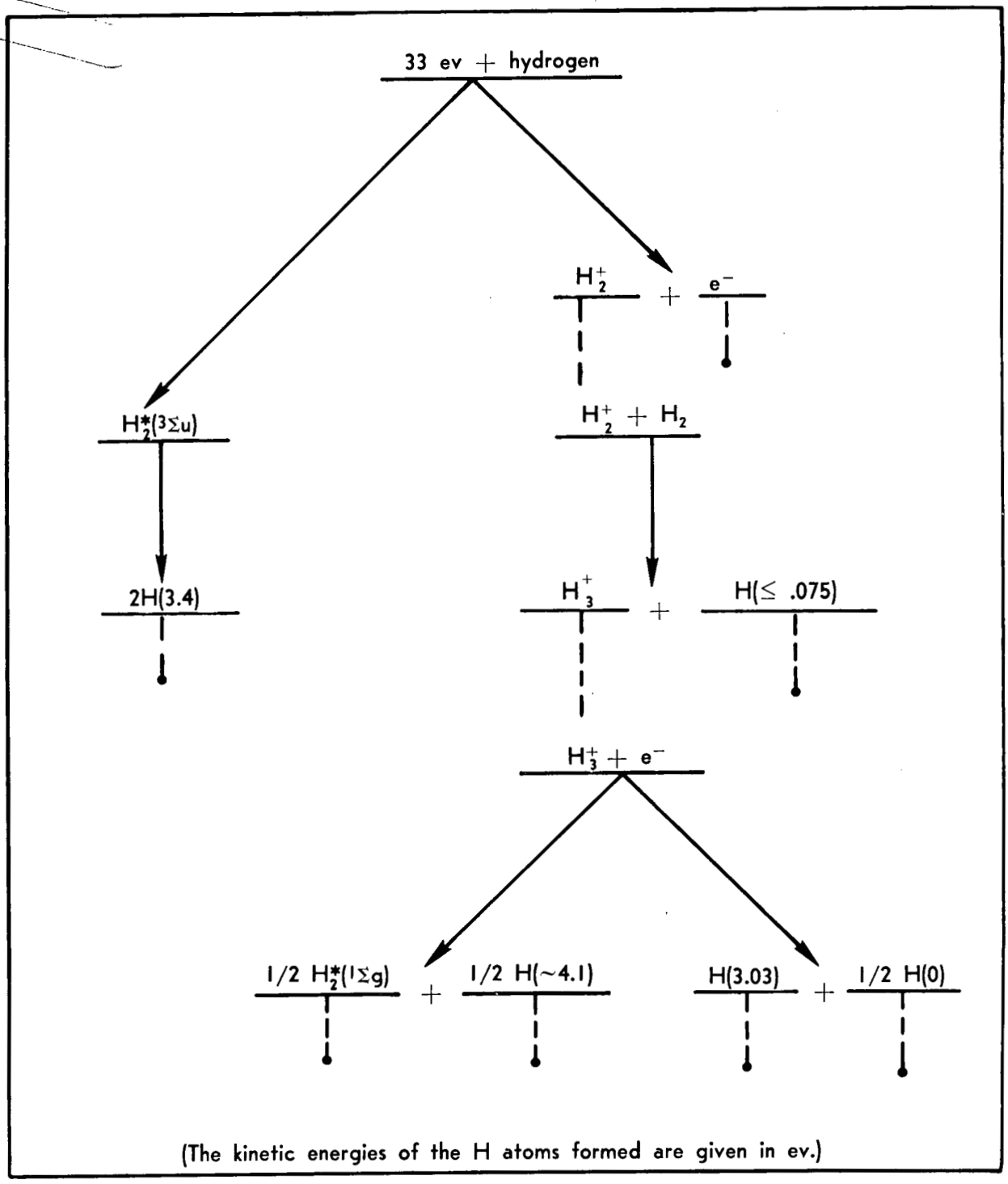

Figure 1. Principal Ionic and Dissociative Events Resulting from the Irradiation of Hydrogen

CLOSED LOOP DYNAMICS OF NUCLEAR ROCKET ENGINES WITH BLEED TURBINE DRIVE

by
Harold P. Smith, Jr.
Department of Nuclear Engineering
University of California
Berkeley, California

ABSTRACT

A previous work on open loop dynamics of nuclear rocket engines (1) is expanded to include integral temperature error feedback control of reactivity and proportional pressure error feedback control of propellant flow with first order lags placed between the desired controller positions and the actual positions. The resulting series of ordinary, non-linear, differential equations are approximated by a linear model in order to analyze the low-frequency dynamics. It is shown that the low and high frequencies may be decoupled and that the proposed method of control is stable for small variations away from any point of steady-state operation. Algebraic equations, in terms of design parameters, are derived for control settings which yield optimum response characteristics. It is further shown that the asymptotic response is improved by reduction of the mechanical inertia of the turbopump but is independent of the thermal inertia of the core.

The analysis is corroborated by analog simulation of the non-linear model for the case of low-power--high-power transition, using only feedback control for flow and reactivity variation.

INTRODUCTION

In a previous paper (1), an analysis was presented showing that conventional nuclear rocket engines can be designed to be inherently stable and do not need external control in order to maintain a steady operational power level. It is equally important that the engine follow a prescribed optimum flight program and adjust its performance in the event of fluctuations during operation. Feedback control of engine parameters is suitable for this provided the controlled system has rapid response, small overshoot, and closed loop stability.

In order to investigate the dynamics of the controlled engine, the previous mathematical model of the open loop (non-controlled) engine is expanded to include the dynamics of external feedback and controller motion. A linear approximation of this model is subjected to analysis in order to estimate stability limits and response characteristics. The non-linear model is simulated by analog computer techniques, and results are given for controlled transition from low to full power.

Throughout the study, the attempt is made to obtain general results that will have application to a variety of engine designs but will not exceed the bounds of reasonable engineering accuracy.

MATHEMATICAL MODEL OF THE ENGINE DYNAMICS

Review of Open Loop Equations

The open loop equations describing the system are the same as those derived in the earlier paper. They are repeated below but preceded by a list of the major assumptions made in their derivation.

1. The distributions of neutron density, temperature, and pressure within the core are adequately described by space independent variables.
2. The standard neutron and precursor equations are applicable.
3. Propellant flow in the main rocket nozzle and turbine nozzles is choked.
4. Power density in the core is proportional to neutron density.
5. Radiative and conductive heat transfer from the core can be neglected in comparison with convective core heat transfer to the propellant.
6. The high-frequency effects associated with propellant compressibility and inertia are effectively damped by the thermal inertia of the core and mechanical inertia of the turbomachinery. (Felix and Bohl (2).)
7. Propellant core entrance stagnation temperature is negligible when compared to the core exit temperature.
8. The rate of change of reactivity with temperature at constant propellant density is negative, $(\partial\delta/\partial T)_{P/T} < 0$; the rate of change of reactivity with propellant density at constant core temperature is positive, $\left(\frac{\partial\delta}{\partial(P/T)}\right)_T > 0$.

The use of standard statements of reactor dynamics, fluid flow, and heat transfer in conjunction with these assumptions is sufficient to derive the following set of equations. The notation is standard.

$$\tau_n \frac{dn'}{dt} = \delta' n' - n' + \sum_{i=1}^{i=N} \frac{\beta_i}{\beta} C_i' \qquad (1)$$

$$\tau_{ci} \frac{dC_i'}{dt} = n' - C_i' \tag{2}$$

$$\tau_T \frac{dT'}{dt} = n' - P'\sqrt{T'} \tag{3}$$

$$\tau_p \frac{dP'}{dt} = P'V'\sqrt{T'} - \frac{(P')^2}{\sqrt{T'}} \tag{4}$$

$$\delta' = \delta_r' - \alpha_c \sqrt{T'} + \alpha_h \frac{P'}{T'} \tag{5}$$

Control Equations

$$\delta_{rs}' = G_1 \int_o^t (\sqrt{T_s'} - \sqrt{T'})dt \tag{6}$$

No proportional feedback is attempted since the large control rod inertial precludes efficient rod response to a proportional error signal. With this simplification, a first order lag between the desired rod position and the actual position should be sufficient for adequate response simulation.

$$\tau_r \frac{d\delta_r'}{dt} = \delta_{rs}' - \delta_r' \tag{7}$$

Since the mechanical inertia of the control valve is small, both integral and proportional feedback of the core exit pressure error is utilized. The attempt is made to rely on proportional control for attaining the desired system pressure; the integral control is used only to eliminate the steady-state error that arises with sole use of proportional control,

$$V_s' = G_2 \int_o^t (P_s' - P')dt + G_3(P_s' - P') \tag{8}$$

A first order lag is introduced between the desired valve position and the actual position.

$$\tau_v \frac{dV'}{dt} = V_s' - V' \tag{9}$$

ANALYSIS OF SYSTEM STABILITY AND RESPONSE

The values of the controllers, G_1, G_2, G_3, are to be such that not only is the system stable, but an optimum response is obtained to a desired engine operation program. In order to investigate the external feedback effect of the controllers upon the system, a linear model of the dynamic equations, accurate for small perturbations about any point of steady-state operation, is made. The accuracy of the model will be tested by analog simulation of the complete set of non-linear equations. With this approximation the stability and impulse response of the linear set of equations is investigated as a function of the controllers.

The following assumptions are made to simplify the analysis:

1. The prompt neutron lifetime is set equal to zero. This approximation is correct for frequencies less than those associated with the inverse lifetime (3) and for reactivities less than prompt critical. Since we have already excluded the high-frequency effects of propellant inertia and compressibility, this assumption does not

further restrict the analysis.

2. The dynamic effects of the delayed neutron precursor groups are adequately expressed by one group of delayed neutrons with parameters, τ_c and β, chosen such that the approximation is accurate for low frequency.

3. Integral feedback control of pressure is eliminated from the analysis since it has been incorporated only to remove the steady-state error of proportional feedback and not as a primary means of control.

4. The time delays associated with the rod and valve response are neglected. As long as the control rods are not driven by a proportional error signal, this approximation should be valid, although not conservative.

The Laplace transformation of the characteristic equation is

$$m(s) = P_p(s) + \frac{G_1}{2\tau_T} P_z(s) + \frac{G_3}{\tau_p} \left\{ Z_p(s) + \frac{G_1}{2\tau_T} Z_z(s) \right\} = 0 \quad (10)$$

where

$$P_p(s) = s^4 + s^3 \left(\frac{\alpha_T + \frac{1}{2}}{\tau_T} + \frac{1}{\tau_p} \right) + s^2 \left(\frac{\alpha_T - \alpha_p}{\tau_T \tau_p} + \frac{\alpha_T}{\tau_c \tau_T} + \frac{\frac{3}{2}}{\tau_T \tau_p} \right) + s \left(\frac{\alpha_T - \alpha_p}{\tau_c \tau_T \tau_p} \right)$$

$$P_z(s) = \left(s + \frac{1}{\tau_c}\right) \left(s + \frac{1}{\tau_p}\right)$$

$$Z_p(s) = s^3 + \frac{s^2}{\tau_T} \left(\alpha_T + \frac{1}{2}\right) + s \frac{\alpha_T}{\tau_c \tau_T}$$

$$Z_z(s) = s + \frac{1}{\tau_c}$$

$$\alpha_T = \frac{\partial \delta'}{\partial T'} \qquad \alpha_p = \frac{\partial \delta'}{\partial p'}$$

The characteristic equation can be further simplified by incorporating the following considerations:

1. The high frequency roots of (10) are well removed from the low frequency region of the s plane. These roots can be neglected.

2. α_T is set equal to α_p. This places the closed loop system at the point of marginal open loop stability and is hence a conservative assumption. Calculations show that this approximation is close to the real situation.

3. The thermal time constant, τ_T, cancels from the characteristic equation in all terms but one, and in that term it is insignificant in comparison to other terms provided the analysis is restricted to high thrust engines.

The root loci of Equation (10) which depend upon the values of G_1 and G_3, determine the stability and response of the linear approximation to the rocket engine dynamics. The root loci are presented in Figure 1. The shape of the system root locus as a function of G_3 is not radically changed as G_1 takes on a variety of values. Therefore, certain general conclusions can be drawn.

1. Stability. The system remains stable for all positive values of G_1 and G_3, even when the system parameters are allowed wide variation from our calculated values. The introduction of the proposed control system leads to no low-frequency instability

within the range of practical design or interest.

2. Decoupling of high and low frequencies. The root locus remains in the low frequency region of the s plane ($|s| \approx \frac{2}{\tau_p}$) for all values of G_1 and G_3 of practical interest. The high frequency root loci do not move into this region for the same range of controllers.

3. Operation away from open loop marginal stability ($\alpha_T > \alpha_p$). The starting point of each root locus for a given value of G_1 is displaced slightly to the left if $\alpha_T > \alpha_p$. This only enhances and cannot jeopardize the stability and response of the system.

4. Asymptotic response proportional to $1/\tau_c$. No combination of G_1 and G_3 can remove the system root at $s = -1/\tau_c$. Consequently, the asymptotic response of the system cannot be faster than times associated with delayed neutron precursors. However, the analysis utilized the zero neutron lifetime approximation which is applicable only when the total reactivity is less than prompt critical. It is not surprising, therefore, that the response of the system is restricted to delayed neutron time constants.

5. Asymptotic response proportional to $1/\tau_p$. Since it is possible for the nuclear rocket engines to safely respond to reactivity inputs greater than prompt critical (1), the above analysis was repeated in which it was assumed that all neutrons are emitted promptly. The root loci are the same within the region, $|s| \approx 2/\tau_p$ with the exception that there are no poles or zeroes at or near $s = -1/\tau_c$, as expected. Under these conditions, the dominant root is of the order of $1/\tau_p$ and the asymptotic response of the system is associated with the mechanical inertia of the turbopump system.

6. Optimum point of control. Although the values of G_1 and G_3 have little effect on the position of the system root near $s = -1/\tau_c$, they do have a significant effect on the other two system root loci. The optimum position of these roots occurs where the loci again meet the real axis at the point labeled $-s_o$ in Figure 1. This occurs when the following equation is satisfied:

$$G_3 = 2\xi + \xi^2 \qquad (11)$$

where

$$\xi^2 = \frac{G_1 \tau_p}{2\alpha_T}$$

The value of the double root at $s = -s_o$ is

$$s_o = \frac{1}{\tau_p}(\xi^2 + \xi) \qquad (12)$$

The speed of response of the terms in the time domain associated with the roots at $s = -s_o$ increases as the value of s_o increases. Therefore, optimum control results whenever G_1 or G_3 or both take on their maximum practical value, subject to satisfaction of Eq.(11).

7. Optimum control as a function of power level. Most parameters of the system are functions of the power level. Therefore, the values of G_3 or G_1, or both must be changed in order to operate at optimum control for various operational power levels.

8. Response as a function of power level. If G_1 and G_3 are adjusted, such that (12) is satisfied, the root at $-s_o$ is moved to a more negative value as the power is increased, thus improving the response. Unfortunately, $1/\tau_c$ is independent of power level, so that one would expect that at full power where only small changes of reactivity will be required that the asymptotic response will be geared to the delayed neutron response. Nevertheless, the

response of the closed loop nuclear rocket engine should improve with power level just as the open loop response improves at high power (1).

ANALOG SIMULATION OF LOW-POWER--HIGH-POWER CONTROLLED TRANSITION

The non-linear dynamic equations (1 through 9), using two groups of delayed neutrons, were simulated on an analog computer. In order to provide an exacting test of the linear analysis, as well as to investigate a possible method of bringing the rocket to full power, the engine was assumed to be operating at a relatively low power (T = 1000°R, P = 275 psi), and then brought to full power (T = 5000°R, P = 1500 psi) by requiring a step change in desired temperature and pressure, adjusting the controller gains to acceptable values, and allowing the engine to proceed to full power under its own feedback control system.

A rapid transition is desired since efficient use of the engine demands that the propellant not be carried to high altitudes before being utilized. Since the full power operating point will be only slightly less than that which the materials can withstand, the transition, although rapid, can have only very small overshoot.

In theory, it should be possible to bring the engine to full power almost as rapidly as desired and with small overshoot, if one has unlimited amounts of control available. In the nuclear rocket, this would mean very large and extremely mobile control rods, as well as oversized and responsive flow machinery.

Although there are many reasons for not building huge control mechanisms, a workable rocket engine demands primarily that the structural weight be as low as possible. Consequently, total control rod worth will probably be less than 15% $\delta k/k$ and control rod speeds less than 0.6%/sec.

An oversized control valve and turbine can increase the speed of transition to full power, and thereby increase the over-all efficiency of the engine, but the heavier turbine will reduce the burn-out velocity. Consequently, the amount of oversize must be computed by considering specific missions and trajectories. Two transitions are simulated: Case I, using a turbine capable of 1.33 times the full power flow, and Case II, using 3.00 times the full power flow.

The restrictions on maximum control rod velocity and maximum valve position determine the maximum values of G_1 and G_3. If one assumes that it is undesirable to change the value of controller gain after the transition to full power has begun and that the gains should remain unchanged at full power, then G_1 and G_3 should satisfy Eq. (12) at full power with either G_1 or G_3 set at its maximum value. Using this criterion and our calculated values of the various design parameters, the optimum control point is obtained by setting

$$G_1 = 0.6 \text{ sec}^{-1}$$
$$G_3 = 0.07$$

Figure 2 presents the time variation of temperature, pressure, control rod position, and valve setting simulated for low-power--high-power transition, with

$$G_1 = 0.5 \text{ sec}^{-1}$$
$$G_2 = 0.002 \text{ sec}^{-1}$$
$$G_3 = 0.07$$

The controller gains were varied over a considerable range in order to investigate the optimum response. It is easily seen that the predictions of optimum control settings made from the linear model are in good agreement with those settings that yielded the optimum simulated response, using the complete set of non-linear equations.

Figure 2 also presents the time history of the same variables for transition using an oversized valve and turbine. As can be seen from the figure, the turbine operated at peak capacity for only a few seconds, but the transition time was reduced from 15 to 10 seconds. It is unlikely that this increase in response speed justifies the increased structural weight of the oversized flow machinery in attaining efficient rocket performance.

Transition was also simulated for various values of the parameters, β, ℓ, α_c, α_h, τ_T, τ_p, τ_{ci}. Only variation of the pressure time constant, τ_p, had any significant effect. The transition time was directly proportional to τ_p, as predicted by the analysis, demonstrating the importance to the engine dynamics of keeping the turbopump inertia to a minimum.

Since reactivity inputs were allowed to exceed one dollar, it is not surprising that variation of the yield fraction and the precursor delay constants had little effect.

It has been mentioned that the low-frequency neutron kinetics are adequately represented by the zero lifetime approximation; therefore, variation of ℓ is expected to have little effect on the system, as was the case.

Variation of the temperature time constant, τ_T, caused no visible effect on the transition, which is in agreement with the predictions of the analysis.

Variation of the reactivity coefficients changed the values of the controller gains needed to maintain optimum control, but when these changes were incorporated, the transition appeared to be essentially the same.

ACKNOWLEDGMENT

The author would like to thank Professor Alan H. Stenning for his many helpful suggestions and criticisms.

NOMENCLATURE

C_i delayed neutron precursor concentration

G_1 scaled integral temperature error gain

G_2 scaled integral pressure error gain

G_3 scaled proportional pressure error gain

ℓ prompt neutron lifetime

m(s) system characteristic equation

n neutron density

N number of precursor groups

P core entrance stagnation pressure

P_s desired core entrance stagnation pressure

P_z, P_p polynomials of s, defined in text

s Laplace conjugate of time

s_o absolute value of root of m(s) = 0, associated with optimum response

T core exit stagnation temperature

T_s desired core exit stagnation temperature

V dimensionless ratio of turbine inlet pressure to core inlet pressure. V is a function only of the control value setting.

V_s desired pressure ratio

Z_z, Z_p polynomials of s, defined in text

α_c dimensionless reactivity-core temperature coefficient

α_h dimensionless reactivity-propellant density coefficient

α_p dimensionless reactivity-pressure coefficient

α_T dimensionless reactivity-temperature coefficient

β_i effective precursor group yield

β effective precursor yield

δ reactivity

δ_r control rod reactivity

δ_{rs} desired control rod reactivity

τ_c effective delayed neutron time constant

τ_{ci} delayed neutron group time constant

τ_n prompt neutron time constant

τ_p pressure time constant

τ_r control rod time constant

τ_T thermal time constant

τ_v control value time constant

ξ dimensionless temperature controller

Superscript

quantity scaled by its steady-state value; reactivity is scaled by β.

REFERENCES

1. H.P. Smith, Jr. and A.H. Stenning, "Open Loop Stability and Response of Nuclear Rocket Engines," Nuclear Sci. and Eng. 11, 76, (1961).

2. B.R. Felix and R.J. Bohl, "Dynamic Analysis of a Nuclear Rocket Engine System," J.Am. Rocket Soc. 29, 853 (1959).

3. D.S. St. John, "Reaction Stability," AEC Research and Development Report DP-517, Sept. 1960.

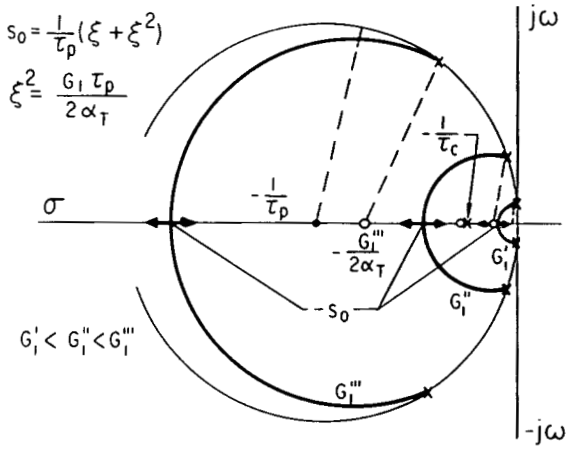

Fig. 1

ROOT LOCUS OF $P_p'(s) + \frac{G_1}{2} P_z'(s) + \frac{G_3}{\tau_p}\left\{Z_p'(s) + \frac{G_1}{2} Z_z(s)\right\} = 0$

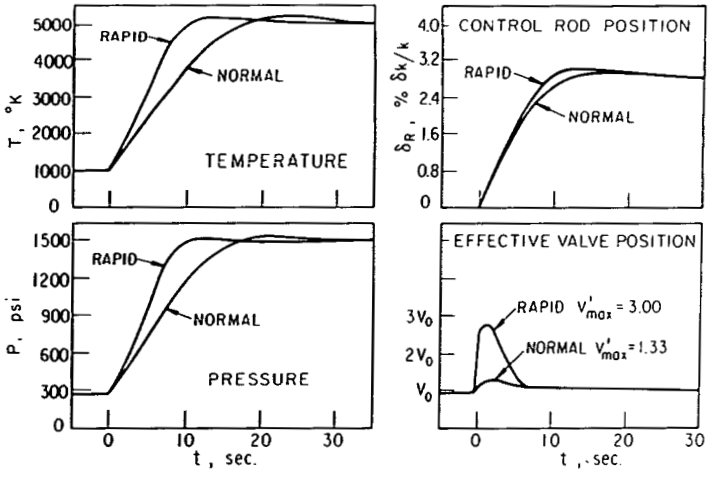

Fig. 2 LOW-POWER — HIGH POWER TRANSITION

ENVIRONMENTAL STUDIES RELATED TO NUCLEAR ROCKET FLIGHT

by

Arnold B. Joseph*
and
Isaac Van der Hoven**

A brief presentation of the kinds of atmospheric, oceanographic, and geohydrologic studies underway in 1962 pertinent to developing an understanding of the possible pathways that may be taken be accidental releases of radioactivity. Reference is made to existing standards and criteria and procedures for assessing possible impact of such radioactivity.

The nuclear rocket safety problems are manifold and the associated environmental safety studies are equally manifold and intricate. Many of the studies are truly on the frontiers of the environmental sciences. Or to put it another way, on the basis of the environmental studies associated with nuclear rocket flight, the environmental sciences will have a better understanding of the mechanisms of nature. This paper is directed to discussing the development of this understanding and to indicate the kinds and purpose of the environmental studies underway or planned. This paper will not attempt to vouch-safe the environmental safety of nuclear flight for the data are too sparse. For those interested, preliminary analyses of possible effects have been made by others.(1) (2)

An understanding of man's environment is the essential link between nuclear rocket propulsion technology and its effect upon man. In an over-simplified version the environment referred to is comprised of the atmosphere, the hydrosphere, and the lithosphere. The particular environment of concern is the region around the launch facilities and the environment in or over which the reactor will operate. The environmental studies are concerned with an understanding of the mechanisms of transferring the nuclear hazard through the environment to man so as to enable one to evaluate what is the consequence of the hazard to man.

With respect to the levels of radiation which pose a hazard to man, guides and standards are in existence and are published as recommendations from such groups as the Federal Radiation Council, National Committee on Radiation Protection, International Commission of Radiological Protection, and the National Academy of Sciences. Obviously, in the nuclear rocket program, we will gear our engineer-

*Sanitary Engineer, Division of Reactor Development, USAEC, Washington 25, D. C.

**Meteorologist, Environmental Meteorological Research Project, U. S. Weather Bureau, Washington 25, D. C.

ing and operational efforts to stay within these guides and limits. However, proper interpretation of these limits is necessary. This is because the recognized guides are written in terms of lifetime exposures to steady concentrations. The accident situation at the pad or in flight is neither lifetime nor steady. Consequently, to make a realistic appraisal of the consequences of any accident involving more than readily acceptable lifetime tolerances it is necessary to have a good idea of just how much above these lifetime Maximum Permissible Concentrations man may be exposed and for how much time. In a nutshell, we need to be in a position to predict the time-space distribution of radioactivity that may be released to the environment in a nuclear rocket accident.

Atmosphere

As a starting point in understanding the mechanisms of the transport of fission products in the atmosphere it is desirable to know the initial shape and composition of the energy release sphere or plume formed by the excursion. This will largely be a function of the physical characteristics of the excursion, but the shape and initial height of rise of the cloud will also be a function of atmospheric conditions such as wind speed, ambient temperature, and the rate of change of temperature in the vertical. Specifically, to predict the behavior and fate of released radioactive materials it is necessary to know the magnitude of the energy release, the fraction of gaseous fission activity released, the particulate materials and their size distributions that would become airborne, and the time history of the chemistry of these released materials. In the event of an excursion in air there are two primary-direct means and several secondary-indirect means by which man can be exposed. The primary-direct exposures are by external beta-gamma radiation from immersion in or passing by of the cloud and by internal radiation through direct inhalation of the cloud. The indirect means are by fallout contamination of habitable areas and of water and food supplies.

A general equation describing atmospheric diffusion from a continuously emitting gaseous source is given by:

$$\chi = \frac{Q}{\pi \sigma_y \sigma_z u} \exp\left[-\frac{1}{2}\left(\frac{y^2}{\sigma_y^2} + \frac{h^2}{\sigma_z^2}\right)\right] \quad [1]$$

which results from the assumption of a Gaussian distribution and the requirement of mass continuity. In the equation X is the ground concentration, Q the source emission rate, σ_y and σ_z the standard deviation of the crosswind and vertical effluent distribution respectively, h the effective stack height, u the mean wind speed in the x-direction and x, y, z the usual cartesian coordinates. The equation is related to the well-known Sutton diffusion equation by the relationships:

$$\sigma_y^2 = \frac{1}{2} C_y^2 x^{2-n} \quad [2]$$

$$\sigma_z^2 = \frac{1}{2} C_z^2 x^{2-n} \quad [3]$$

where Cy, Cz, and n are the empirically determined diffusion parameters.

To improve our estimation of the possible effects of an accidental excursion release to man it is necessary to improve our knowledge of the applicability of expressions such as equation [1], which essentially means a knowledge of the critical parameters. The source term, Q, as it appears in equation [1] is a continuously emitting point source. Modifications can be made to the equation to include instantaneous sources, and in fact, any source configuration in space and time which can be mathematically described. For example,

Figure 1 shows the infinite integrated exposure from an instantaneous unit source for various source configurations, such as point and line sources. If the source is composed of small particulates, modifications to the equation can be made using a deposition velocity to compute the ground deposition as shown by Van der Hoven[3]. The point to be made is that the source configuration, which in large part is a function of the physical conditions causing the excursion, needs to be defined if a model such as equation [1] is to be applied.

A series of diffusion field experiments at Cape Canaveral called Project Ocean Breeze has been conducted by the Air Force Cambridge Research Laboratories in an attempt to better define the important atmospheric diffusion parameters. A known, ground-based, continuously emitting source was used as a gaseous tracer whose air concentration was measured out to three miles downwind by volumetric samplers. From these experiments the parameters in a prediction equation similar to equation [1] were evaluated. A telemetered meteorological data acquisition network has been established to serve as input data to the prediction equation which is programmed on a computer as part of the system. The tentative conclusion of the experiment was that within a factor of 2, the diffusive quality of the atmosphere at Cape Canaveral was similar to the empirical relationship determined in an extensive Great Plains diffusion experiment. Further experiments are being conducted to see if there is a seasonal effect. The applicability of these types of data needs to be evaluated for elevated sources and for travel distances on the order of tens of miles.

A further problem in atmospheric dispersion, especially for distances greater than a few miles, is the downwind trajectory of the plume center line as opposed to the diffusion about this centerline. There is a need to tabulate various typical low level (about 500' from surface) trajectories and relate them to surface meteorological measurements. Angell and Pack[4] have demonstrated by the analysis of some low level constant volume balloon flights tracked by radar from Wallops Island that obtaining trajectories near the surface for tens of miles are feasible on an operational basis.

On a larger scale, information is needed on the fate of radioactive materials discharged during nuclear powered flight and re-entry from orbit. Machta[5] has made a study on the transfer of tracer material from the stratosphere to the ground and discusses such items as tropospheric and stratospheric residence times and the effect of the zone of injection on relative air concentrations and deposition rates at the ground. This type of information will influence whether it is advisable to use an explosive destruct system to disintegrate the reactor at high altitudes, whether to depend on re-entry burnup, or whether to actually attempt to bring the reactor back to the surface intact. (see Figures 2, 3)

Hydrosphere

The hydrological studies are similar to the atmospheric in that we are evaluating the mechanisms, in a quantitative fashion, that may carry the potential hazard of the nuclear rocket to man. The mechanisms of transfer are unlike the atmospheric connections, however, because man does not live in the water environment. Hence, except in possible cases of immersion, the transmission of the potential hazard is indirect - through the mechanisms of the resources in the hydrosphere.

The possibilities of introduction, accidentally or operational, of the radioactive source into the hydrosphere have been described elsewhere.[1] [2] The hydrosphere here includes any surface water body which may receive the rocket and includes the ocean as well as inshore tributaries.

The future meanderings of the material in the water is in part predetermined by the physical and chemical form of the material when it is introduced. e.g., Pieces or fragments larger than 10 microns with density greater than water generally sink to the bottom and if soluble they can be expected to remain there. Gaseous materials on the other hand can be expected to diffuse out and may or may not go into solution and be quickly sorbed whereas argon while somewhat soluble is essentially non-reactive. An excursion in water likely results in a spectrum of radioactive molecules different from an excursion in air because of the differing chemical reactants in the water. Source term studies now being undertaken are concerned with not only identifying the fission products but also the neutron induced radionuclides and the chemical forms of these at the physical conditions at introduction. The studies are also concerned with chemical property changes which take place after coming in contact with the water. Initial theoretical studies and some preliminary lab experiments indicate that fission products from an operated core sample are only slightly leachable in water.(2) Definition of the activation products and studies of their physical and chemical forms in sea waters are now being undertaken. Other factors such as the possible enhancement of leaching by direct biological interactions are also to be investigated.

Figure 4 illustrates schematically a kind of equilibrium in the dynamic chemical, physical, and biological processes taking place in the sea. When a foreign chemical load is introducted, this equilibrium will be disturbed as the introduced materials take their place in the system.

The newly introduced chemicals may go into solution or suspension and be physically borne by the water and move along with it. They may go to the bottom to become in effect a part of the bottom or go into solution (dissolve) at a slow rate. If in suspension or solution they may be sorbed out of the water by suspended mineral matter and settle out slowly. The dissolved chemicals may be taken up by plants or plankton and become part of the food chain - perhaps eventually to reach man. Some elements can be reconcentrated by certain organisms by thousandfold factors which makes this factor draw particular attention and study.

The material that goes into solution appears to hold the most concern because it is most likely to enter the food chain first. It is fortunate in a way that once in solution it is then subject to the relatively rapid natural forces which act to spread it out - to dilute and disperse it. This is fortunate because the introductions are not continuous the movements tend to discourage reconcentration actions as well.

How the material will be dispersed depends largely on where in the system it is introduced. Generally, if it goes into solution in the shallow or mixed layer it will be mixed and dispersed more rapidly than if it goes in the cold, slow moving deep waters of 1,000 fathoms or greater. However, the mixed layer is the layer of greatest biological activity including the harvesting of sea foods.

There are several theories to explain the physical dispersion and diffusion of soluble materials introduced into the ocean. Schonfeld(6), Pritchard, and Carpenter(7) and Okubo(8) review the merits and demerits of equations by Joseph and Sender, Ozmidov and Obukhov as well as their own. Basically, these are similar to the Fickian distribution equation:

$$S(r, t) = \frac{M}{4 \quad kt} \; e^{-\frac{r^2}{4kt}}$$

That is the concentration of a substance in solution, as a function of time and space is proportional to the amount of the substance introduced M, time t, distance or space travelled r and some measure of diffusion k. Clearly, there is not full agreement among the experts on a single mathematical model to quantatatively predict cases of oceanic diffusion.

The variances are concerned primarily with a measure of diffusion, k. Depending on the equation, the diffusion parameter has the dimensions L/T, L^2/T or $L^{2/3}/T$. Theoretical estimates of time, space distributions vary from measured concentrations by factors of 4 to 10 or more. In confirming their formulae or those of others investigators are now making direct measurements of diffusion of contaminants using the rhodamine dye tracer technique was perfected by the Chesapeake Bay Institute. This technique is described by Pritchard and Carpenter.(8) The experts are in agreement, however, in noting that diffusion undoubtedly does vary from place to place and time to time depending on boundary conditions, depth, vertical stability (temperature and salinity distributions), tidal currents and wind driven currents, and that the best obtainable measure of diffusion and dispersion is the direct observation; which is what we are doing.

A series of dye releases in the coastal waters off Cape Canaveral were made in March and again in August 1962 (see Figure 5).

In the spring series, 200 pounds of rhodamine B were released in each of three areas, in shallow water north and south of the shoal and in the deeper water off shore. The distribution of the dye was measured with five self-balancing fluorometers. The results may be considered in terms of the rate of decrease of the peak concentration. The average rate of peak concentration decrease was found to be proportional to the minus third power of time. The first experiment conformed most closely to this rate while the second experiment showed a more rapid decrese and the third a less rapid decrease. It was tentatively postulated that the nearness to shore caused these differences. In particular the second experiment was quite close to the shore and shoal, so that extensive shear of the tracer patch occurred and the distribution was strongly elliptical. The results of the spring experiments can be summarized in terms of an average rate of decrease of peak concentration as indicated by the following table.(9)

Ratio of peak concentration to amount introduced vs time

(Hours)	c/m (Pounds/m^3 per pound released)
1	5.42×10^{-4}
10	5.42×10^{-7}
24	3.93×10^{-8}
48	4.93×10^{-9}
100	5.42×10^{-10}

Studies of transport in the waters off Cape Canaveral - those with a higher statistical probability of introduction due to a malfunction during the early launch period - are also being made. Measurements are being made of the range of current velocities that may be expected, their vertical profile, the direction of motion, and correlated with surface wind observations.

Transponding buoys, designed to respond to a particular radio signal, each supporting a cargo parachute 28' in diameter at certain depths below the surface were employed to determine the speed of the non-tidal drift. The parachutes obtain a good "grip" on the water, and in every instance of recovery were open to the extent that they had to be cut loose rather than recovered. The tech-

nique employed was to set buoy and parachute adrift and attempt to locate it at least once each day. In some instances these experiments coincided with the dye experiments and greatly aided in locating the area in which to sample the dye concentration. Results of these experiments are plotted in Figure 6. Depth of parachute appeared to have no particular significance, i.e., the whole water column to the depth to which parachutes were used, normally not deeper than 2/3 the depth, appeared to move uniformly. The buoys, and apparently the water, followed the wind at about 1/20 the wind speed with the exception of the offshore stations, i.e., east of 80°15' where influence of the Gulf Stream was felt and the drift was northerly in spite of the wind.(10)
The stretch of water from the shoreline out to the Blake Escarpment approximately 220 miles off shore and down to the bottom are being studied. Physical motion studies are also being considered for the presently conceived RIFT (Reactor-in-flight test) impact area and a third group of studies may be undertaken for the downrange areas depending on the operational plans for the vehicle.

An assessment of the possible effects on man through the food web mechanism is underway. The first step here is to make an accurate census - to determine all the species existent from the elemental forms like phytoplankton to the more complex forms like edible fishes. This will be followed and supplemented by uptake studies where necessary on the important organisms in the food chain. When completed we hope to be able to predetermine where in the chain radioactive materials may be found and the concentrations expected.

Concentration Guides for Sea Water

The National Academy of Sciences has established concentration guides or maximum permissible concentrations of radioisotopes in sea water.(11) These differ from maximum permissible concentrations in fresh water on two counts - one, they consider that the activity may be returned to man directly via marine plants and animals and two, that sea water, unlike fresh water is a solution of almost all the elements. The first factor is important because marine biota can reconcentrate introduced radioelements; the second factor because isotopic dilution can reduce possible effects of activity. In considering a particular isotope one must consider whether the hazard is to the gastro intestinal tract as food passed through the body or to a particular organ which accumulates the isotope. For the group of isotopes that affect the GI-tract, the concentration of isotope per unit volume of marine food is controlling and for the critical organ group the specific activity (the ratio of the radioactive to the non-radioactive element in the marine environment) is limiting. Mathematically, the permissible specific activity in sea water (for critical organs) is

$$I = \frac{Irb}{Inb} Ine \left(1 + \frac{K}{B}\right) \text{ where}$$

Irb = maximum permissible concentration of the isotope in the critical organ.

Inb = concentration of the element in the organ

Ine = concentration of the element in sea water

K = decay factor = $\frac{0.69}{T\ 1/2}$ (half life)

B = biological factor = $\frac{0.69}{Tb\ 1/2}$ (biological half life)

and the permissible specific activity in sea water based on GI tract consideration is

$$I_{GI} = 10 \frac{(MPC)w}{F} \quad \text{where}$$

(MPC)w = the maximum permissible drinking water concentrations

F = the concentration factor in marine organisms.

Table I shows the relative differences in the various permissible concentrations.

TABLE I

Comparison of Permissible Sea Water Concentrations With MPC Values for Drinking Water[11]

Isotope	MPC for Drinking Water uc/ml	Permissible Sea Water Concentrations Specific Activity Of Critical Organ uc/ml	Permissible Sea Water Concentrations GI Tract Consideration uc/ml
P^{32}	2×10^{-5}	4.5×10^{-9}	--
S^{35}	6×10^{-5}	1.1×10^{-3}	--
Ca^{45}	9×10^{-6}	1.2×10^{-4}	--
Cr^{51}	2×10^{-3}	--	2×10^{-5}
Fe^{55}	8×10^{-4}	1.4×10^{-6}	--
Fe^{59}	6×10^{-5}	--	6×10^{-9}
Co^{60}	5×10^{-5}	--	5×10^{-8}
Zn^{65}	1×10^{-4}	7×10^{-9}	--
Sr^{90}	1×10^{-7}	3.3×10^{-6}	--
Nb^{95}	1×10^{-4}	--	5×10^{-6}
Ru^{106}	1×10^{-5}	--	1×10^{-7}
I^{131}	2×10^{-6}	1.6×10^{-6}	--
Cs^{137}	2×10^{-5}	1.3×10^{-7}	--
Ce^{144}	1×10^{-5}	--	1×10^{-8}

Using permissible sea water concentrations of isotopes such as developed by the NAS-NRC for guides and having determined the manner in which the activities are expected to behave when introduced in the water environment, we will then be in position to evaluate the possible effects on man. This evaluation will generally follow the course illustrated schematically in Figure 7.

Lithosphere

The lithosphere problems appear to be of secondary nature at this time in considering the time-space distributions of activity and the possible rates of return to man because the activities are postulated to be either solid or airborne and their means of entry to ground waters involve a dissolution step.

Nevertheless, a study is being undertaken to describe the near surface ground water system in order to determine the extent to which water supplies may be affected by an accident over land. This will take into account geologic, mineralogic, and chemical data as these bear on underground transport of activity. These studies will also provide a basis for decontamination or other applied safety measures in the event of an accident. The possible effects of local deposition are being examined as well, especially with regard to the contamination of vegetation which enters into a food chain.

Summary

At this stage of development, although there appears to be an overbearing potential of radioactivity inherent in the nuclear rocket flight system, preliminary examination of the source term and an understanding of the effects exerted by the various environments on its distribution, indicate that under appropriate control, nuclear propulsion systems can be radiologically tolerated. Accurate quantitative information on the possible release mechanisms, the actual materials themselves - their chemistry and physics and the possible movement of these materials through the environments must be collected and evaluated in order to develop rational safety controls.

An intuitive feeling for the possible fate and effects of released activities is shown in Figure 8. Preliminary information on the time-space distributions of activity following releases indicates that the atmospheric route to man is the most direct. On the fortuitous side the very mechanisms which make it most direct also act to dilute and disperse it most readily. Meteorological investigations are aimed at quantitatively defining the time-space distribution of radioactivity, depending on the source term.

Preliminary studies of hypothesized radioactive introductions into the hydrologic environment indicate that the potential exposure problems are probably not as severe as in the atmospheric environment. A local area would be contaminated and like the atmosphere the physical forces on the water would tend to disperse the contaminant. But because the radioactive elements can be transposed to a biological or geochemical phase, there is a tendency to restrict freedom of movement. As a consequence, hydrologic problems are more enduring than the atmospheric problems.

The terrestrial problems appear to be the least significant at present. They would be mostly local and essentially die out at the rate decay of the activity. However, an important consideration of the radioactive deposition on vegetation which may be reconcentrated in the food chain.

All the environments require further study in order to be convincingly quantitative about fate and effects.

REFERENCES

1. Nuclear Safety Study, Dix, G. P., et al, Final Report MND-2517, (S), Martin Nuclear Division, Martin Marietta Corporation, 1961.

2. Nuclear Safety Aspects of the Rover Program, Graves, G. A., et al, LA-2409 (S), Los Alamos Scientific Laboratory, 1960.

3. A Diffusion-Deposition Model for Particulate Effluent from Ground-Tested Nuclear Engines, Van der Hoven, I., Accepted for Publication, Int. J. of Water and Air Pollution, 1962.

4. An Analysis of Some Low Level Constant Volume Balloon (tetroon) Flights from Wallops Island, Angell, J. K. and Pack, D. H., Weather Bureau Manuscript, 1961.

5. Transfer of Tracer Material from the Stratosphere to the Ground Level, Machta, L., Weather Bureau Manuscript, 1962.

6. Radioactive Waste Disposal Into the Sea, Safety Series No. 5, International Atomic Energy Agency, Vienna, Austria, 1961.

7. Measurement of Turbulent Diffusion in Estuarine and Inshore Waters, Pritchard and Carpenter, Proceedings of Symposium on Tidal Rivers, Helsinki, July 1960.

8. A Review of Theoretical Models for Turbulent Diffusion in the Sea, Akira Okubo, Draft Chesapeake Bay Institute Technical Report, 1962.

9. Preliminary Report on Dye Diffusion Studies off Cape Canaveral, Memorandum Report to AEC, July 1962.

10. Preliminary Report on Non-Tidal Drift Experiments off Cape Canaveral, Bumpus, D. F., Memorandum Report to AEC, July 1962.

11. The Biological Effects of Atomic Radiation, Summary Reports, National Academy of Sciences-National Research Council, 1960.

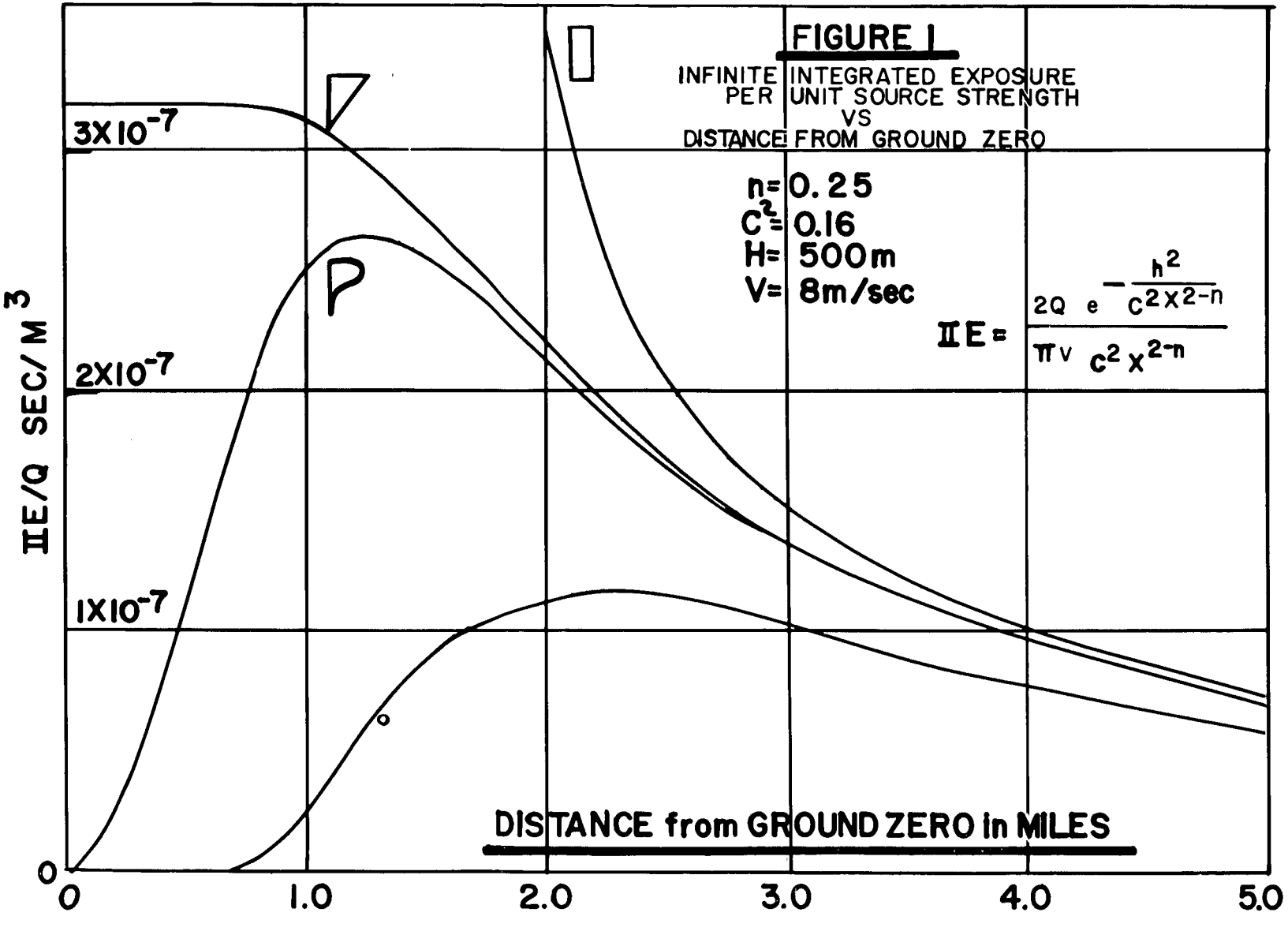

Effect of source configuration on down-wind exposure.

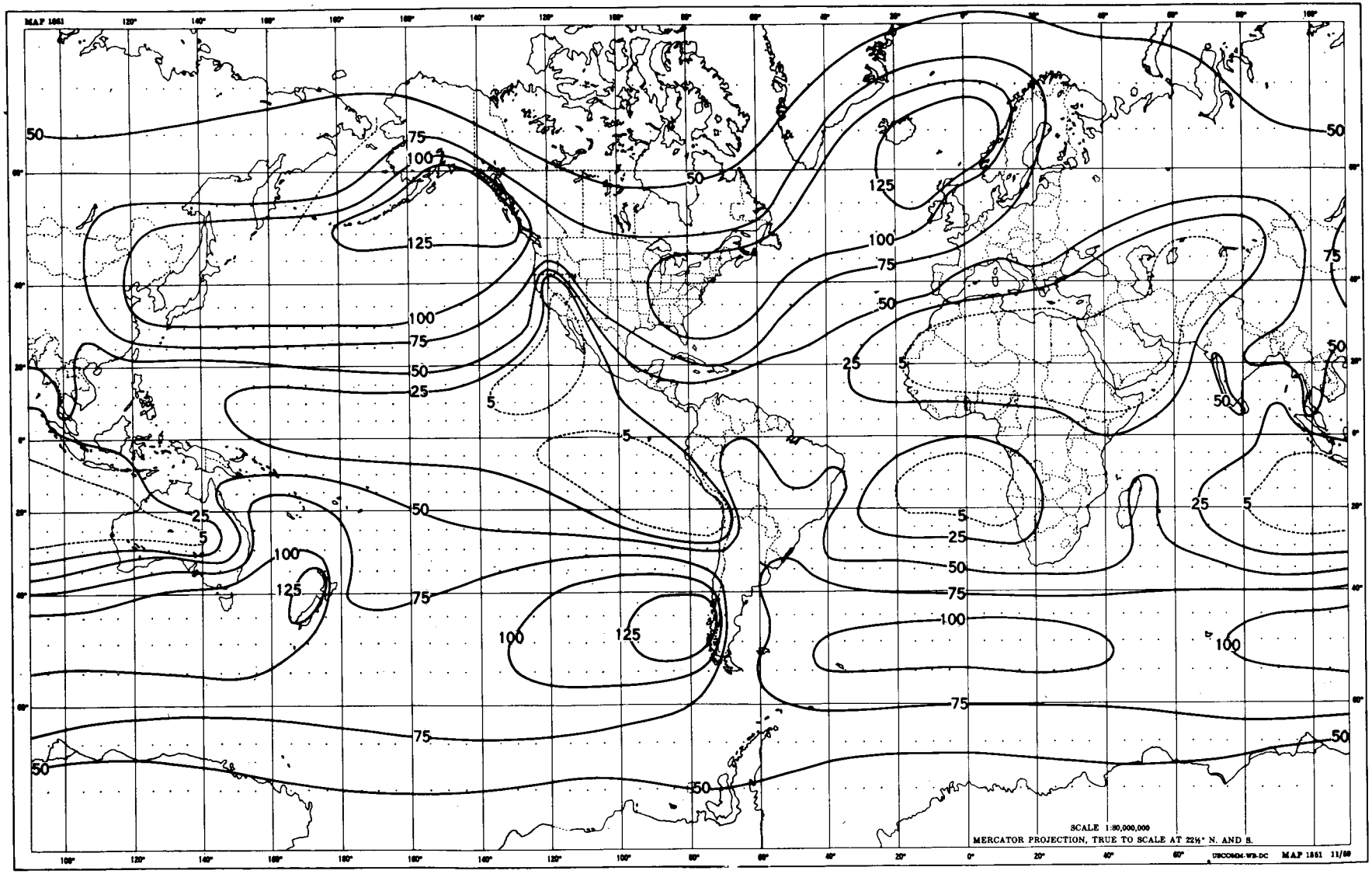

Figure 2 Relative deposition of tracer material partitioned equally in the stratosphere of each hemisphere.

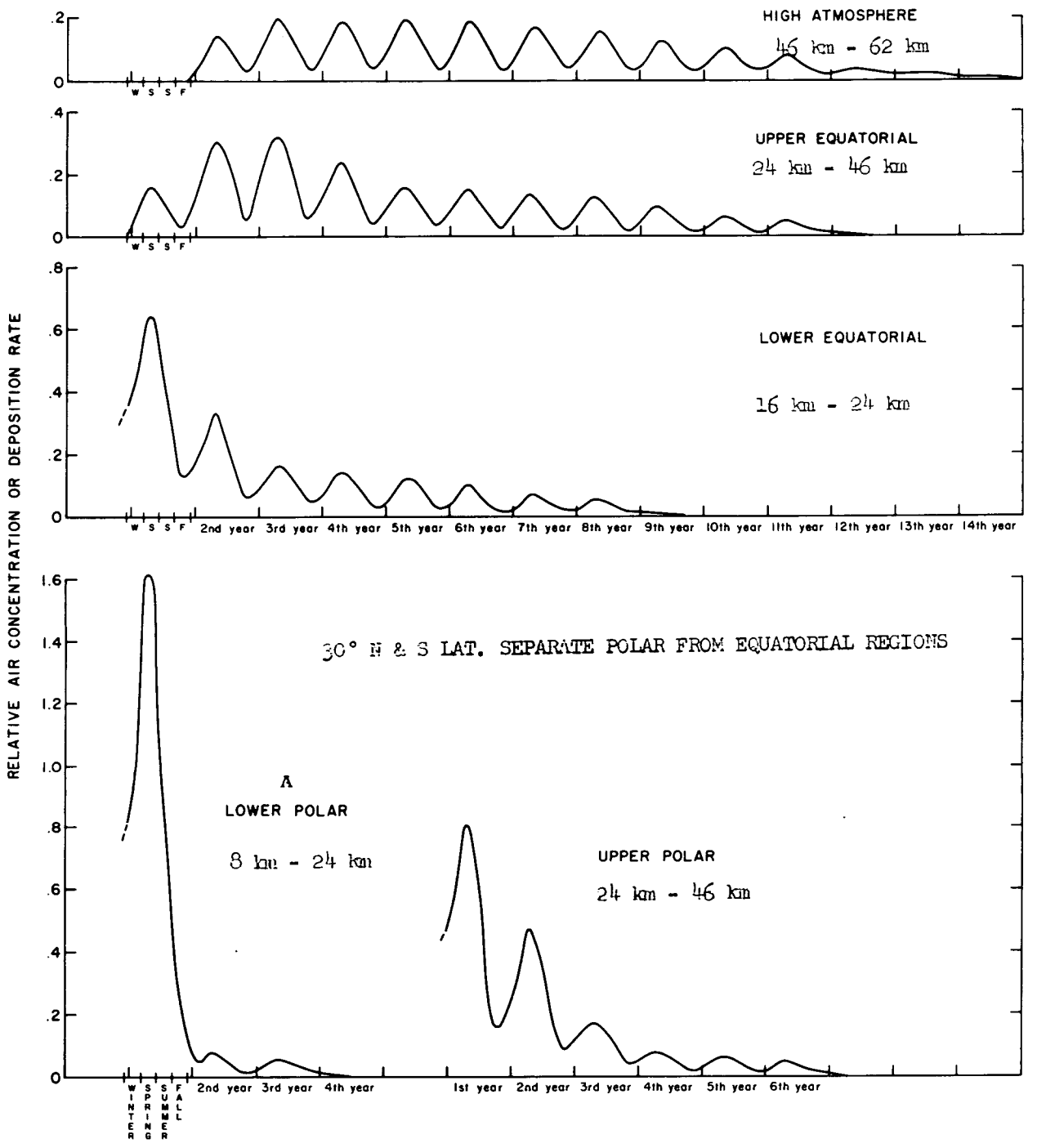

Figure 3 Time history of deposited and air concentration from each of five stratosphere regions.

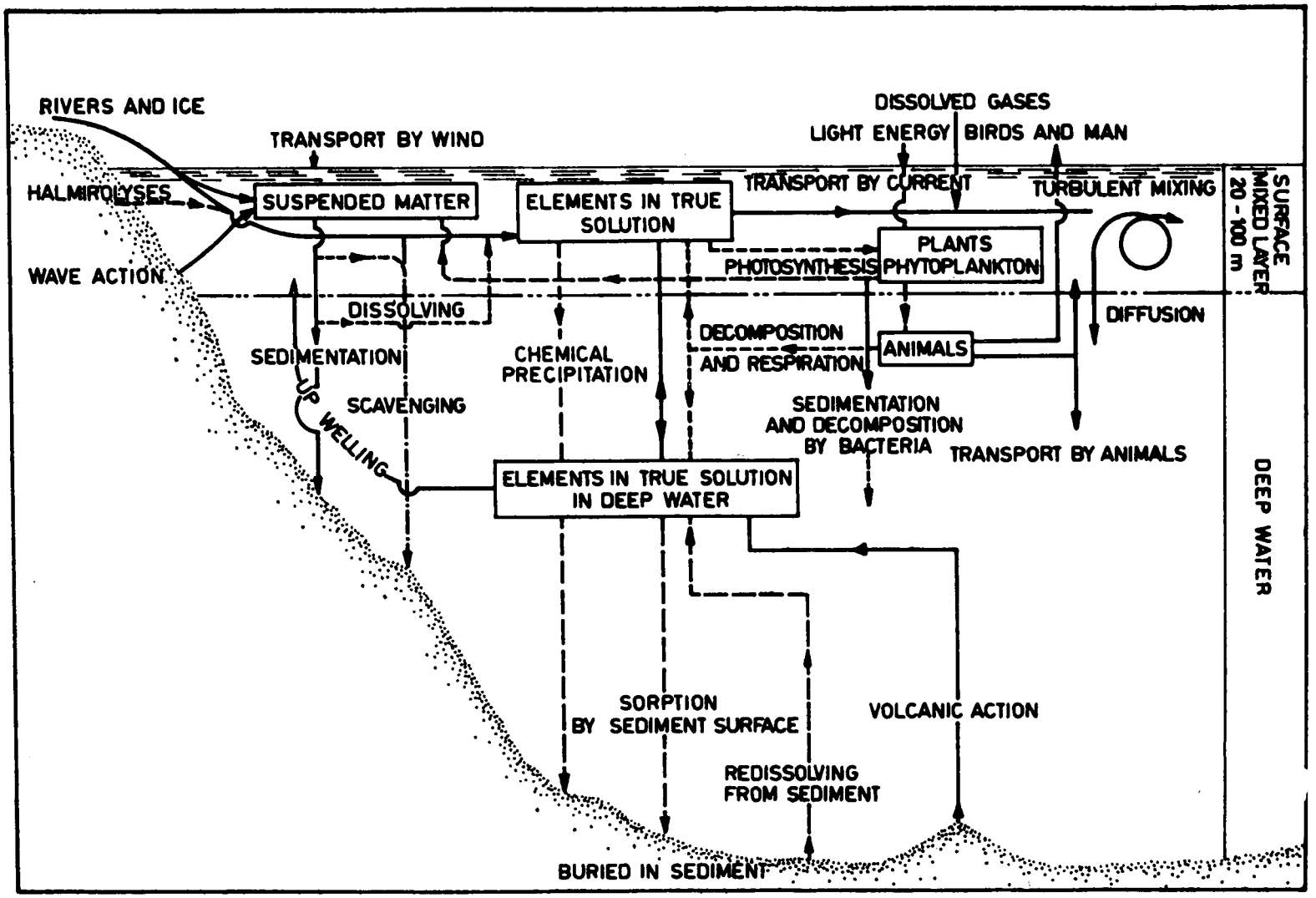

Figure 4 Scheme of major physical and geological processes in the sea.

——— Physical (mainly dynamic) processes
— — — Chemical processes
- - - - - - Biological processes
——·——· Combined processes

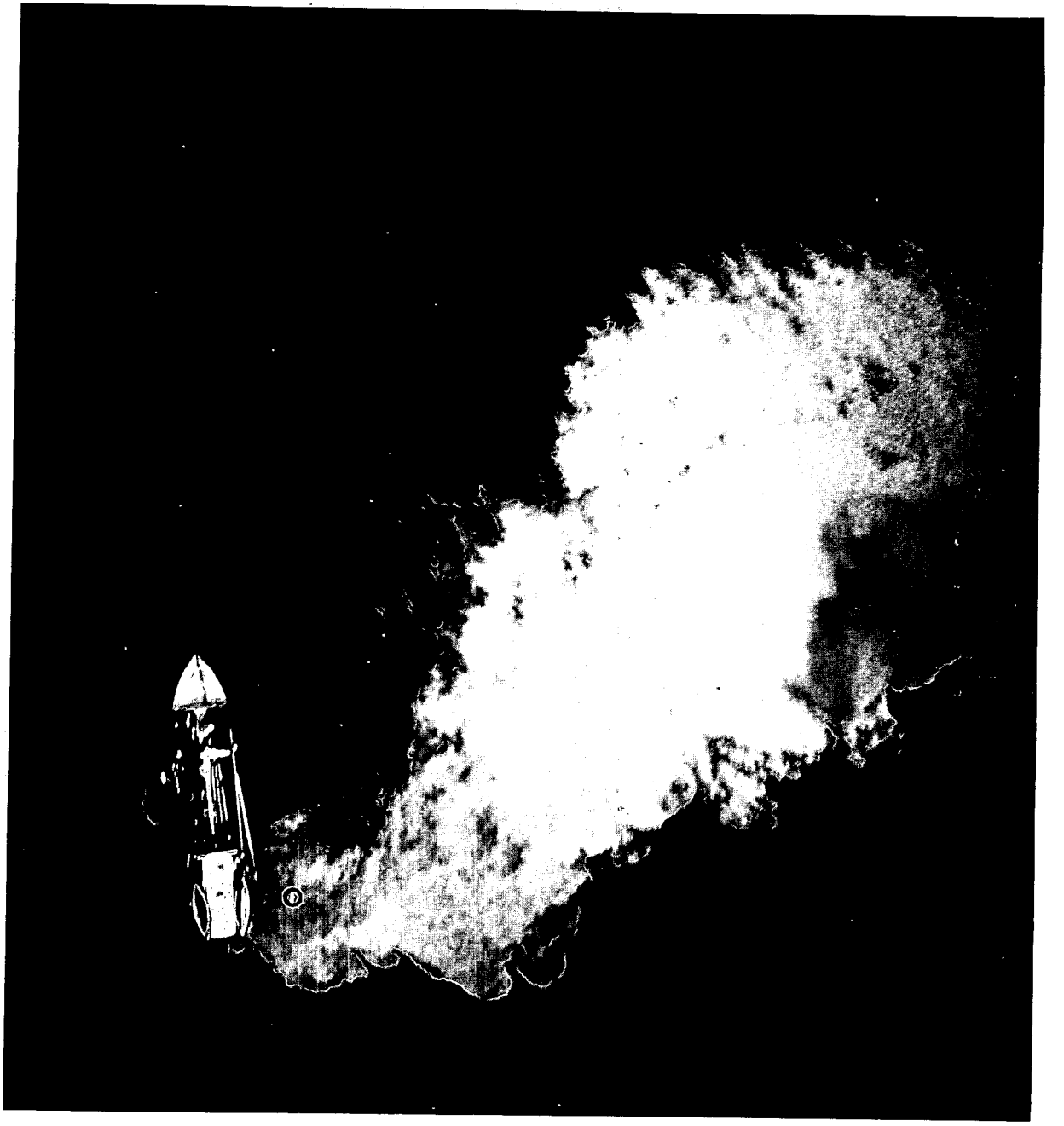

Figure 5 Rhodamine B dye released on lee side of ship.

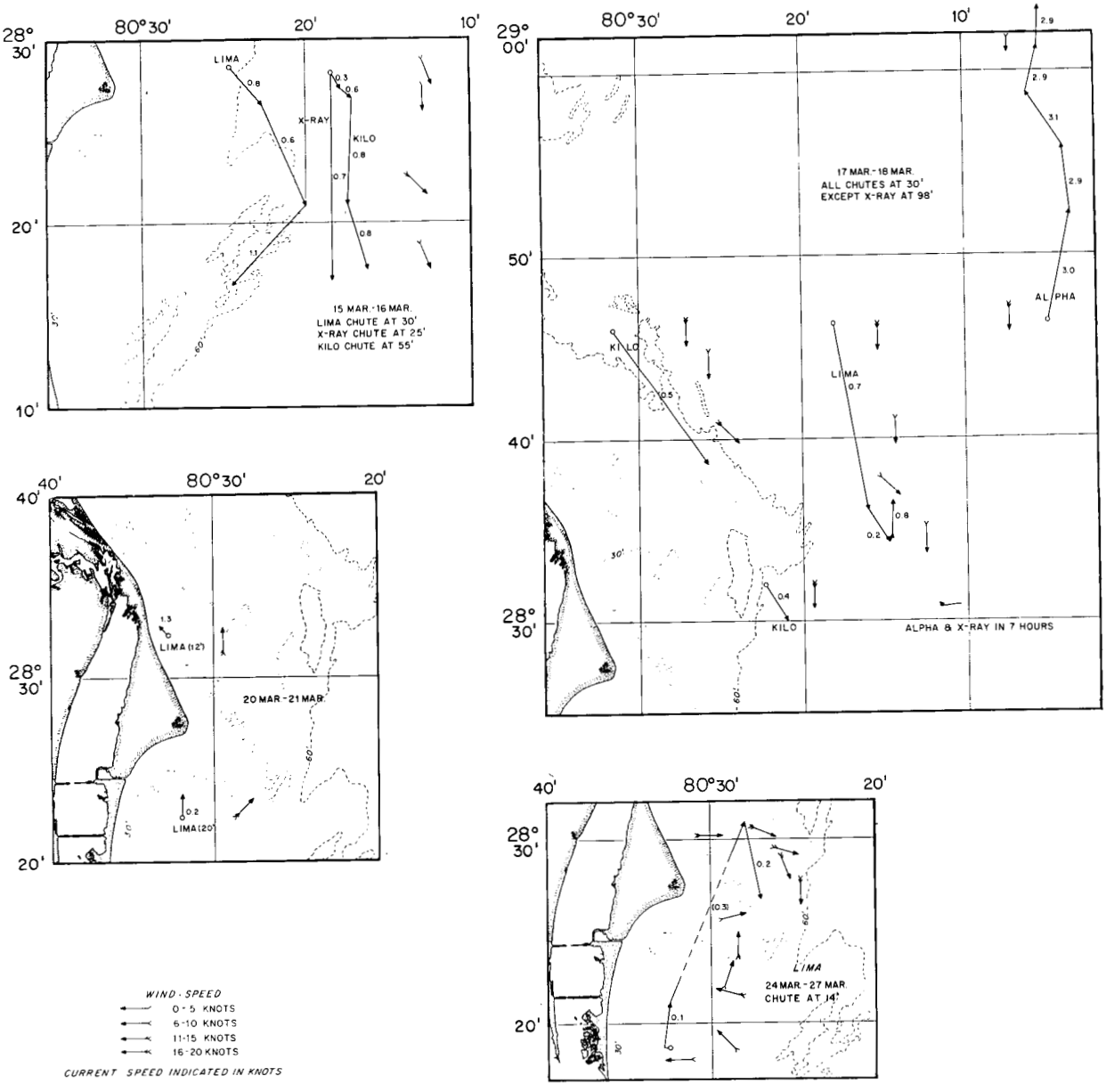

Figure 6 Drift of drogued telemetering buoys off Cape Canaveral 15 to 27 March 1962.

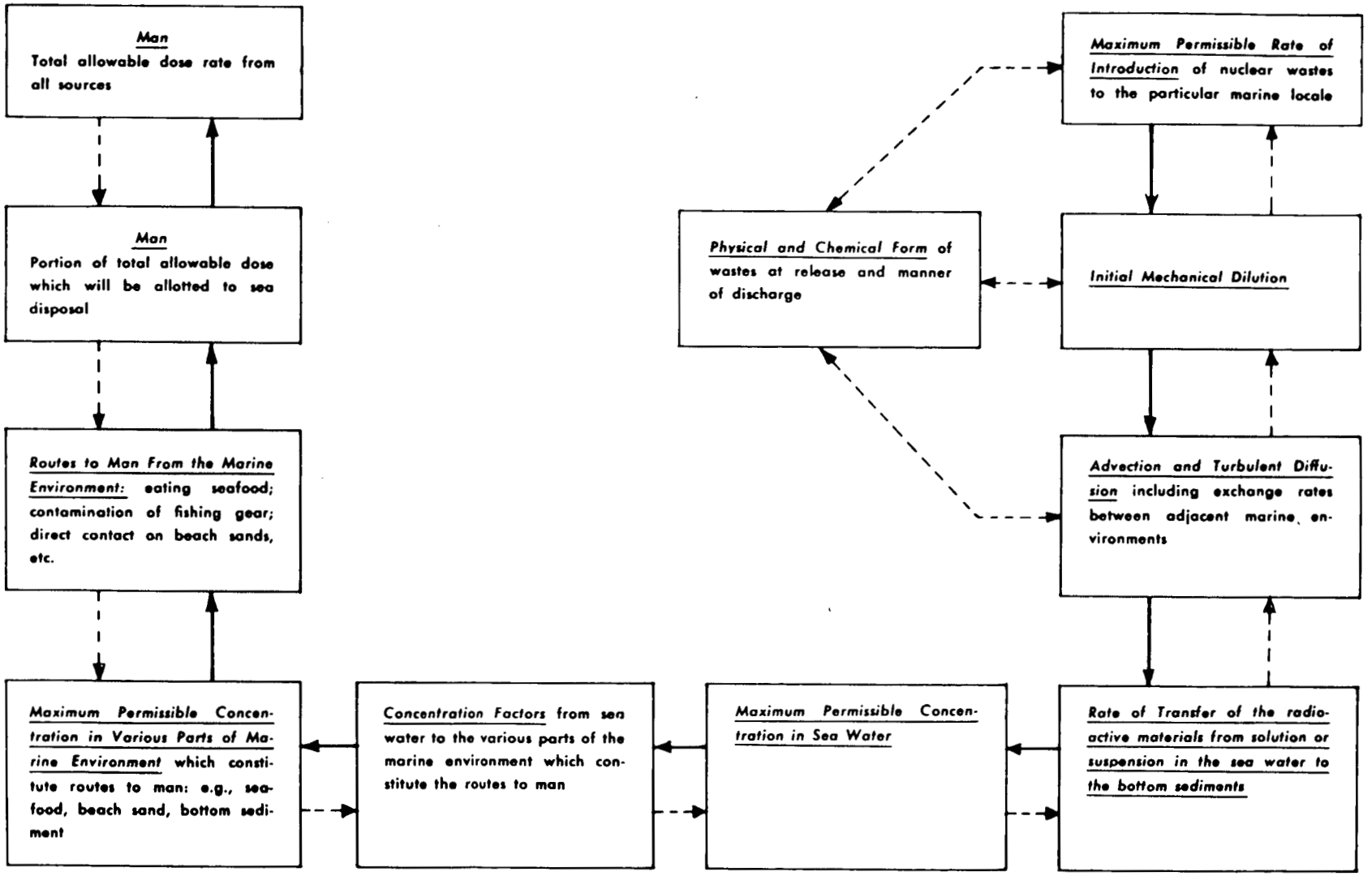

Figure 7 Schematic presentation of considerations in evaluating marine area receiving radioactivity.

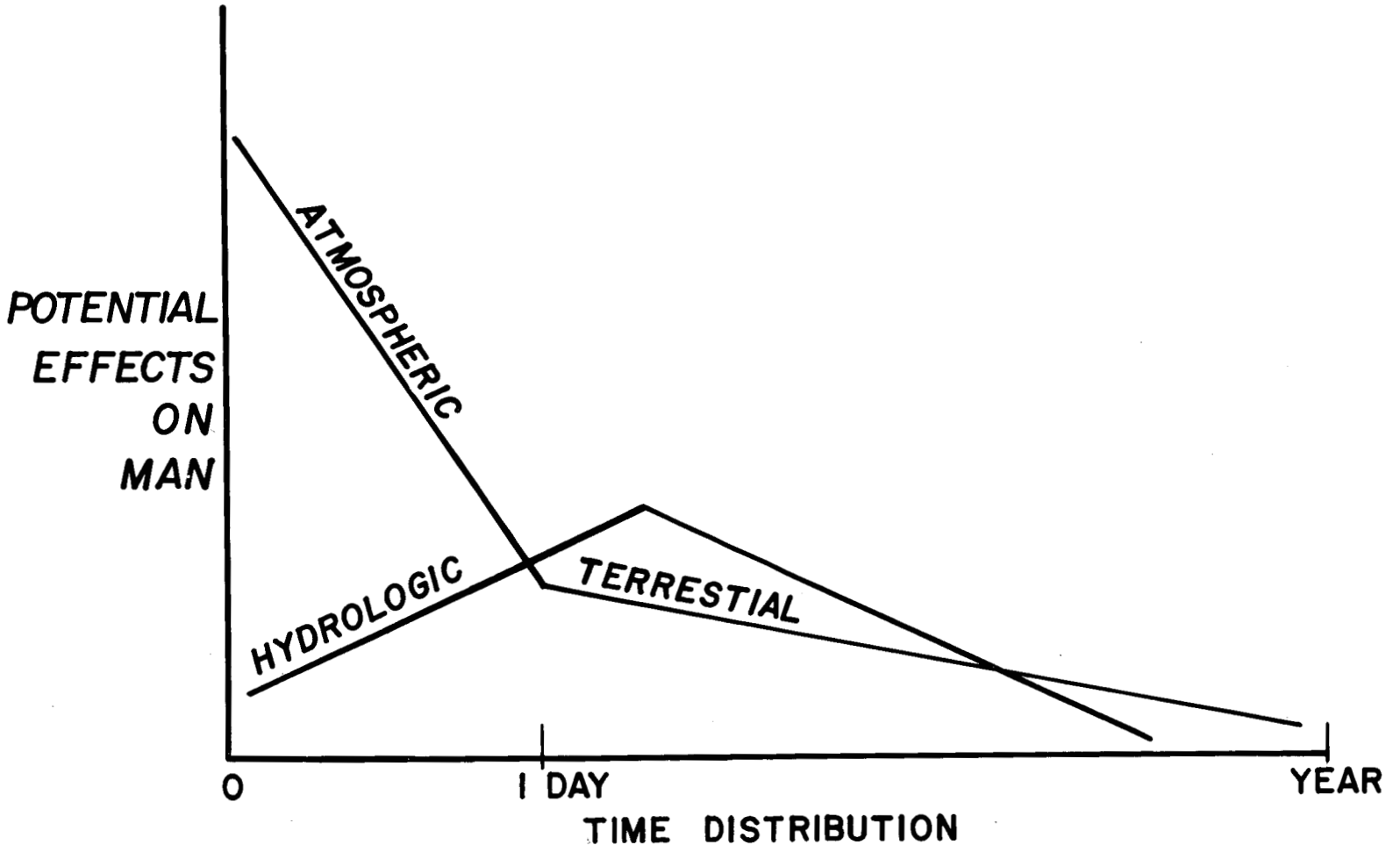

Figure 8 Intuitive representation of possible fate and effects of released activities.

REVIEW OF PLUTO REACTOR TEST FACILITY DEVELOPMENT

William C. Miller
Lawrence Radiation Laboratory, University of California
Livermore, California

This summary of the Pluto Test facility development was prepared for those who are presently involved in facility engineering work, and for those who in the future will be using and designing Pluto-type facilities. The subject material covers:

History and description of the facility
Design requirements
Proposed system designs
Typical blowdown operation

HISTORY AND DESCRIPTION

The history of the Pluto test site had its beginning when the Laboratory was planning for the testing of Tory I, a Rover-type reactor. The site was selected, construction budgets were prepared, and operational schemes were devised. During the final design stage the Laboratory's assignment was changed from developing a Rover-type reactor to developing a Pluto-type reactor. The designs and operating schemes were changed accordingly, and construction was started in 1958. Since that time there have been four phases of construction which have added utilities and structures but principally more air capacity.

The site covers 4 square miles in an area known as Jackass Flats. It is located 28 miles northwest of Mercury, in the Nevada Test Site.

For operating reasons the site was divided into three functional areas: control, test, and disassembly (see Fig. 1) The control area is the center for the administrative, operational, and all other nonhazardous functions. It consists of a complex of buildings which support the testing activities, the prominent one being the control building, which is the terminus for all facility and test item data transmission and control functions.

The test area bunker serves as ground zero for the testing operations. It houses the equipment required to furnish controlled heated air to the test reactor.

The disassembly area includes structures and equipment necessary to assemble, disassemble, and adjust Pluto-type reactors.

DESIGN REQUIREMENTS

Tory II-A and Tory II-C in the design requirement list below are two reactors which were to be tested in series. The facility was designed to test the Tory II-A first, then it was modified to suit the Tory II-C requirements.

1. Budget – Construction shall be completed without exceeding the authorized budget:

Tory II-A	(Phase 1) $1.2 million	$8.7 million	$18.0 million
	(Phase 2) 7.5 million		
Tory II-C	(Phase 3) 1.3 million	9.3 million	
	(Phase 4) 8.0 million		

*2. Safety – Design facility to provide minimum hazard to public, operating personnel, and the test reactor. The design rule shall be to use equipment and techniques with proven reliability.
*3. Air Supply – Provide air storage at 3000 to 4000 psi:
Tory II-A, 120,000 pounds;
Tory II-C, 1,200,000 pounds.
*4. Air Heater – Provide heat source capable of delivering:
Tory II-A, 900 pps @ 1050°F for 90 seconds plus ramps;
Tory II-C, 2000 pps @ 1050°F for 300 seconds plus ramps.
5. Air Control – Design air control system which will have manual, manual servo, and fully automatic capability. Provide 60-second ramps on flow profile. Control to ±5% on preprogrammed profile; control to ±2% on actual flow.
6. Cooling Water – Provide nozzle and reflector cooling for the Tory II-A reactor only.
*7. Reactor Transport – Provide method of transporting, connecting, and disconnecting a reactor by remote control methods.
8. Disassembly – Provide building and equipment capable of assembling and disassembling the Tory II-A and Tory II-C reactors.
*9. Electric Power – Provide electric power system in which undesirable transients are not transmitted to the reactor control and data system.
10. Operations – Consider the long prenuclear periods of activity as well as the brief nuclear testing periods when designing to the above nine requirements.

Some of the items in the generalized requirement list above have been reviewed and presented in other papers (see references). This paper will discuss only those items marked with an asterisk. The following describes the system designs that were proposed as satisfying the requirements.

PROPOSED SYSTEM DESIGNS

Safety (Radiation)

Before the mechanical systems could be designed a plan for personnel safety had to be devised. The three-functional-area system was selected. The distance between control and test areas (8200 feet) was calculated on radiation levels anticipated during normal high power testing which would reduce the radiation level to 10 mr/hr at the control building. The distance between control and disassembly (3600 feet) was calculated on the basis of γ attenuation in air if a reactor were parked outside the disassembly building for an indefinite period.

Because personnel must enter the test bunker when a reactor is in its test position, it was decided to create a "no man's land" on the surface, around the test zero point. The radius was calculated to be 1000 feet, but subsequent experimentation reduced this radius to 500 feet. An earth-shielded access tunnel runs from the perimeter of the circle to the bunker. A rule was established that nothing was to be designed that would require frequent maintenance unless it was outside the "no man's land" circle or placed in the bunker.

Air Supply

Three systems were evaluated: manifolded pipe, large pressure vessels and underground.

Large pressure vessels and underground were eliminated by the requirement for proven reliability. The manifolded pipe was selected because of its long history of pressure and shock reliability in the oilwell industry. The air storage system for Tory II-A consists of 18,000 feet of 9-inch, N-80 oilwell casing which holds 120,000 pounds at 3600 psi. The storage system for the Tory II-C consists of the above, plus 112,000 feet of 10-inch, P-110 casing. The total storage is now 1,200,000 pounds at 3600 psi.

Air Heater

Two systems were proposed which could provide heated air: "vitiated" and heat sink. The "vitiated" system, which burns propane in the air stream, appeared attractive in cost, but it presented potential hazards of explosion and thermal shock. The heat sink system was selected, and for Tory II-A it consisted of 200,000 pounds of 7/8-inch-diameter rods fixed in a cross-rod matrix. It was heated by a furnace in an indirect closed-loop circuit. The Tory II-C system is of the pebble-bed type, and has four vessels containing 2 million pounds of 1-inch-diameter stainless steel balls. It is heated by an oil-fired furnace in a direct open-loop circuit.

Reactor Transport

After a brief study comparing monorail, cable car, and railroad systems, the railroad was selected. Subsequently, the battery locomotive, diesel-electric, and electric trolley were evaluated. The battery locomotive was chosen. The decision was based on reliability, cost, smoothness of operation, and the fact that no maintenance would be required in the test area. The locomotive selected weighs 17 tons, has radio and manual controls, and has a 1000-ampere-hour battery which can drive the locomotive 8 miles before recharging.

Electric Power

The systems proposed here were designed around methods which would prevent power line transients from affecting the reactor control and instrumentation system. The Tory II-A system had a 69-kV high line for general utility plus three 125-kVA generators for running reactor-associated equipment. Control power was taken from a 50-kVA MG set.

Because of synchronization problems between the MG set and the generators, the system was redesigned for Tory II-C. This system has three basic circuits: commercial power for items not critical to line fluctuations, utility power from the three generators for items that must operate during reactor testing, and instrument power from two generators supplying a dc system for reactor control and data systems.

TYPICAL BLOWDOWN

The facility operations that are required to perform a typical nuclear blowdown test are best described in chronological order. X is the time at which test air passes through the reactor.

X - 100 hours:	Compressors started, will run until X - 2 hours.
X - 80 hours:	Check out facility instrumentation; i. e., calibrate all pressure and temperature sensors.
X - 55 hours:	Check out all facility equipment that must operate during test run.
X - 40 hours:	Start hot air furnace, will run until X - 2 hours.
X - 24 hours:	Prerun meeting, discuss schedule and test run plan.
X - 2 hours:	Manually check position of all valves.
X - 1 hour:	Unlock master block valve, clear bunker area of all personnel.
X - 45 minutes:	Assemble operating crew.
X - 10 minutes:	Start low pressure blowers.
X - 8 minutes:	Establish inlet temperature on blower air.
X - 30 seconds:	Valve out blower air.
X - 0 second:	Start test air through reactor.
X + 90 seconds:	Start nozzle cooling air flow.
X + 120 seconds:	Start automatic air flow program.
X + 540 seconds:	Automatic flow program complete, switch to manual.
X + 560 seconds:	Reduce inlet temperature.
X + 1000 seconds:	Stop nozzle cooling flow.

X + 1500 seconds: Switch from test air to blower air.
X + 2500 seconds: Secure all systems.
X + 2 hours: Conduct facility radiation survey.

After 24 hours the reactor can be moved from the test bunker to the disassembly building. Now the facility can be made ready for the next scheduled test.

REFERENCES

H. L. Reynolds and C. E. Walter, "Hot Box, A High-Temperature Critical Facility," UCRL-5483.

J. W. Hadley, "Tory II-A," UCRL-5484.

W. H. Moran, "Design and Construction of the Site 401 Disassembly Facility," UCRL-6100.

C. E. Walter and W. C. Miller, "Nuclear Ramjet Reactor Test Facility Requirements," UCRL-6576.

E. Arbtin, E. A. Platt, and W. L. Ross, "Engineering Review of the Phase IV Pebble Bed Air Heater Design," UCID-4437.

/rd

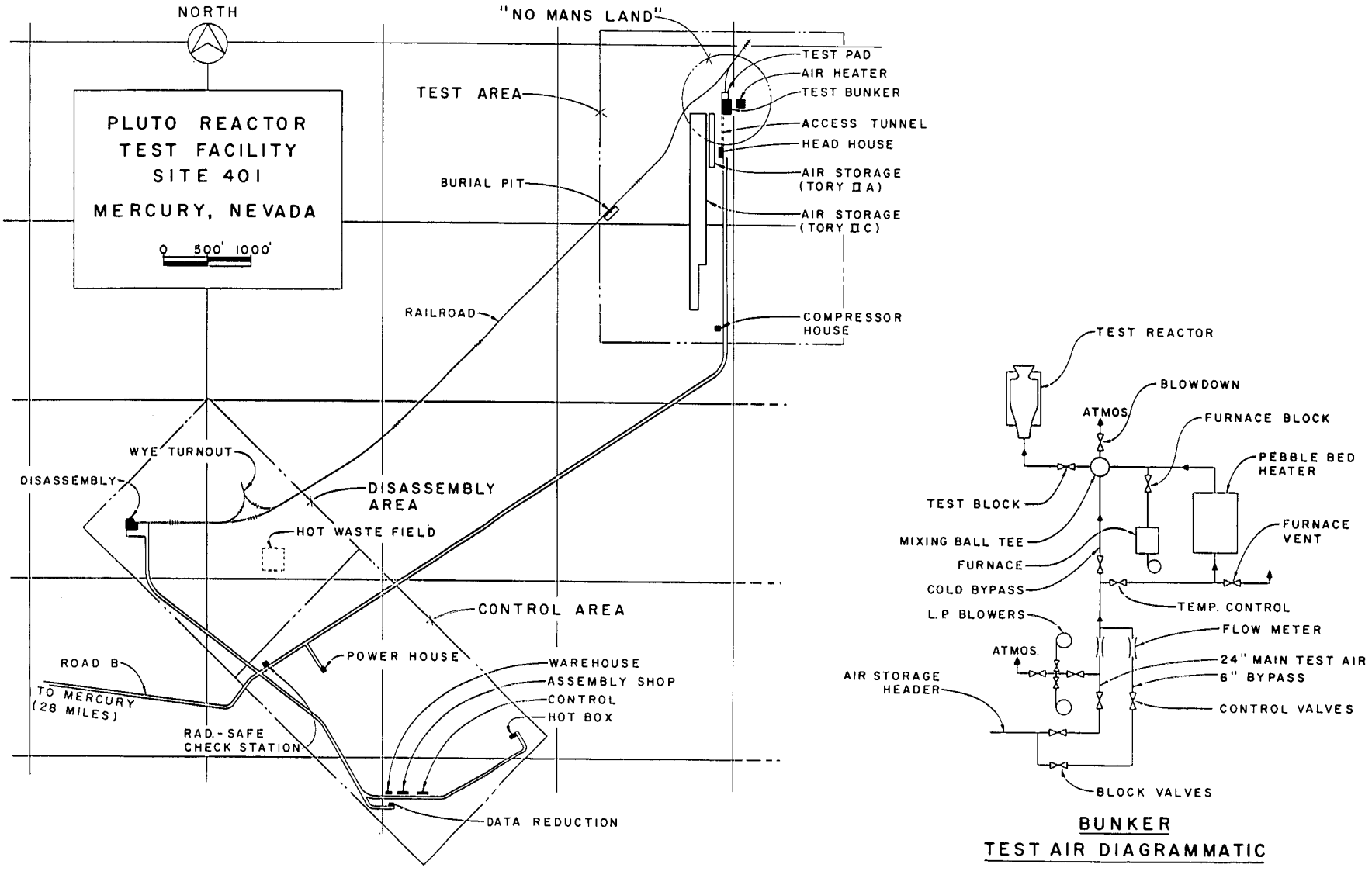

Fig. 1. Pluto reactor test facility and test air schematic.

CONVECTIVE HEAT TRANSFER AND WALL FRICTION AT HIGH TEMPERATURE

by P.M. Magee, D.M. McEligot, M.E. Davenport*, and G. Leppert

Department of Mechanical Engineering, Stanford University

Local heat transfer coefficients and friction factors for turbulent flow of air, nitrogen and helium have been obtained in 1/8-inch diameter smooth tubes. Unheated starting lengths of 1.5 to 3 inches were followed by heated lengths of approximately 20 inches. Within the accuracy of the measurements, the same correlations can be used for all three gases.

Entering Reynolds numbers in various runs range from 13,500 to more than 200,000, the highest flow rates being accompanied by choking at the tube exit. Calculated Mach numbers in the region of the test section where friction factors and heat transfer coefficients were measured vary from 0.02 to more than 0.4. Maximum tube wall temperatures range from 160 to 1890°F, wall-to-bulk temperature ratios to 2.45, and heat fluxes to 259,000 Btu/(hr)(sq ft), while the gas pressure ranges from a few atmospheres to about twenty.

The primary measurements made in this program include tube wall temperature and static pressure at various stations along the heated length; gas inlet and outlet temperatures and pressures; and electrical power input to the tube. Consequently, the local heat transfer and friction coefficients depend on calculated local bulk temperatures obtained from energy balances. However, each test section was calibrated for radial and axial heat loss, with the result that over-all energy balances show agreement to a few per cent between calculated and measured gas exit temperature.

* Present address: Department of Mechanical Engineering, Texas Technological College, Lubbock, Texas.

Figure 1 shows the experimental heat transfer data for air correlated by the relation

$$N_{Nu} = 0.021\, N_{Re}^{0.8} N_{Pr}^{0.4} \left(\frac{T_w}{T_b}\right)^{-0.5} \left[1 + \left(\frac{x}{D}\right)^{-0.7}\right] \qquad (1)$$

in which all properties are evaluated at bulk temperature. The plot includes temperature data at values of x/D from 2.6 to 100. It should be noted that as the heat flux is increased the points in the entrance region ($x/D < 30$) are at first overcorrected, then later undercorrected, by the combination of the temperature ratio and axial distance parameters. The equation is most effective when the heat flux parameter, q^+, equals 0.002.

Many experimental investigators [4, 5, 6, 7] have used a so-called film temperature, midway between the wall and the bulk temperature, to correlate average heat transfer data at high temperature ratios, and Deissler, as the result of a variable properties analysis [3], suggested that a 0.4 reference temperature, $T_r = T_b + 0.4\,(T_w - T_b)$, be used for correlating local heat transfer data. While the present authors prefer the formulation of equation 1, the data obtained in the present investigation can be correlated, as in Figure 2, by

$$N_{Nu,f} = 0.019\, N_{Re,f,m}^{0.8} N_{Pr,f}^{0.4} \left[1 + \left(\frac{x}{D}\right)^{-0.7}\right] \qquad (2)$$

where fluid properties are evaluated at film temperature, $T_f = T_b + 0.5(T_w - T_b)$. The modified film Reynolds number is defined, following Humble et al. [6], by

$$N_{Re,f,m} = \frac{DV\rho_f}{\mu_f} = \frac{GD}{\mu_f} \cdot \frac{\rho_f}{\rho_b}$$

With equation 2, as with the previous equation, the data in the entrance region are not as well correlated as those downstream.

For comparison with earlier investigations the average heat transfer parameters have also been calculated following the definitions

of Humble et al. [6]. Although film properties are usually used for such correlations, the relationship shown in Figure 3 is in agreement with the trends reported in reference 6. The average heat transfer data for air are correlated by

$$N_{Nu,av} = 0.021\, N_{Re,av}^{0.8}\, N_{Pr,av}^{0.4} \left(\frac{T_{w,av}}{T_{b,av}}\right)^{-0.5} \qquad (3)$$

for long tubes ($L/D > 60$) at Reynolds numbers exceeding 25,000.

As shown in Figure 4, local friction factors in the downstream region follow the Karman-Nikuradse relation,

$$\frac{1}{\sqrt{4f}} = 2 \log_{10} (N_{Re} \sqrt{4f}) - 0.8 \qquad (4)$$

when based on fluid properties evaluated at the bulk temperature. Increasing the heat flux appears to cause a slight reduction in the friction factor. In the thermal entry region, local friction factors are higher, and this trend becomes more pronounced at lower values of the Reynolds number and higher values of the heat flux parameter, q^+.

The film temperature concept did not provide a useful correlation of the local friction factor data. Although no comparable data on local friction factors have been published, average values for high temperature gas flow have been reported [1, 6, 7]. The present results, when averaged over the heated length, are in good agreement with these references.

Acknowledgements

This research was performed at Stanford University under AEC contracts AT(04-3)-247 and AT(04-3)-326 Project No. 5.

References

1. Barnes, J.F., and J.D. Jackson, Journ. Mech. Eng. Sci., 3, No. 4, 303 (1961).

2. Deissler, R.G., NACA TN 3016, Oct. 1953.

3. Deissler, R.G., and C.S. Eian, NACA TN 2629, February 1952.

4. Durham, F.P., R.C. Neal and H.J. Newman, Reactor Heat Transfer Conference, New York, November 1, 1956.

5. Fowler, J.M., and C.F. Warner, ARS Journal, 30, No. 3, 266 (March 1960).

6. Humble, L.V., W.H. Lowdermilk and L.G. Desmon, NACA Report 1020, 1951.

7. Taylor, M.F., and T.A. Kirchgessner, NASA TN D-133, Oct. 1959.

Nomenclature

f	Fanning friction factor, $\tau_w / \frac{1}{2}\rho V^2$
H_i	Inlet stagnation enthalpy
N_{Nu}	Nusselt number, hD/k
N_{Pr}	Prandtl number, $\mu c_p/k$
N_{Re}	Reynolds number, GD/μ
q^+	Heat flux parameter [2], q''_w/GH_i
$\frac{x}{D}$	Distance parameter

Subscripts:

f	evaluated at film temperature
i	evaluated at inlet temperature
w	evaluated at wall temperature

The lack of a subscript on a non-dimensional parameter indicates that properties are evaluated at bulk temperature.

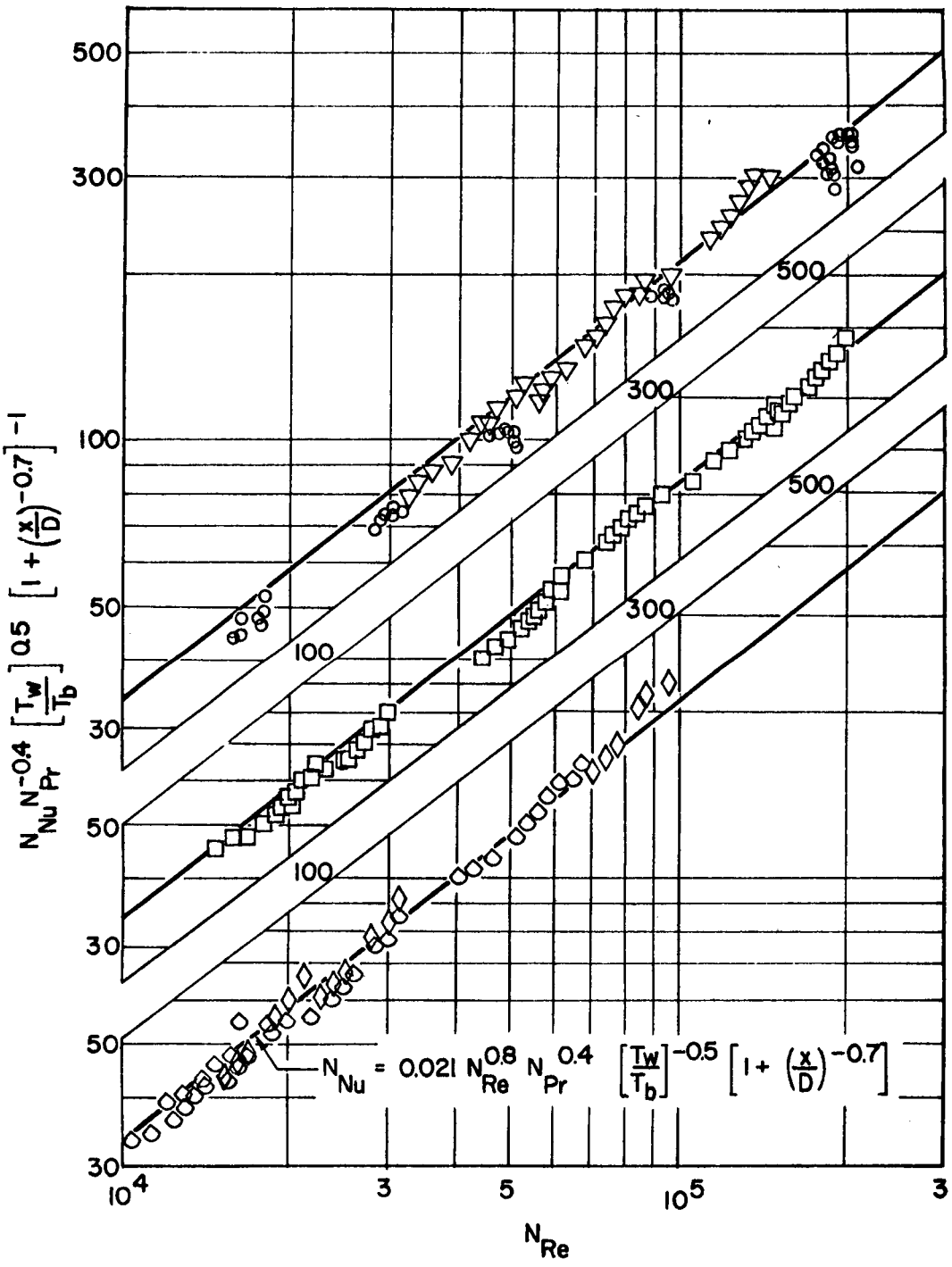

Fig. 1 Local heat transfer results for air based on bulk properties.

Symbol	Heat Flux Parameter, q^+
○	< 0.0005
□	0.0016-0.0023
▽	0.0026-0.0030
△	0.0033-0.0034
◇	> 0.0038

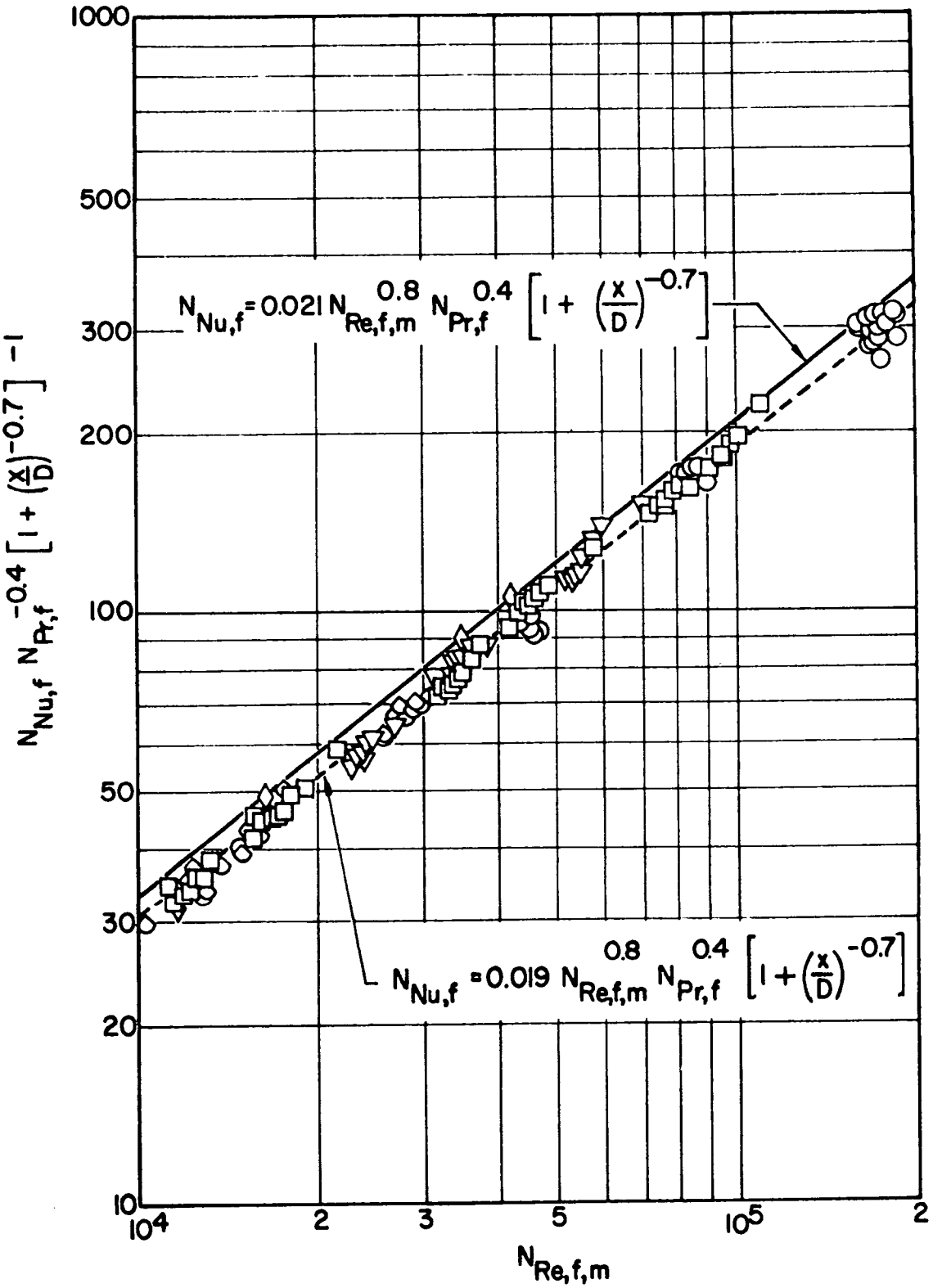

Fig. 2 Local heat transfer results for air based on film properties. Symbols as in figure 1.

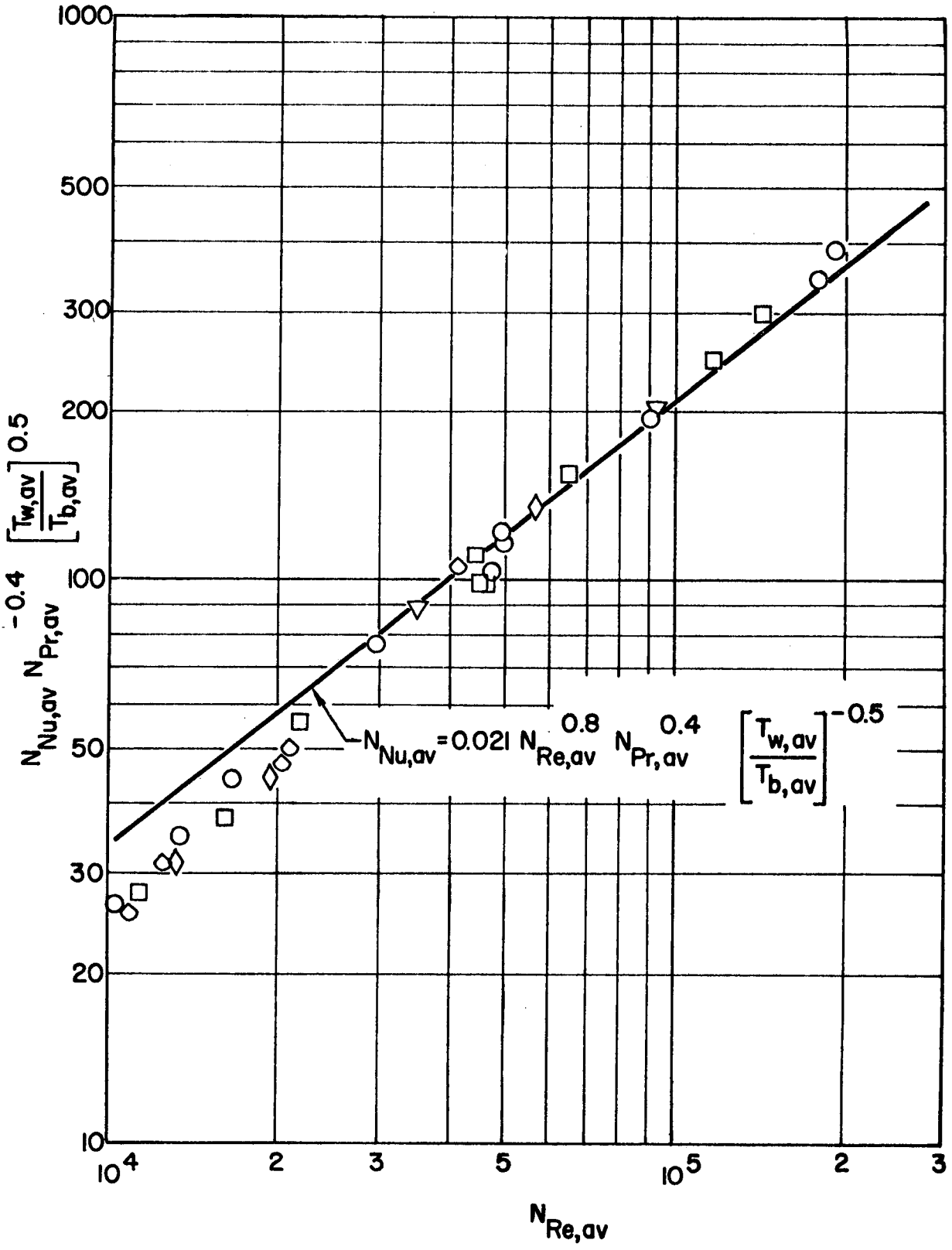

Fig. 3 Average heat transfer results for air based on bulk properties. Symbols as in figure 1.

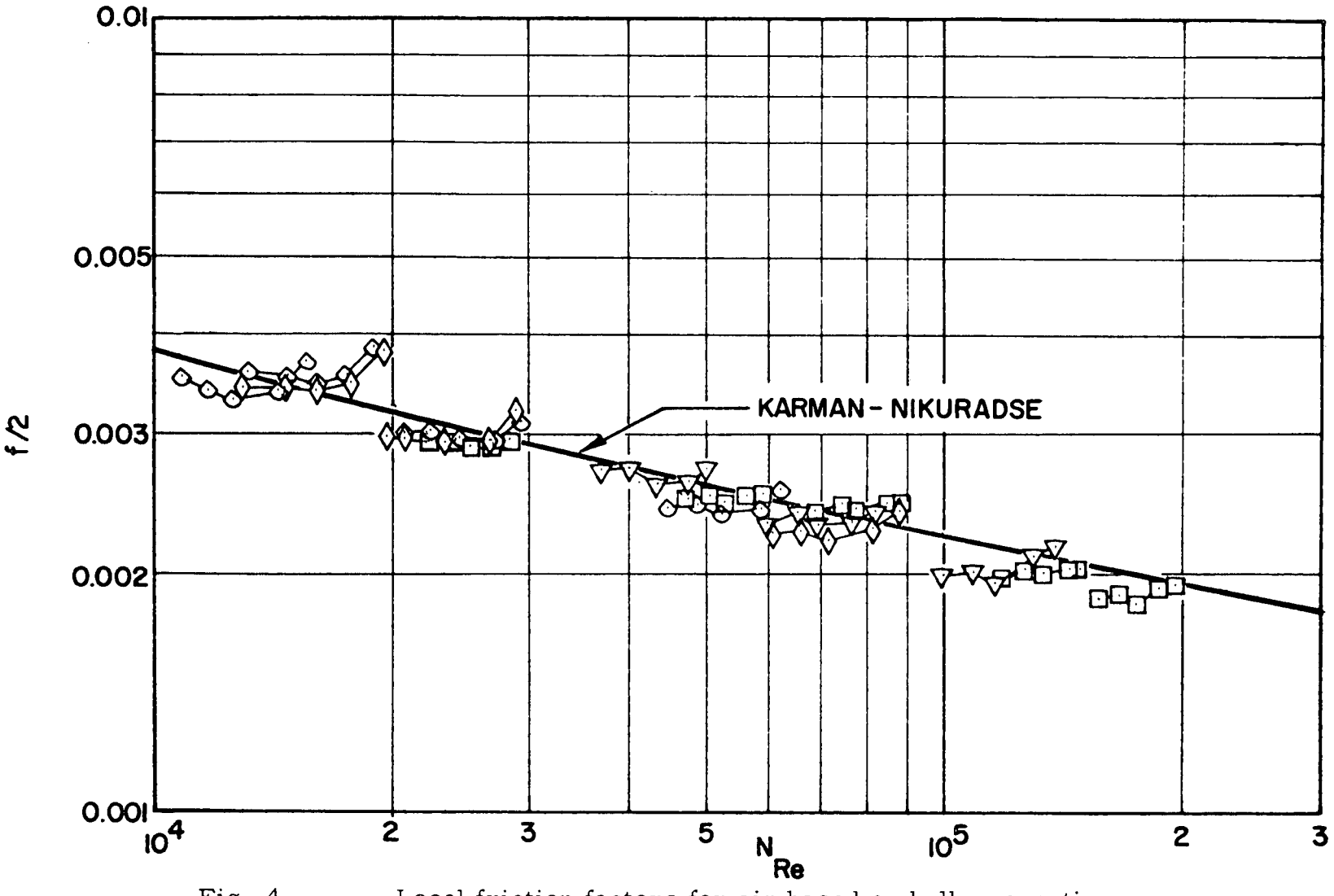

Fig. 4 Local friction factors for air based on bulk properties. $q^+ > 0.0016$, $\frac{x}{D} > 9$, Mach No. < 0.23. Solid lines connect points on same run. Symbols as in figure 1.

ON THE HYDRODYNAMICS OF A COAXIAL FLOW GASEOUS REACTOR

By Robert G. Ragsdale and Herbert Weinstein

Lewis Research Center
National Aeronautics and Space Administration
Cleveland, Ohio

Introduction

The concept of a coaxial flow gaseous reactor is presented in reference 1, and will be but briefly described here. The containment criterion, common to all gaseous reactor schemes, is met by introducing a slow moving stream of fissionable gas into a surrounding, fast moving stream of hydrogen propellant. The hydrodynamic analysis of such a system must include both mass and momentum interchange between the two streams, and is additionally complicated by heat transfer and criticality considerations. The approach here has been to first restrict attention to an isothermal, laminar coaxial flow system.[2] This basic analysis has been extended in this paper to include turbulence by introducing an eddy diffusivity into the laminar equations.

Experimental measurements have been made on an air-bromine coaxial flow system. Measured values of the variation of inner stream (bromine) density with axial position are compared with the analysis for both laminar and turbulent flow of the outer (air) stream. The purpose of this study is to verify the fundamental diffusion and momentum transfer analysis. Though the additional complexities associated with flow instability and nuclear heat generation are as yet unexplored, the results presented here provide necessary information about the basic mixing process in a coaxial flow gaseous reactor.

Analysis

The assumptions and restrictions made in deriving the equation set for the model shown in figure 1 are: (1) the entire flow field is at steady state and constant temperature and pressure, (2) axial symmetry exists, (3) the fluids mix ideally, and (4) the usual boundary layer assumptions apply.

The equation set consists of the continuity equation with the steady state and axial symmetry assumptions; the momentum equation, which is the axial component Navier-Stokes equation including the body force term, with the boundary layer, steady state, axial symmetry, constant pressure and constant temperature assumptions; and the diffusion equation[3] with the axial symmetry and steady state assumptions. These three equations are taken through a transformation to an axial length-stream function coordinate set.

The resulting equations are:

$$\text{momentum:}\quad \frac{\partial \bar{u}}{\partial \bar{z}} = \frac{\beta + 1}{Re_{1,0}} \cdot \frac{\partial}{\partial \psi}\left[\bar{\mu}\bar{r}^2\bar{u}(\beta C + 1)\frac{\partial \bar{u}}{\partial \psi}\right] + \frac{\beta C}{F\bar{u}(\beta C + 1)} \tag{1}$$

$$\text{diffusion:}\quad \frac{\partial C}{\partial \bar{z}} = \frac{(\beta C + 1)^2}{Re_{1,0}\cdot Sc_{1,0}} \cdot \frac{\partial}{\partial \psi}\left[\overline{Dr}^2\bar{u}\frac{\partial C}{\partial \psi}\right] \tag{2}$$

where

$\bar{u} = \dfrac{\text{Local axial velocity}}{\text{Initial inner stream velocity}}$;

F = Initial inner stream Froude number

$\bar{z} = \dfrac{\text{Axial distance}}{\text{Initial inner stream radius}}$;

$\bar{\mu} = \dfrac{\text{Local mixture viscosity}}{\text{Inner stream viscosity}}$

$\beta = \dfrac{\text{Mol. wt. of inner stream}}{\text{Mol. wt. of outer stream}} - 1$;

C = Inner stream mole fraction

$\bar{r} = \dfrac{\text{Radial distance}}{\text{Initial inner stream radius}}$

$\bar{D} = \dfrac{\text{Local binary diff. coeff.}}{\text{Inner stream self-diff. coeff.}}$

$Sc_{1,0}$ = Initial inner stream Schmidt number

$Re_{1,0}$ = Initial inner stream Reynolds number

ψ = stream function

Because of the cylindrical geometry, the radial distance does not drop out of the equations as it would in a two-dimensional system as Pai[4] showed, so a form of the continuity equation must be carried along in the numerical integration to relate $\bar{r}$ and ψ. The form used is obtained by assuming again $\partial\psi/\partial\bar{r} \gg \partial\psi/\partial\bar{z}$ and dropping the term containing the smaller derivative:

$$\text{continuity:}\quad \int_0^{\bar{r}} \bar{r}'d\bar{r}' = \int_0^{\psi} \frac{1}{\bar{u}(\beta C + 1)}\, d\psi' \tag{3}$$

These equations are integrated numerically from the initial face at the nozzle entrance downstream to a face beyond the end of the potential core.

The laminar analysis is extended to include turbulent flow by introducing eddy diffusivity factors into the molecular viscosity and diffusivity terms in the above equations. This is done in the usual manner:

$$\mu_{turb} = \mu_{lam}\,(1 + \rho\epsilon/\mu_{lam})$$

$$D_{turb} = D_{lam}\,(1 + \epsilon/D_{lam})$$

for both fluids. In addition, the value of $(\rho\epsilon/\mu)$ in the inner stream is allowed to vary axially from a low initial value up to the constant value of the $(\rho\epsilon/\mu)$ in the outer stream according to the form:

$$(\rho\epsilon/\mu)_1 = (\rho\epsilon/\mu)_{1,0} + a_1(\bar{z})^{a_2}.$$

Experiment

The air-bromine coaxial flow test set-up is shown schematically in figure 2. Metered air is introduced through a tube bundle, and flows downward in a five

inch by five inch Lucite channel. A metered bromine stream is injected into the air stream two feet downstream from the tube bundle through a one-half inch diameter monel tube. The test section was operated at five psia, the vapor pressure of bromine at room temperature. A photograph of the test apparatus is shown in figure 3.

Radial average bromine concentrations were measured at one-inch intervals downstream from the point of injection by a light absorption technique. One-eighth inch diameter collimated light beams were passed through the bromine stream, and intercepted by photomultiplier detectors. Concentration was calculated from the measured light attenuation from Beer's law.

The calculated concentrations at the various axial stations were normalized to the value at the injection point, and are thus independent of the absolute value of absorption coefficient. This concentration ratio, C^*, is plotted as a function of the distance from the injection point, $\bar{z}$, normalized to the initial bromine stream radius. Two flow conditions are reported here; one is for laminar flow of both streams, and the other for turbulent.

Discussion of Results

Figure 4(a) shows a comparison of the experimental data with the analysis for laminar flow. The Reynolds number of the airstream is 2075, and the initial air-to-bromine velocity ratio is 4.3. The initial bromine Reynolds number, based on the diameter of the injection tube, is 200. The agreement is satisfactory in view of the relatively complex flow mechanism under consideration. Two factors are worthy of note here. First, though the Reynolds numbers of both the air and bromine streams are within the laminar regime, the discontinuity resulting from the finite thickness of the injection tube tended to introduce a certain amount of turbulence. Second, the analytical line is a true radial average, while the experimental conditions only approximate this, since the light beams were of finite diameter. Both of these considerations would tend to cause the data to fall somewhat below the predicted line. The results of both the laminar and turbulent analyses include gravitational effects, expressed in equation (1) in terms of a Froude number.

For laminar flow, the conditions of the experiment are used as input to the analysis, and the predicted variation of concentration with axial position is obtained. For turbulent flow, the situation is not so well defined. In addition to the measurable parameters, one more quantity is required but unavailable. That is the value of a turbulence level factor, $(\rho\epsilon/\mu)$. In the outer stream, this factor is considered constant. In the bromine stream, the turbulence factor is allowed to vary from some initial value (zero, if the bromine stream is initially laminar) up to the $(\rho\epsilon/\mu)$ in the airstream.

It is possible, however, to estimate this parameter from the Reynolds number, based on existing pipe flow data. This was done, and for the turbulent case considered here, the $(\rho\epsilon/\mu)$ of the airstream was estimated to be from 21 to 37. For this run, the air Reynolds number was 19,900, and the initial bromine Reynolds number was 1900. The initial air-to-bromine velocity ratio was 4.4.

Figure 4(b) shows the experimental data for these conditions. The predicted line for laminar flow is shown for comparison. The analytical line for turbulent flow was obtained by taking a turbulence factor of 30 for both the air and bromine streams. Since this value is within the range expected from pipe flow information, the procedure seems justified; though, admittedly, this probably masks certain experimental inaccuracies. A more realistic approach would be to consider some initially low turbulence level factor in the bromine stream, and allow it to increase axially to the airstream value. The point of view here is

that, for the purposes of this paper, it is sufficient to show that the assumption of equal turbulence levels in the two streams yields satisfactory results.

Additional data, over a range of flow conditions, will be required to determine a relationship between turbulence level and Reynolds number for a coaxial flow system. The three flow regimes of interest are: (1) laminar flow of both streams, (2) turbulent flow of both streams, and (3) laminar flow of the inner stream and turbulent flow of the outer stream. The general agreement of the experimental data and the analysis for both turbulent flow (with an assumed value of $\rho\epsilon/\mu$) and laminar flow cases presented here indicates that the important physical mechanisms for mass and momentum transfer are adequately described by the analytical expressions.

REFERENCES

1. Weinstein, Herbert, and Ragsdale, Robert G.: A Coaxial Flow Reactor - A Gaseous Nuclear-Rocket Concept. ARS preprint 1518-60, Dec. 5, 1960.

2. Weinstein, Herbert, and Todd, Carroll A.: A Numerical Solution of the Problem of Mixing of Laminar Coaxial Streams of Greatly Different Densities - Isothermal Case. NASA TN D-1534 (to be published).

3. Bird, R. B., Stewart, W. E., and Lightfoot, E. C.: Notes on Transport Phenomena. Wiley & Sons, New York, 1958.

4. Pai, Shih-I: Fluid Dynamics of Jets. Van Nostrand Co., New York, 1958.

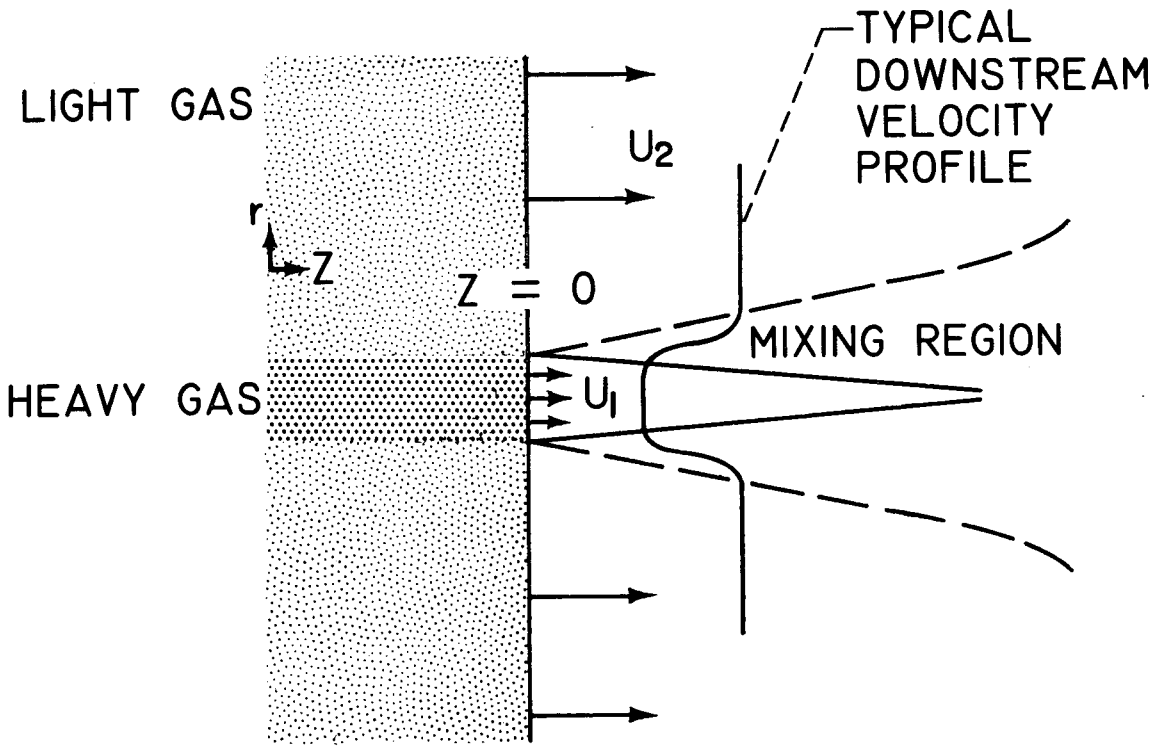

Figure 1. - Coaxial flow model.

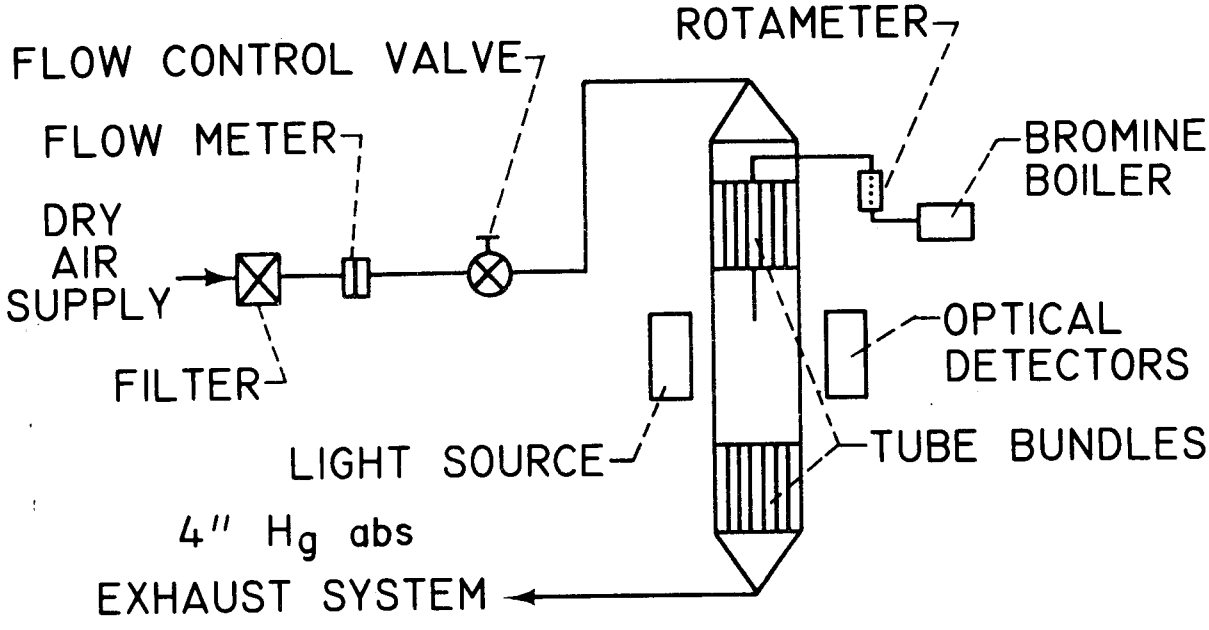

Figure 2. - Schematic of air-bromine system.

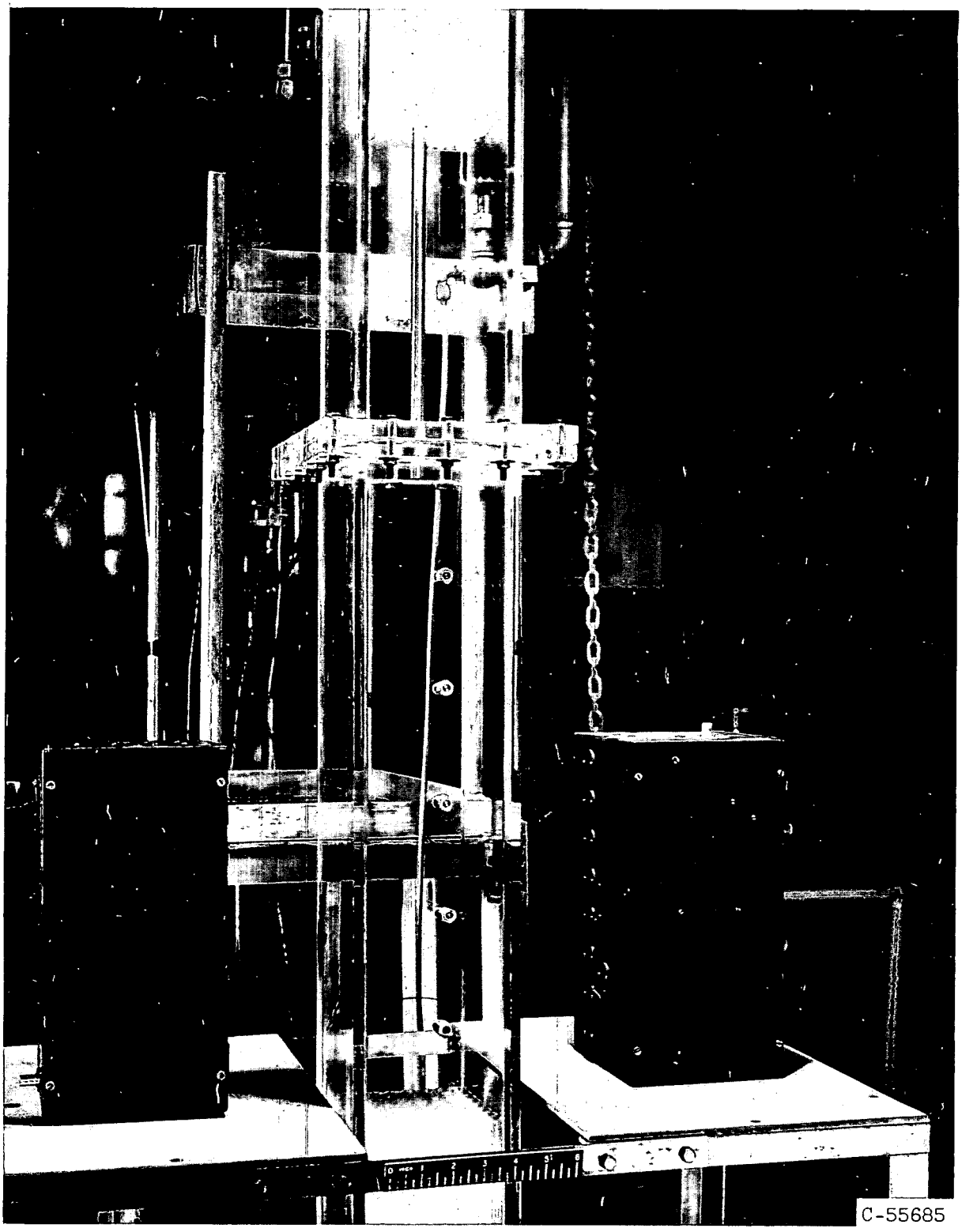

Figure 3 Air-bromine test apparatus.

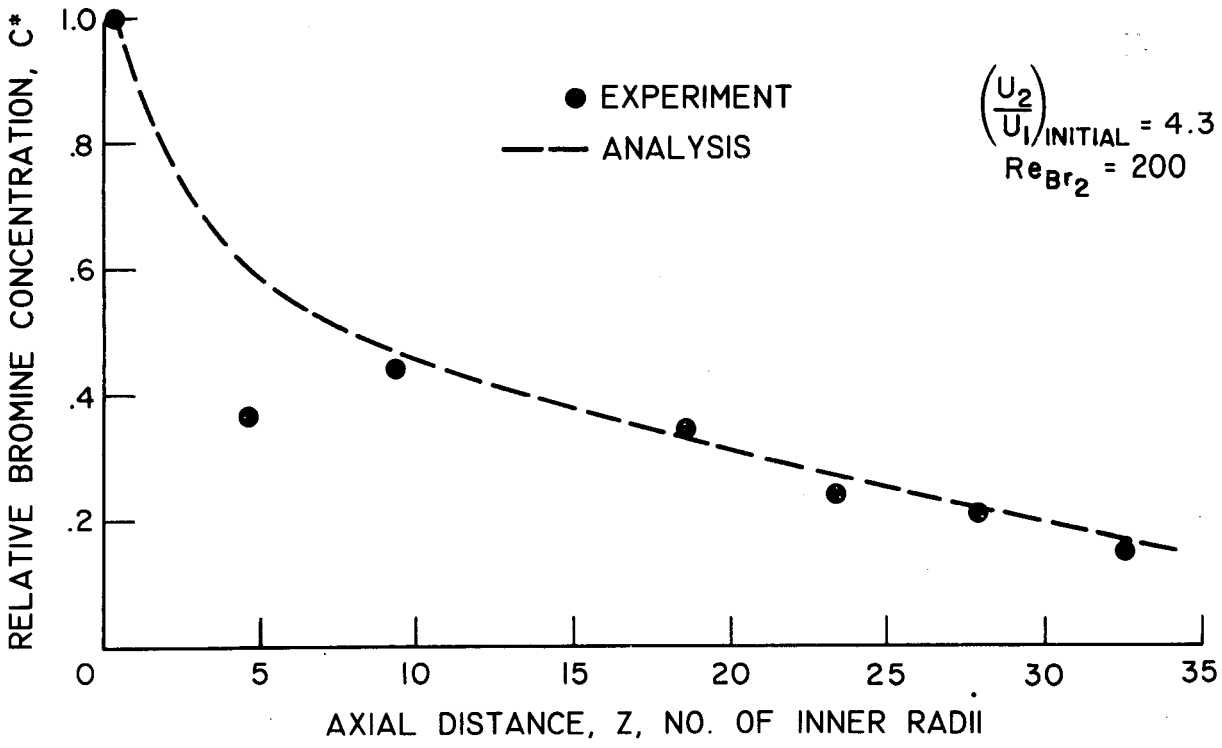

(a) Laminar flow (Re_{air} = 2075).

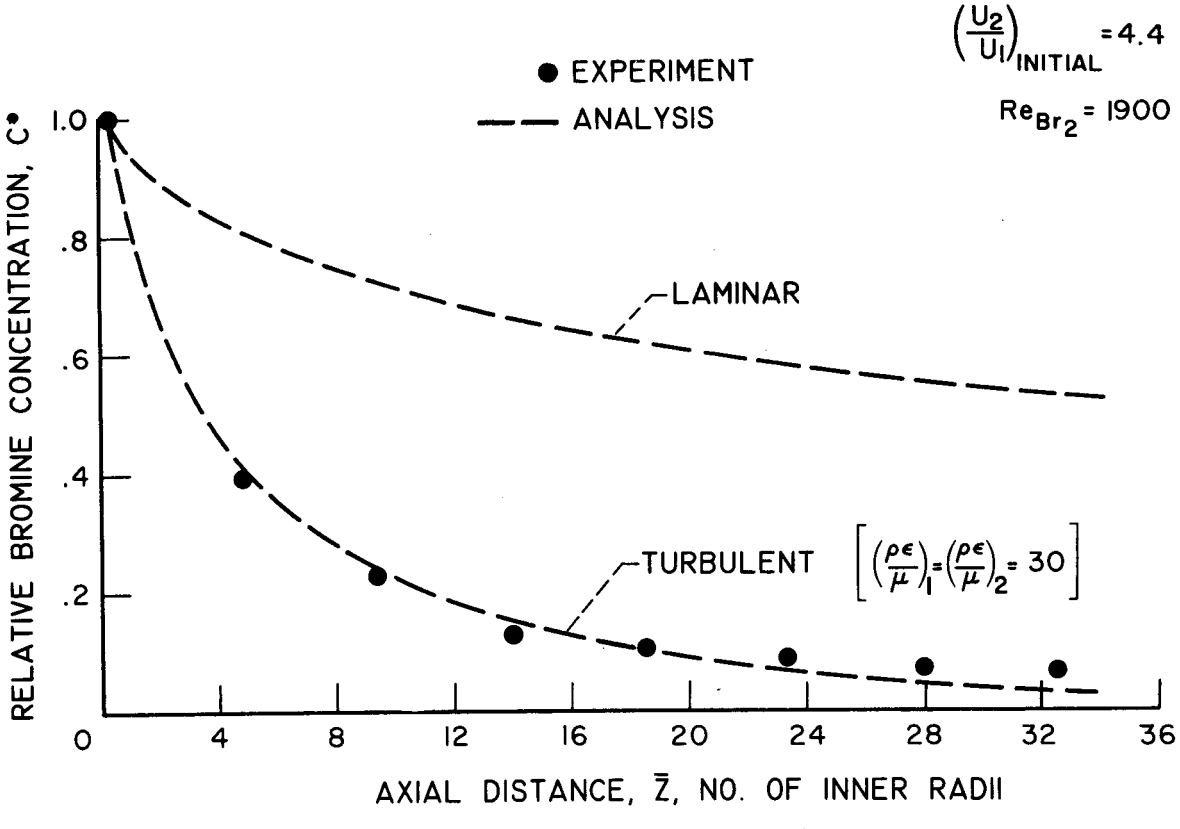

(b) Turbulent flow (Re_{air} = 19,900).

Figure 4. - Air-bromine coaxial flow tests.

RADIANT HEAT TRANSFER TO ABSORBING GASES WITH FLOW AND CONDUCTION

By T. H. Einstein

Lewis Research Center
National Aeronautics and Space Administration
Cleveland, Ohio

INTRODUCTION

During the past five years there has been a significant increase of interest in the problem of radiant heat transfer to absorbing gases. Recent activity in this area has been motivated by the advent of heat transfer problems arising in space vehicle reentry, MHD energy conversion, and energy transport in a gaseous nuclear reactor.

Hottel was one of the earliest workers in this field, having investigated radiant heat transfer from furnace gases as early as 1927. Although other workers have recently become active in the field by obtaining analytical solutions for heat transfer and temperature distributions (1), (2), (3), Hottel's analysis (4) of the heat transfer problem remains probably the most realistic since it is applicable to real (nongray) gases and may be applied to geometries of almost arbitrary shape.

There has been very little done so far in obtaining generalized results for radiation to a flowing gas or for combined radiation and conduction. Adrianov, (3), investigated radiation heat transfer to a flowing gas, but some of the assumptions in his analysis render his results valid only for the case of weak absorbtion in the gas. Viskanta, (2), has presented a rather complete analytical treatment of combined radiation and conduction between two infinite parallel plates separated by an absorbing gas, but only a few specific results were presented.

It is the purpose of this investigation to expand on the work done by both Adrianov and Viskanta which is cited above. The method used in the present analysis is a modification of Hottel's zoning technique (4). Results are obtained for a gray gas in a rectangular channel formed by two black, parallel flat plates of finite length, and are presented in generalized form for the case of radiation to flowing gases and also for combined radiation and conduction.

ANALYSIS

A two-dimensional analysis of radiation heat transfer is made for a gray gas enclosed in a rectangular channel formed by two black parallel flat plates of finite length and infinite width. A sketch of this configuration is shown in figure 1. A rigorous treatment of this problem requires the solution of the following two dimension integro-differential equation which represents the heat balance on an infinitesimal volume, dV, at any point in the channel.

$$+ 4k\sigma T^4(\vec{r}_o) + Gc_p \left.\frac{\partial T(\vec{r})}{\partial x}\right|_{\vec{r}=\vec{r}_o} - \lambda \left.\frac{\partial^2 T(\vec{r})}{\partial y^2}\right|_{\vec{r}=\vec{r}_o}$$

$$= k \int\int\int \sigma T^4(\vec{r}) f(\vec{r} - \vec{r}_o)dv + k \int\int \sigma T_s^4(\vec{r}) g(\vec{r} - \vec{r}_o)da \quad (1)$$

An explanation of the various terms in equation (1) is given below

k absorbtion coefficient of the gas

$+ rk\sigma T^4(\vec{r}_o)$ energy emitted per unit volume at $\vec{r} = \vec{r}_o$

$Gc_p \left.\frac{\partial T}{\partial x}\right|_{r=r_o}$ rate of enthalpy increase of the flowing gas at $\vec{r} = \vec{r}_o$

$\lambda \frac{\partial^2 T(\vec{r})}{\partial y^2}$ net conduction heat transfer per unit volume

$\int\int\int$ radiation absorbed from emission due to surrounding gas volume and radiation absorbed from emission of flat plate surfaces, respectively

If the conduction and convection terms are removed in equation (1), its solution is greatly simplified since the equation will then be linear in the emissive power σT^4. If in addition the length of the channel also becomes infinite, the integrals can be partially evaluated in closed form in terms of exponential-integral functions, as was done by Usiskin (1).

In the absence of these simplifying restrictions, the only feasible way to solve this problem appears to be application of a method similar to Hottel's where the two-dimensional integral-differential equation (1) is approximated by a system of algebraic equations. This is done by first dividing the region between the plates up into a 10×10 array of rectangular zones, 100 zones in all. The gas temperature variation within each of these zones may be approximated by a two-dimensional linear function. Heat balance equations in the form of equations in the form of equation (1) are now written for infinitesimal volume elements located at the center of each of 100 zones. The integral on the right of equation (1) is approximated by a finite summation over all the zones and surfaces. The derivatives are replaced by numerical approximations obtained from fitting a paraboloid through the temperatures of the zone in question and those of its adjacent neighbors in both directions. Each of the 100 zones is labeled by a dual subscript (i,j), i is the position along the length of the channel and j represents the position in the transverse direction. The resulting system of nonlinear algebraic equations, which is given below, are then solved for the 100 values of T_{ij}, the gas temperatures at the center of the zones, for a given set of boundary conditions (plate and end temperatures).

The conditions of the two ends of the channel are represented by assuming that the ends are porous black plugs having the same temperature as the effective gas temperature at the ends. The equations to be solved are thus:

$$+ 4k\sigma T_{ij}^4 + Gc_p \frac{\left(T_{i+1,j} - T_{i-1,j}\right)}{2\,\Delta x} - \lambda \frac{\left(T_{i,j+1} + T_{i,j-1} - 2T_{ij}\right)}{\Delta y^2}$$

$$= k \sum_{m,n=1}^{10} \sigma T_{m,n}^4 f(\vec{r}(m,n) - \vec{r}(i,j))\Delta v$$

$$+ k \sum_{m,n=1}^{10} \sigma T_s^4(m,n) g(\vec{r}(m,n) - \vec{r}(i,j))\Delta a \qquad i=1,10;\ j=1,10 \qquad (2)$$

The principal difference between the present approach and that of Hottel's is that here the heat balance is taken on an infinitesimal volume of the center of the zone, rather than on the entire zone. This approach results in a large reduction in the effort required to compute the "exchange factors" $f(\vec{r})$ and $g(\vec{r})$. Since the system of 100 equations (2) is generally nonlinear due to the presence of convection and conduction terms, it was solved using the Newton-Raphson iterative method for nonlinear algebraic equations. This method rapidly converges and the correct solution is obtained after only a few iterations.

RESULTS AND DISCUSSION

The system of equations described by equation (2) was solved on an IBM 7090 computer for a gray gas of constant absorptivity enclosed in a black walled rectangular channel of aspect ratio, L/D, of ten and for a range of optical thickness τ_o, $(0.1 \leq \tau_o \leq 6)$, $\tau = kD$, where k is the gas absorptivity and D is the plate spacing. Cases were run for either combined convection and radiation or combined conduction and radiation, for a wide range of gas flow rates and thermal conductivities. The walls of the channel were considered to be at constant temperatures. To establish a reference several cases were run for radiation only, without flow or conduction.

Figure 2 illustrates the heat transfer between the two plates for the case of a stagnant nonconducting gas. Since in this case equation (1) is linear in the emissive power, σT^4, the heat transfer results may be normalized by dividing by the difference in the emissive powers of the two plates. The results given in figure 2 compare favorably with those obtained by Usiskin, (1), for infinite parallel flat plates. The agreement is not perfect because of end effects due to the finite length of the channel.

In order to discuss the effect of conduction on radiation in a stagnant gas it is desirable to present the results in some type of nondimensional parametric form to obtain complete generality. Equation (1) may be nondimensionalized by dividing through by $k\sigma T_*^4$ where T_* is the temperature of the hotter plate. It can also be shown that the integrals on the right, for a given temperature field, are a function only of τ_o, and the channel aspect ratio L/D. On the basis of the above observations it can be shown that the solution of equation (1) is a unique function of the boundary conditions (ratio of cold plate and end

temperatures to T_*), and of the following set of dimensionless parameters $\left(\frac{\lambda/D}{\sigma T_*^3}, \tau_o, \frac{L}{D}\right)$. For the sake of brevity the parameter $\frac{\lambda/D}{\sigma T_*^3}$ will be designated N_{CR}. Figure 3 shows the effect of combined conduction and radiation on the transverse temperature profile for the cases of both weak gas radiation ($\tau_o = 0.2$), and a relatively opaque gas ($\tau_o = 3.0$). In both cases, the temperature gradient and therefore the heat conduction at the cold wall were substantially higher than those for pure conduction (linear temperature profile). At the hot wall the temperature gradient may be either greater or less than that for pure conduction, depending upon the value of N_{CR} and the opacity of the gas.

Another effect of combined radiation and conduction is that the total heat transferred is greater than the sum of the heat transfer for radiation and conduction, taken separately. This effect is shown in figure 4 where the ratio of combined heat transfer to the sum of both components taken separately is plotted versus τ_o for various values of N_{CR}. This augmentation is due to interaction between radiation and conduction resulting from the nonlinear nature of the combined process. There is no augmentation for the case $\tau_o = 0$ since the gas is then not involved in the radiation transfer process, and the energy transport by conduction and that by radiation are independent. For large values of τ_o, the radiation transport becomes similar to a diffusion process (Rosseland approximation) and again the interaction with conduction diminishes.

For the discussion of the effect of gas flow on radiation without conduction it is again desirable to present the results in the form of dimensionless parameters. In the discussion to follow both plates are at the same, constant temperature T^* and the gas enters the channel from one end through the black porous plug at a temperature T_i. The gas flow is in the direction of length L, as shown in figure 1. The results to be given are for slug flow, G is constant. In a manner similar to that described earlier, the solution to equation (1) is a function of the dimensionless inlet temperature (T_i/T_*) and the following set of dimensionless parameters $\left(\frac{Gc_p}{\sigma T_*^3}, \tau_o, \frac{L}{D}\right)$. The parameter $\frac{Gc_p}{\sigma T_*^3}$ is known as the Boltzmann number N_{Bo} and was also used by Adrianov (3) in presenting his results. In figure 5, the parameter $\Lambda = \frac{T_o - T_i}{T_* - T_i}$ represents the ratio of the actual heat transferred to the gas to the maximum theoretically possible. The striking feature of figure 4 is that for a given value of N_{Bo} the heat transfer to the gas goes through a maximum with increasing τ_o. The reason for this behavior is that as τ_o increases the layers of gas next to the wall effectively absorb most of the radiation from the wall and thereby shield the bulk of the gas stream from any direct radiation. Because of this the bulk of the gas absorbs less radiation with increasing τ_o, resulting in reduced overall heat transfer.

The effect of this self shielding can also be seen by comparing the transverse temperature profiles at the channel exit for a weak and a strongly absorbing gas as shown in figure 6. At $\tau_o = 1.0$ there is very little self shielding and the temperature profile across the channel is fairly flat. For a higher degree of gas opacity at the same value of Λ, $\tau_o = 4.0$, the temperature profile shows the variation expected, the temperatures next to the wall being higher but the temperatures in the remainder of the stream being reduced due to the heavy self shielding.

The preceding remarks have indicated some of the effects of conduction and gas flow on radiant heat transfer to absorbing gases. The interaction between conduction and radiation results in an increase in net heat transfer in comparison to the sum of the conduction and radiation heat transfer taken separately. For the case of radiation to a flowing gas from a constant temperature surface, the net heat transferred to the gas goes through a maximum as the gas absorbtivity is increased.

REFERENCES

1. Usiskin, C. M., and Sparrow, E. M.: Thermal Radiation Between Parallel Plates Separated by an Absorbing-Emitting Nonisothermal Gas. Int. Jour. Heat and Mass Transfer, vol. I, no. 1, June 1960.

2. Viskanta, R., and Grosh, R. J.: Heat Transfer by Simultaneous Conduction and Radiation in an Absorbing Medium. ASME Trans., sec. C, vol. 84, no. 1, Feb. 1962.

3. Adrianov, V. N., and Shorin, S. N.: Radiant Heat Transfer in a Flowing Radiating Medium. Izvestiga Akademii Nauk S.S.S.R. 1958. (AEC trans. 3928.)

4. Hottel, H. C., and Cohen, E. S.: Radiant Heat Exchange in a Gas Filled Enclosure: Allowance for Nonuniformity of Gas Temperature. A.I.Ch.E. Jour., vol. 4, no. 1, Mar. 1958.

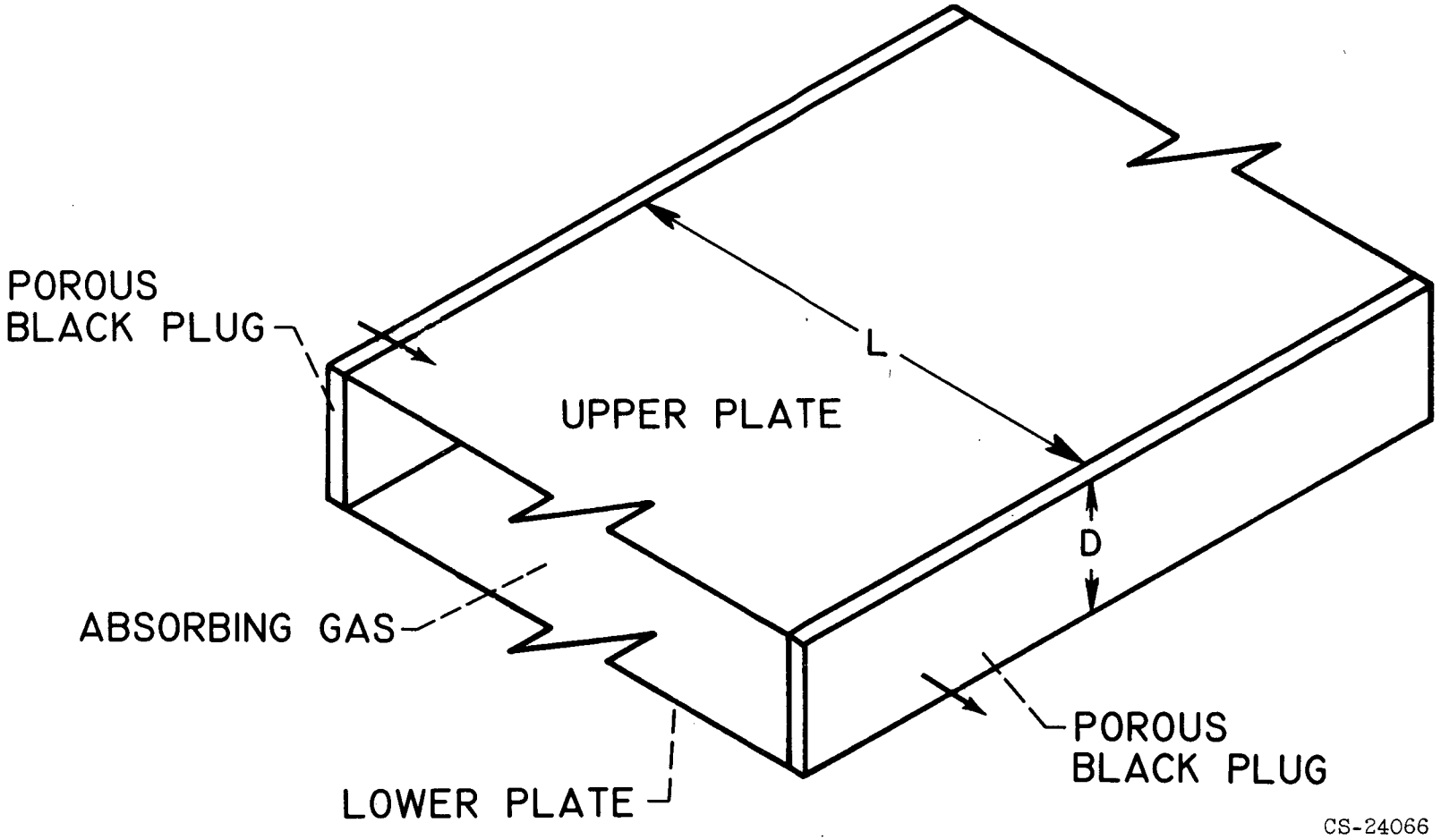

Fig. 1. - Sketch of rectangular channel configuration.

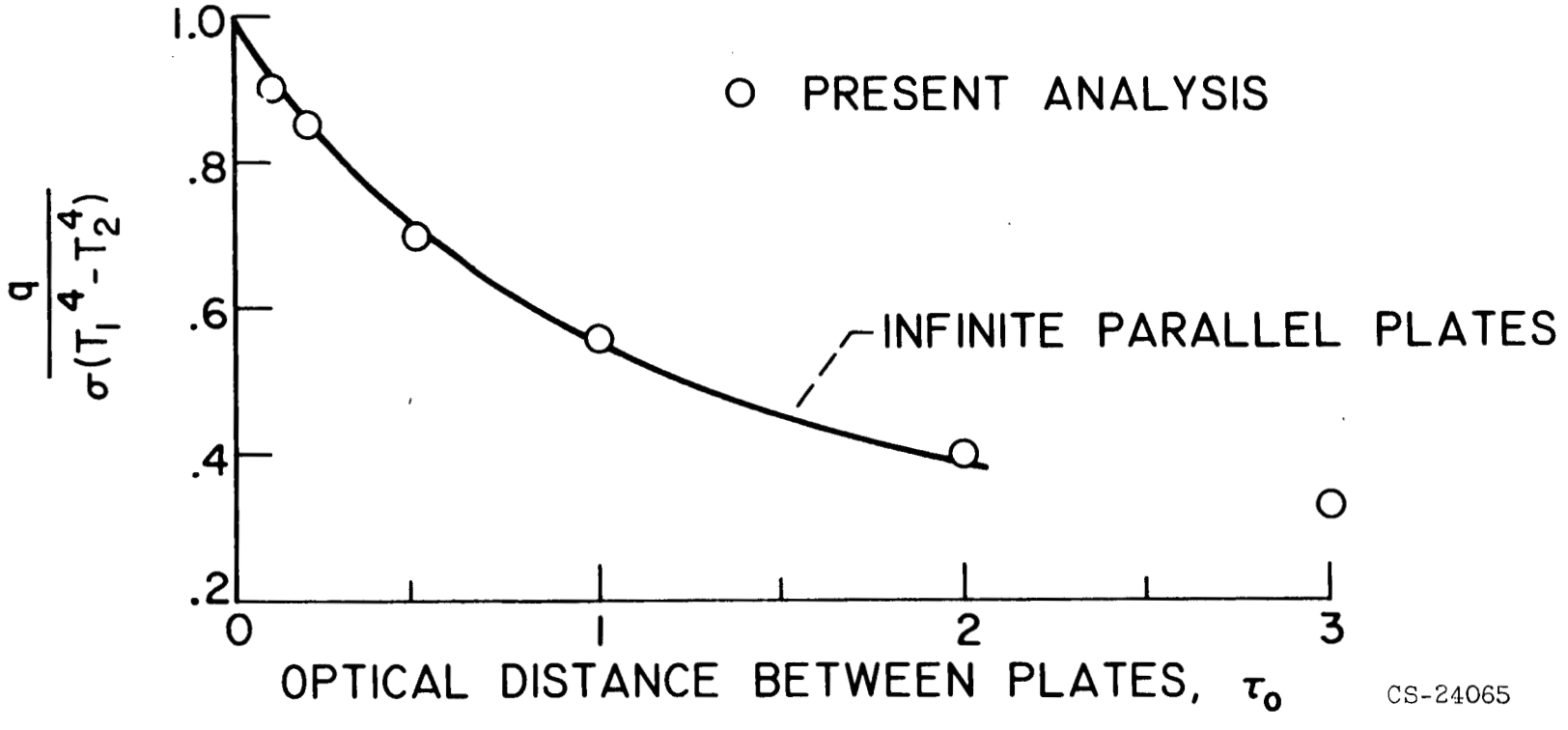

Fig. 2. - Dimensionless heat transfer between the plates for pure radiation (no conduction or flow).

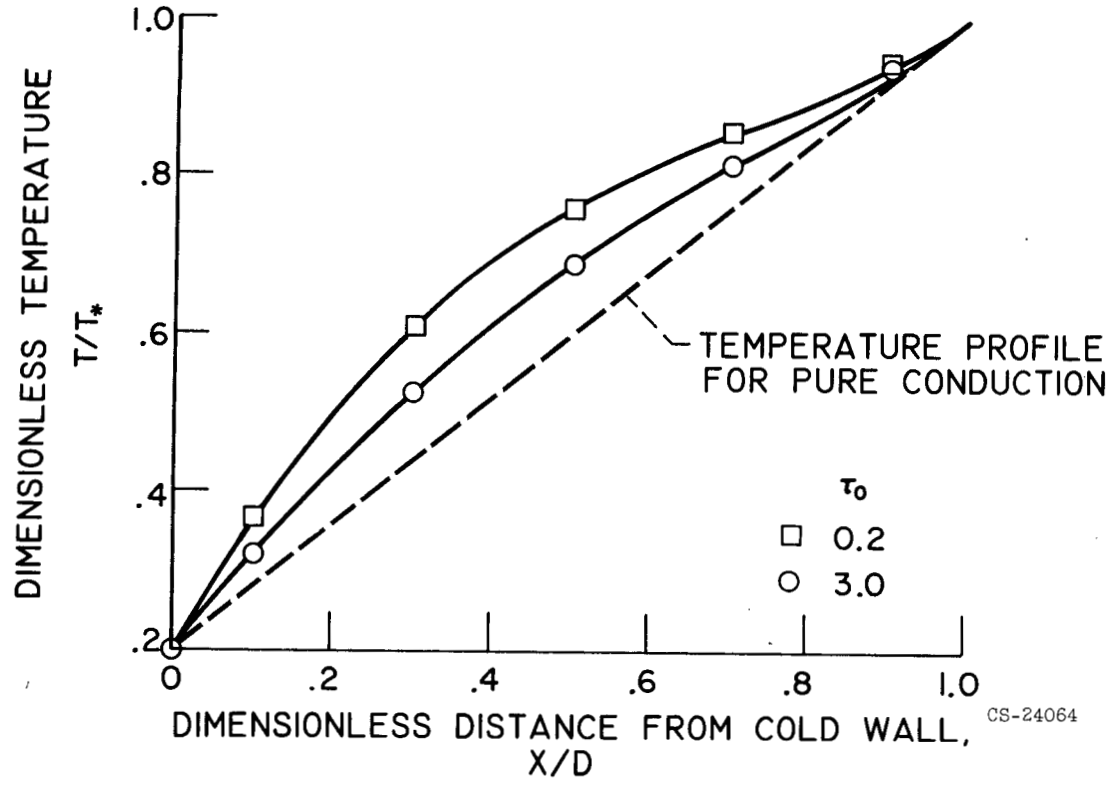

Fig. 3. - Temperature profiles for combined conduction and radiation. N_{CR} = .208, $T_c/T_* = 0.2$.

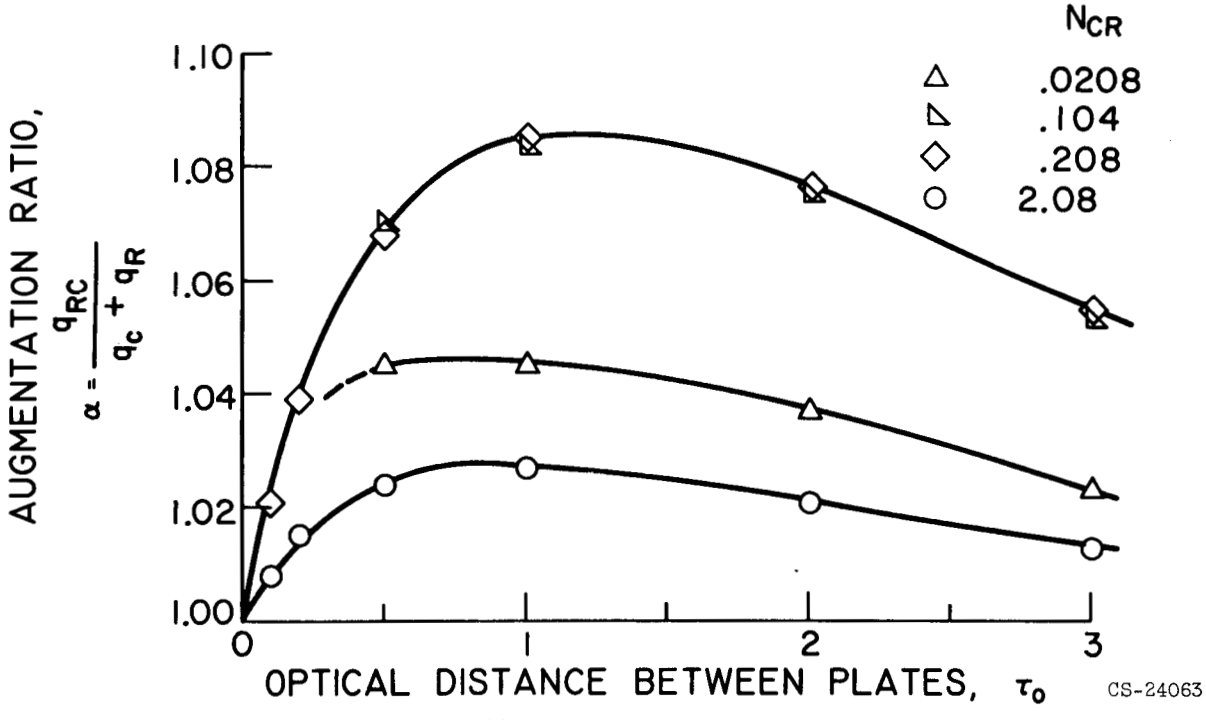

Fig. 4. - Augmentation ratio versus τ_0 for combined radiation and conduction.

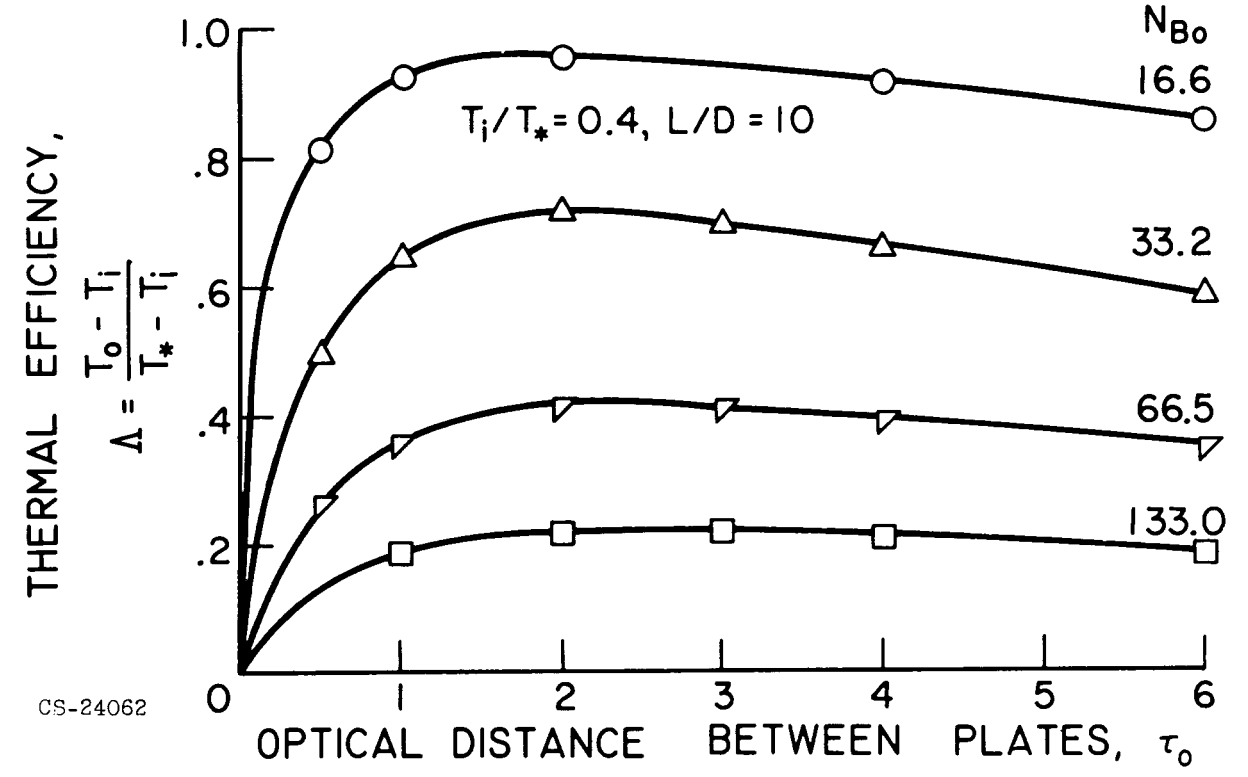

Fig. 5. - Dimensionless heat transfer to gas in a rectangular channel as a function of gas capacity.

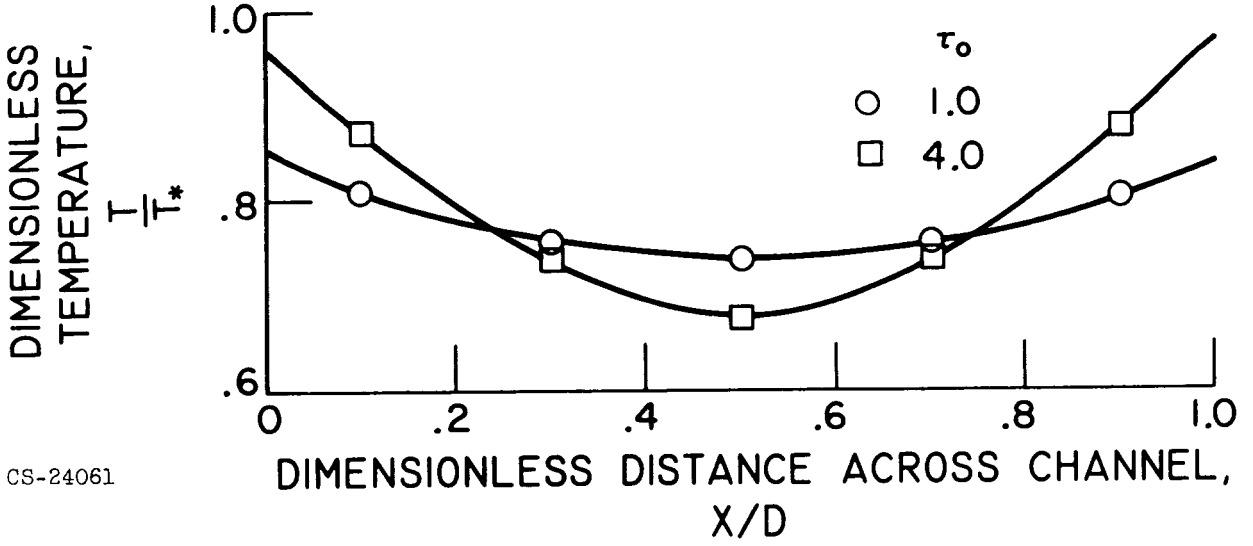

Fig. 6. - Dimensionless transverse temperature profile at channel exit. L/D = 10, T_i/T_* = 0.4, Λ = .65.

EXPERIMENTAL SPECTRAL TRANSMISSIVITY OF CARBON PARTICLE CLOUDS

By Chester D. Lanzo

Lewis Research Center
National Aeronautics and Space Administration
Cleveland, Ohio

INTRODUCTION

Radiation heat transfer is an important consideration at the temperature levels associated with current and advanced nuclear rocket concepts. The primary mode of heat transfer to the hydrogen propellant in a coaxial flow gaseous nuclear rocket is radiation; and since hydrogen is transparent at temperatures below 6000° K, the necessity of seeding with an absorbing material is evident.[1] There are many complex problems attendant to the use of high temperature, seeded hydrogen gas as a propellant, and information necessary to select a proper seed material is unavailable.

To provide a means of initially estimating the required seeding densities in a gaseous reactor, a study of the transmissivity of carbon particle clouds at room temperature was undertaken at Lewis Research Center. The investigation was conducted in two phases. First, spectral transmissivity measurements were made with a spectrophotometer. Then, total transmissivity was determined with a xenon arc source and a total radiation detector. Good agreement was obtained with the two methods, and therefore only the spectral results are presented here.

EXPERIMENT

In all of the tests the seeding powders were dispersed in distilled water to minimize problems caused by particle settling. The absorption contribution of the water was eliminated by comparing each sample transmissivity with that of a reference cell containing only water. Four carbon powders (diameters of 0.08, 0.15, 0.45, and 1.40 microns) were studied to investigate the effect of particle size on transmissivity. Particle sizes were all determined with a Fischer Sub-Seive Sizer.

Spectral transmissivities of the various particles were measured with a Beckman model DK-1 recording spectrophotometer which provided the following features: a quartz monochromater, with a hydrogen or tungsten lamp, and a photomultiplier or lead sulfide detector. Transmissivities were measured over a range of wavelengths from 0.2 to 1.0 microns.

Figure 1 illustrates the system under consideration. Radiant energy of intensity I_o and wavelength λ traverses a particle cloud for a distance l,

and is attenuated to the emerging intensity I. The particle system is defined by N, the number of particles per unit volume of dispersion; the particle density $\bar{\rho}$; and R, the particle radius. The purpose of the measurements is to provide information from which the transmissivity of a seeded medium can be easily estimated.

All of the data are presented in the form of the measured quantity, transmissivity I/I_o. If no radiation is removed from the incoming beam by scattering, then these values are readily transformed into absorptivities. Light scattering by small particles is a complicated process, and is the subject of a number of textbooks. Though a detailed study of scattering is beyond the scope of this study, two items are worthy of note. One point is that the light beam was of small diameter (1/8 in.) compared to that of the sample cell (2 cm, see fig. 1); and the optics of the spectrophotometer used are such that any scattered light emerging from the end face of the cell is intercepted by the detector, and thus does not contribute to any apparent absorption. Secondly, some brief measurements made on a typical dispersion indicate that the attenuation of the incoming beam due to scattering was less than 1 percent. So, it is assumed that scattering is not an important factor for the range of conditions considered here, and that the measured attenuations represent true absorption.

DISCUSSION OF RESULTS

The transmissivity of carbon particle dispersions was measured over a range of wavelengths with a spectrophotometer. The results are shown in figure 2 for a particle diameter of 0.15 micron. The transmissivity of the particles is seen to be essentially independent of wavelength from 0.2 to 1.0 microns. Two sets of measurements are shown, for particle densities of 0.12×10^{-4} and 0.2×10^{-4} grams per cc. Any dependence of transmissivity on wavelength is within the deviation of the data, and the results show that for the conditions of interest here the transmissivity of carbon particles can be considered independent of wavelength.

A procedure of successive dilutions was used to determine the effect of particle concentration on transmissivity. The results for four particle diameters of 0.08, 0.15, 0.45, and 1.40 microns are shown in figure 3. Monochromatic light, wavelength of 0.36 micron, was used, and the path length was 10 cm in all cases. The variation of transmissivity with particle concentration follows the exponential dependency stated by Beer's law:

$$I/I_o = e^{-E\bar{\rho}l}$$

where E is the specific extinction coefficient. The fact that Beer's law is operative suggests that E is a true absorption coefficient, and that a large percentage of scattering is not present.[2]

Although it is advantageous that transmissivity has a simple exponential dependency with concentration, it is not generally useful unless the specific extinction coefficient E is known as a function of particle size. To obtain a correlation for all particle sizes, the data were plotted in terms of an extinction coefficient per particle ϵ/N, obtained from:

$$I/I_o = e^{-\epsilon l}$$

and

$$N = \frac{1}{\frac{4}{3}\pi R^2} \quad \frac{\bar{\rho}}{\rho}$$

where $\bar{\rho}$, N, R, and l are as previously defined, and ρ is the material density, taken to be 1.6 gm/cc for carbon. A value of ϵ was obtained from the slopes of the lines shown in figure 3 for each particle size.

Figure 4 shows ϵ/N as a function of particle radius R. As particle size decreases, it can be shown[3] that ϵ/N should become proportional to $R.^6$ A dashed line with this slope is shown in figure 4, and is in good agreement with the line through the data.

For large particles, it is also possible to anticipate the relation of ϵ/N with particle radius. Here, the absorption mechanism should be physically similar to a "shutter," or blocking effect, and ϵ/N becomes proportional to $R.^2$ A line with this slope is shown in figure 4 to be in good agreement with the data for large radii. It is of interest to note that ϵ/N can be viewed as an absorption cross sectional area, and thus the ratio of ϵ/N to the physical cross sectional area of a particle has significance. This ratio is 0.052 for the smallest particle tested, and progressively increases to a value of 0.91 for the largest. The fact that this ratio approaches unity for large particles is the equivalent to the expected proportionality of ϵ/N to R^2 shown in figure 4.

The applicability of the results shown in figure 4 to a gaseous reactor seeding problem can be exemplified as follows. A typical problem would be to estimate the seeding density required to attenuate a given radiant energy to 5 percent of its initial intensity in a path length of 100 centimeters. Assuming that 1 micron particles are available, figure 4 gives $\epsilon/N = 7.8\times10^{9}$. From the attenuation requirement, $I/I_o = 0.05$, and $\epsilon = 0.0299$ for a path length of 100 cm. Thus the required particle concentration is 3.84×10^{6} particles per cc. For a material density of 1.6 gm/cc, the required seeding density is 3.2×10^{-6} grams per cc.

CONCLUDING REMARKS

It is reasonable to assume that carbon dispersion data obtained at room temperature will not duplicate transmissivities which will occur at elevated temperatures in a gaseous medium such as hydrogen. The purpose here is to establish that reasonable attenuation of radiation is possible for seeding densities which are sufficiently small to be of interest for gaseous reactor applications.

Further, although the measurements presented are related to the seeding problem in a gaseous reactor, carbon particles are not necessarily best for this purpose. Tantalum carbide, for example, has been considered elsewhere,[4] and other materials may ultimately prove to be more useful than the ones investigated to date. In addition to transmissivity, other factors will require consideration; the choice of a seeding agent may be dictated by the minimum partical size attainable with various materials, or by chemical stability in the presence of hydrogen at elevated temperatures.

REFERENCES

1. Weinstein, Herbert, and Ragsdale, Robert G.: A Coaxial Flow Reactor - A Gaseous Nuclear-Rocket Concept. ARS preprint 1518-60, Dec. 1960.

2. Lothian, G. F.: Absorption Spectrophotometry. MacMillan Co., New York, 1958.

3. Charyk, J. V., editor: Physical Measurements in Gas Dynamics and Combustion. Princeton Univ. Press, pp. 289-304, 1954.

4. Spencer, D. F.: Thermal and Criticality Analysis of the Plasma Core Reactor. JPL TR 32-188, Jan. 1962.

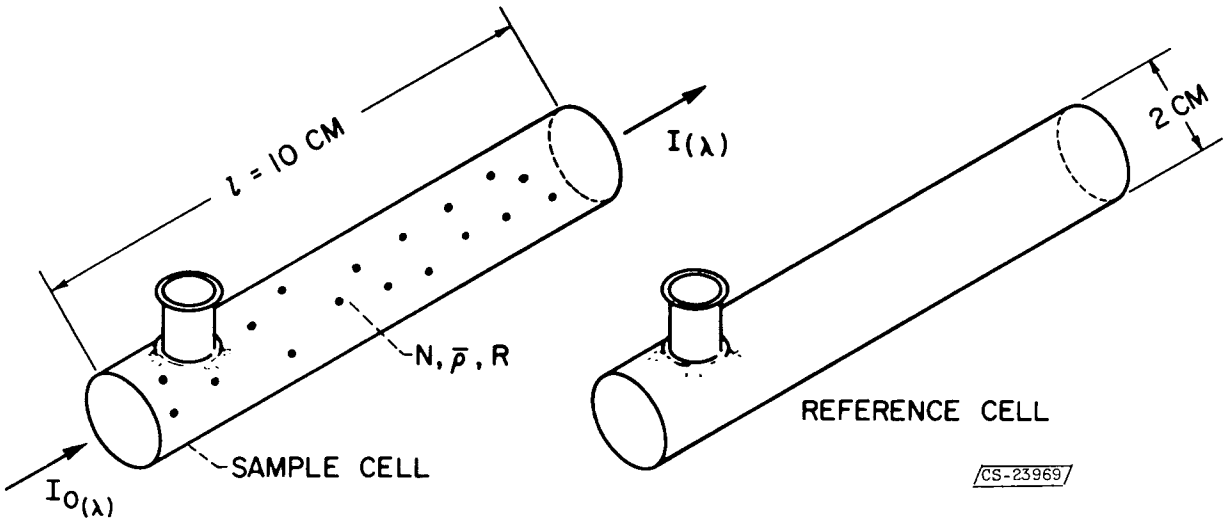

Fig. 1. - Absorption cells, and system under consideration.

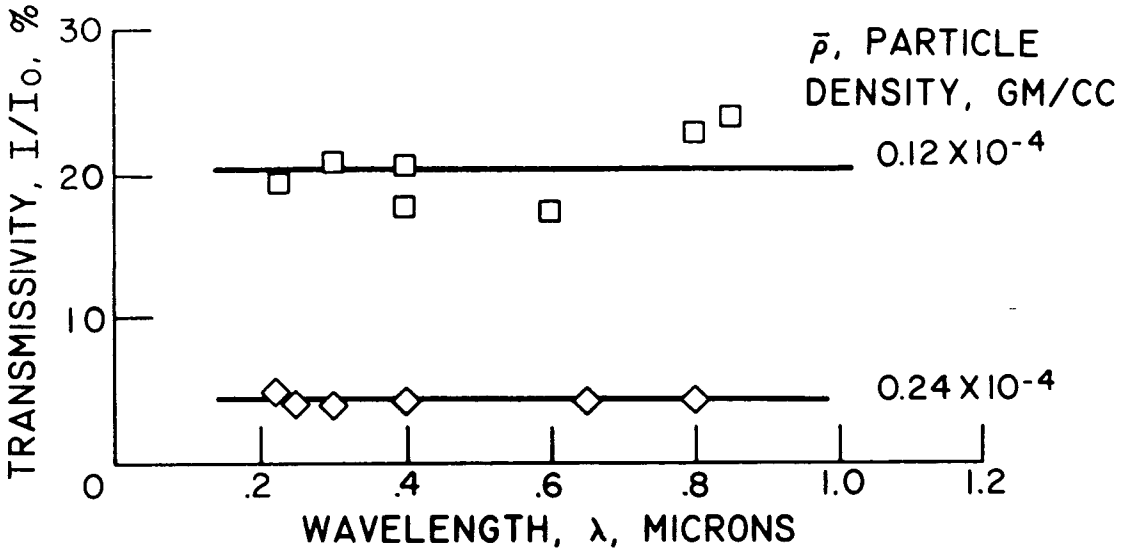

Fig. 2. - Spectral transmissivity of 0.15 micron carbon particles (path length = 10 CM).

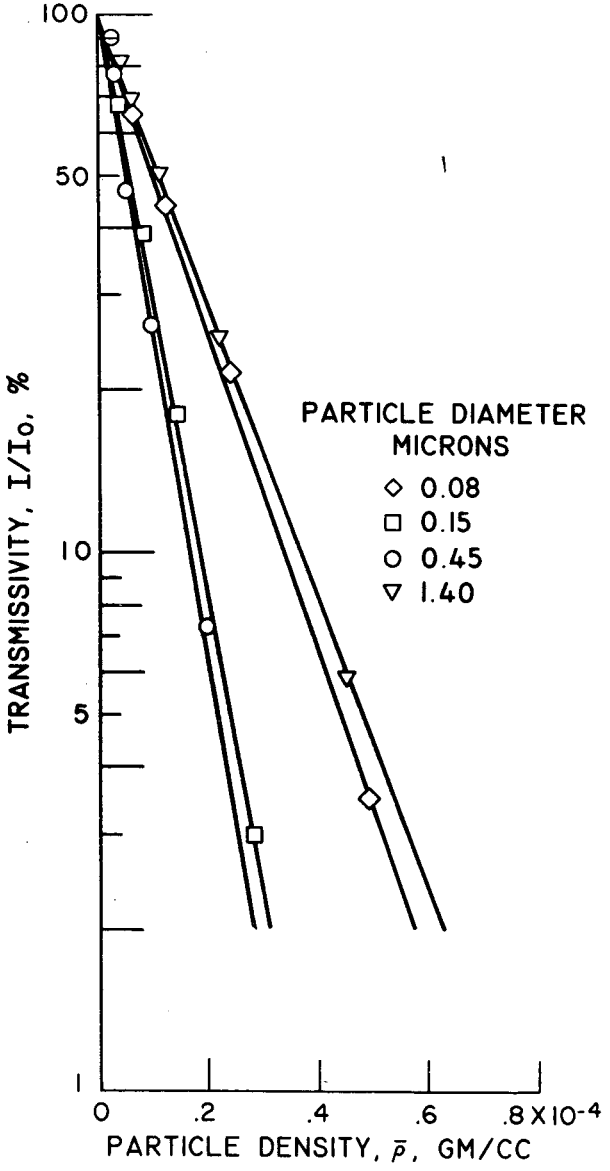

Fig. 3. - Effect of particle density on spectral transmissivity, λ = 0.36 microns.

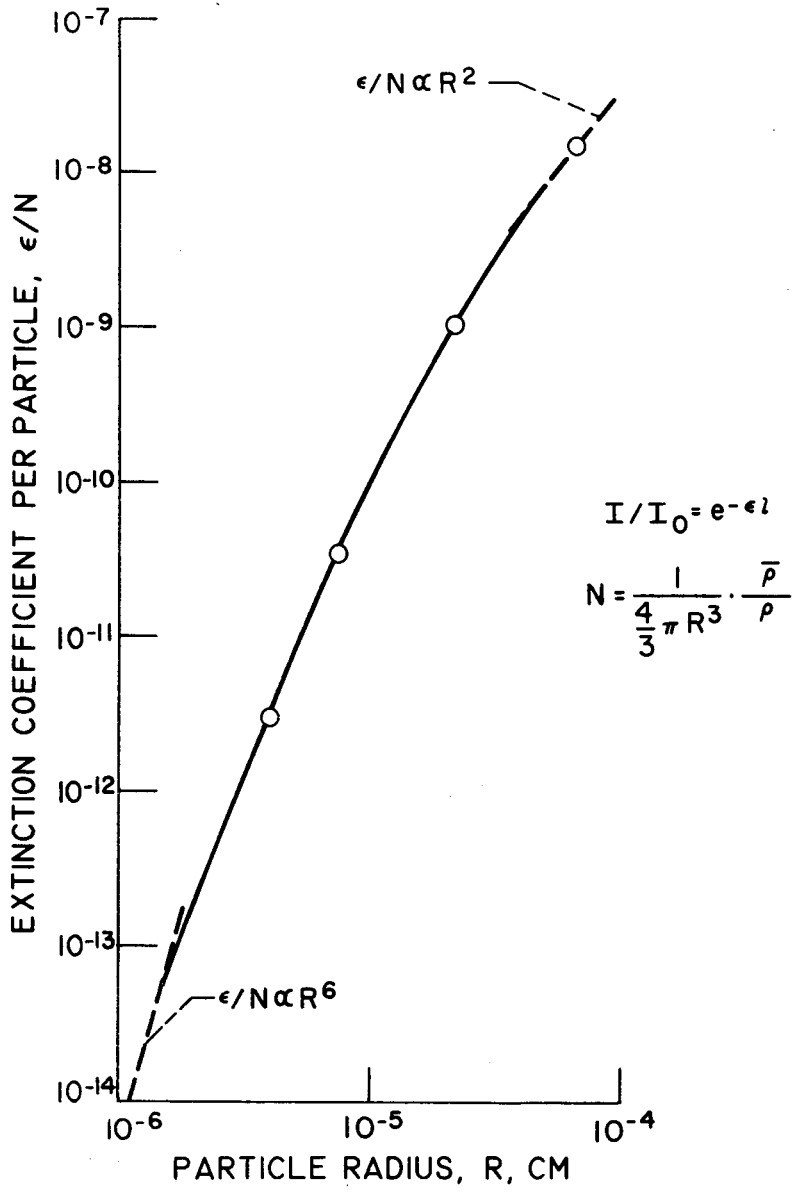

Fig. 4. - Correlation of carbon spectral data.

TWO-DIMENSIONAL DIFFUSION CALCULATIONS ON CO-AXIAL CAVITY REACTORS

By Robert E. Hyland

Lewis Research Center
National Aeronautics and Space Administration
Cleveland, Ohio

Introduction

In the last few years there have been an increasing number of ideas and schemes on the retention of gaseous nuclear fuel in a cavity reactor. Some methods proposed make use of hydrodynamic forces, such as the vortex type discussed by Kerrebrock and Meghreblian[1], and the co-axial flow type described by Weinstein and Ragsdale[2]. Other methods require magnetic forces to contain the fuel in the cavity, such as proposed by Spencer[3] and Nelson[4]. There have been other proposals with variations on these methods. With the exception of the vortex type, one common requirement imposed on the fuel is that it be centrally located, away from the cavity walls. In an arrangement such as this, it is expected that the critical mass requirements will be higher than that of a uniformly filled cavity.

In a previous analysis on spherical geometries[5], this increase in critical mass was indicated as being less than 25 percent for fuel-to-cavity radius ratios down to 0.5, for cavity radii ranging from 70 to 175 cm. In a cylindrical cavity reactor the fuel would be centrally located only with respect to the radius. As shown in figure 1, the fuel region runs the entire length of the cavity. It is anticipated that this would allow a further decrease in the fuel-to-cavity radius ratio without an increase in the critical mass.

Conditions of Analysis

The moderator-reflector region, as shown in figure 1, completely surrounds the cavity. The thickness of this region is maintained at 100 cm for all calculations. Graphite and D_2O were considered as moderator materials; and U^{235} and Pu^{239} as nuclear fuels. The radius of the cavity was varied in a few cases, but for the majority of the computations was held constant at 150 cm, along with a reactor cavity L/D (length-to-diameter) ratio of 1.0.

The cavity radius was chosen on examination of the combined continuity equations for the propellant (hydrogen) and the fuel (uranium or plutonium), expressed as a velocity ratio in a coaxial flow reactor[2]:

$$\frac{u_{H_2}}{u_F} = \frac{(w_{H_2}/w_F)(M_F/M_{H_2})(\overline{T}_{H_2}/\overline{T}_F)}{\left(\frac{1}{r_F/r_{H_2}}\right)^2 - 1}$$

To minimize mixing losses it is assumed that the average velocity ratio must be on the order of 100 or less. With the mass flow, molecular weight, and temperature ratios relatively invariant, the radius ratio r_F/r_{H_2} becomes the dominant factor. Small radius ratios ease the hydrodynamic restrictions on the velocity ratio required, but lead to high operating pressures because of the increase in critical densities. Combining these factors, a value of 150 cm was assumed for a reasonable cavity radius, and 0.17 for a fuel-to-cavity radius ratio. Inasmuch as these are only guesses as to reasonable values, they should not be taken as final or recommended values; they are, however, suitable for discussion here.

To determine the effect of changing radius ratio on criticality, the fuel region radius was varied and critical densities were obtained. The region of the cavity outside of the fuel region contained hydrogen with a density of 0.8×10^{21} atoms/cc. Although diffusion of neutrons in the hydrogen was considered, removal and absorption cross-sections were taken as zero. All of the results presented here were based on calculations of criticality obtained with PDQ02, a two-dimensional reactor code written[6] for the IBM 704. Neutron macroscopic cross sections for the materials were basically obtained by flux weighting cross sections from BNL 325[7]. For the high temperature "thermal" cross sections, the effect of Doppler broadening was taken into account. This was done primarily because of low energy level resonances in plutonium and uranium. For a given geometry the fuel density was varied until a criticality factor of 1.00 was obtained.

Discussion of Results

In general, cavity reactors are considered thermal in the sense that most of the absorptions of neutrons by the fuel occur at thermal energies. In a cavity reactor the neutrons are born in the fuel at high energies and quickly diffuse into the reflector-moderator region. Here they are thermalized and find their way back into the fuel region to be absorbed and start a new generation of neutrons. As the fuel region is decreased in diameter, the probability that returning neutrons will intersect it again is reduced. Therefore, to maintain criticality the ones which do pass through the fuel must have a higher probability of being absorbed. This means that as the fuel radius is decreased, the fuel density must increase. As the fuel density increases, the thermal flux drops off more rapidly through the fuel region. An example of this is shown in figure 2. For three different fuel radii, the flux decreases more rapidly as the fuel radius is decreased, and the fuel density is increased to maintain criticality.

Since the fuel volume is decreasing, an increase in fuel density does not necessarily mean that the critical mass has increased. Several configurations were computed to determine the effect on critical mass as the fuel radius is decreased. This is indicated in figure 3. The lower curve is for a cavity radius of 40 cm, and L/D of 2, and illustrates that, based on diffusion theory,

the fuel region can be reduced in radius by factors of 5 and 6 with no appreciable increase in critical mass.

The remaining curves are for a cavity radius of 150 cm. The dashed line extensions are extrapolations to end points (cavity completely filled with fuel). The end points for the D_2O cases were determined from a buckling analogy[5]. All of the curves for U^{235} indicate that the fuel radius can be reduced by factors of 5 or 6, that is, fuel-to-cavity radius ratios of 0.2 to 0.167, without increasing the critical mass by more than 25 percent. The curve for Pu^{239} fuel indicates a sharp increase in critical mass at a radius ratio of about 0.25, or a factor of 4 in decreased radius. Although this is less of a reduction in fuel radius than afforded by the U^{235}, the critical mass is much less (10 kg compared with 30 kg at 0.4 radius ratio) under the same conditions.

As was previously indicated, a fuel radius of 25 cm appears to be in the region of interest. Maintaining this fuel radius and a cavity radius of 150 cm, several calculations were performed to determine changes in critical mass due to variations in temperature and materials. The results are shown in table I. Case (1), as shown in the table, had U^{235} as the fuel, and D_2O as the moderator (100 cm thick). Since D_2O was used, the neutrons were assumed to be at room temperature (70° F). The critical mass for this case is seen to be 6.3 kg. In the next case, as shown in the diagram with table I, a void region through the D_2O with the same diameter as the fuel region was added to one end to obtain some indication of the effect of an exhaust nozzle; the increase in critical mass was small (5 percent).

In the third case, the D_2O was replaced with graphite. The increase in critical mass from 6.3 to 65 kg is due primarily to the increased absorption in the graphite moderator, as is shown in table II. Therefore, an increase in the thermal temperature to near an operating temperature (approximately 5300° F) should decrease the critical mass. This is shown by the results for case 4. Case 5 was run to determine the effect of replacing U^{235} with Pu^{239}. The indicated result is that the critical mass decreases from 38 to 27 kg.

Table II gives a neutron balance for each case. Since this is a balance of neutrons, and a fixed fraction of neutrons must be absorbed in the fuel, any increase of absorptions in nonfuel regions must be accompanied by a decrease in leakage. One noticeable fact is that even though less fuel is required using Pu^{239}, more neutrons must be absorbed in the fuel. This is due to the larger portion of the neutrons absorbed in the Pu^{239} that do not produce fission neutrons. The decrease in critical mass for Pu^{239} results from the fact that although the probability of a fission per absorption is less than for U^{235}, the probability of an absorption is sufficiently greater to override this effect.

Concluding Remarks

From the two-dimensional calculations performed on cylindrical cavity reactors, it appears that the fuel region can be reduced in radius inside a cavity more than appeared possible from spherical results. The calculations indicate that if graphite is to be required for high temperature use, an increase in critical mass will result, though not as much as would be indicated by the use of room temperature cross sections.

The calculations also show that critical mass can be reduced by using Pu^{239} rather than U^{235}. A single calculation of the effect of a nozzle opening through the reflector-moderator showed only a slight increase in critical mass. Inasmuch as D_2O is a better moderator, it would seem worthwhile to consider a possible combination of D_2O and graphite into a two-region moderator-reflector

with high temperature capability and reduced neutron absorptions. Finally, in view of some of the steep flux gradients in a cavity reactor, it is estimated that transport theory would predict, in certain cases, larger critical masses than diffusion theory; this has been indicated by a few preliminary one-dimensional calculations.

References

1. Kerrebrock, J. L., and Meghreblian, R. V.: Vortex Containment for Gaseous-Fission Rocket. Jour. of the Aerospace Sciences, Vol. 28, no. 9, Sept. 1961.

2. Weinstein, H., and Ragsdale, R. G.: Co-Axial Flow Reactor - A Gaseous Nuclear-Rocket Concept. Preprint 1518-60, ARS, 1960.

3. Spencer, D. F.: The Plasma Core Reactor. Jet Propulsion Lab. Tech. Report No. 32-104, April 1961.

4. Nelson, S. T.: The Plasma Core Reactor. Preprint ARS-ORNL Space Nuclear Conference, Gatlinburg, Tenn., May 1961.

5. Ragsdale, R., and Hyland, R.: Some Nuclear Calculations of U^{235}-D_2O Gaseous-Core Cavity Reactors. NASA TN D-475, Oct., 1961.

6. Bilodeau, G. G., et al.: PDQ-An IBM-704 Code to Solve the Two-Dimensional Few-Group Neutron-Diffusion Equation. WAPD TM-70.

7. Hughes, D. J., and Schwartz, R. B.: Neutron Cross Sections. BNL 325 2nd Edition, July 1958.

TABLE I. - FUEL INVESTMENTS FOR 2-D (R,Z)

DIFFUSION ANALYSIS - CAVITY REACTORS

Case	Refl.	Fuel	Temp.	Nozzle	Critical mass, kg
1	D_2O	U-235	70° F	No	6.3
2	D_2O	U-235	70° F	Yes	6.6
3	C	U-235	70° F	No	65.0
4	C	U-235	5300° F	No	38.0
5	C	Pu-239	5300° F	No	27.0

Refl. thick = 100 cm
Cavity L/D = 1.0
Cavity radius = 150 cm
Fuel radius = 25 cm

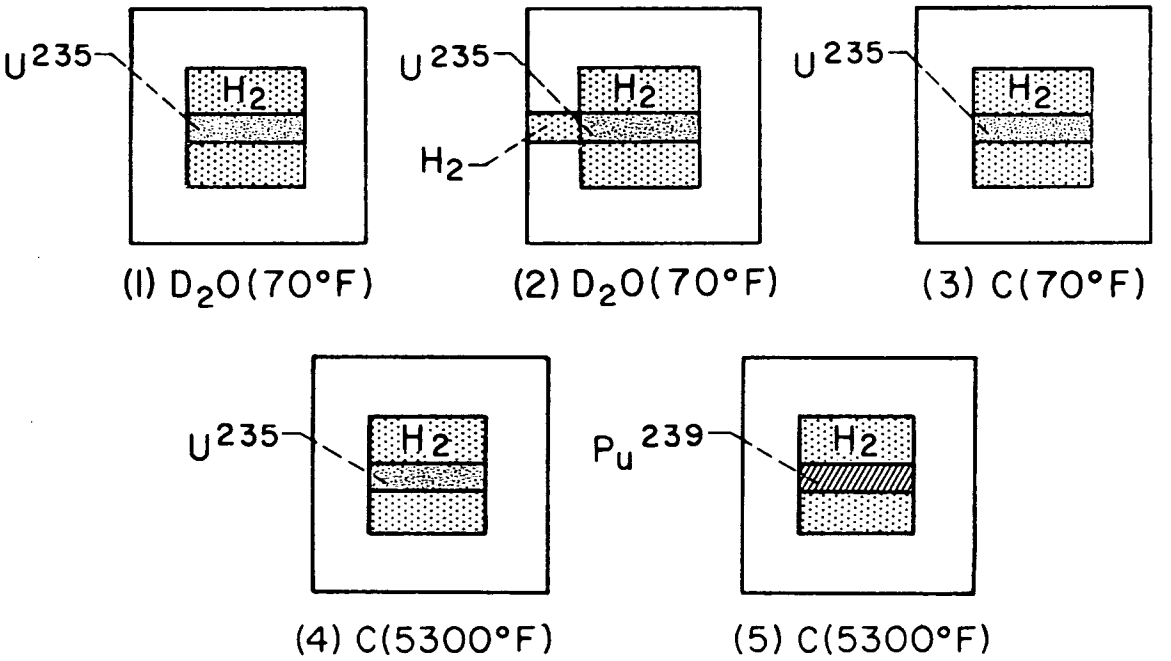

TABLE II. - NEUTRON BALANCES FOR 2-D (R,Z)

DIFFUSION ANALYSIS - CAVITY REACTORS

Case	Refl.	Fuel	Absorptions		Leakage	Total
			Fuel	Nonfuel		
1	D_2O (70° F)	U-235	484	67	449	1000
2*	D_2O (70° F)	U-235	484	63	453	1000
3	C (70° F)	U-235	488	318	194	1000
4	C (5300° F)	U-235	482	144	374	1000
5	C (5300° F)	Pu-239	553	124	323	1000

*With exhaust nozzle.

Refl. thick = 100 cm
Cavity L/D = 1.0
Cavity radius = 150 cm
Fuel radius = 25 cm

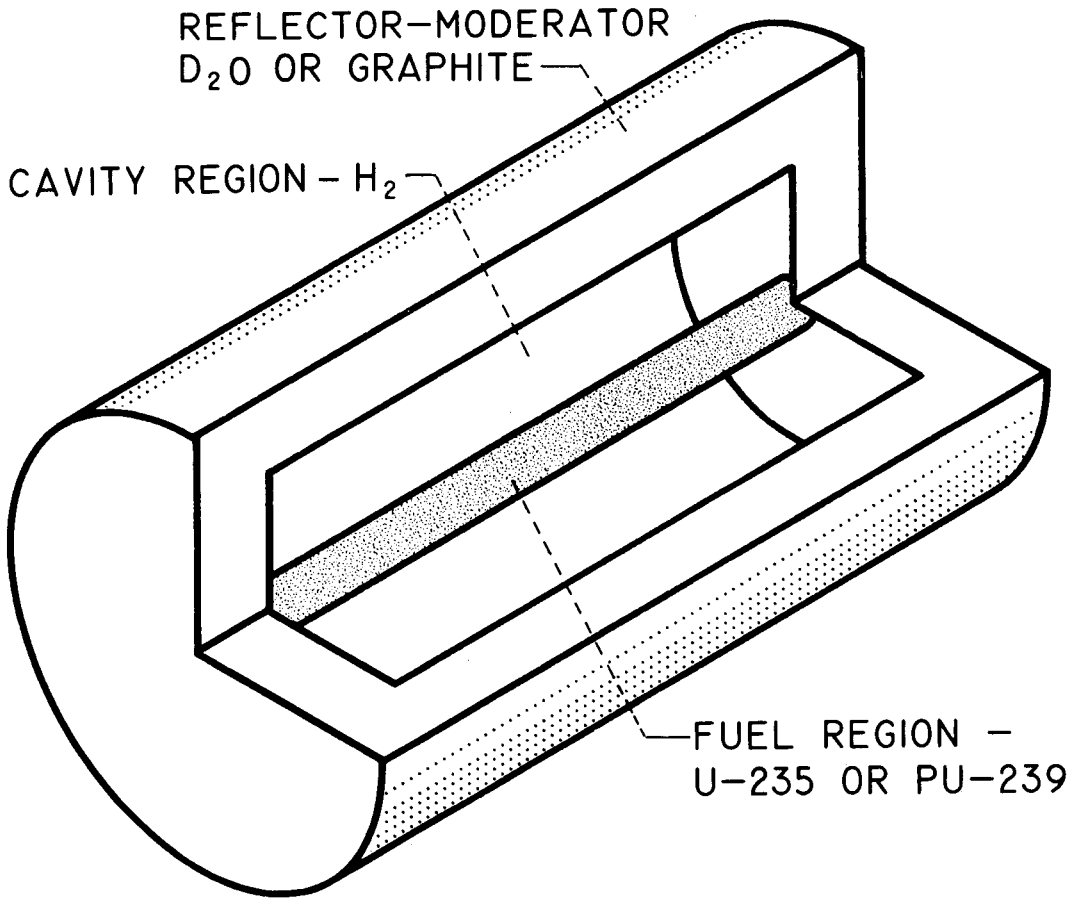

Fig. 1. - 2 dimensional cavity reactor model.

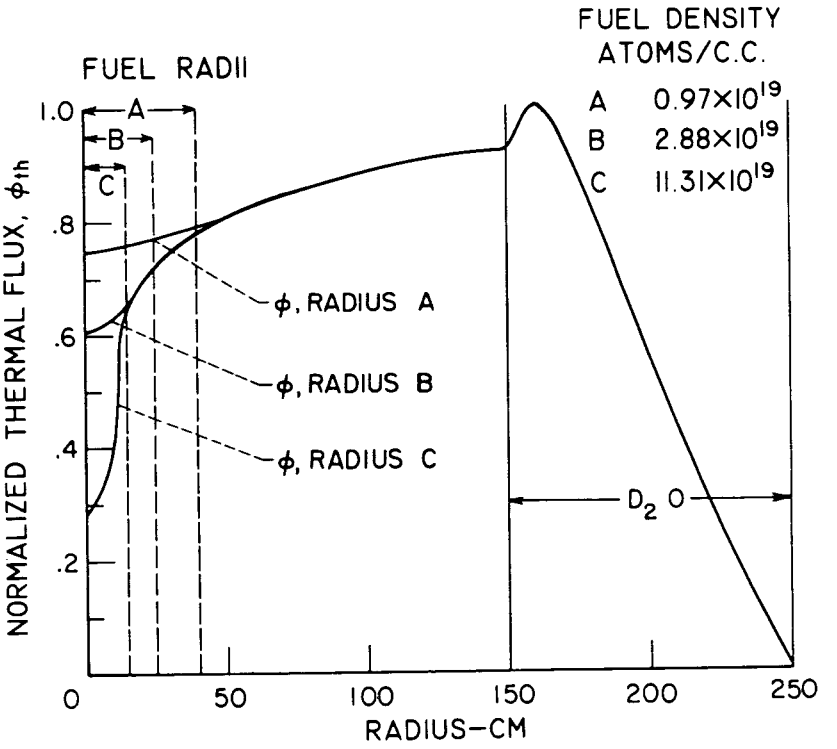

Fig. 2. - Thermal flux effect for reduced fuel (U^{235}) radii. (Cavity L/D = 1.0, K_{eff} = 1.0.)

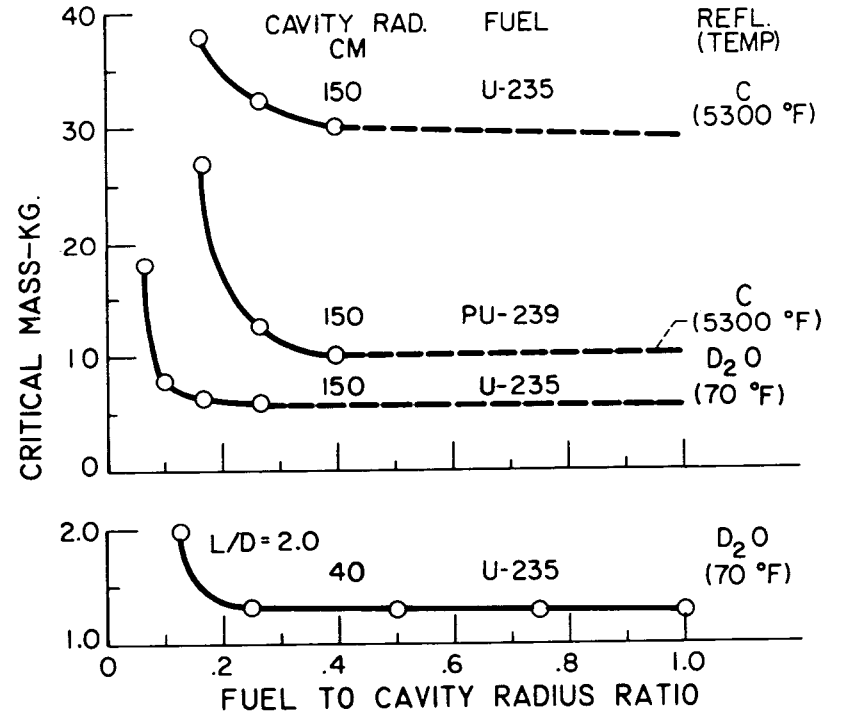

Fig. 3. - Decreased fuel radius effect on critical mass of cyl. cavity reactors. 2-D (R,Z) PDQ02 results K_{eff} = 1.00, L/D = 1.0, reflector thickness = 100 CM.

NASA RESEARCH ON THE COAXIAL FLOW GASEOUS NUCLEAR ROCKET

By Robert G. Ragsdale and Frank E. Rom

Lewis Research Center
National Aeronautics and Space Administration
Cleveland, Ohio

The Concept

An increasing amount of attention in recent years has been directed to a nuclear rocket engine which would employ both the propellant and fuel in a gaseous state.[1,2,3,4] Though the problems imposed by fuel containment are severe, the performance potential associated with specific impulses up to 3000 seconds and thrust-to-reactor-weight ratios on the order of one is sufficient to warrant the current effort. This paper will describe the gaseous reactor concept and the associated research program underway at Lewis Research Center.

The coaxial flow gaseous reactor is illustrated in figure 1. The essence of this scheme is that the nuclear fuel gas is injected into the reactor cavity at a much lower velocity (on the order of 1/100) than that of the surrounding hydrogen propellant. The hydrogen is heated to temperatures beyond materials limits by thermal radiation from the fissioning fuel. The containment criterion is satisfied if the initial velocity deficit provides a fuel residence time that is sufficiently (100 times) larger than that of the propellant. As in any gaseous reactor device, the primary problems are hydrodynamics, heat transfer, and nucleonics.

Problem Areas

Diffusion of the nuclear fuel into the faster moving hydrogen stream reduces the average fuel density in the reactor cavity. Acceleration of the inner stream by momentum transfer also reduces the fuel concentration. The fuel density can be increased by raising the operating pressure in the reactor, but there is obviously a limit on this. It is the purpose of the hydrodynamic analysis to describe the mass and momentum transfer process, and to predict to what extent the inner stream will be "swept out" of the reactor. Room temperature studies of an air-bromine coaxial flow set-up yield useful information to check the analysis, and provide a means of empirically extending it to include the turbulent flow regime.

Elementary considerations show that the primary mode of energy transfer from the fuel region is thermal radiation.[3] This radiation must be attenuated by the propellant gas, and not reach the reactor cavity walls. Since hydrogen at the maximum permissible wall temperature, say 5000° R, is transparent, the necessity of seeding the inlet propellant is apparent.[3] A solid particle seed

material, such as graphite dust, might be adequate up to its melting temperature of 6800° R. Hydrogen itself will begin to attenuate the radiation at temperatures above 12,000° R. The intermediate temperature region probably represents the most difficult, and relatively unexplored, heat transfer problem. An initial step in this direction has been to determine the transmissivity of clouds of small particles as a function of wavelength, particle density, diameter, and material at room temperature. A second approach has been to analytically study the temperature profiles which will exist in an absorbing, re-emitting, conducting propellant as it flows through a coaxial reactor.

Nuclear calculations are necessary to determine the effect of geometry and materials on reactor criticality. The primary geometric characteristic of interest is that the fuel region is considerably withdrawn into the reactor cavity. Other nucleonic information required is the effect on critical mass of: (1) moderator thickness, temperature, and materials; (2) an exhaust nozzle opening; (3) a fuel region temperature that is higher than that of the moderator region; (4) the fuel material; and (5) the presence of hydrogen gas between the fuel and moderator regions. Such effects have been investigated with a two-dimensional, four-group diffusion program.

Performance Capability

Initial results of the above studies are combined here to provide a consistent "reference case" for the coaxial flow nuclear rocket concept. It must be emphasized that this example calculation in no way represents either the best, or the most probable performance. It is simply one that is consistent with the best information we have to date on hydrodynamic containment, heat transfer, and nucleonics. The following table summarizes the important dimensions and other powerplant characteristics using Pu-239 as the fuel:

Dimensions:	
Cavity length	10 ft
Cavity diameter	10 ft
Fuel core diameter	2 ft
Moderator-reflector thickness	3.3 ft
Over-all reactor length	16.6 ft
Over-all reactor diameter	16.6 ft
Flow Conditions:	
Fuel core velocity (average)	0.2 ft/sec
Fuel core Reynolds number	1800
Hydrogen velocity (average)	17 ft/sec
Propellant-to-fuel velocity ratio (initial)	158
Propellant-to-fuel mass flow ratio	57
Cavity pressure (fuel 100 percent singly ionized)	2200 psia
Weight-percent carbon particles in propellant	1 percent
Temperatures:	
Fuel region (average)	20,000° R
Hydrogen region (average)	10,000° R
Inner moderator (graphite)	5,000° R
Outer moderator (D_2O)	70° R
Performance:	
Specific impulse	2500 sec
Thrust	98,000 lb
Weight (moderator)	154,000 lb
Thrust-to-weight ratio	0.64

Because the specific impulse is higher, but the powerplant thrust-to-weight ratio is less, it is not immediately apparent if the coaxial flow system yields improved performance over that of an advanced solid-core nuclear rocket with a specific impulse of 1000 seconds and a thrust-to-weight ratio of 30. Figure 2, obtained from information given in reference 5, allows such a comparison for a typical interplanetary mission. The curves in figure 2 show the required specific impulse as a function of thrust-to-weight ratio to accomplish the mission with an equal or lighter weight vehicle. The gross weight of the coaxial flow reference vehicle given here is seen to be approximately 65 percent of that required by a solid core nuclear rocket.

An alternate, and perhaps more striking, advantage of a high impulse gas-core system is shown in figure 3.[5] Here the total trip time is shown as a function of specific impulse for an initial vehicle of 1.7×10^6 pounds in an Earth orbit. The required trip time of a coaxial flow gaseous rocket is 160 to 200 days, a considerable gain over the 460 day requirement of a solid-core nuclear system. A secondary, but important, advantage of shorter trip time capability is the resulting increased flexibility in choice of depart and return times.

In view of the complex interdependency of nuclear, hydrodynamic, and heat transfer characteristics, the calculation presented here is at best an estimate. It does, however, illustrate the extremely attractive performance potential of a coaxial flow nuclear rocket. Much work has been done to date on the various aspects of this concept. Much more remains to be done.

References

1. Ragsdale, Robert G.: NASA Research on the Hydrodynamics of the Gaseous Vortex Reactor. NASA TN D-288, Sept. 1960.

2. Kerrebrock, Jack L., and Meghreblian, Robert V.: Vortex Containment for the Gaseous-Fission Rocket. JPL TR 34-205, Sept. 1961.

3. Weinstein, Herbert, and Ragsdale, Robert G.: A Coaxial Flow Reactor - A Gaseous Nuclear-Rocket Concept. ARS preprint 1518-60, Dec. 1960.

4. Spencer, D. F.: Thermal and Criticality Analysis of the Plasma Core Reactor. JPL TR 32-188, Jan. 1962.

5. Himmel, S. C., et al.: Nuclear-Rocket Vehicles for Mars and Venus Missions. Presented at ARS/ORNL Space-Nuclear Conference, May 3-5, 1961, Gatlinburg, Tenn.

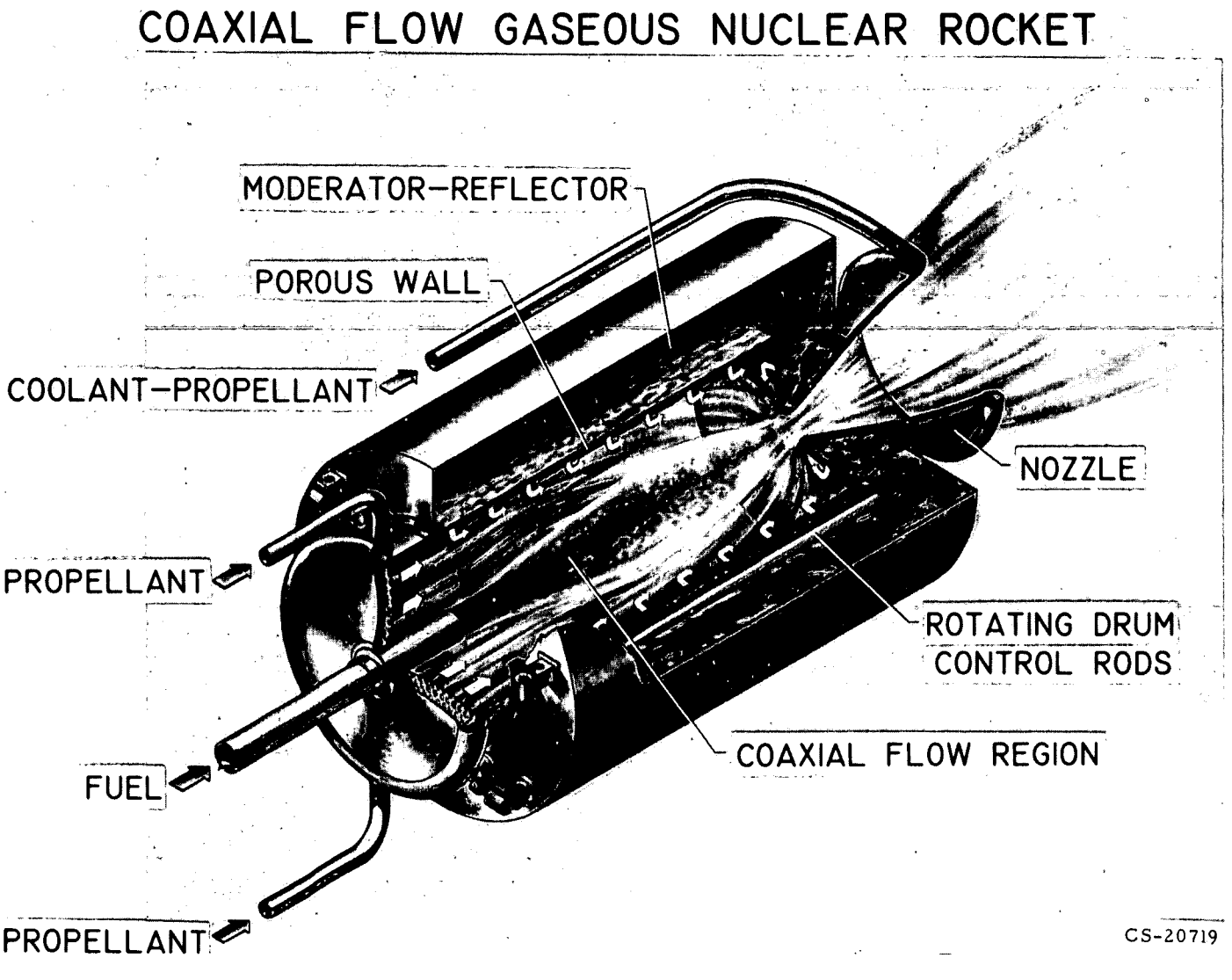

Figure 1 Coaxial flow gaseous nuclear rocket.

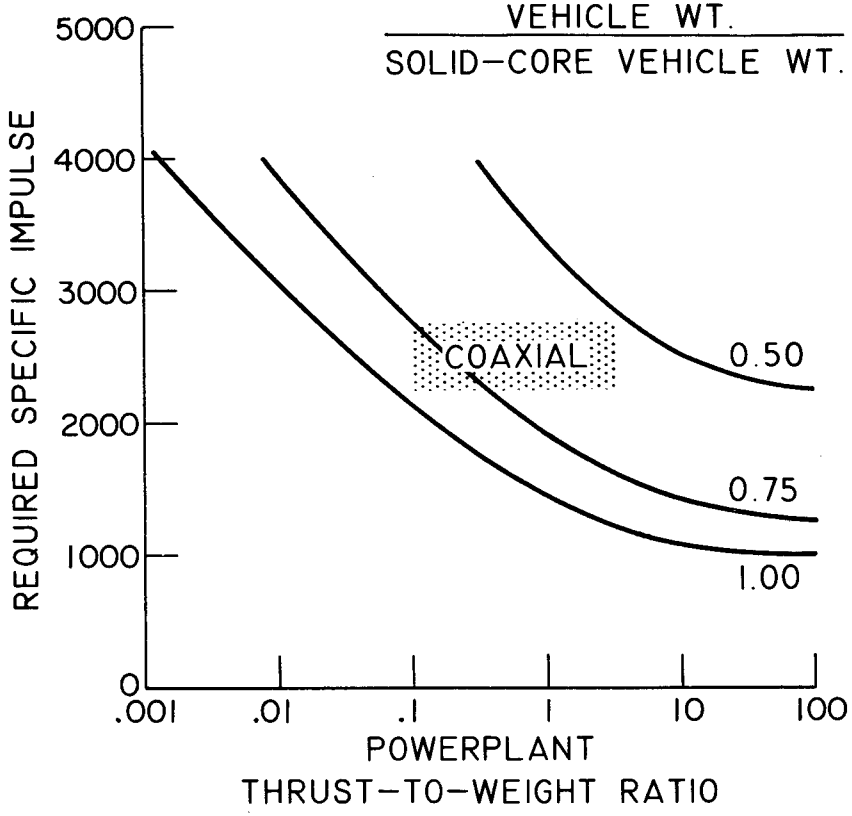

Fig. 2. - Effect of powerplant thrust-to-weight ratio on specific impulse required to equal or better the performance of a vehicle powered with an advanced solid-core nuclear rocket powerplant with a specific impulse of 1000 sec. 7-man, 460d venus mission (taken from ref. 5).

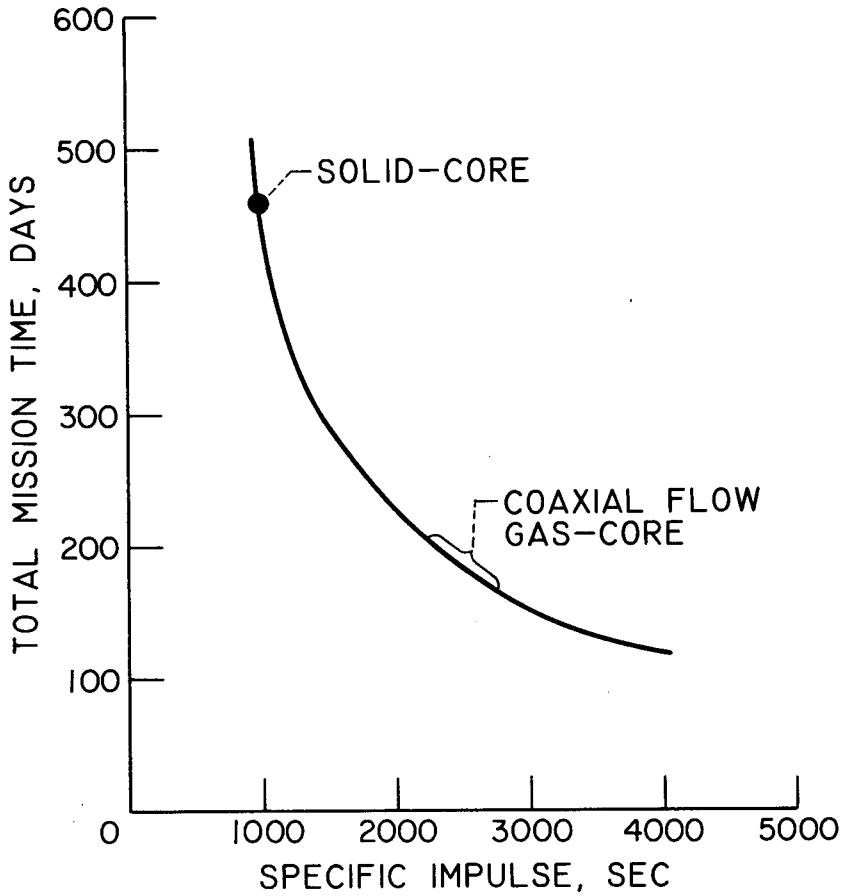

Fig. 3. - Effect of specific impulse on mission time. 7-man venus mission; initial weight in orbit, 1.7×10^6 pounds; thrust per powerplant weight $>10^{-1}$ (taken from ref. 5).

Choking Two-Phase Flow of Hydrogen: Some Idealized Solutions

R. V. Smith
Cryogenic Engineering Laboratory
National Bureau of Standards
Boulder, Colorado

Two-phase, single-component flow is more complex than single phase flow because of the additional degrees of freedom of mass, momentum and energy transport between the phases; these lead to many possible flow patterns. Methods for determining these patterns do not yet exist, and therefore the accurate prediction of the behavior of two-phase flow systems cannot be made. The work presented in this report considers extreme-model flow cases, intended to bracket the actual choking flow values which will occur.

To determine the choking condition this paper analyzes three models of saturated, two-phase fluid flow: (see Figure 1). (IA1) The two-phases are sufficiently mixed to be considered homogeneous, and adequate time is available so that thermal equilibrium exists in the fluid throughout the process. This is called the homogeneous, thermal equilibrium model. (IA2) The two phases are homogeneous and are at the same pressure and temperature but there has been insufficient time for any mass transfer between the phases. This is called the homogeneous, metastable model. (IB) The two phases flow separately and unmixed, but uniform temperature is assumed at each point. Maximum flow is assumed to occur when the vapor reaches sonic velocity. This is called the separated-phase, vapor-choking model. Figure 1 also shows models for the isentropic and Fanno flow processes considered in this paper, and the analytical expressions from which all the equations used in preparing Figures 3 through 6 were developed. No general solution charts such as Figure 6 for Case IIA are shown for Cases IIB and IIC, however, a complete set of solutions for all flow cases will be presented in a subsequent National Bureau of Standards Publication. Some flow situations where upstream, rather than choking point, data are given may be handled by Figures 3, 4 and 5 as shown in Example 1. For Fanno flow, if p_s is known, or can be determined, Figure 6 provides for a rapid determination of choking flow data.

In Figure 2 the results of the analyses are compared with test results of various investigators in order to show the general regions of utility of the various models. From Figure 2, for higher qualities, the vapor choking model is seen to generally predict the experimental results from adiabatic. constant-flow area systems.[10, 11, 13, 17]* The homogeneous, thermal equilibrium and the homogeneous, metastable models tend to bracket the experimental results of low quality, adiabatic systems using short tubes, nozzles, small clearances.[6, 7, 8, 9, 12, 15, 16] Three points from a system in which heat was added are also shown.[14] The results from the ideal models may also be useful in correlating the results of systems where the flow patterns deviate appreciably from the patterns assumed.

For a general design guide, the homogeneous models will most closely fit situations where the system promotes mixing (valves, elbows, small clearances) and where the quality (vapor fraction) is low. Conversely, the separated model may predict the behavior where the flow is relatively undisturbed (constant area flow, venturi or nozzle flow) and where the quality is high.

The homogeneous, metastable model is designed to describe the cases where the time necessary for vaporization is limited. For example, this would be the case where the quality is low and the interface area available for required vaporization to produce thermal equilibrium is small.

Example 1:

> It is desired to determine the choking flow rate for liquid and vapor hydrogen flowing through a short nozzle. The fluid enters the nozzle with a quality of 0.01 and a pressure of 1.84 atmospheres. Discharge pressure of the H_2 is one atmosphere.

* Numbers in brackets indicate references at the end of the paper.

Solution:

Since the quality at choking will be low, the homogeneous model solutions will be used. G_c values will be determined for three cases:

(1) Thermal equilibrium in the flow, thermal equilibrium at choking, Case IIB1a, Figure 1.

(2) Thermal equilibrium in the flow, metastable choking. This case is a mixture of Case IIB1a and IIB1b shown in Figure 1. The case presumes the pressure drop may be slow enough in the flow to the choking point to maintain equilibrium, but at the high choking point velocity, metastable conditions will prevail.

(3) Metastable flow, metastable choking, Case IIB1b, Figure 1.

Case (1)

The first step is to determine a p_s value for this system. This is done by making an imaginary extension of the flow section upstream to the point where the fluid is a saturated liquid. Assuming p_s = 2 atm., from Figure 5, (isentropic flow) $\frac{p_s - p}{p_s}$ = 0.08 for nozzle entrance conditions. Solving this expression for p_s shows that the initial assumption of p_s = 2 atm. is correct.

Again, from Figure 5, for p_s = 2 atm. and p = 1 atm., x = 0.058. Then, from Figure 3,

$$G_{c(HO)(TH)} = 112 \ \frac{\text{grams}}{\text{cm}^2 - \text{sec}}$$

Case (2)

Figure 2 for p_c = 1 atm and x_c = 0.058 shows

$$G_{c(MET)(TH)} = 1.4 \, G_{c(HO)(TH)}$$

then

$$G_{c(HO)(MET)} = 156 \frac{\text{grams}}{\text{cm}^2 - \text{sec}}$$

Case (3)

Metastable flow indicates no quality change in flow, so from Figure 3, for $p_c = 1$ atm and $x_c = 0.01$, $G_{c(HO)(TH)} = 135 \frac{\text{grams}}{\text{cm}^2 - \text{sec}}$ and from Figure 2, $G_{c(HO)(MET)} = 2.72\, G_{c(HO)(TH)} = 370 \frac{\text{grams}}{\text{cm}^2 - \text{sec}}$.

Results of previous investigations would indicate the actual G_c value will be between the values obtained for Case (2) and Case (3) above. Case (1) should represent an extreme lower limit for a value of G_c.

Example 2:

Hydrogen is flowing adiabatically through a tube such that saturated liquid conditions are reached when $p_s = 2$ atm.

a) If the tube length is 125 cm. the two phase friction factor is estimated at 0.01 and the tube diameter is 2.5 cm. What is the maximum discharge pressure at which choking will occur?

b) What is the maximum discharge rate?

Solution:

a) $$\frac{fL_{tp}}{D} = \frac{0.01 \times 125}{2.5}$$

$$= 0.5$$

From Figure 6

$p_c/p_s = 0.745$

$p_c = 1.48$ atm.

b) Then

$$G_c = 168 \frac{\text{grams}}{\text{cm}^2 - \text{sec}}.$$

It should be recognized that these values are obtained from homo-

geneous, thermal equilibrium models for a low quality at discharge ($x = 0.025$ from Figure 4). Assuming metastability at choking with $x = 0.025$ Figure 2 shows $G_{c(HO)(MET)} = 350 \frac{\text{grams}}{\text{cm}^2 - \text{sec}}$. This would generally represent the upper limit for G_c.

Example 3:

> Hydrogen with a quality of 0.8 is discharging through an orifice-like opening. The pressure of the hydrogen at discharge is one atmosphere. What is the maximum mass flow rate?

Solution:

For high quality, the results from the separated-phase vapor-choking model will be determined. For a short flow section we will assume metastable flow. Therefore the quality at discharge will be 0.8 also.

From Figure 3

$$G_{c(HO)(TH)} = 47 \frac{\text{grams}}{\text{cm}^2 - \text{sec}} .$$

Then from Figure 2

$$G_{c(VC)} = 1.13 - G_{c(HO)(TH)}$$

$$= 53.2 \frac{\text{grams}}{\text{cm}^2 - \text{sec}} .$$

Since this flow case would probably involve a vena contracta, the actual flow area in the G_c value should be determined by multiplying the exit for minimum flow area by an appropriate coefficient of discharge.

Bibliography

Analytical Expressions

[1] Holtzman, D., Unpublished Report. Aerojet-General Corp., Azusa, Calif.

[2] Karplus, H. B. "The Velocity of Sound in a Liquid Containing Gas Bubbles" Armour Research Foundation Report 4132-12.

[3] Martinelli, R. C. and Nelson, D. B. "Prediction of Pressure Drop During Forced Circulation Boiling of Water" Trans ASME, 70 695 (1948).

[4] Sajben, M. "Adiabatic Flow of Flashing Liquids in Pipes" Trans ASME J. of Basic Eng. 83, 619-631 (1961).

[5] Tangren, R. F., Dodge, C. H. and Seifert, H. S. "Compressibility Effects in Two Phase Flow" J. of Applied Phys. 20 7, 637-645 (1949).

Experimental Results

[6] Agnostinelli, A. and Salemann, V. "Prediction of Flashing Water Flow Through Fine Annular Clearances" Trans. ASME 80, 1138-42 (1958).

[7] Bailey, J. F. "Metastable Flow of Saturated Water" Trans. ASME 73, 1109-16 (1951).

[8] Benjamin, M. W. and Miller, J. G. "The Flow of Flashing Mixtures of Water and Steam through Pipes" Trans. ASME 64, 657-99 (1942).

[9] Burnell, J. G. "The Flow of Boiling Water through Nozzles, Orifices and Pipes" Engineering 164, 572-76 (1947).

[10] Faletti, D. W. "Two Phase Critical Flow of Steam-Water Mixtures" Ph. D. Thesis, University of Washington, (1959).

[11] Fauske, H. "Critical, Two-Phase, Steam-Water Flows" Proceedings of the 1961 Heat Transfer and Fluid Mechanics Institute, R. C. Binder et al. (Ed.), Stanford University Press.

[12] Hesson, J. L. and Peck, R. E. "Flow of Two-Phase Carbon Dioxide Through Orifices" A. I. Ch. E. J., 207-10 (1958).

[13] Isbin, H. S., Moy, J. E. and Cruz, A. J. R. "Two-Phase, Steam-Water, Critical Flow" A. I. Ch. E. J. 3, 361-65 (1957).

[14] Leppert, G. Jacob, M., Reynolds, J. B. "Pressure Drop During Forced Circulation Boiling" Heat Transfer Symposium, A. I. Ch. E., (1955).

[15] Linning, D. L. "The Adiabatic Flow of Evaporating Fluids in Pipes of Uniform Bore" Proc. Inst. Mech. Eng. 1B, 64-75 (1952-53).

[16] Silver, R. S. and Mitchell, J. A. "Discharge of Saturated Water Through Nozzles" Trans. North East Coast Inst. Eng. and Shipbuilders" 62, (1945-46).

[17] Zaludek, F. R. "The Low Pressure Critical Discharge of Steam-Water Mixtures from Pipes" HW-68934REV Hanford Lab., Richland, Wash.

Fluid Properties

[18] Coremans, J. M. J., Van Itterbeck, H., Beenakker, J. J. M., Knapp, H. F. P. and Zandenbergen, P., Physica 24, (1958).

[19] Friedman, A. S., National Bureau of Standards, Washington, D. C., unpublished (1954).

[20] Mullins, J. C., Ziegler, W. T. and Kirk, B. S. Tech. Rep. No. 1 Project No. A-593 Eng. Expr. Sta. Geo. Inst. of Tech. (1961).

[21] Roder, H. M., Goodwin, R. D. NBS Tech. Note 130, PB 161631 (1962).

[22] Van Itterbeck, A., Van Dael, W. and Cops, A. Physics 27 (1961).

Notation

a	=	acoustic velocity
A	=	total flow-cross-section area
D	=	pipe diameter
f	=	friction factor
G	=	mass flow flux, $\dot{m}/A$
h	=	enthalpy
ℓ	=	any length in direction of flow
L	=	total or specific length in direction of flow
$\dot{m}$	=	mass rate of flow
p	=	pressure
s	=	entropy
u	=	velocity
v	=	specific volume
x	=	ratio of vapor weight to mixture weight
ρ	=	density $(\frac{1}{v})$
μ	=	viscosity

Subscripts

1	=	inlet flow condition
c	=	critical (mass-limiting) conditions
f	=	liquid
g	=	vapor
fg	=	difference between vapor value & liquid value i.e. $v_{fg} = v_g - v_f$
(HO)(TH)	=	value obtained by use of a homogeneous, thermal equilibrium model
(HO)(MET)	=	value obtained by use of a homogeneous, metastable model
o	=	stagnation value
s	=	saturated liquid point in the flow system or isentropic process
tp	=	two-phase
(VC)	=	value obtained by use of a separated phase, vapor choking model

ANALYTICAL EXPRESSIONS

CHOKING:

$$a = \left(\frac{\partial P}{\partial \rho}\right)_s \quad (1)$$

$$G_c = \frac{\dot{m}_c}{A} = -\left(\frac{\partial P}{\partial v}\right)_s \quad (2)$$

FLOW:

ASSUMPTIONS

One dimensional, Adiabatic, Steady state, Horizontal

MOMENTUM

$$u\,du + v\,dp + \frac{fu^2}{2D}\,d\ell = 0 \quad (3)$$

CONTINUITY

$$\dot{m} = \frac{Au}{v} \quad (4)$$

ENERGY

$$h_0 = h + \frac{u^2}{2} = \text{constant} \quad (5)$$

FLUID PROPERTIES

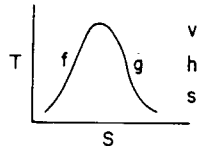

$$\left.\begin{aligned} v &= v_f + x v_{fg} \\ h &= h_f + x h_{fg} \\ s &= s_f + x s_{fg} \end{aligned}\right\} \quad (6)$$

MODELS

I. CHOKING:

A. HOMOGENEOUS
1. Thermal equilibrium
2. Metastable

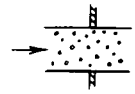

B. SEPARATED PHASE VAPOR CHOKING

II. FLOW:

A. FANNO
1. Homogeneous Thermal equilibrium

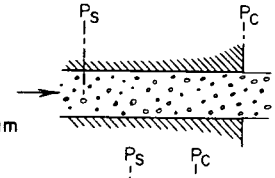

B. ISENTROPIC
1. Homogeneous
a. Thermal equilibrium
b. Metastable

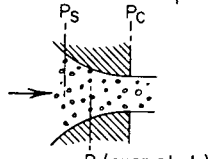

C. SEPARATED PHASE VAPOR CHOKING

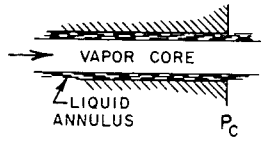

Figure 1. Analytical expression and model summary.

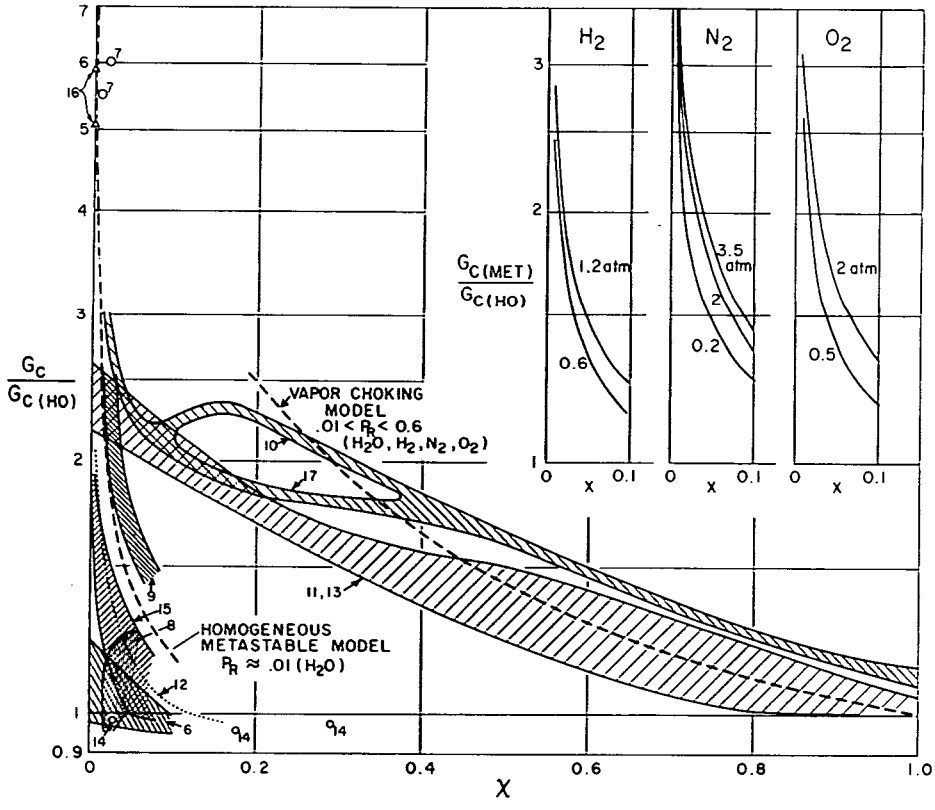

Figure 2. A summary of experimental, two-phase, choking studies with curves from the idealized solutions of this paper. Numbers indicate references in the bibliography. P_R = reduced pressure.

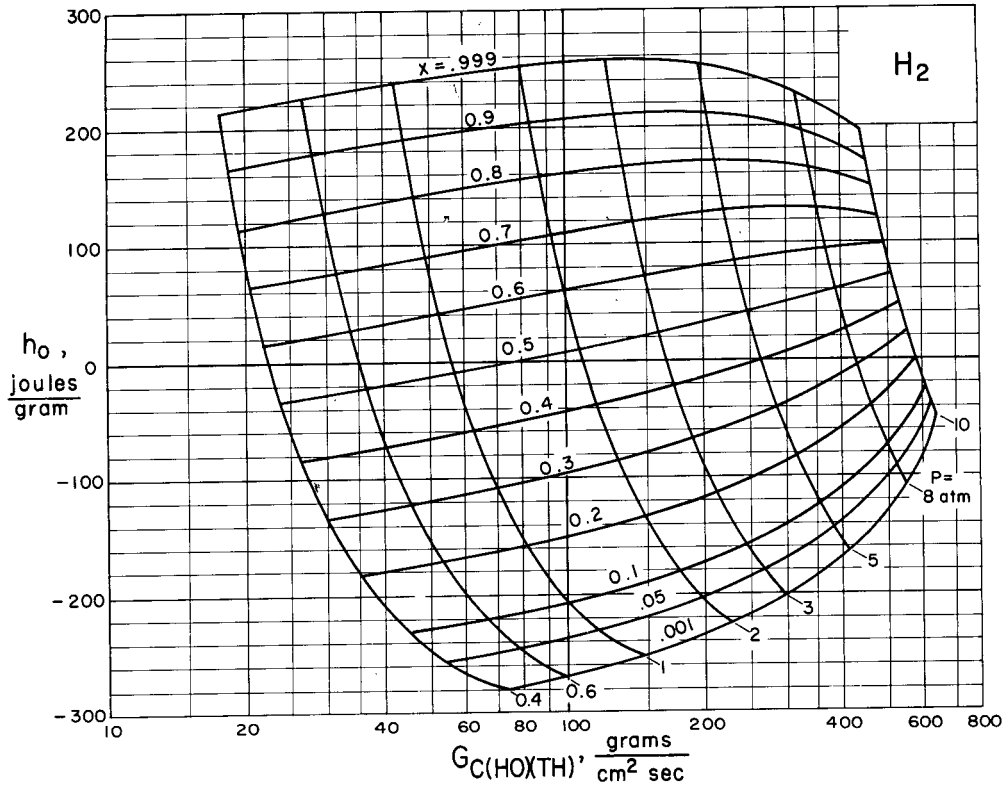

Figure 3. Mass-limiting flow predictions at the point of choking for H_2; homogeneous, thermal equilibrium model, Case IA1, Figure 1.

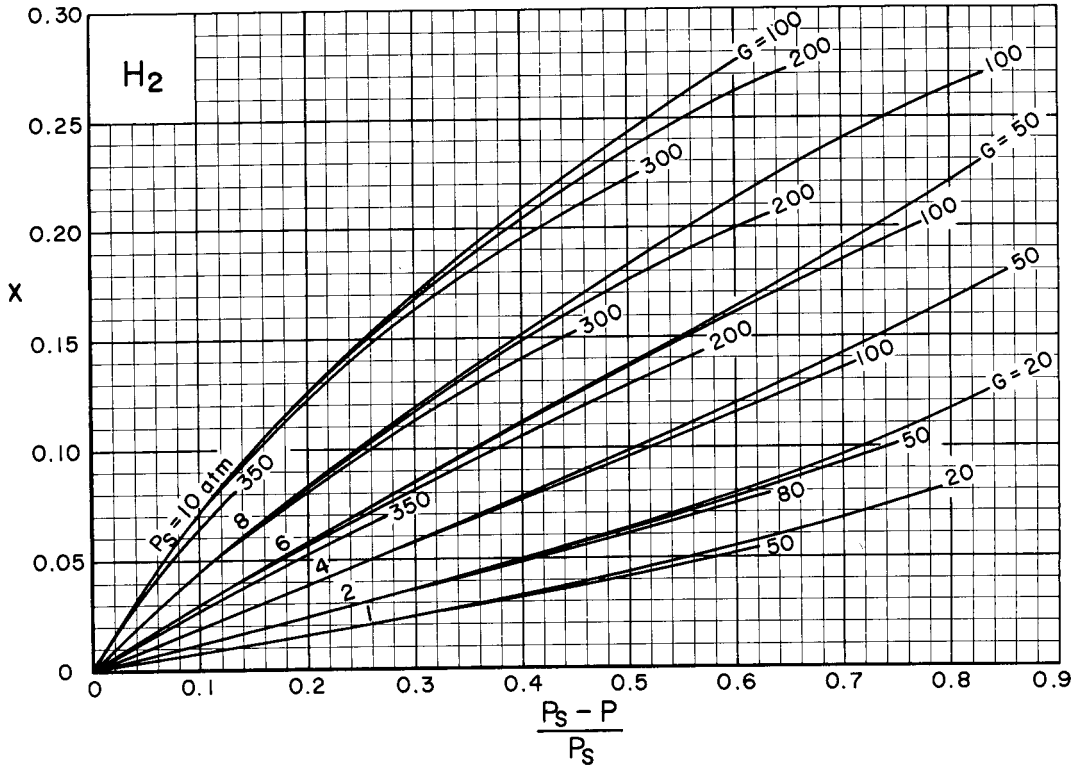

Figure 4. Quality as a function of pressure for a constant-area flow of H_2; homogeneous, thermal equilibrium model, Case IIA1, Figure 1.

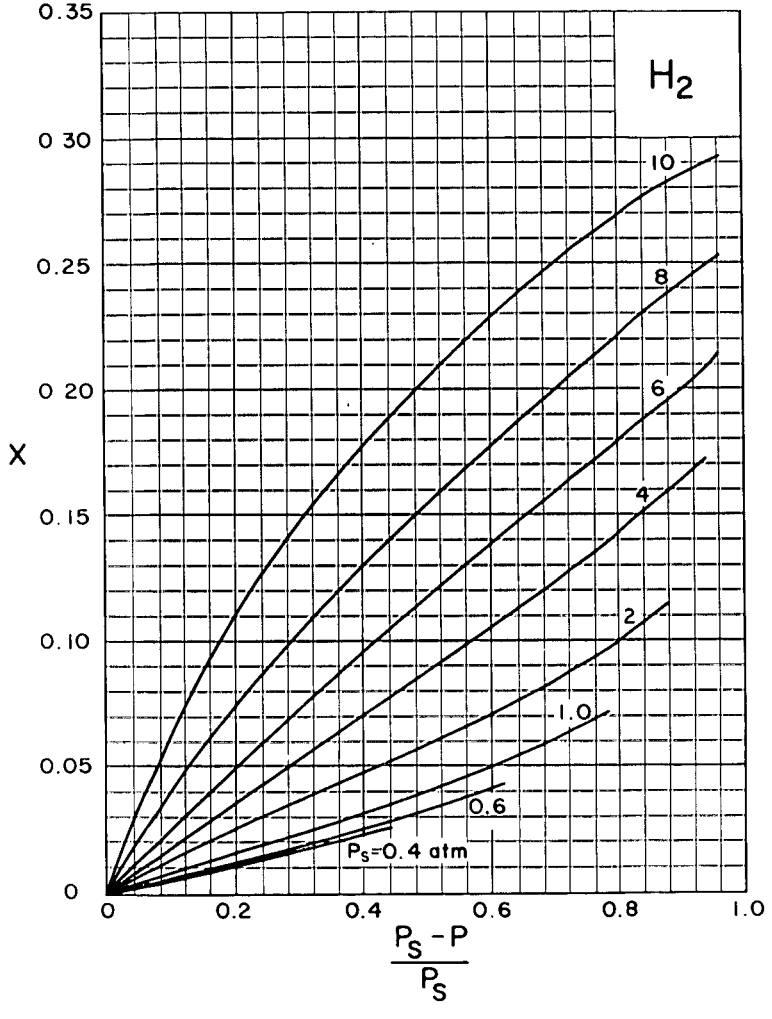

Figure 5. Quality as a function of pressure for an isentropic flow of H_2, homogeneous, thermal equilibrium model, Case IIB1a, Figure 1.

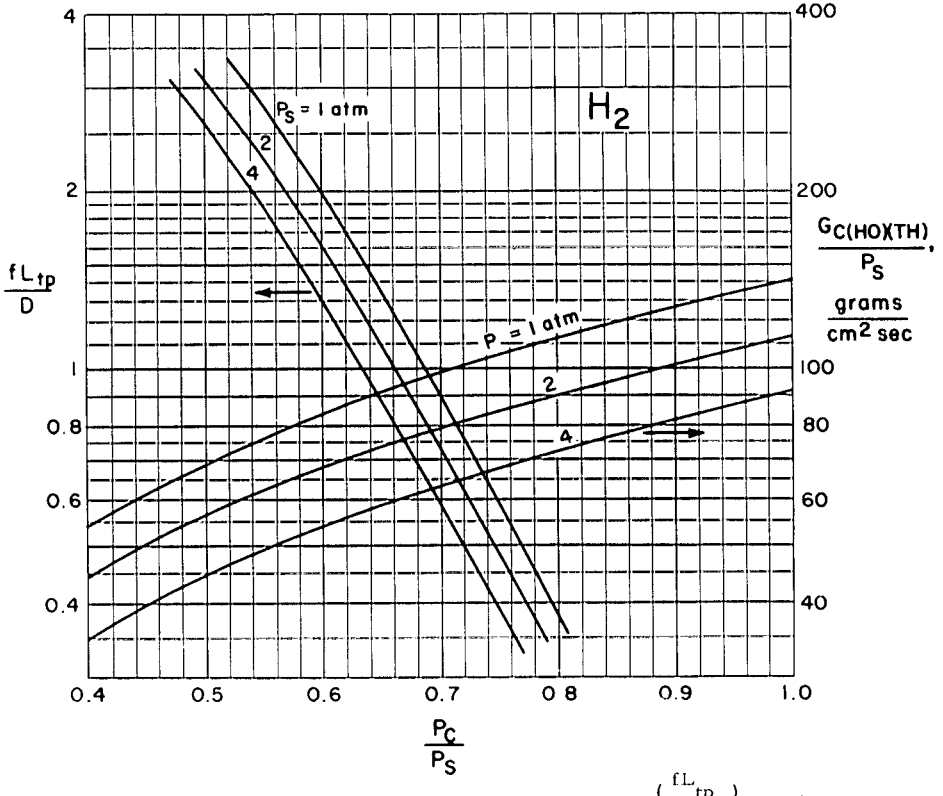

Figure 6. Geometry and friction factor parameter $\frac{(fL_{tp})}{D}$ and mass flow rate parameter (G_c/p_s) versus the ratio of the choking pressure to the flow pressure where the fluid is a saturated liquid, Case IIA1, Figure 1.

TRANSIENT TEMPERATURE HISTORY WITH UNIFORM ENERGY GENERATION FOR PLATE, CYLINDER, AND SPHERE WITH EXTENSIVE TABLES OF RESULTS

J. D. Seader[1] and H. Wolf[2]

INTRODUCTION

In the utilization of nuclear energy for power or propulsion, adequate provision must be made for maintaining structural components within specified temperature limits. A determination of the spatial temperature history of such components is, therefore, required for different boundary conditions. In many cases the energy generation rate may be considered sufficiently uniform to permit a solution on that basis. Heisler (1)[3] has prepared charts for estimating temperature histories in plates, cylinders, and spheres for different values of surface conductance (surface temperature changing with time) with special emphasis on Fourier numbers less than 0.2. Reference (1) also gives charts of temperature variation with position for the case where the surface temperature is maintained at the initial, uniform temperature of the solid for Fourier numbers less than 0.2 with uniform internal energy generation. The analytical solutions for the plate, cylinder, and sphere

---

1. Principal Scientist, Research Center, Rocketdyne Div. NAA, Canoga Park, California.

2. Associate Professor of Mechanical Engineering, University of Arkansas, Fayetteville, Arkansas

3. Numbers in parentheses indicate references at end of paper.

have been derived in detail from the partial differential equation for conduction in solids by Carslaw and Jaeger (2) for this case.

It is the purpose of this paper to present the results of an application of Laplace transform techniques to the solution of the transient conduction problem for the plate, cylinder and sphere with uniform internal energy generation, but for the more general case where the surface temperature is maintained constant at a value different from the initial uniform temperature of the solid. Previously, a solution for this case has been available (5) only for the plate. The technique of applying the Laplace transforms to the solution of differential equations is well known; the method of superposition of solutions has also been utilized in cases similar to the one described herein.

The advantage of using the Laplace transform technique, as presented here, is that its linearity property readily leads to a solution in terms of already available analytical solutions. Thus, existing (2) graphical solutions can be utilized to make calculations. For greater accuracy, however, the solutions have been calculated to six decimal places and are presented in extensive tables.

ANALYSIS

The geometries treated are the sphere, cylinder, and plate; the analysis will be outlined for the sphere (of diameter 2a) and only the results presented for the cylinder and plate.

The differential equation for transient conduction in a sphere (temperature a function of radius only and constant isotropic properties) is given by

$$\partial t/\partial \theta = \alpha \partial^2 t/\partial r^2 + (2\alpha/r)\,\partial t/\partial r + G \qquad (1)$$

It is convenient to rewrite equation 1 in terms of the following dimensionless and temperature parameters: Let

$$\xi = r/a \qquad A = G\,a^2/\alpha$$
$$\phi = \alpha\theta/a^2 \qquad T = t - t_o \tag{2}$$

The resulting equation is

$$\partial T/\partial \phi = \partial^2 T/\partial \xi^2 + (2/\xi)\,\partial T/\partial \xi + A \tag{3}$$

The boundary conditions for the case under consideration are given as Case III in Table I, wherein uniform internal energy generation, uniform initial temperature, and constant surface temperature at $\phi = 0^+$ (which is different from the initial, uniform temperature) are specified. Also included in Table I are boundary conditions for two other cases for which analytical solutions are already available. The solution for Case III is obtained in terms of the known solutions to Cases I and II.

Table I

Boundary Conditions for Equation 3

	Case I	Case II	Case III
1) Energy generation	0	A	A
2) $T(\xi, 0^-)$ for $0 \leq \xi \leq 1$	0	0	0
3) $T(1, \phi)$ for $\phi > 0^+$	T_1	0	T_1
4) $T(0, \phi)$ for all ϕ	Finite	Finite	Finite

To obtain a solution for Case III, the Laplace transform of equation 3 is taken with respect to ϕ, the boundary conditions are translated from $T(\xi, \phi)$ to $t(\xi, s)$, and the linearity property of the transform is applied. Accordingly, the Laplace transform (3) with respect to ϕ is denoted by the lower case letter of the function under consideration

$$t(\xi, s) = L\{T(\xi, \phi)\}; \tag{4}$$

the transform with respect to ϕ of the first derivative, $\partial T/\partial \phi$, is given by

$$L\left\{T_{\phi}(\xi,\phi)\right\} = s\,t(\xi,s) - T(\xi,0); \tag{5}$$

and the transforms with respect to ϕ of the first and second derivatives, $\partial T/\partial \xi$ and $\partial^2 T/\partial \xi^2$, are

$$\begin{aligned} L\left\{T_{\xi}(\xi,\phi)\right\} &= t_{\xi}(\xi,s) \\ L\left\{T_{\xi\xi}(\xi,\phi)\right\} &= t_{\xi\xi}(\xi,s) \end{aligned} \tag{6}$$

where the subscripts on T and t denote differentiation with respect to that variable.

From boundary condition 2) in Table I and the application of equations 5 and 6 to equation 3, one obtains

$$t_{\xi\xi}(\xi,s) + (2/\xi)\,t_{\xi}(\xi,s) - st(\xi,s) = -A/s \tag{7}$$

as the differential equation in terms of the transform $t(\xi,s)$ corresponding to equation 3. The remaining transformed boundary conditions applicable to equation 7 are listed in Table II.

Table II

Boundary Conditions for Equation 7

	Case I	Case II	Case III
1) Energy generation	0	A	A
2) $t(1,s)$ for $s>0^+$	T_1/s	0	T_1/s
3) $t(0,s)$ for all s	Finite	Finite	Finite

Solution for Case I. With $A = 0$, equation 7 becomes homogenious and of the second order. The solution is given by Kamke (4) as follows:

$$t(\xi,s) = C_1(\cosh \xi \sqrt{s})/\xi + C_2(\sinh \xi \sqrt{s})/\xi \qquad (8)$$

Application of boundary conditions 2) and 3) in Table II gives $C_1 = 0$ and C_2 such that

$$t_I(\xi,s) = \frac{T_1}{\xi s} \frac{\sinh \xi \sqrt{s}}{\sinh \sqrt{s}} \qquad (9)$$

Solution for Case II. Consideration of the uniform energy generation phenomena requires a particular solution to be added to the homogenious solution of equation 8. The solution given by Kamke (4) for the homogenious part of equation 7 was based upon the substitution $u = t\xi$; equation 7 takes the following form upon making this substitution,

$$\partial^2 u/\partial \xi^2 - su = -A\xi/s. \qquad (10)$$

The expression $u_1 = A\xi/s^2$ can be seen to satisfy equation 10 as the particular solution, so that the complete solution is given by

$$u = C_1 \cosh \xi \sqrt{s} + C_2 \sinh \xi \sqrt{s} + A\xi/s^2 \qquad (11)$$

or

$$t(\xi,s) = C_1(\cosh \xi \sqrt{s})/\xi + C_2(\sinh \xi \sqrt{s})/\xi + A/s^2. \qquad (12)$$

Boundary condition 3) requires $C_1 = 0$ for $t(0,s)$ to be finite and boundary condition 2) yields C_2. Thus

$$t_{II}(\xi,s) = \frac{A}{s^2} - \frac{A}{\xi s^2} \frac{\sinh \xi \sqrt{s}}{\sinh \sqrt{s}} \qquad (13)$$

Solution for Case III. The solution for this case is given by equation 12. As before, boundary condition 3) requires $C_1 = 0$. The surface temperature boundary condition 2), $t(1,s) = T_1/s$, permits evaluation of C_2 yielding the following expression for the transform function:

$$t_{III}(\xi,s) = \frac{A}{s^2} + \frac{T_1}{\xi s}\frac{\sinh \xi\sqrt{s}}{\sinh\sqrt{s}} - \frac{A}{\xi s^2}\frac{\sinh\xi\sqrt{s}}{\sinh\sqrt{s}} \qquad (14)$$

From an inspection of equations 9, 13 and 14 it may be seen that the transform for Case III is the sum of the transforms for Cases I and II. Accordingly, because of the linearity property of the transform, the solution is given in terms of the inverse transforms by

$$T_{III}(\xi,\phi) = T_I(\xi,\phi) + T_{II}(\xi,\phi) \qquad (15)$$

where the functions T_I and T_{II} are given in (2).

The above development has been given specifically for the sphere; it can be shown that parallel developments for the plate and cylinder lead to the same result as expressed by equation 15 for the solution to Case III. A summary of the transform equations is presented in Table III.

A more convenient way of expressing $T_{III}(\xi,\phi)$ is as follows:

$$T_{III}(\xi,\phi) = T_1 Y_a + (A/M) Y_b \qquad (16)$$

where the subscripts a and b refer to Cases I and II respectively; and $M = 2,4,6$ for the plate, cylinder, and sphere respectively. The functions Y_a and Y_b are repeated here from (2) for convenience:

Plate

$$Y_a = 1 - (4/\pi)\sum_{n=0}^{\infty}\frac{(-1)^n e^{\frac{-(2n+1)^2\pi^2\phi}{4}}\cos\frac{(2n+1)\pi\xi}{2}}{(2n+1)} \qquad (17)$$

$$Y_b = 1 - \xi^2 - \frac{32}{\pi^3}\sum_{n=0}^{\infty}\frac{(-1)^n e^{\frac{-(2n+1)^2\pi^2\phi}{4}}\cos\frac{(2n+1)\pi\xi}{2}}{(2n+1)^3} \qquad (18)$$

Table III

Summary of Transform Equations

Geometry Basic Equation		Transformed Differential Equation
$T_\phi = T_{\xi\xi} + A$	Plate	$t_{\xi\xi} - st = -A/s$
$T_\phi = T_{\xi\xi} + T_\xi/\xi + A$	Cylinder	$t_{\xi\xi} + t_\xi/\xi - st = -A/s$
$T_\phi = T_{\xi\xi} + 2T_\xi/\xi + A$	Sphere	$t_{\xi\xi} + 2t_\xi/\xi - st = -A/s$

Solutions to Transformed Differential Equations

Case I, A = 0 $t_I(\xi,s)$	Case II, A = A $t_{II}(\xi,s)$	Case III, A = A $t_{III}(\xi,s)$
$(T_1/s)\,B_p$	$(1 - B_p)\,A/s^2$	$(T_1/s - A/s^2)\,B_p + A/s^2$
Plate	where $B_p = \dfrac{e^{\sqrt{s}\,\xi}}{1 + e^{2\sqrt{s}}} + \dfrac{e^{-\sqrt{s}\,\xi}}{1 + e^{-2\sqrt{s}}}$	
$(T_1/s)\,B_c$	$(1 - B_c)\,A/s^2$	$(T_1/s - A/s^2)\,B_c + A/s^2$
Cylinder	where $B_c = I_o(\xi\sqrt{s})/I_o(\sqrt{s})$	
$(T_1/s)\,B_s$	$(1 - B_s)\,A/s^2$	$(T_1/s - A/s^2)\,B_s + A/s^2$
Sphere	where $B_s = (\sinh \xi\sqrt{s})/\xi \sinh \sqrt{s}$	

Cylinder

$$Y_a = 1 - 2\sum_{n=1}^{\infty} e^{-\beta_n^2 \phi}\left[J_o(\xi\beta_n)/\beta_n J_1(\beta_n)\right] \tag{19}$$

$$Y_b = 1 - \xi^2 - 8\sum_{n=1}^{\infty} e^{-\beta_n^2 \phi}\left[J_o(\xi\beta_n)/\beta_n^3 J_1(\beta_n)\right] \tag{20}$$

where β_n are the roots of $J_o(\beta) = 0$.

Sphere

$$Y_a = 1 + \frac{2}{\pi\xi}\sum_{n=1}^{\infty} \frac{(-1)^n}{n} e^{-n^2\pi^2\phi}\left[\sin(n\pi\xi)\right] \tag{21}$$

$$Y_b = 1 - \xi^2 + \frac{12}{\pi^3\xi}\sum_{n=1}^{\infty} \frac{(-1)^n}{n^3} e^{-n^2\pi^2\phi}\left[\sin(n\pi\xi)\right] \tag{22}$$

AVAILABLE SOLUTIONS

Only small charts are presented in (2) giving Y_a and Y_b for limited values of ϕ as functions of ξ from which approximate estimates for Case III can be made. Accordingly, extensive tables of Y_a and Y_b have been computed from the equations 17 through 22 for ξ from 0 to 1.0 in increments of 0.05 over the following ranges:

Plate:	$0.1 \leq \phi \leq 2.0$ (25 values)
Cylinder:	$0.1 \leq \phi \leq 0.9$ (25 values)
Sphere:	$0.1 \leq \phi \leq 0.6$ (25 values)

The tables presented in Appendixes A, B, and C give values of Y_a and Y_b

to six decimal places, the values of the series sums, and the number of terms required for convergence. Compilations of the IBM 7090 Fortran programs employed for the computations are also included.

ACKNOWLEDGMENT

The authors express their appreciation to the management of Rocketdyne for supporting this work and for permission to publish the results.

REFERENCES

(1) M. P. Heisler, "Temperature Charts for Internal Heat Generation", Trans. ASME, Vol. 78, Aug. 1956, p. 1187.

(2) H. S. Carslaw and J. C. Jaeger, "Conduction of Heat in Solids", Second Edition, Clarendon Press, Oxford, England, 1959, pp. 101, 131, 200, 204, 234, 244.

(3) R. V. Churchill, "Modern Operational Methods in Engineering", First Ed., McGraw-Hill Book Co., New York, 1944, p. 85.

(4) E. Kamke, "Differentialgleichungen", Second Ed., Chelsea Pub. Co., New York, 1948, p. 424.

(5) H. M. Nelson, "Temperature Distribution with Simultaneous Platten and Dielectric Heating", Brit. Journal of Applied Physics, Vol. 3, 1952, p. 79.

NOMENCLATURE

A	Temperature generation function, $G\,a^2/\alpha$, R.
a	Sphere or cylinder radius, ft.
C_1, C_2	Integration constants.
e	Base for natural logarithms.
G	Temperature generation rate, R/hr.
$I_o(z)$	Modified Bessel function of first kind, zero order corresponding to $J_o(iz)$.
$J_o(z)$	Bessel function of first kind, zero order.
L	Thickness of plate, ft.
$L\{\ \}$	Laplace transform.
M	Constant, 2, 4, 6 for plate, cylinder, and sphere respectively.
n	Series index.
r	Radial distance, ft.
s	Laplace parameter corresponding to ϕ.
t	Temperature, R, and Laplace transform of T.
t_o	Uniform initial temperature of solid, R.
t_1	Surface temperature, R.
T	Temperature excess $t - t_o$, R.
T_1	Temperature excess $t_1 - t_o$, R.
u	The variable $t\xi$.
x	Distance from centerline of plate, ft.
Y_a	Temperature function, T/T_1, for Case I.
Y_b	Temperature function, MT/A, for Case II.
α	Thermal diffusivity of solid, ft^2/hr.
θ	Time, hr.
ξ	Position ratio, r/a for sphere and cylinder, x/L for plate.
ϕ	Fourier number, $\alpha\theta/L^2$ or $\alpha\theta/a^2$.

APPENDIX A

TEMPERATURE HISTORY FOR THE PLATE

The results presented in the tables apply to the following geometry:

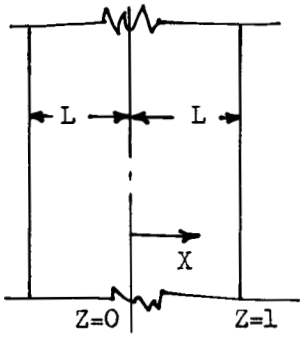

$Z = \xi = X/L$

The position ratio

The following special terms were employed in the computer program:

$$TM1 = (-1)^n/(2n + 1) = (\cos(n\pi))/(2n + 1)$$

$$TM2 = (-1)^n/(2n + 1)^3 = TM1/(2n + 1)^2$$

$$CTM = \cos((2n + 1)\pi Z/2)$$

$$ETM = \exp((2n + 1)^2\pi^2\phi/4)$$

XN = n, the series index

The individual series terms in Equation (17) and (18) were designated as follows:

$$SERA = (4/\pi)\ TM1(CTM)/ETM$$

$$SERB = (32/\pi^3)CTM(TM2)/ETM$$

The series sums were designated as ASER and BSER, and N gives the number of terms required to converge to the tolerance TOL (a value of TOL = 0.0000001 was employed throughout). The values Y_a and Y_b were calculated as

$$YA = 1 - ASER$$

$$YB = 1 - Z^2 - BSER$$

The data cards require DZ and TOL on the first card, then each value of PHI (the Fourier number ϕ) is entered on a separate card, as many as desired. The computations were made on the IBM 7090 with the Fortran System.

```
C     TRSCND     P-005      5-12-61                                          00000010
C                                                                           00000020
C     PROGRAMMER-H. WOLF                                                    00000030
C                                                                           00000040
C     SYNOPSIS  - CALC. OF TEMP. HISTORY IN A FLAT PLATE FOR ZERO AND       00000050
C                 FINITE SURFACE TEMP. WITH ZERO INITIAL TEMP.              00000060
C                 THROUGHOUT                                                00000070
C                                                                           00000080
C     PURPOSE   - GENERATE TABLES OF VALUES                                 00000090
C                                                                           00000100
C     SYMBOLS   -                                                           00000110
C                                                                           00000112
C            Z - POSITION RATIO                DZ - UPDATING FACTOR ON Z  00000114
C          TOL - TOLERANCE ON CONVERG.          N - NO OF TERMS REQD       00000116
C          PHI - FOURIER NUMBER                                             00000120
C                                                                           00000130
C              SEE NOTES FOR SPECIALIZED NOMENCLATURE OF PARTS OF           00000140
C              SERIES TERMS                                                 00000150
C                                                                           00000160
C             *---*              *-*-*-*              *---*                 00000170
C                                                                           00000180
C     MAIN CALCULATIONS                                                     00000190
C                                                                           00000200
    5 READ INPUT TAPE 5,10, DZ, TOL                                         00000210
   10 FORMAT(F12.1, F12.7)                                                  00000220
   15 READ INPUT TAPE 5,16. PHI                                             00000225
   16 FORMAT(6F12.6)                                                        00000230
   20 Z = 0.                                                                00000240
   22 IF(PHI - 10.) 40, 40, 250                                             00000250
   40 WRITE OUTPUT TAPE 6, 45, PHI                                          00000280
   45 FORMAT(1H1///45X,  20HTRANSIENT CONDUCTION// 36X,  37HTEMPERATURE      00000290
     1RATIO TERMS FOR THE PLATE/// 45X,14HFOURIER NO. = F4.2 /// 21X,       00000300
     2 67H Z          YA           YB           ASER         BSER        Z   00000310
     3    N//1H )                                                           00000315
   25 ASER = 0.000000                                                       00000316
   30 BSER = 0.000000                                                       00000317
   35 XN = 0.0                                                              00000318
   50 PI = 3.14159265358979323846                                           00000320
   55 PI2 = PI*PI                                                           00000330
   60 AN = 2.*XN + 1.                                                       00000340
   65 PI3 = PI2*PI                                                          00000350
   70 TM1 = COSF(XN*PI)/AN                                                  00000360
   75 TM2 = TM1/(AN*AN)                                                     00000370
   80 X = AN*AN*PI2*PHI/4.                                                  00000380
   85 IF( X - 86.) 90, 90, 105                                              00000390
   90 ETM = EXPF(X)                                                         00000400
  100 GO TO 135                                                             00000410
  105 XB = X/1000.                                                          00000420
  110 D = EXPF(XB)                                                          00000430
  115 D1 = D**10.                                                           00000440
  120 D2 = D1**10.                                                          00000450
  130 ETM = D2**10.                                                         00000460
  135 CTM = COSF(AN*PI*Z/2.)                                                00000470
  140 SERA = 4.*TM1*CTM/(ETM*PI)                                            00000480
  145 SERB = 32.*TM2*CTM/(ETM*PI3)                                          00000490
  160 ASER1 = ASER + SERA                                                   00000520
  165 A1 = ABSF(ASER1)                                                      00000530
  170 A  = ABSF(ASER)                                                       00000540
  175 B  = ABSF(A1 - A)                                                     00000550
  180 ASER = ASER + SERA                                                    00000560
  185 BSER = BSER + SERB                                                    00000570
  190 IF(TOL - B) 195, 195, 202                                             00000580
  195 XN = XN + 1.                                                          00000590
  200 GO TO 50                                                              00000592
  202 IF(XN - 1.) 203, 205, 205                                             00000594
  203 XN = XN +1.                                                           00000596
  204 GO TO 50                                                              00000598
  205 XN = XN + 1.                                                          00000600
  206 CTM1 = ABSF(CTM)                                                      00000604
  207 IF(CTM - .0000001) 50, 50, 208                                        00000606
  208 IF(Z - .99) 210, 210, 209                                             00000608
  209 YA = 1.0000001                                                        00000610
      YB =  .0000001                                                        00000612
      ASER =.0000001                                                        00000614
      BSER =.0000001                                                        00000616
      XN = 0.                                                               00000617
      GO TO 214                                                             00000618
  210 YA = 1. - ASER                                                        00000620
  212 YB = 1. - Z*Z - BSER                                                  00000622
  214 N = XFIXF(XN)                                                         00000624
      YA = ABSF(YA)                                                         00000626
      YB = ABSF(YB)                                                         00000628
  216 WRITE OUTPUT TAPE 6, 220, Z,YA,YB,ASER,BSER, Z, N                     00000632
  220 FORMAT(F25.2, 2F12.6,F13.6, F12.6, F8.2, I6)                          00000640
  225 Z = Z + DZ                                                            00000650
  230 IF(Z - 1.01) 25, 25. 15                                               00000660
  250 CALL EXIT                                                             00000710
  255 STOP                                                                  00000720
      END(1,0,0,0,0,0,0,0,0,0,0,0,0,0,0)
```

EXTERNAL FORMULA NUMBERS WITH CORRESPONDING INTERNAL FORMULA NUMBERS AND OCTAL LOCATIONS

EFN	IFN	LOC	EFN	IFN	LOC	EFN	IFN	LOC	EFN	IFN	LOC
10	1	00000	16	2	00000	45	3	00000	220	4	00000
5	6	00014	5	7	00017	15	8	00024	15	9	00027
20	10	00032	22	11	00034	40	12	00040	40	13	00043
25	14	00046	30	15	00050	35	16	00052	50	17	00054
55	18	00056	60	19	00061	65	20	00065	70	21	00070
75	22	00077	80	23	00105	85	24	00114	90	25	00120
100	26	00125	105	27	00126	110	28	00131	115	29	00136
120	30	00144	130	31	00152	135	32	00160	140	33	00170
145	34	00200	160	35	00210	165	36	00213	170	37	00216
175	38	00221	180	39	00225	185	40	00230	190	41	00233
195	42	00237	200	43	00242	202	44	00243	203	45	00247
204	46	00252	205	47	00253	206	48	00256	207	49	00261
208	50	00266	209	51	00273	210	57	00306	212	58	00311
214	59	00317	216	62	00334	216	63	00337	225	64	00356
230	65	00361	250	66	00366	255	67	00371			

STORAGE NOT USED BY PROGRAM

DEC	OCT	DEC	OCT
349	00535	32561	77461

LOCATIONS OF NAMES IN TRANSFER VECTOR

	DEC	OCT		DEC	OCT		DEC	OCT		DEC	OCT
EXP(3	7	00007	EXP	6	00006	EXIT	8	00010	COS	5	00005
(FIL)	4	00004	(FPT)	0	00000	(RTN)	2	00002	(STH)	3	00003
(TSH)	1	00001									

STORAGE LOCATIONS FOR VARIABLES NOT APPEARING IN DIMENSION, EQUIVALENCE OR COMMON SENTENCES

	DEC	OCT		DEC	OCT		DEC	OCT		DEC	OCT
ETM	348	00534	DZ	347	00533	D	346	00532	D2	345	00531
D1	344	00530	CTM	343	00527	CTM1	342	00526	BSER	341	00525
B	340	00524	ASER	339	00523	ASER1	338	00522	A	337	00521
AN	336	00520	A1	335	00517	N	334	00516	PHI	333	00515
PI2	332	00514	PI3	331	00513	PI	330	00512	SERA	329	00511
SERB	328	00510	TM1	327	00507	TM2	326	00506	TOL	325	00505
XB	324	00504	XN	323	00503	X	322	00502	YA	321	00501
YB	320	00500	Z	319	00477						

TRANSIENT CONDUCTION

TEMPERATURE RATIO TERMS FOR THE PLATE

FOURIER NO. = 0.01

Z	YA	YB	ASER	BSER	Z	N
0.	0.000000	0.020000	1.000000	0.980000	0.	13
0.05	0.000000	0.020000	1.000000	0.977500	0.05	31
0.10	0.000000	0.020000	1.000000	0.970000	0.10	16
0.15	0.000000	0.020000	1.000000	0.957500	0.15	12
0.20	0.000000	0.020000	1.000000	0.940000	0.20	12
0.25	0.000000	0.020000	1.000000	0.917500	0.25	15
0.30	0.000001	0.020000	0.999999	0.890000	0.30	13
0.35	0.000004	0.020000	0.999996	0.857500	0.35	13
0.40	0.000022	0.020000	0.999978	0.820000	0.40	15
0.45	0.000101	0.020000	0.999899	0.777500	0.45	13
0.50	0.000407	0.019999	0.999593	0.730001	0.50	12
0.55	0.001463	0.019996	0.998537	0.677504	0.55	12
0.60	0.004616	0.019985	0.995384	0.620015	0.60	8
0.65	0.013328	0.019948	0.986672	0.557552	0.65	13
0.70	0.033895	0.019839	0.966105	0.490161	0.70	15
0.75	0.077100	0.019552	0.922900	0.417948	0.75	14
0.80	0.157299	0.018864	0.842701	0.341136	0.80	13
0.85	0.288844	0.017368	0.711156	0.260132	0.85	12
0.90	0.479500	0.014403	0.520500	0.175597	0.90	12
0.95	0.723673	0.009017	0.276327	0.088483	0.95	13
1.00	1.000000	0.000000	0.000000	0.000000	1.00	0

FOURIER NO. = 0.02

Z	YA	YB	ASER	BSER	Z	N
0.	0.000001	0.040000	0.999999	0.960000	0.	9
0.05	0.000002	0.040000	0.999998	0.957500	0.05	9
0.10	0.000007	0.040000	0.999993	0.950000	0.10	16
0.15	0.000021	0.040000	0.999979	0.937500	0.15	11
0.20	0.000063	0.040000	0.999937	0.920000	0.20	9
0.25	0.000177	0.039999	0.999823	0.897501	0.25	9
0.30	0.000465	0.039998	0.999535	0.870002	0.30	13
0.35	0.001154	0.039994	0.998846	0.837506	0.35	11
0.40	0.002700	0.039984	0.997300	0.800016	0.40	10
0.45	0.005960	0.039959	0.994040	0.757541	0.45	9
0.50	0.012419	0.039904	0.987581	0.710096	0.50	9
0.55	0.024449	0.039784	0.975551	0.657716	0.55	11
0.60	0.045500	0.039539	0.954500	0.600462	0.60	8
0.65	0.080118	0.039060	0.919882	0.538440	0.65	9
0.70	0.133614	0.038172	0.866386	0.471828	0.70	9
0.75	0.211300	0.036607	0.788700	0.400893	0.75	9
0.80	0.317310	0.033973	0.682690	0.326027	0.80	10
0.85	0.453255	0.029740	0.546745	0.247760	0.85	10
0.90	0.617075	0.023229	0.382925	0.166771	0.90	9
0.95	0.802587	0.013623	0.197413	0.083877	0.95	9
1.00	1.000000	0.000000	0.000000	0.000000	1.00	0

FOURIER NO. = 0.03

Z	YA	YB	ASER	BSER	Z	N
0.	0.000089	0.060000	0.999911	0.940000	0.	8
0.05	0.000123	0.059999	0.999877	0.937501	0.05	8
0.10	0.000246	0.059998	0.999754	0.930002	0.10	16
0.15	0.000523	0.059996	0.999477	0.917504	0.15	11
0.20	0.001092	0.059991	0.998908	0.900009	0.20	9
0.25	0.002200	0.059981	0.997800	0.877519	0.25	8
0.30	0.004267	0.059959	0.995733	0.850041	0.30	8
0.35	0.007964	0.059915	0.992036	0.817585	0.35	11
0.40	0.014306	0.059830	0.985694	0.780170	0.40	10
0.45	0.024745	0.059672	0.975255	0.737828	0.45	9
0.50	0.041227	0.059387	0.958773	0.690613	0.50	8
0.55	0.066193	0.058893	0.933807	0.638607	0.55	7
0.60	0.102470	0.058064	0.897530	0.581936	0.60	8
0.65	0.153042	0.056716	0.846958	0.520784	0.65	9
0.70	0.220671	0.054595	0.779329	0.455405	0.70	9
0.75	0.307434	0.051364	0.692566	0.386136	0.75	8
0.80	0.414216	0.046586	0.585784	0.313414	0.80	8
0.85	0.540291	0.039730	0.459709	0.237770	0.85	7
0.90	0.683091	0.030165	0.316909	0.159835	0.90	9
0.95	0.838256	0.017180	0.161744	0.080321	0.95	9
1.00	1.000000	0.000000	0.000000	0.000000	1.00	0

TRANSIENT CONDUCTION

TEMPERATURE RATIO TERMS FOR THE PLATE

FOURIER NO. = 0.04

Z	YA	YB	ASER	BSER	Z	N
0.	0.000814	0.079992	0.999186	0.920008	0.	7
0.05	0.000988	0.079990	0.999012	0.917510	0.05	7
0.10	0.001563	0.079983	0.998437	0.910017	0.10	16
0.15	0.002702	0.079968	0.997298	0.897532	0.15	11
0.20	0.004700	0.079939	0.995300	0.880061	0.20	9
0.25	0.008020	0.079885	0.991980	0.857615	0.25	7
0.30	0.013333	0.079791	0.986667	0.830209	0.30	7
0.35	0.021558	0.079629	0.978442	0.797871	0.35	7
0.40	0.033896	0.079358	0.966104	0.760642	0.40	10
0.45	0.051830	0.078915	0.948170	0.718585	0.45	6
0.50	0.077100	0.078209	0.922900	0.671791	0.50	8
0.55	0.111612	0.077114	0.888388	0.620386	0.55	7
0.60	0.157299	0.075457	0.842701	0.564543	0.60	7
0.65	0.215925	0.073007	0.784075	0.504493	0.65	7
0.70	0.288844	0.069472	0.711156	0.440528	0.70	9
0.75	0.376759	0.064487	0.623241	0.373013	0.75	8
0.80	0.479500	0.057611	0.520500	0.302389	0.80	8
0.85	0.595883	0.048533	0.404117	0.229168	0.85	7
0.90	0.723673	0.036070	0.276327	0.153930	0.90	7
0.95	0.859684	0.020185	0.140316	0.077315	0.95	7
1.00	1.000000	0.000000	0.000000	0.000000	1.00	0

FOURIER NO. = 0.05

Z	YA	YB	ASER	BSER	Z	N
0.	0.003131	0.099956	0.996869	0.900044	0.	6
0.05	0.003562	0.099948	0.996438	0.897552	0.05	6
0.10	0.004931	0.099922	0.995069	0.890078	0.10	16
0.15	0.007466	0.099871	0.992534	0.877629	0.15	11
0.20	0.011560	0.099781	0.988440	0.860219	0.20	9
0.25	0.017783	0.099633	0.982217	0.837867	0.25	7
0.30	0.026896	0.099395	0.973104	0.810605	0.30	6
0.35	0.039852	0.099021	0.960148	0.778479	0.35	6
0.40	0.057789	0.098446	0.942211	0.741554	0.40	6
0.45	0.081995	0.097579	0.918005	0.699921	0.45	6
0.50	0.113848	0.096298	0.886152	0.653702	0.50	8
0.55	0.154730	0.094445	0.845270	0.603055	0.55	7
0.60	0.205904	0.091814	0.794096	0.548186	0.60	7
0.65	0.268382	0.088148	0.731618	0.489352	0.65	6
0.70	0.342782	0.083136	0.657218	0.426864	0.70	6
0.75	0.429195	0.076405	0.570805	0.361095	0.75	6
0.80	0.527089	0.067523	0.472911	0.292477	0.80	6
0.85	0.635256	0.056001	0.364744	0.221499	0.85	7
0.90	0.751830	0.041300	0.248170	0.148701	0.90	7
0.95	0.874367	0.022836	0.125633	0.074664	0.95	7
1.00	1.000000	0.000000	0.000000	0.000000	1.00	0

FOURIER NO. = 0.06

Z	YA	YB	ASER	BSER	Z	N
0.	0.007785	0.119851	0.992215	0.880149	0.	6
0.05	0.008536	0.119832	0.991464	0.877668	0.05	6
0.10	0.010871	0.119769	0.989129	0.870231	0.10	16
0.15	0.015039	0.119650	0.984961	0.857850	0.15	11
0.20	0.021453	0.119456	0.978547	0.840544	0.20	9
0.25	0.030691	0.119153	0.969309	0.818347	0.25	7
0.30	0.043483	0.118695	0.956517	0.791305	0.30	6
0.35	0.060699	0.118018	0.939301	0.759482	0.35	6
0.40	0.083318	0.117036	0.916682	0.722964	0.40	6
0.45	0.112380	0.115634	0.887620	0.681866	0.45	6
0.50	0.148930	0.113667	0.851070	0.636333	0.50	8
0.55	0.193939	0.110951	0.806061	0.586549	0.55	5
0.60	0.248217	0.107263	0.751783	0.532737	0.60	7
0.65	0.312323	0.102329	0.687677	0.475171	0.65	6
0.70	0.386477	0.095829	0.613523	0.414171	0.70	6
0.75	0.470487	0.087393	0.529513	0.350107	0.75	6
0.80	0.563703	0.076600	0.436297	0.283400	0.80	6
0.85	0.665006	0.062986	0.334994	0.214514	0.85	7
0.90	0.772830	0.046044	0.227170	0.143956	0.90	7
0.95	0.885234	0.025235	0.114766	0.072265	0.95	7
1.00	1.000000	0.000000	0.000000	0.000000	1.00	0

TRANSIENT CONDUCTION

TEMPERATURE RATIO TERMS FOR THE PLATE

FOURIER NO. = 0.08

Z	YA	YB	ASER	BSER	Z	N
0.	0.024839	0.159232	0.975161	0.840768	0.	5
0.05	0.026214	0.159170	0.973786	0.838330	0.05	5
0.10	0.030409	0.158975	0.969591	0.831025	0.10	5
0.15	0.037627	0.158627	0.962373	0.818873	0.15	11
0.20	0.048200	0.158089	0.951800	0.801911	0.20	9
0.25	0.062571	0.157309	0.937429	0.780191	0.25	7
0.30	0.081272	0.156214	0.918728	0.753786	0.30	6
0.35	0.104901	0.154710	0.895099	0.722790	0.35	5
0.40	0.134080	0.152680	0.865920	0.687320	0.40	5
0.45	0.169420	0.149977	0.830580	0.647523	0.45	5
0.50	0.211476	0.146424	0.788524	0.603576	0.50	5
0.55	0.260696	0.141810	0.739304	0.555690	0.55	5
0.60	0.317374	0.135890	0.682626	0.504110	0.60	7
0.65	0.381611	0.128380	0.618389	0.449120	0.65	6
0.70	0.453276	0.118959	0.546724	0.391041	0.70	6
0.75	0.531983	0.107268	0.468017	0.330232	0.75	6
0.80	0.617082	0.092915	0.382918	0.267085	0.80	5
0.85	0.707664	0.075475	0.292336	0.202026	0.85	5
0.90	0.802589	0.054494	0.197411	0.135506	0.90	5
0.95	0.900524	0.029498	0.099476	0.068002	0.95	5
1.00	1.000000	0.000000	0.000000	0.000000	1.00	0

FOURIER NO. = 0.10

Z	YA	YB	ASER	BSER	Z	N
0.	0.050695	0.197746	0.949305	0.802254	0.	5
0.05	0.052529	0.197619	0.947471	0.799881	0.05	5
0.10	0.058078	0.197227	0.941922	0.792773	0.10	5
0.15	0.067473	0.196543	0.932527	0.780956	0.15	11
0.20	0.080929	0.195521	0.919071	0.764479	0.20	9
0.25	0.098721	0.194092	0.901279	0.743408	0.25	7
0.30	0.121175	0.192167	0.878825	0.717833	0.30	6
0.35	0.148639	0.189634	0.851361	0.687866	0.35	5
0.40	0.181458	0.186356	0.818542	0.653644	0.40	5
0.45	0.219944	0.182168	0.780056	0.615332	0.45	5
0.50	0.264349	0.176878	0.735651	0.573122	0.50	5
0.55	0.314833	0.170264	0.685167	0.527236	0.55	5
0.60	0.371440	0.162073	0.628560	0.477927	0.60	7
0.65	0.434073	0.152022	0.565927	0.425478	0.65	6
0.70	0.502479	0.139799	0.497521	0.370201	0.70	6
0.75	0.576241	0.125061	0.423759	0.312439	0.75	6
0.80	0.654777	0.107440	0.345223	0.252560	0.80	5
0.85	0.737349	0.086543	0.262651	0.190957	0.85	5
0.90	0.823082	0.061958	0.176918	0.128042	0.90	5
0.95	0.910988	0.033257	0.089012	0.064243	0.95	5
1.00	1.000000	0.000000	0.000000	0.000000	1.00	0

FOURIER NO. = 0.15

Z	YA	YB	ASER	BSER	Z	N
0.	0.135778	0.288573	0.864222	0.711427	0.	4
0.05	0.138072	0.288232	0.861928	0.709268	0.05	4
0.10	0.144958	0.287200	0.855042	0.702800	0.10	4
0.15	0.156454	0.285440	0.843546	0.692060	0.15	11
0.20	0.172586	0.282897	0.827414	0.677103	0.20	9
0.25	0.193382	0.279488	0.806618	0.658012	0.25	7
0.30	0.218864	0.275111	0.781136	0.634889	0.30	6
0.35	0.249043	0.269637	0.750957	0.607863	0.35	5
0.40	0.283907	0.262917	0.716093	0.577083	0.40	5
0.45	0.323412	0.254774	0.676588	0.542726	0.45	4
0.50	0.367475	0.245013	0.632525	0.504987	0.50	4
0.55	0.415962	0.233413	0.584038	0.464087	0.55	4
0.60	0.468684	0.219731	0.531316	0.420269	0.60	4
0.65	0.525390	0.203704	0.474610	0.373796	0.65	4
0.70	0.585766	0.185048	0.414234	0.324952	0.70	4
0.75	0.649435	0.163462	0.350565	0.274038	0.75	6
0.80	0.715957	0.138628	0.284043	0.221372	0.80	5
0.85	0.784836	0.110213	0.215164	0.167287	0.85	5
0.90	0.855529	0.077874	0.144471	0.112127	0.90	5
0.95	0.927453	0.041256	0.072547	0.056245	0.95	5
1.00	1.000000	0.000000	0.000000	0.000000	1.00	0

TRANSIENT CONDUCTION

TEMPERATURE RATIO TERMS FOR THE PLATE

FOURIER NO. = 0.20

Z	YA	YB	ASER	BSER	Z	N
0.	0.227688	0.370386	0.772312	0.629614	0.	4
0.05	0.229947	0.369816	0.770053	0.627684	0.05	4
0.10	0.236714	0.368094	0.763286	0.621906	0.10	4
0.15	0.247968	0.365187	0.752032	0.612313	0.15	11
0.20	0.263673	0.361038	0.736327	0.598962	0.20	9
0.25	0.283773	0.355569	0.716227	0.581931	0.25	7
0.30	0.308194	0.348679	0.691806	0.561321	0.30	6
0.35	0.336843	0.340247	0.663157	0.537253	0.35	5
0.40	0.369599	0.330128	0.630401	0.509872	0.40	5
0.45	0.406317	0.318160	0.593683	0.479340	0.45	4
0.50	0.446824	0.304159	0.553176	0.445841	0.50	4
0.55	0.490915	0.287922	0.509085	0.409578	0.55	4
0.60	0.538353	0.269229	0.461647	0.370771	0.60	4
0.65	0.588872	0.247844	0.411128	0.329656	0.65	4
0.70	0.642170	0.223512	0.357830	0.286488	0.70	4
0.75	0.697916	0.195969	0.302084	0.241531	0.75	6
0.80	0.755752	0.164935	0.244248	0.195065	0.80	5
0.85	0.815292	0.130122	0.184708	0.147378	0.85	5
0.90	0.876131	0.091232	0.123869	0.098768	0.90	5
0.95	0.937845	0.047961	0.062155	0.049539	0.95	5
1.00	1.000000	0.000000	0.000000	0.000000	1.00	0

FOURIER NO. = 0.25

Z	YA	YB	ASER	BSER	Z	N
0.	0.314554	0.443212	0.685446	0.556788	0.	3
0.05	0.316627	0.442425	0.683373	0.555075	0.05	3
0.10	0.322834	0.440052	0.677166	0.549948	0.10	3
0.15	0.333144	0.436064	0.666856	0.541436	0.15	3
0.20	0.347504	0.430409	0.652496	0.529591	0.20	9
0.25	0.365839	0.423015	0.634161	0.514485	0.25	7
0.30	0.388053	0.413789	0.611947	0.496211	0.30	6
0.35	0.414028	0.402622	0.585972	0.474878	0.35	5
0.40	0.443621	0.389383	0.556379	0.450617	0.40	5
0.45	0.476670	0.373925	0.523330	0.423575	0.45	4
0.50	0.512987	0.356082	0.487013	0.393918	0.50	4
0.55	0.552364	0.335672	0.447636	0.361828	0.55	4
0.60	0.594570	0.312500	0.405430	0.327500	0.60	4
0.65	0.639353	0.286354	0.360647	0.291146	0.65	3
0.70	0.686439	0.257010	0.313561	0.252990	0.70	3
0.75	0.735539	0.224233	0.264461	0.213267	0.75	3
0.80	0.786344	0.187777	0.213656	0.172223	0.80	3
0.85	0.838532	0.147389	0.161468	0.130111	0.85	3
0.90	0.891767	0.102809	0.108233	0.087191	0.90	3
0.95	0.945707	0.053769	0.054293	0.043731	0.95	3
1.00	1.000000	0.000000	0.000000	0.000000	1.00	0

FOURIER NO. = 0.30

Z	YA	YB	ASER	BSER	Z	N
0.	0.393196	0.507752	0.606804	0.492248	0.	3
0.05	0.395053	0.506769	0.604947	0.490731	0.05	3
0.10	0.400614	0.503808	0.599386	0.486192	0.10	3
0.15	0.409847	0.498843	0.590153	0.478657	0.15	3
0.20	0.422698	0.491827	0.577302	0.468173	0.20	9
0.25	0.439093	0.482696	0.560907	0.454804	0.25	7
0.30	0.458935	0.471368	0.541065	0.438632	0.30	6
0.35	0.482109	0.457744	0.517891	0.419756	0.35	5
0.40	0.508479	0.441709	0.491521	0.398291	0.40	5
0.45	0.537887	0.423129	0.462113	0.374371	0.45	4
0.50	0.570157	0.401859	0.429843	0.348141	0.50	4
0.55	0.605097	0.377737	0.394903	0.319763	0.55	4
0.60	0.642495	0.350589	0.357505	0.289411	0.60	4
0.65	0.682121	0.320227	0.317879	0.257273	0.65	3
0.70	0.723734	0.286454	0.276266	0.223546	0.70	3
0.75	0.767077	0.249061	0.232923	0.188439	0.75	3
0.80	0.811881	0.207833	0.188119	0.152168	0.80	3
0.85	0.857865	0.162544	0.142135	0.114956	0.85	3
0.90	0.904744	0.112966	0.095256	0.077034	0.90	3
0.95	0.952221	0.058864	0.047779	0.038637	0.95	3
1.00	1.000000	0.000000	0.000000	0.000000	1.00	0

TRANSIENT CONDUCTION

TEMPERATURE RATIO TERMS FOR THE PLATE

FOURIER NO. = 0.35

Z	YA	YB	ASER	BSER	Z	N
0.	0.463323	0.564857	0.536677	0.435143	0.	3
0.05	0.464973	0.563698	0.535027	0.433802	0.05	3
0.10	0.469913	0.560213	0.530087	0.429787	0.10	3
0.15	0.478114	0.554377	0.521886	0.423123	0.15	3
0.20	0.489525	0.546149	0.510475	0.413851	0.20	9
0.25	0.504078	0.535472	0.495922	0.402028	0.25	7
0.30	0.521686	0.522273	0.478314	0.387727	0.30	6
0.35	0.542241	0.506465	0.457759	0.371035	0.35	5
0.40	0.565619	0.487944	0.434381	0.352056	0.40	5
0.45	0.591678	0.466594	0.408322	0.330906	0.45	4
0.50	0.620259	0.442285	0.379741	0.307715	0.50	4
0.55	0.651188	0.414873	0.348812	0.282627	0.55	4
0.60	0.684274	0.384205	0.315726	0.255795	0.60	4
0.65	0.719315	0.350114	0.280685	0.227386	0.65	3
0.70	0.756096	0.312426	0.243904	0.197574	0.70	3
0.75	0.794389	0.270957	0.205611	0.166543	0.75	3
0.80	0.833958	0.225516	0.166042	0.134485	0.80	3
0.85	0.874557	0.175904	0.125443	0.101596	0.85	3
0.90	0.915936	0.121919	0.084064	0.068081	0.90	3
0.95	0.957837	0.063354	0.042163	0.034146	0.95	3
1.00	1.000000	0.000000	0.000000	0.000000	1.00	0

FOURIER NO. = 0.40

Z	YA	YB	ASER	BSER	Z	N
0.	0.525513	0.615352	0.474487	0.384647	0.	3
0.05	0.526974	0.614038	0.473026	0.383462	0.05	3
0.10	0.531349	0.610088	0.468651	0.379912	0.10	3
0.15	0.538610	0.603479	0.461390	0.374021	0.15	3
0.20	0.548714	0.594177	0.451286	0.365823	0.20	9
0.25	0.561599	0.582129	0.438401	0.355371	0.25	7
0.30	0.577185	0.567273	0.422815	0.342727	0.30	6
0.35	0.595378	0.549529	0.404622	0.327971	0.35	5
0.40	0.616066	0.528808	0.383934	0.311192	0.40	5
0.45	0.639121	0.505005	0.360879	0.292495	0.45	4
0.50	0.664403	0.478006	0.335597	0.271994	0.50	4
0.55	0.691757	0.447683	0.308243	0.249817	0.55	4
0.60	0.721013	0.413902	0.278987	0.226098	0.60	4
0.65	0.751991	0.376514	0.248009	0.200986	0.65	3
0.70	0.784502	0.335366	0.215498	0.174634	0.70	3
0.75	0.818345	0.290295	0.181655	0.147205	0.75	3
0.80	0.853309	0.241131	0.146691	0.118869	0.80	3
0.85	0.889181	0.187701	0.110819	0.089799	0.85	3
0.90	0.925738	0.129825	0.074262	0.060175	0.90	3
0.95	0.962754	0.067319	0.037246	0.030161	0.95	3
1.00	1.000000	0.000000	0.000000	0.000000	1.00	0

FOURIER NO. = 0.50

Z	YA	YB	ASER	BSER	Z	N
0.	0.629223	0.699455	0.370777	0.300545	0.	3
0.05	0.630365	0.697881	0.369635	0.299619	0.05	3
0.10	0.633787	0.693155	0.366213	0.296845	0.10	3
0.15	0.639466	0.685259	0.360534	0.292241	0.15	3
0.20	0.647367	0.674164	0.352633	0.285836	0.20	9
0.25	0.657443	0.659832	0.342557	0.277668	0.25	7
0.30	0.669630	0.642212	0.330370	0.267788	0.30	6
0.35	0.683854	0.621242	0.316146	0.256258	0.35	5
0.40	0.700028	0.596853	0.299972	0.243147	0.40	5
0.45	0.718050	0.568963	0.281950	0.228537	0.45	4
0.50	0.737812	0.537481	0.262188	0.212519	0.50	4
0.55	0.759190	0.502310	0.240810	0.195190	0.55	4
0.60	0.782053	0.463343	0.217947	0.176657	0.60	4
0.65	0.806260	0.420465	0.193740	0.157035	0.65	3
0.70	0.831661	0.373554	0.168339	0.136446	0.70	3
0.75	0.858101	0.322486	0.141899	0.115015	0.75	3
0.80	0.885416	0.267126	0.114584	0.092874	0.80	3
0.85	0.913438	0.207339	0.086562	0.070161	0.85	3
0.90	0.941994	0.142984	0.058006	0.047016	0.90	3
0.95	0.970907	0.073919	0.029093	0.023581	0.95	3
1.00	1.000000	0.000000	0.000000	0.000000	1.00	0

TRANSIENT CONDUCTION

TEMPERATURE RATIO TERMS FOR THE PLATE

FOURIER NO. = 0.60

Z	YA	YB	ASER	BSER	Z	N
0.	0.710291	0.765170	0.289709	0.234830	0.	3
0.05	0.711184	0.763394	0.288816	0.234106	0.05	3
0.10	0.713858	0.758061	0.286142	0.231939	0.10	3
0.15	0.718296	0.749159	0.281704	0.228341	0.15	3
0.20	0.724470	0.736664	0.275530	0.223336	0.20	9
0.25	0.732343	0.720546	0.267657	0.216954	0.25	7
0.30	0.741867	0.700765	0.258133	0.209235	0.30	6
0.35	0.752982	0.677275	0.247018	0.200225	0.35	5
0.40	0.765620	0.650019	0.234380	0.189981	0.40	5
0.45	0.779703	0.618934	0.220297	0.178566	0.45	4
0.50	0.795144	0.583950	0.204856	0.166050	0.50	4
0.55	0.811848	0.544990	0.188152	0.152510	0.55	4
0.60	0.829712	0.501970	0.170288	0.138030	0.60	4
0.65	0.848626	0.454802	0.151374	0.122698	0.65	3
0.70	0.868474	0.403389	0.131526	0.106611	0.70	3
0.75	0.889132	0.347635	0.110868	0.089866	0.75	3
0.80	0.910474	0.287434	0.089526	0.072566	0.80	3
0.85	0.932368	0.222680	0.067632	0.054820	0.85	3
0.90	0.954679	0.153265	0.045321	0.036736	0.90	3
0.95	0.977269	0.079076	0.022731	0.018425	0.95	3
1.00	1.000000	0.000000	0.000000	0.000000	1.00	0

FOURIER NO. = 0.70

Z	YA	YB	ASER	BSER	Z	N
0.	0.773637	0.816517	0.226363	0.183483	0.	2
0.05	0.774335	0.814583	0.225665	0.182917	0.05	2
0.10	0.776424	0.808776	0.223576	0.181224	0.10	2
0.15	0.779892	0.799087	0.220108	0.178413	0.15	2
0.20	0.784716	0.785498	0.215284	0.174502	0.20	2
0.25	0.790868	0.767984	0.209132	0.169516	0.25	2
0.30	0.798309	0.746516	0.201691	0.163484	0.30	2
0.35	0.806994	0.721055	0.193006	0.156445	0.35	5
0.40	0.816869	0.691559	0.183131	0.148441	0.40	5
0.45	0.827872	0.657979	0.172128	0.139521	0.45	4
0.50	0.839937	0.620258	0.160063	0.129742	0.50	4
0.55	0.852989	0.578337	0.147011	0.119163	0.55	4
0.60	0.866947	0.532152	0.133053	0.107848	0.60	4
0.65	0.881726	0.481631	0.118274	0.095869	0.65	3
0.70	0.897233	0.426701	0.102767	0.083299	0.70	3
0.75	0.913375	0.367284	0.086625	0.070216	0.75	3
0.80	0.930050	0.303301	0.069950	0.056699	0.80	3
0.85	0.947157	0.234667	0.052843	0.042833	0.85	3
0.90	0.964589	0.161297	0.035411	0.028703	0.90	3
0.95	0.982240	0.083104	0.017760	0.014396	0.95	3
1.00	1.000000	0.000000	0.000000	0.000000	1.00	0

FOURIER NO. = 0.80

Z	YA	YB	ASER	BSER	Z	N
0.	0.823133	0.856637	0.176867	0.143363	0.	2
0.05	0.823678	0.854579	0.176322	0.142921	0.05	2
0.10	0.825310	0.848402	0.174690	0.141598	0.10	2
0.15	0.828020	0.838098	0.171980	0.139402	0.15	2
0.20	0.831789	0.823654	0.168211	0.136346	0.20	2
0.25	0.836596	0.805050	0.163404	0.132450	0.25	2
0.30	0.842410	0.782263	0.157590	0.127737	0.30	2
0.35	0.849196	0.755263	0.150804	0.122237	0.35	5
0.40	0.856911	0.724017	0.143089	0.115983	0.40	5
0.45	0.865509	0.688486	0.134491	0.109014	0.45	4
0.50	0.874936	0.648627	0.125064	0.101373	0.50	4
0.55	0.885134	0.604393	0.114866	0.093107	0.55	4
0.60	0.896040	0.555733	0.103960	0.084267	0.60	4
0.65	0.907587	0.502593	0.092413	0.074907	0.65	3
0.70	0.919704	0.444915	0.080296	0.065085	0.70	3
0.75	0.932316	0.382637	0.067684	0.054863	0.75	3
0.80	0.945345	0.315698	0.054655	0.044302	0.80	3
0.85	0.958711	0.244033	0.041289	0.033467	0.85	3
0.90	0.972332	0.167573	0.027668	0.022427	0.90	3
0.95	0.986123	0.086252	0.013877	0.011248	0.95	3
1.00	1.000000	0.000000	0.000000	0.000000	1.00	0

TRANSIENT CONDUCTION

TEMPERATURE RATIO TERMS FOR THE PLATE

FOURIER NO. - 0.90

Z	YA	YB	ASER	BSER	Z	N
0.	0.861806	0.887984	0.138194	0.112016	0.	2
0.05	0.862232	0.885829	0.137768	0.111671	0.05	2
0.10	0.863507	0.879363	0.136493	0.110637	0.10	2
0.15	0.865624	0.868579	0.134376	0.108921	0.15	2
0.20	0.868570	0.853467	0.131430	0.106533	0.20	2
0.25	0.872325	0.834011	0.127675	0.103489	0.25	2
0.30	0.876868	0.810193	0.123132	0.099807	0.30	2
0.35	0.882170	0.781991	0.117830	0.095509	0.35	5
0.40	0.888199	0.749377	0.111801	0.090623	0.40	5
0.45	0.894916	0.712322	0.105084	0.085178	0.45	4
0.50	0.902282	0.670793	0.097718	0.079207	0.50	4
0.55	0.910250	0.624752	0.089750	0.072748	0.55	4
0.60	0.918772	0.574159	0.081228	0.065841	0.60	4
0.65	0.927794	0.518972	0.072206	0.058528	0.65	3
0.70	0.937261	0.459146	0.062739	0.050854	0.70	3
0.75	0.947115	0.394633	0.052885	0.042867	0.75	3
0.80	0.957296	0.325385	0.042704	0.034615	0.80	3
0.85	0.967739	0.251350	0.032261	0.026150	0.85	3
0.90	0.978382	0.172477	0.021618	0.017523	0.90	3
0.95	0.989157	0.088711	0.010843	0.008789	0.95	3
1.00	1.000000	0.000000	0.000000	0.000000	1.00	0

FOURIER NO. = 1.00

Z	YA	YB	ASER	BSER	Z	N
0.	0.892023	0.912477	0.107977	0.087523	0.	2
0.05	0.892356	0.910247	0.107644	0.087253	0.05	2
0.10	0.893352	0.903555	0.106648	0.086445	0.10	2
0.15	0.895006	0.892395	0.104994	0.085105	0.15	2
0.20	0.897308	0.876761	0.102692	0.083239	0.20	2
0.25	0.900242	0.856639	0.099758	0.080861	0.25	2
0.30	0.903792	0.832017	0.096208	0.077983	0.30	2
0.35	0.907934	0.802874	0.092066	0.074626	0.35	5
0.40	0.912645	0.769192	0.087355	0.070808	0.40	5
0.45	0.917894	0.730947	0.082106	0.066553	0.45	4
0.50	0.923649	0.688112	0.076351	0.061888	0.50	4
0.55	0.929875	0.640658	0.070125	0.056842	0.55	4
0.60	0.936533	0.588555	0.063467	0.051445	0.60	4
0.65	0.943582	0.531769	0.056418	0.045731	0.65	3
0.70	0.950979	0.470265	0.049021	0.039735	0.70	3
0.75	0.958679	0.404006	0.041321	0.033494	0.75	3
0.80	0.966633	0.332954	0.033367	0.027046	0.80	3
0.85	0.974793	0.257068	0.025207	0.020432	0.85	3
0.90	0.983109	0.176308	0.016891	0.013692	0.90	3
0.95	0.991528	0.090633	0.008472	0.006867	0.95	3
1.00	1.000000	0.000000	0.000000	0.000000	1.00	0

FOURIER NO. = 1.20

Z	YA	YB	ASER	BSER	Z	N
0.	0.934080	0.946567	0.065920	0.053433	0.	2
0.05	0.934283	0.944232	0.065717	0.053268	0.05	2
0.10	0.934892	0.937225	0.065108	0.052775	0.10	2
0.15	0.935902	0.925544	0.064098	0.051956	0.15	2
0.20	0.937307	0.909183	0.062693	0.050817	0.20	2
0.25	0.939098	0.888135	0.060902	0.049365	0.25	2
0.30	0.941265	0.862391	0.058735	0.047609	0.30	2
0.35	0.943794	0.831941	0.056206	0.045559	0.35	5
0.40	0.946670	0.796772	0.053330	0.043228	0.40	5
0.45	0.949874	0.756870	0.050126	0.040630	0.45	4
0.50	0.953388	0.712217	0.046612	0.037783	0.50	4
0.55	0.957189	0.662798	0.042811	0.034702	0.55	4
0.60	0.961253	0.608593	0.038747	0.031407	0.60	4
0.65	0.965557	0.549582	0.034443	0.027918	0.65	3
0.70	0.970073	0.485742	0.029927	0.024258	0.70	3
0.75	0.974774	0.417052	0.025226	0.020448	0.75	3
0.80	0.979630	0.343488	0.020370	0.016512	0.80	3
0.85	0.984611	0.265026	0.015389	0.012474	0.85	3
0.90	0.989688	0.181641	0.010312	0.008359	0.90	3
0.95	0.994828	0.093308	0.005172	0.004192	0.95	3
1.00	1.000000	0.000000	0.000000	0.000000	1.00	0

TRANSIENT CONDUCTION

TEMPERATURE RATIO TERMS FOR THE PLATE

FOURIER NO. = 1.40

Z	YA	YB	ASER	BSER	Z	N
0.	0.959756	0.967380	0.040244	0.032620	0.	2
0.05	0.959880	0.964980	0.040120	0.032520	0.05	2
0.10	0.960252	0.957781	0.039748	0.032219	0.10	2
0.15	0.960868	0.945781	0.039132	0.031719	0.15	2
0.20	0.961726	0.928976	0.038274	0.031024	0.20	2
0.25	0.962819	0.907363	0.037181	0.030137	0.25	2
0.30	0.964142	0.880935	0.035858	0.029065	0.30	2
0.35	0.965686	0.849686	0.034314	0.027814	0.35	5
0.40	0.967442	0.813609	0.032558	0.026391	0.40	5
0.45	0.969398	0.772695	0.030602	0.024805	0.45	4
0.50	0.971543	0.726934	0.028457	0.023066	0.50	4
0.55	0.973864	0.676315	0.026136	0.021185	0.55	4
0.60	0.976345	0.620826	0.023655	0.019174	0.60	4
0.65	0.978973	0.560456	0.021027	0.017044	0.65	3
0.70	0.981730	0.495191	0.018270	0.014809	0.70	3
0.75	0.984599	0.425017	0.015401	0.012483	0.75	3
0.80	0.987564	0.349920	0.012436	0.010080	0.80	3
0.85	0.990605	0.269885	0.009395	0.007615	0.85	3
0.90	0.993704	0.184897	0.006296	0.005103	0.90	3
0.95	0.996842	0.094941	0.003157	0.002559	0.95	3
1.00	1.000000	0.000000	0.000000	0.000000	1.00	0

FOURIER NO. = 1.60

Z	YA	YB	ASER	BSER	Z	N
0.	0.975431	0.980085	0.024569	0.019915	0.	2
0.05	0.975507	0.977647	0.024493	0.019853	0.05	2
0.10	0.975734	0.970330	0.024266	0.019670	0.10	2
0.15	0.976110	0.958136	0.023890	0.019364	0.15	2
0.20	0.976634	0.941060	0.023366	0.018940	0.20	2
0.25	0.977301	0.919101	0.022699	0.018399	0.25	2
0.30	0.978109	0.892256	0.021891	0.017744	0.30	2
0.35	0.979052	0.860520	0.020948	0.016980	0.35	5
0.40	0.980123	0.823889	0.019877	0.016111	0.40	5
0.45	0.981318	0.782357	0.018682	0.015143	0.45	4
0.50	0.982627	0.735918	0.017373	0.014082	0.50	4
0.55	0.984044	0.684566	0.015956	0.012934	0.55	4
0.60	0.985559	0.628294	0.014441	0.011706	0.60	4
0.65	0.987163	0.567095	0.012837	0.010405	0.65	3
0.70	0.988846	0.500959	0.011154	0.009041	0.70	3
0.75	0.990598	0.429879	0.009402	0.007621	0.75	3
0.80	0.992408	0.353846	0.007592	0.006154	0.80	3
0.85	0.994265	0.272851	0.005735	0.004649	0.85	3
0.90	0.996157	0.186885	0.003843	0.003115	0.90	3
0.95	0.998072	0.095938	0.001928	0.001562	0.95	3
1.00	1.000000	0.000000	0.000000	0.000000	1.00	0

FOURIER NO. = 1.80

Z	YA	YB	ASER	BSER	Z	N
0.	0.985001	0.987842	0.014999	0.012158	0.	2
0.05	0.985047	0.985380	0.014953	0.012120	0.05	2
0.10	0.985185	0.977992	0.014815	0.012008	0.10	2
0.15	0.985415	0.965678	0.014585	0.011822	0.15	2
0.20	0.985735	0.948437	0.014265	0.011563	0.20	2
0.25	0.986143	0.926268	0.013857	0.011232	0.25	2
0.30	0.986636	0.899167	0.013364	0.010833	0.30	2
0.35	0.987211	0.867134	0.012789	0.010366	0.35	5
0.40	0.987865	0.830164	0.012135	0.009836	0.40	5
0.45	0.988595	0.788255	0.011405	0.009245	0.45	4
0.50	0.989394	0.741403	0.010606	0.008597	0.50	4
0.55	0.990259	0.689604	0.009741	0.007896	0.55	4
0.60	0.991184	0.632854	0.008816	0.007146	0.60	4
0.65	0.992163	0.571148	0.007837	0.006352	0.65	3
0.70	0.993190	0.504480	0.006809	0.005520	0.70	3
0.75	0.994260	0.432847	0.005740	0.004653	0.75	3
0.80	0.995365	0.356243	0.004635	0.003757	0.80	3
0.85	0.996498	0.274662	0.003501	0.002838	0.85	3
0.90	0.997654	0.188098	0.002346	0.001902	0.90	3
0.95	0.998823	0.096546	0.001177	0.000954	0.95	3
1.00	1.000000	0.000000	0.000000	0.000000	1.00	0

TRANSIENT CONDUCTION

TEMPERATURE RATIO TERMS FOR THE PLATE

FOURIER NO. = 2.00

Z	YA	YB	ASER	BSER	Z	N
0.	0.990843	0.992578	0.009157	0.007422	0.	2
0.05	0.990871	0.990100	0.009129	0.007899	0.05	2
0.10	0.990956	0.982669	0.009044	0.007331	0.10	2
0.15	0.991096	0.970283	0.008904	0.007217	0.15	2
0.20	0.991291	0.952941	0.008709	0.007059	0.20	2
0.25	0.991540	0.930643	0.008460	0.006857	0.25	2
0.30	0.991841	0.903387	0.008159	0.006613	0.30	2
0.35	0.992192	0.871171	0.007808	0.006329	0.35	5
0.40	0.992592	0.833995	0.007408	0.006005	0.40	5
0.45	0.993037	0.791856	0.006963	0.005644	0.45	4
0.50	0.993525	0.744752	0.006475	0.005248	0.50	4
0.55	0.994053	0.692680	0.005947	0.004820	0.55	4
0.60	0.994618	0.635637	0.005382	0.004363	0.60	4
0.65	0.995215	0.573622	0.004785	0.003878	0.65	3
0.70	0.995843	0.506630	0.004157	0.003370	0.70	3
0.75	0.996496	0.434660	0.003504	0.002840	0.75	3
0.80	0.997170	0.357706	0.002830	0.002294	0.80	3
0.85	0.997862	0.275767	0.002138	0.001733	0.85	3
0.90	0.998568	0.188839	0.001432	0.001161	0.90	3
0.95	0.999282	0.096918	0.000718	0.000582	0.95	3
1.00	1.000000	0.000000	0.000000	0.000000	1.00	0

APPENDIX B

TEMPERATURE HISTORY FOR THE CYLINDER

The results presented apply to the infinite cylinder as follows:

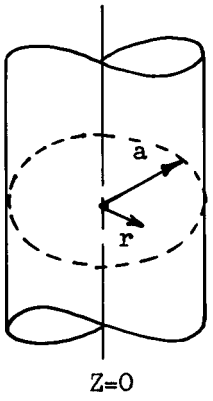

$Z = \xi = r/a$

The position ratio

The following special terms were employed in the computer program:

$$ET1 = \beta_n \, \mathrm{Exp}(\beta_n^2 \phi)$$

$$ET2 = \beta_n^2 \, ET1$$

$$TJ = J_o(Z\beta_n)/J_1(\beta_n)$$

XN = n, the series index

The individual series terms in Equations (19) and (20) were designated as follows:

$$SERA = 2TJ/ET1$$

$$SERB = 8TJ/ET2$$

The series sums were designated by ASER and BSER, and N gives the number of terms required to converge to the tolerance TOL (a value of Tol = 0.0000001 was employed throughout). The values Y_a and Y_b were calculated as

$$YA = 1 - ASER$$

$$YB = 1 - Z^2 - BSER$$

The data cards require DZ and TOL on the first card, then each value of PHI (the Fourier number ϕ) is entered on a separate card; as many as desired. The computations were made on the IBM 7090 with the Fortran system.

```
C     TRSCND      A-005       5-12-61                                          00500020
C                                                                              00500030
C     PROGRAMMER H. WOLF                                                       00500040
C                                                                              00500050
C     SYNOPSIS-  CALCULATION OF TRANSIENT CONDUCTION HISTORY FOR THE           00500060
C                CYLINDER AS A FUNCTION OF FOURIER NUMBER AND POSITION        00500070
C                RATIO WITH ZERO AND FINITE SURFACE TEMP. AND WITH ZERO       00500080
C                INITIAL TEMP. THROUGHOUT.                                    00500090
C                                                                             00500095
C     PURPOSE -  GENERATE TABLES OF VALUES                                     00500100
C                                                                              00500105
C                                                                              00500110
C     SYMBOLS -                                                                00500112
C          Z - POSITION RATIO                PHI - FOURIER NUMBER            00500114
C         DZ - UPDATING FACTOR ON Z          TOL - TOLERANCE ON CONVERG.     00500116
C          N - NO. OF TERMS REQD.             TJ - BESEL FUNCT TERM          00500118
C       B(I) - SLNS OF J0(X)=0.              ET1 - EXP TERM X B(I)           00500120
C       ASER - SERIES SUM FOR YA             ET2 - EXP TERM X B(I)XB(I)      00500122
C       BSER - SERIES SUM FOR YB                                             00500124
C                                                                              00500126
C            *-*-*                *-*-*-*                 *-*-*              00500128
C                                                                              00500140
C             SEE NOTES FOR SPECIALIZED NOMENCLATURE EMPLOYED FOR             00500150
C             DESIGNATION OF PARTS OF THE SERIES TERMS.                       00500160
C                                                                             00500170
C            *-*-*                *-*-*-*                 *-*-*              00500180
C                                                                              00500190
C     MAIN CALCULATIONS                                                        00500200
C                                                                             00500210
C                                                                              00500220
      DIMENSION  B(30)                                                        00500222
    5 READ INPUT TAPE 5,10, DZ, TOL                                           00500230
   10 FORMAT(F12.4, F12.7)                                                    00500232
   35 READ INPUT TAPE 5, 40, (B(J),J=1,24)                                    00500250
   40 FORMAT(6F12.4)                                                          00500260
   15 READ INPUT TAPE 5,16, PHI                                               00500270
   16 FORMAT(F12.6)                                                           00500272
   18 IF(PHI - 10.) 20, 20, 235                                               00500278
   20 Z = 0.                                                                  00500280
   22 WRITE OUTPUT TAPE 6,23, PHI                                             00500282
   23 FORMAT(1H1///45X,  20HTRANSIENT CONDUCTION// 35X,   40HTEMPERATURE      00500284
     1 RATIO TERMS FOR THE CYLINDER/// 45X, 14HFOURIER NO. = F4.3///21X       00500286
     2,67H Z          YA          YB          ASER        BSER        Z       00500287
     3    N//1H )                                                             00500288
   25 ASER = 0.                                                               00500290
   30 BSER = 0.                                                               00500300
   34 IF(Z - .99)   45,45,36                                                  00500302
   36 YA = 1.000000                                                           00500304
   38 YB = 0.0000001                                                          00500306
   41 ASER = 0.0000001                                                        00500308
   42 BSER = 0.0000001                                                        00500310
      I = 0                                                                   00500311
   43 GO TO 200                                                               00500312
   45 DO195 I=1,24                                                            00500350
   50 X     = B(I)*B(I)*PHI                                                   00500360
   55 IF(X     - 86.) 60,60, 75                                               00500370
   60 ET1 = EXPF(X)    *B(I)                                                  00500380
   65 ET2 = ET1*B(I)*B(I)                                                     00500390
   70 GO TO 100                                                               00500400
   75 XB = X/1000.                                                            00500410
   76 D = EXPF(XB)                                                            00500415
   77 D1 = D**10.                                                             00500420
   80 D2= D1**10.                                                             00500425
   85 ET1 =(D2**10.)*B(I)                                                     00500430
   90 ET2 = ET1*B(I)*B(I)                                                     00500440
  100 TJ  = BESELF(Z*B(I),0,1) /BESELF(B(I),1,1)                              00500450
  110 SERA =(TJ/ET1)*2.                                                       00500460
  120 SERB =(TJ/ET2)*8.                                                       00500470
  145 XN = FLOATF(I)                                                          00500480
  160 ASER1 = ASER + SERA                                                     00500510
  165 A1 = ABSF(ASER1)                                                        00500520
  170 A  = ABSF(ASER)                                                         00500530
  175 BBB = ABSF (A1 - A)                                                     00500540
  180 ASER = ASER + SERA                                                      00500550
  185 BSER = BSER + SERB                                                      00500560
  190 IF(TOL - BBB) 195, 195, 196                                             00500570
  195 CONTINUE                                                                00500580
  196 YA = 1. - ASER                                                          00500582
  197 YB = 1. - Z*Z - BSER                                                    00500584
      IF(YA) 198,198, 200                                                     00500586
  198 ASER = 1.0000001                                                        00500587
      YA = 0.0000001                                                          00500588
  200 WRITE OUTPUT TAPE 6,202, Z, YA, YB, ASER, BSER, Z , I                   00500590
  202 FORMAT(F25.2, 2F12.6, F13.6, F12.6, F8.2, I6)                           00500600
  205 Z = Z + DZ                                                              00500620
  210 IF(Z - 1.01)    25,25,15                                                00500630
  235 CALL EXIT                                                               00500670
      STOP                                                                    00500680
      END(1,0,0,0,0,0,0,0,0,0,0,0,0,0,0)
```

EXTERNAL FORMULA NUMBERS WITH CORRESPONDING INTERNAL FORMULA NUMBERS AND OCTAL LOCATIONS

EFN	IFN	LOC	EFN	IFN	LOC	EFN	IFN	LOC	EFN	IFN	LOC
10	2	00000	40	3	00000	16	4	00000	23	5	00000
202	6	00000	5	8	00014	5	9	00017	35	10	00024
35	14	00034	15	15	00040	15	16	00045	18	17	00052
20	18	00056	22	19	00060	22	20	00065	25	21	00072
30	22	00074	34	23	00076	36	24	00104	38	25	00106
41	26	00110	42	27	00112	43	29	00116	45	30	00117
50	31	00122	55	32	00127	60	33	00133	65	34	00144
70	35	00151	75	36	00153	76	37	00156	77	38	00165
80	39	00175	85	40	00205	90	41	00217	100	42	00224
110	43	00252	120	44	00256	145	45	00262	160	46	00267
165	47	00272	170	48	00275	175	49	00300	180	50	00304
185	51	00307	190	52	00312	195	53	00316	196	54	00322
197	55	00325	198	57	00336	200	59	00344	200	60	00351
205	61	00372	210	62	00375	235	63	00402			

STORAGE NOT USED BY PROGRAM

DEC	OCT	DEC	OCT
390	00606	32561	77461

LOCATIONS OF NAMES IN TRANSFER VECTOR

	DEC	OCT		DEC	OCT		DEC	OCT		DEC	OCT
EXP(3	6	00006	EXP	5	00005	EXIT	8	00010	BESEL	7	00007
(FIL)	4	00004	(FPT)	0	00000	(RTN)	2	00002	(STH)	3	00003
(TSH)	1	00001									

STORAGE LOCATIONS FOR VARIABLES APPEARING IN DIMENSION AND EQUIVALENCE SENTENCES

	DEC	OCT		DEC	OCT		DEC	OCT		DEC	OCT
B	389	00605									

STORAGE LOCATIONS FOR VARIABLES NOT APPEARING IN DIMENSION, EQUIVALENCE OR COMMON SENTENCES

	DEC	OCT		DEC	OCT		DEC	OCT		DEC	OCT
I	359	00547	ET2	358	00546	ET1	357	00545	DZ	356	00544
D	355	00543	D2	354	00542	D1	353	00541	BSER	352	00540
BBB	351	00537	ASER	350	00536	ASER1	349	00535	A	348	00534
A1	347	00533	PHI	346	00532	SERA	345	00531	SERB	344	00530
TJ	343	00527	TOL	342	00526	XB	341	00525	XN	340	00524
X	339	00523	YA	338	00522	YB	337	00521	Z	336	00520

TRANSIENT CONDUCTION

TEMPERATURE RATIO TERMS FOR THE CYLINDER

FOURIER NO. = .010

Z	YA	YB	ASER	BSER	Z	N
0.	0.000000	0.039975	1.000000	0.960025	0.	13
0.05	0.000000	0.039975	1.000000	0.957525	0.05	13
0.10	0.000000	0.039975	1.000000	0.950025	0.10	13
0.15	0.000000	0.039975	1.000000	0.937525	0.15	12
0.20	0.000000	0.039975	1.000000	0.920025	0.20	13
0.25	0.000000	0.039975	1.000000	0.897525	0.25	12
0.30	0.000000	0.039976	1.000000	0.870024	0.30	12
0.35	0.000000	0.039976	1.000000	0.837524	0.35	11
0.40	0.000021	0.039976	0.999979	0.800024	0.40	12
0.45	0.000137	0.039976	0.999863	0.757524	0.45	12
0.50	0.000565	0.039975	0.999435	0.710025	0.50	12
0.55	0.001967	0.039967	0.998033	0.657533	0.55	12
0.60	0.006049	0.039939	0.993951	0.600061	0.60	12
0.65	0.016574	0.039850	0.983426	0.537650	0.65	12
0.70	0.040618	0.039596	0.959382	0.470405	0.70	12
0.75	0.089238	0.038945	0.910762	0.398555	0.75	12
0.80	0.176228	0.037438	0.823772	0.322562	0.80	12
0.85	0.313821	0.034266	0.686179	0.243234	0.85	12
0.90	0.506049	0.028173	0.493951	0.161827	0.90	12
0.95	0.742968	0.017439	0.257032	0.080061	0.95	12
1.00	1.000000	0.000000	0.000000	0.000000	1.00	0

FOURIER NO. = .020

Z	YA	YB	ASER	BSER	Z	N
0.	0.000000	0.079975	1.000000	0.920025	0.	10
0.05	0.000002	0.079975	0.999998	0.917525	0.05	9
0.10	0.000014	0.079975	0.999986	0.910025	0.10	8
0.15	0.000048	0.079975	0.999952	0.897525	0.15	9
0.20	0.000136	0.079975	0.999864	0.880025	0.20	9
0.25	0.000350	0.079973	0.999650	0.857527	0.25	9
0.30	0.000852	0.079968	0.999148	0.830032	0.30	9
0.35	0.001966	0.079955	0.998034	0.797545	0.35	9
0.40	0.004307	0.079925	0.995693	0.760075	0.40	9
0.45	0.008962	0.079855	0.991038	0.717645	0.45	9
0.50	0.017708	0.079704	0.982292	0.670296	0.50	9
0.55	0.033213	0.079393	0.966787	0.618107	0.55	9
0.60	0.059133	0.078781	0.940867	0.561219	0.60	9
0.65	0.099961	0.077636	0.900039	0.499864	0.65	9
0.70	0.160521	0.075593	0.839479	0.434407	0.70	9
0.75	0.245059	0.072118	0.754941	0.365382	0.75	9
0.80	0.356054	0.066468	0.643946	0.293532	0.80	9
0.85	0.493024	0.057680	0.506976	0.219820	0.85	9
0.90	0.651748	0.044578	0.348252	0.145422	0.90	9
0.95	0.824303	0.025823	0.175697	0.071677	0.95	9
1.00	1.000000	0.000000	0.000000	0.000000	1.00	0

FOURIER NO. = .030

Z	YA	YB	ASER	BSER	Z	N
0.	0.000458	0.119970	0.999542	0.880030	0.	8
0.05	0.000542	0.119969	0.999458	0.877531	0.05	8
0.10	0.000826	0.119965	0.999174	0.870035	0.10	8
0.15	0.001419	0.119955	0.998581	0.857545	0.15	8
0.20	0.002534	0.119936	0.997466	0.840064	0.20	8
0.25	0.004530	0.119897	0.995470	0.817603	0.25	7
0.30	0.007977	0.119822	0.992023	0.790178	0.30	8
0.35	0.013731	0.119683	0.986269	0.757817	0.35	8
0.40	0.023007	0.119431	0.976993	0.720569	0.40	7
0.45	0.037433	0.118986	0.962567	0.678514	0.45	8
0.50	0.059055	0.118227	0.940945	0.631773	0.50	8
0.55	0.090257	0.116967	0.909743	0.580533	0.55	7
0.60	0.133585	0.114940	0.866415	0.525060	0.60	8
0.65	0.191439	0.111778	0.808561	0.465722	0.65	8
0.70	0.265676	0.106989	0.734324	0.403011	0.70	7
0.75	0.357172	0.099945	0.642828	0.337555	0.75	8
0.80	0.465422	0.089879	0.534578	0.270121	0.80	8
0.85	0.588283	0.075892	0.411717	0.201608	0.85	7
0.90	0.721947	0.056973	0.278053	0.133027	0.90	8
0.95	0.861214	0.032040	0.138786	0.065460	0.95	8
1.00	1.000000	0.000000	0.000000	0.000000	1.00	0

TRANSIENT CONDUCTION

TEMPERATURE RATIO TERMS FOR THE CYLINDER

FOURIER NO. = .040

Z	YA	YB	ASER	BSER	Z	N
0.	0.003715	0.159902	0.996285	0.840098	0.	7
0.05	0.004083	0.159892	0.995917	0.837608	0.05	7
0.10	0.005259	0.159861	0.994741	0.830139	0.10	7
0.15	0.007467	0.159799	0.992533	0.817701	0.15	7
0.20	0.011097	0.159688	0.988903	0.800312	0.20	7
0.25	0.016734	0.159501	0.983266	0.777999	0.25	7
0.30	0.025178	0.159193	0.974822	0.750807	0.30	6
0.35	0.037462	0.158695	0.962538	0.718805	0.35	7
0.40	0.054850	0.157908	0.945150	0.682092	0.40	7
0.45	0.078804	0.156689	0.921196	0.640811	0.45	7
0.50	0.110902	0.154844	0.889098	0.595156	0.50	7
0.55	0.152721	0.152106	0.847279	0.545394	0.55	7
0.60	0.205662	0.148133	0.794338	0.491867	0.60	7
0.65	0.270757	0.142489	0.729243	0.435011	0.65	6
0.70	0.348451	0.134640	0.651549	0.375360	0.70	7
0.75	0.438421	0.123953	0.561579	0.313547	0.75	7
0.80	0.539454	0.109697	0.460546	0.250303	0.80	7
0.85	0.649409	0.091061	0.350591	0.186439	0.85	7
0.90	0.765295	0.067169	0.234705	0.122831	0.90	7
0.95	0.883486	0.037115	0.116514	0.060385	0.95	7
1.00	1.000000	0.000000	0.000000	0.000000	1.00	0

FOURIER NO. = .050

Z	YA	YB	ASER	BSER	Z	N
0.	0.012890	0.199593	0.987110	0.800407	0.	6
0.05	0.013697	0.199560	0.986303	0.797940	0.05	6
0.10	0.016208	0.199456	0.983792	0.790544	0.10	6
0.15	0.020688	0.199261	0.979312	0.778239	0.15	6
0.20	0.027583	0.198941	0.972417	0.761059	0.20	6
0.25	0.037512	0.198443	0.962488	0.739057	0.25	6
0.30	0.051266	0.197689	0.948734	0.712311	0.30	6
0.35	0.069779	0.196572	0.930221	0.680928	0.35	6
0.40	0.094093	0.194945	0.905907	0.645055	0.40	6
0.45	0.125297	0.192615	0.874703	0.604885	0.45	6
0.50	0.164444	0.189334	0.835556	0.560666	0.50	6
0.55	0.212453	0.184788	0.787547	0.512712	0.55	6
0.60	0.269986	0.178592	0.730014	0.461408	0.60	6
0.65	0.337337	0.170288	0.662663	0.407212	0.65	6
0.70	0.414325	0.159337	0.585675	0.350663	0.70	6
0.75	0.500219	0.145128	0.499781	0.292372	0.75	6
0.80	0.593709	0.126983	0.406291	0.233017	0.80	6
0.85	0.692926	0.104171	0.307074	0.173330	0.85	6
0.90	0.795523	0.075921	0.204477	0.114079	0.90	6
0.95	0.898824	0.041452	0.101176	0.056048	0.95	6
1.00	1.000000	0.000000	0.000000	0.000000	1.00	0

FOURIER NO. = .060

Z	YA	YB	ASER	BSER	Z	N
0.	0.029448	0.238771	0.970552	0.761229	0.	6
0.05	0.030719	0.238697	0.969281	0.758803	0.05	6
0.10	0.034617	0.238464	0.965383	0.751536	0.10	6
0.15	0.041386	0.238043	0.958614	0.739457	0.15	5
0.20	0.051426	0.237383	0.948574	0.722617	0.20	6
0.25	0.065272	0.236407	0.934728	0.701093	0.25	6
0.30	0.083576	0.235009	0.916424	0.674991	0.30	6
0.35	0.107066	0.233047	0.892934	0.644453	0.35	6
0.40	0.136500	0.230339	0.863500	0.609661	0.40	6
0.45	0.172609	0.226656	0.827391	0.570844	0.45	6
0.50	0.216029	0.221715	0.783971	0.528285	0.50	6
0.55	0.267223	0.215177	0.732777	0.482323	0.55	6
0.60	0.326411	0.206640	0.673589	0.433360	0.60	5
0.65	0.393503	0.195641	0.606497	0.381859	0.65	6
0.70	0.468044	0.181656	0.531956	0.328344	0.70	6
0.75	0.549188	0.164105	0.450812	0.273395	0.75	6
0.80	0.635702	0.142363	0.364298	0.217638	0.80	5
0.85	0.725997	0.115765	0.274003	0.161735	0.85	6
0.90	0.818197	0.083627	0.181803	0.106373	0.90	6
0.95	0.910240	0.045261	0.089760	0.052239	0.95	6
1.00	1.000000	0.000000	0.000000	0.000000	1.00	0

TRANSIENT CONDUCTION

TEMPERATURE RATIO TERMS FOR THE CYLINDER

FOURIER NO. = .070

Z	YA	YB	ASER	BSER	Z	N
0.	0.053019	0.277143	0.946981	0.722857	0.	6
0.05	0.054692	0.277010	0.945308	0.720490	0.05	5
0.10	0.059776	0.276596	0.940224	0.713404	0.10	5
0.15	0.068466	0.275865	0.931534	0.701635	0.15	5
0.20	0.081072	0.274750	0.918928	0.685250	0.20	5
0.25	0.098003	0.273155	0.901997	0.664345	0.25	5
0.30	0.119735	0.270952	0.880265	0.639048	0.30	5
0.35	0.146779	0.267975	0.853221	0.609525	0.35	5
0.40	0.179632	0.264016	0.820368	0.575984	0.40	5
0.45	0.218735	0.258823	0.781265	0.538677	0.45	5
0.50	0.264417	0.252095	0.735583	0.497905	0.50	5
0.55	0.316845	0.243479	0.683155	0.454021	0.55	5
0.60	0.375974	0.232571	0.624026	0.407429	0.60	5
0.65	0.441510	0.218916	0.558490	0.358584	0.65	5
0.70	0.512888	0.202012	0.487112	0.307988	0.70	5
0.75	0.589259	0.181311	0.410741	0.256189	0.75	5
0.80	0.669509	0.156236	0.330491	0.203764	0.80	5
0.85	0.752286	0.126181	0.247714	0.151320	0.85	5
0.90	0.836058	0.090529	0.163942	0.099471	0.90	5
0.95	0.919184	0.048666	0.080816	0.048834	0.95	5
1.00	1.000000	0.000000	0.000000	0.000000	1.00	0

FOURIER NO. = .080

Z	YA	YB	ASER	BSER	Z	N
0.	0.082272	0.314454	0.917728	0.685546	0.	5
0.05	0.084249	0.314247	0.915751	0.683253	0.05	5
0.10	0.090227	0.313611	0.909773	0.676389	0.10	5
0.15	0.100343	0.312502	0.899657	0.664998	0.15	5
0.20	0.114816	0.310843	0.885184	0.649157	0.20	5
0.25	0.133924	0.308524	0.866076	0.628976	0.25	5
0.30	0.157981	0.305402	0.842019	0.604598	0.30	5
0.35	0.187305	0.301294	0.812695	0.576206	0.35	5
0.40	0.222184	0.295976	0.777816	0.544024	0.40	5
0.45	0.262837	0.289184	0.737163	0.508316	0.45	5
0.50	0.309378	0.280608	0.690622	0.469392	0.50	5
0.55	0.361775	0.269892	0.638225	0.427608	0.55	5
0.60	0.419826	0.256638	0.580174	0.383362	0.60	5
0.65	0.483134	0.240405	0.516866	0.337095	0.65	5
0.70	0.551094	0.220713	0.448906	0.289287	0.70	5
0.75	0.622898	0.197050	0.377102	0.240450	0.75	5
0.80	0.697548	0.168878	0.302452	0.191122	0.80	5
0.85	0.773886	0.135644	0.226114	0.141856	0.85	5
0.90	0.850635	0.096786	0.149365	0.093214	0.90	5
0.95	0.926454	0.051748	0.073546	0.045752	0.95	5
1.00	1.000000	0.000000	0.000000	0.000000	1.00	0

FOURIER NO. = .090

Z	YA	YB	ASER	BSER	Z	N
0.	0.115629	0.350507	0.884371	0.649493	0.	5
0.05	0.117813	0.350216	0.882187	0.647284	0.05	5
0.10	0.124395	0.349329	0.875605	0.640671	0.10	5
0.15	0.135463	0.347794	0.864537	0.629706	0.15	5
0.20	0.151151	0.345530	0.848849	0.614470	0.20	4
0.25	0.171628	0.342417	0.828372	0.595083	0.25	5
0.30	0.197071	0.338302	0.802929	0.571698	0.30	5
0.35	0.227647	0.332993	0.772353	0.544507	0.35	5
0.40	0.263482	0.326258	0.736518	0.513742	0.40	5
0.45	0.304632	0.317827	0.695368	0.479673	0.45	5
0.50	0.351060	0.307388	0.648940	0.442612	0.50	5
0.55	0.402607	0.294591	0.597393	0.402909	0.55	5
0.60	0.458974	0.279048	0.541026	0.360952	0.60	5
0.65	0.519713	0.260333	0.480287	0.317167	0.65	5
0.70	0.584216	0.237992	0.415784	0.272008	0.70	5
0.75	0.651727	0.211543	0.348273	0.225957	0.75	5
0.80	0.721354	0.180488	0.278646	0.179512	0.80	5
0.85	0.792092	0.144315	0.207908	0.133185	0.85	5
0.90	0.862859	0.102509	0.137141	0.087491	0.90	5
0.95	0.932532	0.054565	0.067468	0.042935	0.95	5
1.00	1.000000	0.000000	0.000000	0.000000	1.00	0

TRANSIENT CONDUCTION

TEMPERATURE RATIO TERMS FOR THE CYLINDER

FOURIER NO. = .100

Z	YA	YB	ASER	BSER	Z	N
0.	0.151632	0.385168	0.848368	0.614832	0.	5
0.05	0.153940	0.384788	0.846060	0.612712	0.05	5
0.10	0.160880	0.383629	0.839120	0.606371	0.10	5
0.15	0.172499	0.381640	0.827501	0.595860	0.15	5
0.20	0.188864	0.378732	0.811136	0.581268	0.20	4
0.25	0.210056	0.374785	0.789944	0.562715	0.25	5
0.30	0.236148	0.369637	0.763852	0.540363	0.30	5
0.35	0.267191	0.363093	0.732809	0.514407	0.35	5
0.40	0.303190	0.354919	0.696810	0.485081	0.40	5
0.45	0.344087	0.344845	0.655913	0.452655	0.45	4
0.50	0.389740	0.332563	0.610260	0.417437	0.50	4
0.55	0.439907	0.317730	0.560093	0.379770	0.55	5
0.60	0.494234	0.299972	0.505766	0.340028	0.60	5
0.65	0.552248	0.278881	0.447752	0.298619	0.65	5
0.70	0.613358	0.254028	0.386642	0.255972	0.70	4
0.75	0.676861	0.224961	0.323139	0.212539	0.75	4
0.80	0.741953	0.191213	0.258047	0.168787	0.80	5
0.85	0.807755	0.152310	0.192245	0.125190	0.85	5
0.90	0.873331	0.107780	0.126669	0.082220	0.90	5
0.95	0.937725	0.057157	0.062275	0.040343	0.95	4
1.00	1.000000	0.000000	0.000000	0.000000	1.00	0

FOURIER NO. = .120

Z	YA	YB	ASER	BSER	Z	N
0.	0.227057	0.450035	0.772943	0.549965	0.	4
0.05	0.229431	0.449466	0.770569	0.548034	0.05	4
0.10	0.236550	0.447740	0.763450	0.542260	0.10	4
0.15	0.248406	0.444806	0.751594	0.532694	0.15	4
0.20	0.264981	0.440573	0.735019	0.519427	0.20	4
0.25	0.286238	0.434917	0.713762	0.502583	0.25	4
0.30	0.312117	0.427680	0.687883	0.482320	0.30	4
0.35	0.342525	0.418667	0.657475	0.458833	0.35	4
0.40	0.377320	0.407651	0.622680	0.432349	0.40	4
0.45	0.416310	0.394372	0.583690	0.403128	0.45	4
0.50	0.459237	0.378539	0.540763	0.371461	0.50	4
0.55	0.505777	0.359832	0.494223	0.337668	0.55	4
0.60	0.555529	0.337908	0.444471	0.302092	0.60	4
0.65	0.608020	0.312398	0.391980	0.265102	0.65	4
0.70	0.662707	0.282917	0.337293	0.227083	0.70	4
0.75	0.718982	0.249065	0.281018	0.188435	0.75	4
0.80	0.776183	0.210434	0.223817	0.149566	0.80	4
0.85	0.833609	0.166615	0.166391	0.110886	0.85	4
0.90	0.890536	0.117198	0.109464	0.072802	0.90	4
0.95	0.946234	0.061785	0.053766	0.035715	0.95	4
1.00	1.000000	0.000000	0.000000	0.000000	1.00	0

FOURIER NO. = .140

Z	YA	YB	ASER	BSER	Z	N
0.	0.302007	0.508855	0.697993	0.491145	0.	4
0.05	0.304300	0.508098	0.695700	0.489402	0.05	4
0.10	0.311164	0.505812	0.688836	0.484188	0.10	4
0.15	0.322565	0.501944	0.677435	0.475556	0.15	4
0.20	0.338439	0.496409	0.661561	0.463591	0.20	4
0.25	0.358694	0.489088	0.641306	0.448412	0.25	4
0.30	0.383203	0.479830	0.616797	0.430170	0.30	4
0.35	0.411805	0.468451	0.588195	0.409049	0.35	4
0.40	0.444294	0.454739	0.555706	0.385261	0.40	4
0.45	0.480419	0.438452	0.519581	0.359048	0.45	4
0.50	0.519883	0.419320	0.480117	0.330680	0.50	4
0.55	0.562336	0.397053	0.437664	0.300447	0.55	4
0.60	0.607378	0.371338	0.392622	0.268662	0.60	4
0.65	0.654564	0.341843	0.345436	0.235657	0.65	4
0.70	0.703401	0.308225	0.296599	0.201775	0.70	4
0.75	0.753361	0.270129	0.246639	0.167371	0.75	4
0.80	0.803885	0.227196	0.196115	0.132804	0.80	4
0.85	0.854394	0.179067	0.145606	0.098433	0.85	4
0.90	0.904301	0.125386	0.095699	0.064614	0.90	4
0.95	0.953023	0.065806	0.046977	0.031695	0.95	4
1.00	1.000000	0.000000	0.000000	0.000000	1.00	0

TRANSIENT CONDUCTION

TEMPERATURE RATIO TERMS FOR THE CYLINDER

FOURIER NO. = .160

Z	YA	YB	ASER	BSER	Z	N
0.	0.373072	0.561819	0.626928	0.438181	0.	4
0.05	0.375211	0.560885	0.624789	0.436615	0.05	4
0.10	0.381614	0.558067	0.618386	0.431933	0.10	4
0.15	0.392230	0.553317	0.607770	0.424163	0.15	4
0.20	0.406979	0.546555	0.593021	0.413445	0.20	4
0.25	0.425744	0.537671	0.574256	0.399829	0.25	4
0.30	0.448374	0.526526	0.551626	0.383474	0.30	4
0.35	0.474680	0.512949	0.525320	0.364551	0.35	4
0.40	0.504434	0.496746	0.495566	0.343254	0.40	4
0.45	0.537373	0.477695	0.462627	0.319805	0.45	4
0.50	0.573191	0.455553	0.426809	0.294447	0.50	4
0.55	0.611546	0.430054	0.388454	0.267446	0.55	4
0.60	0.652060	0.400918	0.347940	0.239082	0.60	4
0.65	0.694321	0.367848	0.305679	0.209652	0.65	4
0.70	0.737888	0.330537	0.262112	0.179463	0.70	4
0.75	0.782298	0.288671	0.217702	0.148829	0.75	4
0.80	0.827069	0.241933	0.172931	0.118068	0.80	4
0.85	0.871711	0.190003	0.128289	0.087497	0.85	4
0.90	0.915733	0.132571	0.084267	0.057429	0.90	4
0.95	0.958649	0.069332	0.041351	0.028168	0.95	4
1.00	1.000000	0.000000	0.000000	0.000000	1.00	0

FOURIER NO. = .180

Z	YA	YB	ASER	BSER	Z	N
0.	0.438730	0.609308	0.561270	0.390692	0.	4
0.05	0.440689	0.608210	0.559311	0.389290	0.05	4
0.10	0.446549	0.604901	0.553451	0.385099	0.10	4
0.15	0.456257	0.599338	0.543743	0.378162	0.15	4
0.20	0.469727	0.591447	0.530273	0.368553	0.20	4
0.25	0.486837	0.581128	0.513163	0.356372	0.25	4
0.30	0.507430	0.568253	0.492570	0.341747	0.30	4
0.35	0.531313	0.552669	0.468687	0.324831	0.35	4
0.40	0.558262	0.534198	0.441738	0.305802	0.40	4
0.45	0.588015	0.512640	0.411985	0.284860	0.45	4
0.50	0.620282	0.487775	0.379718	0.262225	0.50	4
0.55	0.654741	0.459366	0.345259	0.238134	0.55	4
0.60	0.691041	0.427160	0.308959	0.212840	0.60	4
0.65	0.728810	0.390892	0.271190	0.186608	0.65	3
0.70	0.767653	0.350288	0.232347	0.159712	0.70	4
0.75	0.807160	0.305069	0.192840	0.132431	0.75	4
0.80	0.846914	0.254954	0.153086	0.105046	0.80	4
0.85	0.886490	0.199661	0.113510	0.077839	0.85	4
0.90	0.925468	0.138913	0.074532	0.051087	0.90	4
0.95	0.963434	0.072444	0.036566	0.025056	0.95	4
1.00	1.000000	0.000000	0.000000	0.000000	1.00	0

FOURIER NO. = .200

Z	YA	YB	ASER	BSER	Z	N
0.	0.498501	0.651780	0.501499	0.348220	0.	4
0.05	0.500275	0.650532	0.499725	0.346968	0.05	4
0.10	0.505580	0.646777	0.494420	0.343223	0.10	4
0.15	0.514365	0.640474	0.485635	0.337026	0.15	4
0.20	0.526545	0.631557	0.473455	0.328443	0.20	4
0.25	0.542001	0.619936	0.457999	0.317564	0.25	3
0.30	0.560580	0.605495	0.439419	0.304505	0.30	3
0.35	0.582101	0.588095	0.417899	0.289405	0.35	3
0.40	0.606347	0.567577	0.393653	0.272423	0.40	4
0.45	0.633075	0.543762	0.366925	0.253738	0.45	4
0.50	0.662014	0.516450	0.337986	0.233550	0.50	3
0.55	0.692868	0.485431	0.307132	0.212069	0.55	3
0.60	0.725319	0.450477	0.274681	0.189523	0.60	3
0.65	0.759029	0.411352	0.240971	0.166148	0.65	3
0.70	0.793648	0.367813	0.206352	0.142187	0.70	3
0.75	0.828812	0.319611	0.171188	0.117889	0.75	3
0.80	0.864155	0.266496	0.135845	0.093505	0.80	3
0.85	0.899305	0.208217	0.100695	0.069283	0.85	3
0.90	0.933897	0.144531	0.066103	0.045469	0.90	3
0.95	0.967574	0.075200	0.032426	0.022300	0.95	3
1.00	1.000000	0.000000	0.000000	0.000000	1.00	0

TRANSIENT CONDUCTION

TEMPERATURE RATIO TERMS FOR THE CYLINDER

FOURIER NO. = .225

Z	YA	YB	ASER	BSER	Z	N
0.	0.565051	0.698528	0.434949	0.301472	0.	3
0.05	0.566604	0.697115	0.433396	0.300385	0.05	3
0.10	0.571249	0.692862	0.428751	0.297138	0.10	3
0.15	0.578937	0.685736	0.421063	0.291764	0.15	3
0.20	0.589590	0.675679	0.410410	0.284321	0.20	3
0.25	0.603100	0.662611	0.396900	0.274889	0.25	3
0.30	0.619326	0.646431	0.380674	0.263569	0.30	3
0.35	0.638103	0.627019	0.361897	0.250481	0.35	3
0.40	0.659236	0.604235	0.340764	0.235765	0.40	3
0.45	0.682506	0.577923	0.317494	0.219577	0.45	3
0.50	0.707672	0.547910	0.292328	0.202090	0.50	3
0.55	0.734472	0.514012	0.265528	0.183488	0.55	3
0.60	0.762626	0.476032	0.237374	0.163968	0.60	3
0.65	0.791840	0.433767	0.208160	0.143733	0.65	3
0.70	0.821811	0.387004	0.178189	0.122996	0.70	3
0.75	0.852224	0.335529	0.147776	0.101971	0.75	3
0.80	0.882765	0.279125	0.117234	0.080875	0.80	3
0.85	0.913119	0.217578	0.086881	0.059923	0.85	3
0.90	0.942975	0.150675	0.057025	0.039325	0.90	3
0.95	0.972030	0.078214	0.027970	0.019286	0.95	3
1.00	1.000000	0.000000	0.000000	0.000000	1.00	0

FOURIER NO. = .250

Z	YA	YB	ASER	BSER	Z	N
0.	0.623153	0.739051	0.376847	0.260949	0.	3
0.05	0.624506	0.737492	0.375494	0.260008	0.05	3
0.10	0.628550	0.732806	0.371450	0.257194	0.10	3
0.15	0.635244	0.724962	0.364756	0.252538	0.15	3
0.20	0.644516	0.713910	0.355484	0.246090	0.20	3
0.25	0.656269	0.699580	0.343731	0.237920	0.25	3
0.30	0.670380	0.681886	0.329620	0.228114	0.30	3
0.35	0.686701	0.660721	0.313299	0.216779	0.35	3
0.40	0.705059	0.635966	0.294941	0.204034	0.40	3
0.45	0.725262	0.607483	0.274738	0.190017	0.45	3
0.50	0.747098	0.575123	0.252902	0.174877	0.50	3
0.55	0.770336	0.538727	0.229664	0.158773	0.55	3
0.60	0.794734	0.498125	0.205266	0.141875	0.60	3
0.65	0.820036	0.453138	0.179964	0.124362	0.65	3
0.70	0.845977	0.403584	0.154023	0.106416	0.70	3
0.75	0.872288	0.349278	0.127712	0.088222	0.75	3
0.80	0.898698	0.290031	0.101302	0.069969	0.80	3
0.85	0.924936	0.225660	0.075064	0.051840	0.85	3
0.90	0.950735	0.155980	0.049265	0.034020	0.90	3
0.95	0.975838	0.080815	0.024162	0.016685	0.95	3
1.00	1.000000	0.000000	0.000000	0.000000	1.00	0

FOURIER NO. = .275

Z	YA	YB	ASER	BSER	Z	N
0.	0.673672	0.774150	0.326328	0.225850	0.	3
0.05	0.674847	0.772466	0.325153	0.225034	0.05	3
0.10	0.678359	0.767402	0.321641	0.222598	0.10	3
0.15	0.684170	0.758934	0.315830	0.218566	0.15	3
0.20	0.692218	0.747017	0.307782	0.212983	0.20	3
0.25	0.702418	0.731591	0.297582	0.205909	0.25	3
0.30	0.714662	0.712581	0.285338	0.197419	0.30	3
0.35	0.728819	0.689895	0.271181	0.187605	0.35	3
0.40	0.744739	0.663428	0.255261	0.176572	0.40	3
0.45	0.762254	0.633062	0.237746	0.164438	0.45	3
0.50	0.781177	0.598668	0.218823	0.151332	0.50	3
0.55	0.801309	0.560107	0.198691	0.137393	0.55	3
0.60	0.822438	0.517232	0.177562	0.122768	0.60	3
0.65	0.844342	0.469889	0.155658	0.107611	0.65	3
0.70	0.866794	0.417920	0.133206	0.092080	0.70	3
0.75	0.889560	0.361164	0.110440	0.076336	0.75	3
0.80	0.912405	0.299459	0.087595	0.060541	0.80	3
0.85	0.935097	0.232645	0.064903	0.044855	0.85	3
0.90	0.957406	0.160565	0.042594	0.029435	0.90	3
0.95	0.979110	0.083064	0.020890	0.014436	0.95	3
1.00	1.000000	0.000000	0.000000	0.000000	1.00	0

TEMPERATURE RATIO TERMS FOR THE CYLINDER

FOURIER NO. = .300

Z	YA	YB	ASER	BSER	Z	N
0.	0.717502	0.804540	0.282498	0.195460	0.	3
0.05	0.718521	0.802745	0.281479	0.194755	0.05	3
0.10	0.721565	0.797354	0.278435	0.192646	0.10	3
0.15	0.726603	0.788344	0.273397	0.189156	0.15	3
0.20	0.733579	0.775677	0.266421	0.184323	0.20	3
0.25	0.742420	0.759301	0.257580	0.178199	0.25	3
0.30	0.753031	0.739150	0.246969	0.170850	0.30	3
0.35	0.765298	0.715145	0.234702	0.162355	0.35	3
0.40	0.779090	0.687195	0.220910	0.152805	0.40	3
0.45	0.794261	0.655198	0.205739	0.142302	0.45	3
0.50	0.810649	0.619041	0.189351	0.130959	0.50	3
0.55	0.828081	0.578605	0.171919	0.118895	0.55	3
0.60	0.846373	0.533762	0.153627	0.106238	0.60	3
0.65	0.865334	0.484380	0.134666	0.093120	0.65	3
0.70	0.884764	0.430320	0.115236	0.079680	0.70	3
0.75	0.904464	0.371445	0.095536	0.066055	0.75	3
0.80	0.924229	0.307613	0.075771	0.052387	0.80	3
0.85	0.943860	0.238687	0.056140	0.038813	0.85	3
0.90	0.963158	0.164529	0.036842	0.025471	0.90	3
0.95	0.981931	0.085008	0.018069	0.012492	0.95	3
1.00	1.000000	0.000000	0.000000	0.000000	1.00	0

FOURIER NO. = .350

Z	YA	YB	ASER	BSER	Z	N
0.	0.788378	0.853612	0.211622	0.146388	0.	3
0.05	0.789142	0.851641	0.210858	0.145859	0.05	3
0.10	0.791425	0.845721	0.208575	0.144279	0.10	3
0.15	0.795203	0.835835	0.204797	0.141665	0.15	3
0.20	0.800435	0.821956	0.199565	0.138044	0.20	3
0.25	0.807064	0.804043	0.192936	0.133457	0.25	3
0.30	0.815020	0.782048	0.184980	0.127952	0.30	3
0.35	0.824216	0.755911	0.175784	0.121589	0.35	3
0.40	0.834555	0.725564	0.165445	0.114436	0.40	3
0.45	0.845925	0.690931	0.154075	0.106569	0.45	3
0.50	0.858206	0.651927	0.141794	0.098073	0.50	3
0.55	0.871267	0.608462	0.128733	0.089038	0.55	3
0.60	0.884970	0.560442	0.115030	0.079558	0.60	3
0.65	0.899172	0.507766	0.100828	0.069735	0.65	3
0.70	0.913725	0.450331	0.086275	0.059669	0.70	3
0.75	0.928476	0.388034	0.071524	0.049466	0.75	3
0.80	0.943276	0.320770	0.056724	0.039230	0.80	3
0.85	0.957973	0.248435	0.042027	0.029065	0.85	3
0.90	0.972420	0.170927	0.027580	0.019073	0.90	3
0.95	0.986474	0.088146	0.013526	0.009354	0.95	3
1.00	1.000000	0.000000	0.000000	0.000000	1.00	0

FOURIER NO. = .400

Z	YA	YB	ASER	BSER	Z	N
0.	0.841503	0.890369	0.158497	0.109631	0.	3
0.05	0.842076	0.888265	0.157924	0.109235	0.05	3
0.10	0.843786	0.881948	0.156214	0.108052	0.10	3
0.15	0.846617	0.871406	0.153383	0.106094	0.15	3
0.20	0.850536	0.856618	0.149464	0.103382	0.20	3
0.25	0.855503	0.837553	0.144497	0.099947	0.25	3
0.30	0.861463	0.814176	0.138537	0.095824	0.30	3
0.35	0.868352	0.786442	0.131648	0.091058	0.35	3
0.40	0.876097	0.754299	0.123903	0.085701	0.40	3
0.45	0.884614	0.717691	0.115386	0.079809	0.45	3
0.50	0.893813	0.676554	0.106187	0.073446	0.50	3
0.55	0.903596	0.630820	0.096404	0.066680	0.55	3
0.60	0.913859	0.580420	0.086141	0.059580	0.60	3
0.65	0.924496	0.525277	0.075504	0.052223	0.65	3
0.70	0.935394	0.465315	0.064606	0.044685	0.70	3
0.75	0.946441	0.400456	0.053559	0.037044	0.75	3
0.80	0.957524	0.330622	0.042476	0.029378	0.80	3
0.85	0.968530	0.255734	0.031470	0.021766	0.85	3
0.90	0.979348	0.175716	0.020652	0.014284	0.90	3
0.95	0.989872	0.090495	0.010128	0.007005	0.95	3
1.00	1.000000	0.000000	0.000000	0.000000	1.00	0

TRANSIENT CONDUCTION

TEMPERATURE RATIO TERMS FOR THE CYLINDER

FOURIER NO. = .500

Z	YA	YB	ASER	BSER	Z	N
0.	0.911105	0.938513	0.088895	0.061487	0.	3
0.05	0.911426	0.936235	0.088574	0.061265	0.05	3
0.10	0.912385	0.929399	0.087615	0.060601	0.10	3
0.15	0.913973	0.917997	0.086027	0.059503	0.15	3
0.20	0.916172	0.902018	0.083828	0.057982	0.20	3
0.25	0.918958	0.881445	0.081042	0.056055	0.25	3
0.30	0.922301	0.856257	0.077699	0.053743	0.30	3
0.35	0.926165	0.826430	0.073835	0.051070	0.35	2
0.40	0.930509	0.791935	0.069491	0.048065	0.40	2
0.45	0.935286	0.752739	0.064714	0.044761	0.45	2
0.50	0.940446	0.708808	0.059554	0.041192	0.50	2
0.55	0.945933	0.660103	0.054067	0.037397	0.55	2
0.60	0.951689	0.606585	0.048311	0.033415	0.60	2
0.65	0.957655	0.548211	0.042345	0.029289	0.65	3
0.70	0.963767	0.484939	0.036233	0.025061	0.70	3
0.75	0.969963	0.416724	0.030037	0.020776	0.75	2
0.80	0.976178	0.343523	0.023822	0.016477	0.80	2
0.85	0.982351	0.265293	0.017649	0.012207	0.85	2
0.90	0.988418	0.181989	0.011582	0.008011	0.90	2
0.95	0.994320	0.093571	0.005680	0.003929	0.95	2
1.00	1.000000	0.000000	0.000000	0.000000	1.00	0

FOURIER NO. = .600

Z	YA	YB	ASER	BSER	Z	N
0.	0.950143	0.965515	0.049857	0.034485	0.	2
0.05	0.950323	0.963140	0.049677	0.034360	0.05	2
0.10	0.950861	0.956012	0.049139	0.033988	0.10	2
0.15	0.951752	0.944128	0.048248	0.033372	0.15	2
0.20	0.952985	0.927481	0.047015	0.032519	0.20	2
0.25	0.954548	0.906062	0.045452	0.031438	0.25	2
0.30	0.956423	0.879859	0.043577	0.030141	0.30	2
0.35	0.958590	0.848858	0.041410	0.028642	0.35	2
0.40	0.961026	0.813043	0.038974	0.026957	0.40	2
0.45	0.963705	0.772396	0.036295	0.025104	0.45	2
0.50	0.966599	0.726897	0.033401	0.023103	0.50	2
0.55	0.969676	0.676526	0.030324	0.020974	0.55	2
0.60	0.972905	0.621259	0.027095	0.018741	0.60	2
0.65	0.976251	0.561073	0.023749	0.016427	0.65	2
0.70	0.979679	0.495944	0.020321	0.014056	0.70	2
0.75	0.983154	0.425848	0.016846	0.011652	0.75	2
0.80	0.986640	0.350759	0.013360	0.009241	0.80	2
0.85	0.990102	0.270654	0.009898	0.006846	0.85	2
0.90	0.993504	0.185507	0.006496	0.004493	0.90	2
0.95	0.996814	0.095297	0.003186	0.002203	0.95	2
1.00	1.000000	0.000000	0.000000	0.000000	1.00	0

FOURIER NO. = .800

Z	YA	YB	ASER	BSER	Z	N
0.	0.984318	0.989153	0.015682	0.010847	0.	2
0.05	0.984374	0.986692	0.015626	0.010808	0.05	2
0.10	0.984543	0.979309	0.015457	0.010691	0.10	2
0.15	0.984824	0.967003	0.015176	0.010497	0.15	2
0.20	0.985211	0.949771	0.014789	0.010229	0.20	2
0.25	0.985703	0.927611	0.014297	0.009889	0.25	2
0.30	0.986293	0.900519	0.013707	0.009481	0.30	2
0.35	0.986974	0.868491	0.013026	0.009009	0.35	2
0.40	0.987741	0.831521	0.012259	0.008479	0.40	2
0.45	0.988584	0.789604	0.011416	0.007896	0.45	2
0.50	0.989494	0.742733	0.010506	0.007267	0.50	2
0.55	0.990462	0.690903	0.009538	0.006597	0.55	2
0.60	0.991477	0.634105	0.008523	0.005895	0.60	2
0.65	0.992530	0.572333	0.007470	0.005167	0.65	2
0.70	0.993608	0.505579	0.006392	0.004421	0.70	2
0.75	0.994701	0.433835	0.005299	0.003665	0.75	2
0.80	0.995798	0.357093	0.004202	0.002907	0.80	2
0.85	0.996886	0.275347	0.003114	0.002154	0.85	2
0.90	0.997957	0.188587	0.002043	0.001413	0.90	2
0.95	0.998998	0.096807	0.001002	0.000693	0.95	2
1.00	1.000000	0.000000	0.000000	0.000000	1.00	0

TRANSIENT CONDUCTION

TEMPERATURE RATIO TERMS FOR THE CYLINDER

FOURIER NO. = .900

Z	YA	YB	ASER	BSER	Z	N
0.	0.991205	0.993916	0.008795	0.006084	0.	2
0.05	0.991236	0.991438	0.008764	0.006062	0.05	2
0.10	0.991331	0.984004	0.008669	0.005996	0.10	2
0.15	0.991488	0.971613	0.008512	0.005887	0.15	2
0.20	0.991706	0.954263	0.008294	0.005737	0.20	2
0.25	0.991982	0.931954	0.008018	0.005546	0.25	2
0.30	0.992312	0.904683	0.007688	0.005317	0.30	2
0.35	0.992695	0.872447	0.007305	0.005053	0.35	2
0.40	0.993124	0.835244	0.006876	0.004756	0.40	2
0.45	0.993597	0.793071	0.006403	0.004429	0.45	2
0.50	0.994108	0.745924	0.005892	0.004076	0.50	2
0.55	0.994650	0.693800	0.005350	0.003700	0.55	2
0.60	0.995220	0.636694	0.004780	0.003306	0.60	2
0.65	0.995810	0.574602	0.004190	0.002898	0.65	2
0.70	0.996415	0.507520	0.003585	0.002480	0.70	2
0.75	0.997028	0.435444	0.002972	0.002056	0.75	2
0.80	0.997643	0.358370	0.002357	0.001630	0.80	2
0.85	0.998254	0.276292	0.001746	0.001208	0.85	2
0.90	0.998854	0.189207	0.001146	0.000793	0.90	2
0.95	0.999438	0.097111	0.000562	0.000389	0.95	2
1.00	1.000000	0.000000	0.000000	0.000000	1.00	0

APPENDIX C

TEMPERATURE HISTORY FOR THE SPHERE

The results presented in the table apply to the sphere as illustrated.

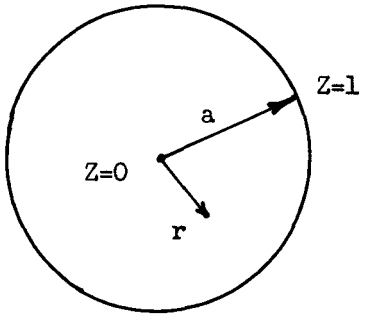

$Z = \xi = r/a$

The position ratio

The following special terms were employed in the computer program.

$$TM1 = (-1)^n/n = (\cos(n\pi))/n$$

$$TM2 = (-1)^n/n^3 = TM1/n^2$$

$$ETM = Z \exp(n^2\pi^2\phi)$$

$$STM = \sin(n\pi Z)$$

XN = n, the series index

The individual series terms in Equations (21) and (22) were designated

$$SERA = (2/\pi)\ TM1(STM)/ETM$$

$$SERB = (12/\pi^3)\ TM2(STM)/ETM$$

The series sums were designated by ASER and BSER, and N gives the number of terms required to converge to the tolerance TOL (a value of TOL = 0.0000001 was employed). The values for Y_a and Y_b were calculated as

$$YA = 1 + ASER$$

$$YB = 1 - Z^2 + BSER$$

The data cards require DZ and TOL on the first card, then each value of PHI (the Fourier No. ϕ) is entered on a separate card; as many as desired. The computations were made on the IBM 7090 with the Fortran system.

```
C     TRSCND      S005        5-15-61                                          00500020
C                                                                            00500030
C     PROGRMR -   H. WOLF                                                    00500035
C                                                                            00500040
C     SYNOPSIS-   CALCULATION OF TEMP HISTORY IN A SPHERE AS A FUNCTION      00500045
C                 OF FOURIER NO AND POSITION RATIO FOR ZERO AND FINITE       00500050
C                 SURFACE TEMP WITH ZERO INITIAL TEMP THROUGHOUT             00500055
C                                                                            00500060
C     PURPOSE -   GENERATE TABLES OF VALUES.                                 00500065
C                                                                            00500070
C     SYMBOLS -                                                              00500075
C           Z - POSITION RATIO, R/A          DZ - UPDATING FACTOR ON Z       00500080
C         TOL - TOLERANCE ON CONVERG         XN - SERIES TERM OR INDEX       00500085
C         STM - SINE TERM                   ETM - EXPONENTIAL TERM           00500090
C        ASER - SERIES SUM FOR YA          BSER - SERIES SUM FOR YB          00500100
C                                                                            00500140
C              SEE NOTES FOR SPECIALIZED NOMENCLATURE EMPLOYED FOR           00500150
C              DESIGNATION OF PARTS OF THE SERIES TERMS.                     00500160
C                                                                            00500170
C              *-*-*              *-*-*-*              *-*-*                 00500180
C                                                                            00500190
C     MAIN CALCULATIONS                                                      00500200
C                                                                            00500210
C                                                                            00500220
    5 READ INPUT TAPE 5,10,DZ, TOL                                           00500230
   10 FORMAT(F12.2, F12.7)                                                   00500235
   12 READ INPUT TAPE 5,13, PHI                                              00500237
   13 FORMAT(F12.6)                                                          00500238
   14 IF(PHI - 10.)  15, 15, 130                                             00500240
   15 Z = 0.000                                                              00500245
   16 WRITE OUTPUT TAPE 6,17, PHI                                            00500250
   17 FORMAT(1H1///45X,  20HTRANSIENT CONDUCTION// 36X,   38HTEMPERATURE     00500252
     1 RATIO TERMS FOR THE SPHERE///   45X, 14HFOURIER NO. = F4.3/// 21X     00500254
     2,67H Z          YA           YB           ASER         BSER        Z   00500256
     3    N//1H )                                                           00500257
   22 ASER = 0.                                                              00500261
      BSER = 0.                                                              00500262
      IF(Z - .99) 25, 25, 23                                                 00500263
   23 YA = 1.000000                                                          00500264
      YB = 0.00000001                                                        00500265
      ASER = 0.00000001                                                      00500266
      BSER = 0.00000001                                                      00500267
      GO TO 160                                                              00500268
   25 XN = 1.                                                                00500270
   29 PI = 3.14159265                                                        00500300
      Y = XN*PI                                                              00500310
   30 TM1 =  COSF(Y)/XN                                                      00500320
   35 TM2 = TM1/(XN*XN)                                                      00500330
      PI2 = 3.14159265*PI                                                    00500340
   40 X = XN*XN*PI2*PHI                                                      00500350
   41 IF(Z) 42,42, 140                                                       00500360
   42 STM = Y                                                                00500370
   43 IF(X-80.) 44,44,170                                                    00500372
   44 ETM = EXPF(X)                                                          00500374
      GO TO 60                                                               00500376
  170 XB = X/1000.                                                           00500378
  172 D = EXPF(XB)                                                           00500380
  174 D1 = D**10.                                                            00500382
  176 D2 = D1**10.                                                           00500384
  178 ETM = D2**10.                                                          00500386
      GO TO 60                                                               00500388
  140 IF(X-80.) 45, 45, 145                                                  00500391
   45 ETM = EXPF(X)*Z                                                        00500392
   46 GO TO 50                                                               00500393
                                                                             00500394
  145 XB = X/1000.                                                           00500395
  150 D = EXPF(XB)                                                           00500396
  151 D1 = D**10.                                                            00500397
  152 D2 = D1**10.                                                           00500398
  153 ETM =(D2**10.)*Z                                                       00500399
   50 YZ = Y*Z                                                               00500410
   55 STM = SINF(YZ)                                                         00500420
   60 SERA =  (2.*TM1*STM)/(ETM*PI)                                          00500430
   65 SERB = (12.*TM2*STM)/(ETM*PI*PI2)                                      00500440
      ASER1 = ASER + SERA                                                    00500492
      A1 = ABSF(ASER1)                                                       00500494
      A  = ABSF(ASER)                                                        00500496
      B  = ABSF(A1-A)                                                        00500498
      ASER = ASER + SERA                                                     00500500
      BSER = BSER + SERB                                                     00500502
      IF(TOL - B) 100,100,103                                                00500504
  100 XN = XN + 1.                                                           00500520
  102 GO TO 29                                                               00500525
  103 IF(XN - 1.) 100,100,180                                                00500527
  180 STM1 = ABSF(STM)                                                       00500529
                                                                             00500530
  182 IF(STM1 -.000001) 100, 100, 185                                        00500531
  185 YA = 1. + ASER                                                         00500532
      YB = 1. - Z*Z + BSER                                                   00500534
```

```
158 N = XFIXF(XN)                                                    00500535
160 WRITE OUTPUT TAPE 6, 165, Z,YA ,YB, ASER, BSER, Z, N             00500538
165 FORMAT(F25.2, 2F12.6, F13.6, F12.6, F8.2, I6)                    00500540
105 Z = Z +DZ                                                        00500545
110 IF(Z - 1.01) 22, 22, 12                                          00500550
130 CALL EXIT                                                        00500580
    STOP                                                             00500590
    END(1,0,0,0,0,0,0,0,0,0,0,0,0,0,0,0)
```

EXTERNAL FORMULA NUMBERS WITH CORRESPONDING INTERNAL FORMULA NUMBERS AND OCTAL LOCATIONS

EFN	IFN	LOC	EFN	IFN	LOC	EFN	IFN	LOC	EFN	IFN	LOC
10	1	00000	13	2	00000	17	3	00000	165	4	00000
5	6	00015	5	7	00020	12	8	00025	12	9	00030
14	10	00033	15	11	00037	16	12	00041	16	13	00044
22	14	00047	23	17	00060	25	22	00071	29	23	00073
30	25	00100	35	26	00106	40	28	00117	41	29	00126
42	30	00131	43	31	00133	44	32	00137	170	34	00145
172	35	00150	174	36	00155	176	37	00163	178	38	00171
140	40	00200	45	41	00204	46	42	00213	145	43	00214
150	44	00217	151	45	00224	152	46	00232	153	47	00240
50	48	00250	55	49	00253	60	50	00260	65	51	00271
100	59	00333	102	60	00336	103	61	00337	180	62	00344
182	63	00347	185	64	00354	158	66	00365	160	67	00374
160	68	00377	105	69	00416	110	70	00421	130	71	00426

STORAGE NOT USED BY PROGRAM

DEC	OCT	DEC	OCT
380	00574	32561	77461

LOCATIONS OF NAMES IN TRANSFER VECTOR

	DEC	OCT		DEC	OCT		DEC	OCT		DEC	OCT
EXP(3	7	00007	EXP	6	00006	EXIT	9	00011	COS	5	00005
SIN	8	00010	(FIL)	4	00004	(FPT)	0	00000	(RTN)	2	00002
(STH)	3	00003	(TSH)	1	00001						

STORAGE LOCATIONS FOR VARIABLES NOT APPEARING IN DIMENSION, EQUIVALENCE OR COMMON SENTENCES

	DEC	OCT		DEC	OCT		DEC	OCT		DEC	OCT
ETM	379	00573	DZ	378	00572	D	377	00571	D2	376	00570
D1	375	00567	BSER	374	00566	B	373	00565	ASER	372	00564
ASER1	371	00563	A	370	00562	A1	369	00561	N	368	00560
PHI	367	00557	PI2	366	00556	PI	365	00555	SERA	364	00554
SERB	363	00553	STM1	362	00552	STM	361	00551	TM1	360	00550
TM2	359	00547	TOL	358	00546	XB	357	00545	XN	356	00544
X	355	00543	YA	354	00542	YB	353	00541	Y	352	00540
YZ	351	00537	Z	350	00536						

TRANSIENT CONDUCTION

TEMPERATURE RATIO TERMS FOR THE SPHERE

FOURIER NO. = .010

Z	YA	YB	ASER	BSER	Z	N
0.	0.000000	0.060000	-1.000000	-0.940000	0.	14
0.05	0.000000	0.060000	-1.000000	-0.937500	0.05	13
0.10	0.000000	0.060000	-1.000000	-0.930000	0.10	13
0.15	0.000000	0.060000	-1.000000	-0.917500	0.15	13
0.20	0.000000	0.060000	-1.000000	-0.900000	0.20	13
0.25	0.000001	0.060000	-0.999999	-0.877500	0.25	13
0.30	0.000003	0.060000	-0.999997	-0.850000	0.30	13
0.35	0.000012	0.060000	-0.999988	-0.817500	0.35	12
0.40	0.000055	0.060000	-0.999945	-0.780000	0.40	12
0.45	0.000224	0.059999	-0.999776	-0.737501	0.45	12
0.50	0.000814	0.059994	-0.999186	-0.690006	0.50	13
0.55	0.002660	0.059978	-0.997340	-0.637522	0.55	12
0.60	0.007797	0.059923	-0.992203	-0.580077	0.60	10
0.65	0.020505	0.059759	-0.979495	-0.517741	0.65	12
0.70	0.048421	0.059312	-0.951579	-0.450688	0.70	10
0.75	0.102827	0.058209	-0.897173	-0.379291	0.75	8
0.80	0.196624	0.055741	-0.803376	-0.304259	0.80	10
0.85	0.339817	0.050711	-0.660183	-0.226789	0.85	12
0.90	0.532778	0.041343	-0.467222	-0.148657	0.90	10
0.95	0.761761	0.025318	-0.238239	-0.072182	0.95	12
1.00	1.000000	0.000000	0.000000	0.000000	1.00	12

FOURIER NO. = .020

Z	YA	YB	ASER	BSER	Z	N
0.	0.000030	0.120000	-0.999970	-0.880000	0.	10
0.05	0.000038	0.120000	-0.999962	-0.877500	0.05	10
0.10	0.000068	0.119999	-0.999932	-0.870001	0.10	9
0.15	0.000142	0.119998	-0.999858	-0.857502	0.15	9
0.20	0.000317	0.119996	-0.999683	-0.840004	0.20	9
0.25	0.000707	0.119991	-0.999293	-0.817509	0.25	9
0.30	0.001551	0.119978	-0.998449	-0.790022	0.30	9
0.35	0.003297	0.119947	-0.996703	-0.757553	0.35	9
0.40	0.006750	0.119878	-0.993250	-0.720122	0.40	9
0.45	0.013243	0.119730	-0.986757	-0.677770	0.45	9
0.50	0.024839	0.119424	-0.975161	-0.630576	0.50	9
0.55	0.044453	0.118823	-0.955547	-0.578677	0.55	9
0.60	0.075834	0.117693	-0.924166	-0.522308	0.60	9
0.65	0.123259	0.115660	-0.876741	-0.461840	0.65	9
0.70	0.190878	0.112167	-0.809122	-0.397833	0.70	9
0.75	0.281733	0.106427	-0.718267	-0.331073	0.75	8
0.80	0.396638	0.097398	-0.603362	-0.262602	0.80	9
0.85	0.533241	0.083788	-0.466759	-0.193712	0.85	9
0.90	0.685639	0.064096	-0.314361	-0.125904	0.90	9
0.95	0.844829	0.036706	-0.155171	-0.060795	0.95	9
1.00	1.000000	0.000000	0.000000	0.000000	1.00	9

FOURIER NO. = .030

Z	YA	YB	ASER	BSER	Z	N
0.	0.001566	0.179971	-0.998434	-0.820029	0.	8
0.05	0.001740	0.179967	-0.998260	-0.817533	0.05	8
0.10	0.002315	0.179953	-0.997685	-0.810047	0.10	8
0.15	0.003451	0.179924	-0.996549	-0.797576	0.15	7
0.20	0.005449	0.179869	-0.994551	-0.780131	0.20	8
0.25	0.008797	0.179768	-0.991203	-0.757732	0.25	9
0.30	0.014222	0.179587	-0.985778	-0.730413	0.30	7
0.35	0.022753	0.179269	-0.977247	-0.698231	0.35	8
0.40	0.035765	0.178723	-0.964235	-0.661277	0.40	7
0.45	0.054988	0.177811	-0.945012	-0.619689	0.45	7
0.50	0.082454	0.176324	-0.917546	-0.573676	0.50	7
0.55	0.120350	0.173963	-0.879650	-0.523537	0.55	7
0.60	0.170784	0.170318	-0.829216	-0.469682	0.60	7
0.65	0.235449	0.164841	-0.764551	-0.412659	0.65	7
0.70	0.315245	0.156837	-0.684755	-0.353163	0.70	7
0.75	0.409912	0.145454	-0.590088	-0.292046	0.75	7
0.80	0.517770	0.129699	-0.482230	-0.230301	0.80	7
0.85	0.635637	0.108458	-0.364363	-0.169042	0.85	7
0.90	0.758990	0.080550	-0.241010	-0.109450	0.90	7
0.95	0.882375	0.044778	-0.117625	-0.052723	0.95	7
1.00	1.000000	0.000000	0.000000	0.000000	1.00	7

TRANSIENT CONDUCTION

TEMPERATURE RATIO TERMS FOR THE SPHERE

FOURIER NO. = .040

Z	YA	YB	ASER	BSER	Z	N
0.	0.010891	0.239656	-0.989109	-0.760344	0.	7
0.05	0.011551	0.239628	-0.988449	-0.757872	0.05	7
0.10	0.013621	0.239539	-0.986379	-0.750461	0.10	7
0.15	0.017375	0.239369	-0.982625	-0.738131	0.15	7
0.20	0.023278	0.239084	-0.976722	-0.720916	0.20	7
0.25	0.032000	0.238627	-0.968000	-0.698873	0.25	7
0.30	0.044413	0.237914	-0.955587	-0.672086	0.30	7
0.35	0.061584	0.236823	-0.938416	-0.640677	0.35	6
0.40	0.084735	0.235184	-0.915265	-0.604816	0.40	7
0.45	0.115177	0.232764	-0.884823	-0.564736	0.45	7
0.50	0.154200	0.229255	-0.845800	-0.520745	0.50	7
0.55	0.202930	0.224260	-0.797070	-0.473240	0.55	7
0.60	0.262165	0.217284	-0.737835	-0.422716	0.60	7
0.65	0.332192	0.207726	-0.667808	-0.369774	0.65	6
0.70	0.412635	0.194881	-0.587365	-0.315119	0.70	6
0.75	0.502345	0.177947	-0.497655	-0.259553	0.75	6
0.80	0.599375	0.156042	-0.400625	-0.203958	0.80	6
0.85	0.701039	0.128233	-0.298961	-0.149267	0.85	6
0.90	0.804082	0.093566	-0.195918	-0.096435	0.90	6
0.95	0.904930	0.051110	-0.095070	-0.046390	0.95	6
1.00	1.000000	0.000000	0.000000	0.000000	1.00	6

FOURIER NO. = .050

Z	YA	YB	ASER	BSER	Z	N
0.	0.034001	0.298384	-0.965999	-0.701616	0.	6
0.05	0.035284	0.298298	-0.964716	-0.699202	0.05	6
0.10	0.039223	0.298028	-0.960777	-0.691972	0.10	6
0.15	0.046089	0.297539	-0.953911	-0.679961	0.15	6
0.20	0.056321	0.296768	-0.943679	-0.663232	0.20	6
0.25	0.070515	0.295619	-0.929485	-0.641881	0.25	6
0.30	0.089391	0.293960	-0.910609	-0.616040	0.30	6
0.35	0.113751	0.291612	-0.886249	-0.585888	0.35	6
0.40	0.144425	0.288343	-0.855575	-0.551657	0.40	6
0.45	0.182191	0.283857	-0.817809	-0.513643	0.45	6
0.50	0.227688	0.277790	-0.772312	-0.472210	0.50	7
0.55	0.281324	0.269700	-0.718676	-0.427800	0.55	6
0.60	0.343171	0.259069	-0.656829	-0.380931	0.60	6
0.65	0.412894	0.245300	-0.587106	-0.332200	0.65	6
0.70	0.489688	0.227726	-0.510312	-0.282274	0.70	6
0.75	0.572260	0.205619	-0.427740	-0.231881	0.75	6
0.80	0.658861	0.178211	-0.341139	-0.181789	0.80	6
0.85	0.747360	0.144710	-0.252640	-0.132790	0.85	6
0.90	0.835366	0.104332	-0.164634	-0.085668	0.90	6
0.95	0.920386	0.056325	-0.079614	-0.041175	0.95	6
1.00	1.000000	0.000000	0.000000	0.000000	1.00	6

FOURIER NO. = .060

Z	YA	YB	ASER	BSER	Z	N
0.	0.071420	0.355287	-0.928580	-0.644713	0.	6
0.05	0.073244	0.355107	-0.926756	-0.642393	0.05	6
0.10	0.078786	0.354551	-0.921214	-0.635449	0.10	6
0.15	0.088247	0.353568	-0.911753	-0.623932	0.15	6
0.20	0.101947	0.352072	-0.898053	-0.607928	0.20	6
0.25	0.120299	0.349939	-0.879701	-0.587561	0.25	6
0.30	0.143778	0.346999	-0.856222	-0.563001	0.30	6
0.35	0.172870	0.343035	-0.827130	-0.534465	0.35	5
0.40	0.208028	0.337777	-0.791972	-0.502223	0.40	6
0.45	0.249606	0.330895	-0.750394	-0.466605	0.45	5
0.50	0.297800	0.322002	-0.702200	-0.427998	0.50	5
0.55	0.352588	0.310645	-0.647412	-0.386855	0.55	5
0.60	0.413682	0.296314	-0.586318	-0.343686	0.60	6
0.65	0.480492	0.278441	-0.519508	-0.299059	0.65	5
0.70	0.552108	0.256410	-0.447892	-0.253590	0.70	5
0.75	0.627315	0.229571	-0.372685	-0.207929	0.75	5
0.80	0.704628	0.197251	-0.295372	-0.162749	0.80	6
0.85	0.782359	0.158774	-0.217641	-0.118727	0.85	5
0.90	0.858700	0.113479	-0.141300	-0.076521	0.90	5
0.95	0.931825	0.060743	-0.068175	-0.036757	0.95	5
1.00	1.000000	0.000000	0.000000	0.000000	1.00	5

TRANSIENT CONDUCTION

TEMPERATURE RATIO TERMS FOR THE SPHERE

FOURIER NO. = .070

Z	YA	YB	ASER	BSER	Z	N
0.	0.119910	0.409592	-0.880090	-0.590408	0.	5
0.05	0.122105	0.409290	-0.877895	-0.588210	0.05	5
0.10	0.128735	0.408366	-0.871265	-0.581634	0.10	5
0.15	0.139919	0.406760	-0.860081	-0.570740	0.15	5
0.20	0.155844	0.404369	-0.844156	-0.555631	0.20	6
0.25	0.176742	0.401051	-0.823258	-0.536449	0.25	5
0.30	0.202856	0.396614	-0.797144	-0.513386	0.30	5
0.35	0.234410	0.390821	-0.765590	-0.486679	0.35	5
0.40	0.271567	0.383382	-0.728433	-0.456618	0.40	6
0.45	0.314383	0.373958	-0.685617	-0.423542	0.45	5
0.50	0.362776	0.362157	-0.637224	-0.387843	0.50	5
0.55	0.416486	0.347537	-0.583514	-0.349963	0.55	5
0.60	0.475051	0.329610	-0.524949	-0.310390	0.60	6
0.65	0.537791	0.307847	-0.462209	-0.269653	0.65	5
0.70	0.603818	0.281687	-0.396182	-0.228314	0.70	5
0.75	0.672044	0.250547	-0.327956	-0.186953	0.75	5
0.80	0.741223	0.213838	-0.258777	-0.146163	0.80	6
0.85	0.809999	0.170973	-0.190001	-0.106527	0.85	5
0.90	0.876964	0.121388	-0.123036	-0.068612	0.90	5
0.95	0.940731	0.064557	-0.059269	-0.032944	0.95	5
1.00	1.000000	0.000000	0.000000	0.000000	1.00	5

FOURIER NO. = .080

Z	YA	YB	ASER	BSER	Z	N
0.	0.175283	0.460760	-0.824717	-0.539240	0.	5
0.05	0.177681	0.460320	-0.822319	-0.537180	0.05	5
0.10	0.184894	0.458979	-0.815106	-0.531021	0.10	5
0.15	0.196976	0.456670	-0.803024	-0.520830	0.15	5
0.20	0.214002	0.453287	-0.785998	-0.506713	0.20	6
0.25	0.236059	0.448673	-0.763941	-0.488827	0.25	5
0.30	0.263214	0.442632	-0.736786	-0.467368	0.30	5
0.35	0.295498	0.434916	-0.704502	-0.442584	0.35	5
0.40	0.332873	0.425234	-0.667127	-0.414766	0.40	6
0.45	0.375205	0.413249	-0.624795	-0.384251	0.45	5
0.50	0.422245	0.398579	-0.577755	-0.351421	0.50	5
0.55	0.473604	0.380803	-0.526396	-0.316697	0.55	5
0.60	0.528745	0.359461	-0.471255	-0.280539	0.60	6
0.65	0.586980	0.334068	-0.413020	-0.243432	0.65	5
0.70	0.647476	0.304113	-0.352524	-0.205887	0.70	5
0.75	0.709279	0.269075	-0.290721	-0.168425	0.75	5
0.80	0.771335	0.228433	-0.228665	-0.131567	0.80	6
0.85	0.832537	0.181675	-0.167463	-0.095825	0.85	5
0.90	0.891762	0.128312	-0.108238	-0.061688	0.90	5
0.95	0.947919	0.067890	-0.052081	-0.029610	0.95	5
1.00	1.000000	0.000000	0.000000	0.000000	1.00	5

FOURIER NO. = .090

Z	YA	YB	ASER	BSER	Z	N
0.	0.233862	0.508494	-0.766138	-0.491506	0.	5
0.05	0.236329	0.507908	-0.763671	-0.489592	0.05	5
0.10	0.243730	0.506126	-0.756270	-0.483874	0.10	5
0.15	0.256069	0.503082	-0.743931	-0.474418	0.15	5
0.20	0.273344	0.498666	-0.726656	-0.461334	0.20	6
0.25	0.295535	0.492721	-0.704465	-0.444779	0.25	5
0.30	0.322590	0.485049	-0.677410	-0.424951	0.30	5
0.35	0.354411	0.475405	-0.645589	-0.402095	0.35	5
0.40	0.390829	0.463505	-0.609171	-0.376495	0.40	6
0.45	0.431598	0.449022	-0.568402	-0.348478	0.45	5
0.50	0.476372	0.431595	-0.523628	-0.318405	0.50	5
0.55	0.524701	0.410825	-0.475299	-0.286675	0.55	5
0.60	0.576027	0.386289	-0.423973	-0.253711	0.60	6
0.65	0.629684	0.357539	-0.370316	-0.219961	0.65	5
0.70	0.684912	0.324113	-0.315088	-0.185887	0.70	4
0.75	0.740870	0.285546	-0.259130	-0.151954	0.75	5
0.80	0.796662	0.241373	-0.203338	-0.118627	0.80	4
0.85	0.851366	0.191142	-0.148634	-0.086358	0.85	5
0.90	0.904063	0.134427	-0.095937	-0.055573	0.90	5
0.95	0.953876	0.070831	-0.046124	-0.026669	0.95	4
1.00	1.000000	0.000000	0.000000	0.000000	1.00	4

TRANSIENT CONDUCTION

TEMPERATURE RATIO TERMS FOR THE SPHERE

FOURIER NO. = .100

Z	YA	YB	ASER	BSER	Z	N
0.	0.292900	0.552688	-0.707100	-0.447312	0.	5
0.05	0.295340	0.551954	-0.704660	-0.445546	0.05	5
0.10	0.302650	0.549730	-0.697350	-0.440270	0.10	5
0.15	0.314802	0.545950	-0.685198	-0.431550	0.15	5
0.20	0.331740	0.540505	-0.668260	-0.419495	0.20	4
0.25	0.353376	0.533242	-0.646624	-0.404258	0.25	5
0.30	0.379581	0.523969	-0.620419	-0.386031	0.30	4
0.35	0.410177	0.512450	-0.589823	-0.365050	0.35	4
0.40	0.444918	0.498412	-0.555082	-0.341588	0.40	4
0.45	0.483494	0.481547	-0.516506	-0.315953	0.45	4
0.50	0.525513	0.461514	-0.474487	-0.288486	0.50	5
0.55	0.570502	0.437944	-0.429498	-0.259556	0.55	4
0.60	0.617911	0.410446	-0.382089	-0.229554	0.60	4
0.65	0.667113	0.378611	-0.332887	-0.198889	0.65	4
0.70	0.717416	0.342022	-0.282584	-0.167978	0.70	4
0.75	0.768079	0.300258	-0.231921	-0.137242	0.75	5
0.80	0.818331	0.252907	-0.181669	-0.107093	0.80	4
0.85	0.867391	0.199567	-0.132609	-0.077933	0.85	4
0.90	0.914494	0.139862	-0.085506	-0.050138	0.90	4
0.95	0.958917	0.073443	-0.041083	-0.024057	0.95	4
1.00	1.000000	0.000000	0.000000	0.000000	1.00	4

FOURIER NO. = .120

Z	YA	YB	ASER	BSER	Z	N
0.	0.405587	0.630676	-0.594413	-0.369324	0.	4
0.05	0.407815	0.629661	-0.592185	-0.367839	0.05	4
0.10	0.414479	0.626594	-0.585521	-0.363406	0.10	4
0.15	0.425517	0.621416	-0.574483	-0.356084	0.15	4
0.20	0.440823	0.614027	-0.559177	-0.345973	0.20	4
0.25	0.460248	0.604292	-0.539752	-0.333208	0.25	5
0.30	0.483595	0.592035	-0.516405	-0.317965	0.30	4
0.35	0.510616	0.577050	-0.489384	-0.300450	0.35	4
0.40	0.541012	0.559096	-0.458988	-0.280904	0.40	4
0.45	0.574431	0.537907	-0.425569	-0.259593	0.45	4
0.50	0.610470	0.513189	-0.389530	-0.236811	0.50	5
0.55	0.648674	0.484629	-0.351326	-0.212871	0.55	4
0.60	0.688544	0.451900	-0.311456	-0.188100	0.60	4
0.65	0.729543	0.414664	-0.270457	-0.162836	0.65	4
0.70	0.771105	0.372578	-0.228895	-0.137422	0.70	4
0.75	0.812646	0.325300	-0.187354	-0.112200	0.75	5
0.80	0.853575	0.272499	-0.146425	-0.087501	0.80	4
0.85	0.893312	0.213855	-0.106688	-0.063645	0.85	4
0.90	0.931299	0.149068	-0.068701	-0.040932	0.90	4
0.95	0.967018	0.077564	-0.032982	-0.019636	0.95	4
1.00	1.000000	0.000000	0.000000	0.000000	1.00	4

FOURIER NO. = .140

Z	YA	YB	ASER	BSER	Z	N
0.	0.505668	0.695859	-0.494332	-0.304141	0.	4
0.05	0.507601	0.694593	-0.492399	-0.302907	0.05	4
0.10	0.513377	0.690779	-0.486623	-0.299221	0.10	4
0.15	0.522928	0.684364	-0.477072	-0.293136	0.15	4
0.20	0.536140	0.675264	-0.463860	-0.284736	0.20	4
0.25	0.552852	0.663358	-0.447148	-0.274142	0.25	5
0.30	0.572859	0.648500	-0.427141	-0.261500	0.30	4
0.35	0.595914	0.630510	-0.404086	-0.246990	0.35	4
0.40	0.621723	0.609186	-0.378277	-0.230814	0.40	4
0.45	0.649955	0.584301	-0.350045	-0.213199	0.45	4
0.50	0.680240	0.555608	-0.319760	-0.194392	0.50	5
0.55	0.712177	0.522848	-0.287823	-0.174652	0.55	4
0.60	0.745334	0.485747	-0.254666	-0.154253	0.60	4
0.65	0.779263	0.444026	-0.220737	-0.133474	0.65	4
0.70	0.813499	0.397406	-0.186501	-0.112594	0.70	4
0.75	0.847574	0.345606	-0.152426	-0.091894	0.75	5
0.80	0.881024	0.288358	-0.118976	-0.071642	0.80	4
0.85	0.913400	0.225404	-0.086600	-0.052096	0.85	4
0.90	0.944277	0.156502	-0.055723	-0.033498	0.90	4
0.95	0.973260	0.081432	-0.026740	-0.016068	0.95	4
1.00	1.000000	0.000000	0.000000	0.000000	1.00	4

TRANSIENT CONDUCTION

TEMPERATURE RATIO TERMS FOR THE SPHERE

FOURIER NO. = .160

Z	YA	YB	ASER	BSER	Z	N
0.	0.591305	0.749897	-0.408695	-0.250103	0.	4
0.05	0.592939	0.748417	-0.407061	-0.249083	0.05	4
0.10	0.597821	0.743964	-0.402179	-0.246036	0.10	4
0.15	0.605885	0.736494	-0.394115	-0.241006	0.15	4
0.20	0.617025	0.725933	-0.382975	-0.234067	0.20	4
0.25	0.631093	0.712183	-0.368907	-0.225317	0.25	5
0.30	0.647902	0.695119	-0.352098	-0.214881	0.30	4
0.35	0.667224	0.674591	-0.332776	-0.202909	0.35	3
0.40	0.688801	0.650428	-0.311199	-0.189572	0.40	4
0.45	0.712339	0.622443	-0.287661	-0.175057	0.45	4
0.50	0.737518	0.590430	-0.262482	-0.159570	0.50	5
0.55	0.763995	0.554173	-0.236005	-0.143327	0.55	4
0.60	0.791407	0.513448	-0.208593	-0.126552	0.60	4
0.65	0.819382	0.468024	-0.180618	-0.109476	0.65	3
0.70	0.847538	0.417671	-0.152462	-0.092329	0.70	3
0.75	0.875498	0.362162	-0.124502	-0.075339	0.75	5
0.80	0.902889	0.301276	-0.097111	-0.058724	0.80	4
0.85	0.929356	0.234803	-0.070644	-0.042697	0.85	4
0.90	0.954562	0.162549	-0.045438	-0.027451	0.90	4
0.95	0.978202	0.084334	-0.021798	-0.013166	0.95	3
1.00	1.000000	0.000000	0.000000	0.000000	1.00	3

FOURIER NO. = .180

Z	YA	YB	ASER	BSER	Z	N
0.	0.663191	0.794497	-0.336809	-0.205503	0.	4
0.05	0.664554	0.792838	-0.335446	-0.204662	0.05	4
0.10	0.668625	0.787849	-0.331375	-0.202151	0.10	4
0.15	0.675347	0.779493	-0.324653	-0.198007	0.15	4
0.20	0.684626	0.767710	-0.315374	-0.192290	0.20	4
0.25	0.696333	0.752416	-0.303667	-0.185084	0.25	3
0.30	0.710305	0.733509	-0.289695	-0.176491	0.30	3
0.35	0.726347	0.710864	-0.273653	-0.166636	0.35	3
0.40	0.744236	0.684339	-0.255764	-0.155661	0.40	3
0.45	0.763723	0.653779	-0.236277	-0.143721	0.45	3
0.50	0.784537	0.619014	-0.215463	-0.130986	0.50	3
0.55	0.806389	0.579866	-0.193611	-0.117634	0.55	3
0.60	0.828979	0.536149	-0.171021	-0.103851	0.60	3
0.65	0.851999	0.487674	-0.148001	-0.089826	0.65	3
0.70	0.875136	0.434253	-0.124864	-0.075747	0.70	3
0.75	0.898081	0.375700	-0.101919	-0.061800	0.75	3
0.80	0.920536	0.311833	-0.079464	-0.048167	0.80	3
0.85	0.942211	0.242482	-0.057789	-0.035018	0.85	3
0.90	0.962840	0.167487	-0.037160	-0.022513	0.90	3
0.95	0.982175	0.086703	-0.017825	-0.010798	0.95	3
1.00	1.000000	0.000000	0.000000	0.000000	1.00	3

FOURIER NO. = .200

Z	YA	YB	ASER	BSER	Z	N
0.	0.722922	0.831217	-0.277078	-0.168783	0.	3
0.05	0.724051	0.829409	-0.275949	-0.168091	0.05	3
0.10	0.727422	0.823975	-0.272578	-0.166025	0.10	3
0.15	0.732986	0.814883	-0.267014	-0.162617	0.15	3
0.20	0.740664	0.802086	-0.259336	-0.157914	0.20	3
0.25	0.750346	0.785512	-0.249654	-0.151988	0.25	3
0.30	0.761895	0.765078	-0.238105	-0.144922	0.30	3
0.35	0.775146	0.740680	-0.224854	-0.136820	0.35	3
0.40	0.789911	0.712202	-0.210089	-0.127798	0.40	3
0.45	0.805982	0.679514	-0.194018	-0.117986	0.45	3
0.50	0.823133	0.642478	-0.176867	-0.107522	0.50	3
0.55	0.841125	0.600946	-0.158875	-0.096554	0.55	3
0.60	0.859708	0.554766	-0.140292	-0.085234	0.60	3
0.65	0.878630	0.503783	-0.121370	-0.073717	0.65	3
0.70	0.897633	0.447842	-0.102367	-0.062158	0.70	3
0.75	0.916466	0.386790	-0.083534	-0.050711	0.75	3
0.80	0.934884	0.320479	-0.065116	-0.039521	0.80	3
0.85	0.952654	0.248769	-0.047346	-0.028731	0.85	3
0.90	0.969559	0.171529	-0.030441	-0.018471	0.90	3
0.95	0.985399	0.088641	-0.014601	-0.008859	0.95	3
1.00	1.000000	0.000000	0.000000	0.000000	1.00	3

TRANSIENT CONDUCTION

TEMPERATURE RATIO TERMS FOR THE SPHERE

FOURIER NO. = .220

Z	YA	YB	ASER	BSER	Z	N
0.	0.772282	0.861410	-0.227718	-0.138590	0.	3
0.05	0.773214	0.859479	-0.226786	-0.138021	0.05	3
0.10	0.775994	0.853676	-0.224006	-0.136324	0.10	3
0.15	0.780582	0.843977	-0.219418	-0.133523	0.15	3
0.20	0.786912	0.830342	-0.213088	-0.129658	0.20	3
0.25	0.794893	0.812712	-0.205107	-0.124788	0.25	3
0.30	0.804409	0.791017	-0.195591	-0.118983	0.30	3
0.35	0.815324	0.765174	-0.184676	-0.112326	0.35	3
0.40	0.827480	0.735085	-0.172520	-0.104915	0.40	3
0.45	0.840707	0.700644	-0.159293	-0.096856	0.45	3
0.50	0.854815	0.661738	-0.145185	-0.088262	0.50	3
0.55	0.869609	0.618245	-0.130391	-0.079255	0.55	3
0.60	0.884882	0.570040	-0.115118	-0.069960	0.60	3
0.65	0.900425	0.516996	-0.099575	-0.060504	0.65	3
0.70	0.916029	0.458985	-0.083971	-0.051015	0.70	3
0.75	0.931488	0.395882	-0.068512	-0.041618	0.75	3
0.80	0.946600	0.327566	-0.053400	-0.032434	0.80	3
0.85	0.961177	0.253922	-0.038823	-0.023578	0.85	3
0.90	0.975040	0.174842	-0.024960	-0.015158	0.90	3
0.95	0.988029	0.090230	-0.011971	-0.007270	0.95	3
1.00	1.000000	0.000000	0.000000	0.000000	1.00	3

FOURIER NO. = .240

Z	YA	YB	ASER	BSER	Z	N
0.	0.812950	0.886217	-0.187050	-0.113783	0.	3
0.05	0.813716	0.884184	-0.186284	-0.113316	0.05	3
0.10	0.816004	0.878078	-0.183996	-0.111922	0.10	3
0.15	0.819780	0.867879	-0.180220	-0.109621	0.15	3
0.20	0.824989	0.853553	-0.175011	-0.106447	0.20	3
0.25	0.831555	0.835053	-0.168445	-0.102447	0.25	3
0.30	0.839383	0.812321	-0.160617	-0.097679	0.30	3
0.35	0.848359	0.785288	-0.151641	-0.092212	0.35	3
0.40	0.858355	0.753874	-0.141645	-0.086126	0.40	3
0.45	0.869228	0.717992	-0.130772	-0.079508	0.45	3
0.50	0.880822	0.677549	-0.119178	-0.072451	0.50	3
0.55	0.892977	0.632444	-0.107023	-0.065056	0.55	3
0.60	0.905522	0.582575	-0.094478	-0.057425	0.60	3
0.65	0.918286	0.527838	-0.081714	-0.049662	0.65	3
0.70	0.931098	0.468128	-0.068902	-0.041872	0.70	3
0.75	0.943787	0.403341	-0.056213	-0.034159	0.75	3
0.80	0.956189	0.333380	-0.043811	-0.026621	0.80	3
0.85	0.968150	0.258148	-0.031850	-0.019352	0.85	3
0.90	0.979524	0.177559	-0.020476	-0.012441	0.90	3
0.95	0.990180	0.091534	-0.009820	-0.005966	0.95	3
1.00	1.000000	0.000000	0.000000	0.000000	1.00	3

FOURIER NO. = .260

Z	YA	YB	ASER	BSER	Z	N
0.	0.846400	0.906591	-0.153600	-0.093409	0.	3
0.05	0.847030	0.904474	-0.152970	-0.093026	0.05	3
0.10	0.848911	0.898119	-0.151089	-0.091881	0.10	3
0.15	0.852015	0.887508	-0.147985	-0.089991	0.15	3
0.20	0.856296	0.872615	-0.143704	-0.087385	0.20	3
0.25	0.861693	0.853399	-0.138307	-0.084101	0.25	3
0.30	0.868126	0.829814	-0.131874	-0.080186	0.30	3
0.35	0.875502	0.801803	-0.124498	-0.075697	0.35	3
0.40	0.883715	0.769300	-0.116285	-0.070700	0.40	3
0.45	0.892647	0.732234	-0.107353	-0.065266	0.45	3
0.50	0.902171	0.690527	-0.097829	-0.059473	0.50	3
0.55	0.912153	0.644098	-0.087847	-0.053402	0.55	3
0.60	0.922455	0.592863	-0.077545	-0.047137	0.60	3
0.65	0.932935	0.536736	-0.067065	-0.040764	0.65	3
0.70	0.943452	0.475630	-0.056548	-0.034370	0.70	3
0.75	0.953868	0.409462	-0.046132	-0.028038	0.75	3
0.80	0.964048	0.338150	-0.035952	-0.021850	0.80	3
0.85	0.973864	0.261616	-0.026136	-0.015884	0.85	3
0.90	0.983198	0.179789	-0.016802	-0.010211	0.90	3
0.95	0.991942	0.092603	-0.008058	-0.004897	0.95	3
1.00	1.000000	0.000000	0.000000	0.000000	1.00	3

TRANSIENT CONDUCTION

TEMPERATURE RATIO TERMS FOR THE SPHERE

FOURIER NO. = .280

Z	YA	YB	ASER	BSER	Z	N
0.	0.873889	0.923319	-0.126111	-0.076681	0.	3
0.05	0.874407	0.921134	-0.125593	-0.076366	0.05	3
0.10	0.875952	0.914574	-0.124048	-0.075426	0.10	3
0.15	0.878502	0.903625	-0.121498	-0.073875	0.15	3
0.20	0.882019	0.888265	-0.117981	-0.071735	0.20	3
0.25	0.886452	0.868462	-0.113548	-0.069038	0.25	3
0.30	0.891736	0.844176	-0.108264	-0.065824	0.30	3
0.35	0.897794	0.815361	-0.102206	-0.062139	0.35	3
0.40	0.904539	0.781963	-0.095461	-0.058037	0.40	3
0.45	0.911874	0.743924	-0.088126	-0.053576	0.45	3
0.50	0.919695	0.701180	-0.080305	-0.048820	0.50	3
0.55	0.927892	0.653665	-0.072108	-0.043835	0.55	3
0.60	0.936350	0.601307	-0.063650	-0.038693	0.60	3
0.65	0.944954	0.544039	-0.055046	-0.033461	0.65	3
0.70	0.953587	0.481788	-0.046413	-0.028212	0.70	3
0.75	0.962137	0.414485	-0.037863	-0.023015	0.75	3
0.80	0.970493	0.342065	-0.029507	-0.017936	0.80	3
0.85	0.978550	0.264462	-0.021450	-0.013038	0.85	3
0.90	0.986210	0.181618	-0.013790	-0.008382	0.90	3
0.95	0.993387	0.093480	-0.006613	-0.004020	0.95	3
1.00	1.000000	0.000000	0.000000	0.000000	1.00	3

FOURIER NO. = .300

Z	YA	YB	ASER	BSER	Z	N
0.	0.896468	0.937053	-0.103532	-0.062947	0.	3
0.05	0.896893	0.934812	-0.103107	-0.062688	0.05	3
0.10	0.898162	0.928084	-0.101838	-0.061916	0.10	3
0.15	0.900256	0.916857	-0.099744	-0.060643	0.15	3
0.20	0.903144	0.901114	-0.096856	-0.058886	0.20	3
0.25	0.906784	0.880828	-0.093215	-0.056672	0.25	3
0.30	0.911124	0.855966	-0.088876	-0.054034	0.30	3
0.35	0.916098	0.826491	-0.083902	-0.051009	0.35	3
0.40	0.921637	0.792359	-0.078363	-0.047641	0.40	3
0.45	0.927659	0.753521	-0.072341	-0.043979	0.45	3
0.50	0.934080	0.709926	-0.065920	-0.040074	0.50	3
0.55	0.940809	0.661517	-0.059191	-0.035983	0.55	3
0.60	0.947753	0.608239	-0.052247	-0.031761	0.60	3
0.65	0.954816	0.550033	-0.045184	-0.027467	0.65	3
0.70	0.961904	0.486842	-0.038096	-0.023158	0.70	3
0.75	0.968922	0.418608	-0.031078	-0.018892	0.75	3
0.80	0.975781	0.345278	-0.024219	-0.014722	0.80	3
0.85	0.982394	0.266798	-0.017606	-0.010702	0.85	3
0.90	0.988682	0.183120	-0.011318	-0.006880	0.90	3
0.95	0.994572	0.094200	-0.005428	-0.003300	0.95	3
1.00	1.000000	0.000000	0.000000	0.000000	1.00	3

FOURIER NO. = .350

Z	YA	YB	ASER	BSER	Z	N
0.	0.936787	0.961570	-0.063213	-0.038430	0.	3
0.05	0.937047	0.959228	-0.062953	-0.038272	0.05	3
0.10	0.937822	0.952199	-0.062178	-0.037801	0.10	3
0.15	0.939101	0.940477	-0.060899	-0.037023	0.15	3
0.20	0.940865	0.924049	-0.059135	-0.035951	0.20	3
0.25	0.943088	0.902901	-0.056912	-0.034599	0.25	3
0.30	0.945738	0.877012	-0.054262	-0.032988	0.30	3
0.35	0.948776	0.846359	-0.051224	-0.031141	0.35	3
0.40	0.952158	0.810915	-0.047842	-0.029085	0.40	3
0.45	0.955835	0.770651	-0.044165	-0.026849	0.45	3
0.50	0.959756	0.725535	-0.040244	-0.024465	0.50	3
0.55	0.963865	0.675533	-0.036135	-0.021967	0.55	3
0.60	0.968105	0.620610	-0.031895	-0.019390	0.60	3
0.65	0.972417	0.560732	-0.027583	-0.016768	0.65	3
0.70	0.976744	0.495862	-0.023256	-0.014138	0.70	3
0.75	0.981028	0.425967	-0.018972	-0.011533	0.75	3
0.80	0.985215	0.351012	-0.014785	-0.008988	0.80	3
0.85	0.989252	0.270966	-0.010748	-0.006534	0.85	3
0.90	0.993091	0.185800	-0.006909	-0.004200	0.90	3
0.95	0.996686	0.095486	-0.003314	-0.002014	0.95	3
1.00	1.000000	0.000000	0.000000	0.000000	1.00	3

TRANSIENT CONDUCTION

TEMPERATURE RATIO TERMS FOR THE SPHERE

FOURIER NO. = .400

Z	YA	YB	ASER	BSER	Z	N
0.	0.961408	0.976539	-0.038592	-0.023461	0.	3
0.05	0.961566	0.974135	-0.038434	-0.023365	0.05	3
0.10	0.962039	0.966923	-0.037961	-0.023077	0.10	3
0.15	0.962820	0.954897	-0.037180	-0.022603	0.15	3
0.20	0.963897	0.938052	-0.036103	-0.021948	0.20	3
0.25	0.965255	0.915377	-0.034745	-0.021123	0.25	3
0.30	0.966872	0.889661	-0.033128	-0.020139	0.30	3
0.35	0.968727	0.858488	-0.031273	-0.019012	0.35	3
0.40	0.970792	0.822244	-0.029208	-0.017756	0.40	2
0.45	0.973037	0.781109	-0.026963	-0.016391	0.45	2
0.50	0.975431	0.735064	-0.024569	-0.014936	0.50	3
0.55	0.977940	0.684089	-0.022060	-0.013411	0.55	2
0.60	0.980528	0.628162	-0.019472	-0.011838	0.60	2
0.65	0.983161	0.567263	-0.016839	-0.010237	0.65	2
0.70	0.985802	0.501369	-0.014198	-0.008631	0.70	2
0.75	0.988418	0.430459	-0.011582	-0.007041	0.75	2
0.80	0.990974	0.354513	-0.009026	-0.005487	0.80	2
0.85	0.993439	0.273511	-0.006561	-0.003989	0.85	2
0.90	0.995782	0.187436	-0.004218	-0.002564	0.90	2
0.95	0.997977	0.096270	-0.002023	-0.001230	0.95	2
1.00	1.000000	0.000000	0.000000	0.000000	1.00	2

FOURIER NO. = .450

Z	YA	YB	ASER	BSER	Z	N
0.	0.976439	0.985677	-0.023561	-0.014323	0.	2
0.05	0.976536	0.983236	-0.023464	-0.014264	0.05	2
0.10	0.976825	0.975911	-0.023175	-0.014089	0.10	2
0.15	0.977302	0.963701	-0.022698	-0.013799	0.15	2
0.20	0.977959	0.946601	-0.022041	-0.013399	0.20	2
0.25	0.978788	0.924605	-0.021212	-0.012895	0.25	2
0.30	0.979776	0.897705	-0.020224	-0.012295	0.30	2
0.35	0.980908	0.865893	-0.019092	-0.011607	0.35	2
0.40	0.982169	0.829160	-0.017831	-0.010840	0.40	2
0.45	0.983539	0.787493	-0.016461	-0.010007	0.45	2
0.50	0.985001	0.740882	-0.014999	-0.009118	0.50	3
0.55	0.986532	0.689313	-0.013468	-0.008187	0.55	2
0.60	0.988112	0.632773	-0.011888	-0.007227	0.60	2
0.65	0.989720	0.571250	-0.010280	-0.006250	0.65	2
0.70	0.991332	0.504731	-0.008668	-0.005269	0.70	2
0.75	0.992929	0.433202	-0.007071	-0.004298	0.75	2
0.80	0.994490	0.356650	-0.005510	-0.003350	0.80	2
0.85	0.995994	0.275065	-0.004006	-0.002435	0.85	2
0.90	0.997425	0.188435	-0.002575	-0.001565	0.90	2
0.95	0.998765	0.096749	-0.001235	-0.000751	0.95	2
1.00	1.000000	0.000000	0.000000	0.000000	1.00	2

FOURIER NO. = .500

Z	YA	YB	ASER	BSER	Z	N
0.	0.985616	0.991256	-0.014384	-0.008744	0.	2
0.05	0.985675	0.988792	-0.014325	-0.008708	0.05	2
0.10	0.985852	0.981399	-0.014148	-0.008601	0.10	2
0.15	0.986143	0.969076	-0.013857	-0.008424	0.15	2
0.20	0.986544	0.951820	-0.013456	-0.008180	0.20	2
0.25	0.987050	0.929627	-0.012950	-0.007873	0.25	2
0.30	0.987653	0.902494	-0.012347	-0.007506	0.30	2
0.35	0.988344	0.870414	-0.011656	-0.007086	0.35	2
0.40	0.989114	0.833382	-0.010886	-0.006618	0.40	2
0.45	0.989951	0.791391	-0.010049	-0.006109	0.45	2
0.50	0.990843	0.744433	-0.009157	-0.005567	0.50	3
0.55	0.991778	0.692502	-0.008222	-0.004998	0.55	2
0.60	0.992743	0.635588	-0.007257	-0.004412	0.60	2
0.65	0.993724	0.573685	-0.006276	-0.003815	0.65	2
0.70	0.994708	0.506783	-0.005292	-0.003217	0.70	2
0.75	0.995683	0.434876	-0.004317	-0.002624	0.75	2
0.80	0.996636	0.357955	-0.003364	-0.002045	0.80	2
0.85	0.997555	0.275013	-0.002445	-0.001487	0.85	2
0.90	0.998428	0.189044	-0.001572	-0.000956	0.90	2
0.95	0.999246	0.097042	-0.000754	-0.000458	0.95	2
1.00	1.000000	0.000000	0.000000	0.000000	1.00	2

TRANSIENT CONDUCTION

TEMPERATURE RATIO TERMS FOR THE SPHERE

FOURIER NO. = .600

Z	YA	YB	ASER	BSER	Z	N
0.	0.994639	0.996741	-0.005361	-0.003259	0.	2
0.05	0.994661	0.994254	-0.005339	-0.003246	0.05	2
0.10	0.994727	0.986794	-0.005273	-0.003206	0.10	2
0.15	0.994835	0.974360	-0.005165	-0.003140	0.15	2
0.20	0.994985	0.956951	-0.005015	-0.003049	0.20	2
0.25	0.995173	0.934566	-0.004827	-0.002934	0.25	2
0.30	0.995398	0.907202	-0.004602	-0.002798	0.30	2
0.35	0.995656	0.874859	-0.004344	-0.002641	0.35	2
0.40	0.995943	0.837533	-0.004057	-0.002467	0.40	2
0.45	0.996255	0.795223	-0.003745	-0.002277	0.45	2
0.50	0.996587	0.747925	-0.003413	-0.002075	0.50	3
0.55	0.996936	0.695637	-0.003064	-0.001863	0.55	2
0.60	0.997295	0.638356	-0.002705	-0.001644	0.60	2
0.65	0.997661	0.576078	-0.002339	-0.001422	0.65	2
0.70	0.998028	0.508801	-0.001972	-0.001199	0.70	2
0.75	0.998391	0.436522	-0.001609	-0.000978	0.75	2
0.80	0.998746	0.359238	-0.001254	-0.000762	0.80	2
0.85	0.999089	0.276946	-0.000911	-0.000554	0.85	2
0.90	0.999414	0.189644	-0.000586	-0.000356	0.90	2
0.95	0.999719	0.097329	-0.000281	-0.000171	0.95	2
1.00	1.000000	0.000000	0.000000	0.000000	1.00	2

STARTUP STUDIES OF A NUCLEAR ROCKET REACTOR

Part 1

COMPUTATIONAL PROCEDURES AND EXPERIMENTAL CHECKS

Rodney S. Thurston and Ray Pollock
University of California
Los Alamos Scientific Laboratory
Los Alamos, New Mexico

Introduction

It was decided in the Fall of 1959 to develop a digital code which could calculate the entire startup transient of a Rover reactor. The power fluctuations which might be caused by admission of high density hydrogen into the core made this study imperative. This paper describes, in three parts, the codes which have been developed to date, experiments which have been and will be run to provide checks for the codes, and startup studies which have been performed by means of the codes.

We needed a code which could calculate wall temperatures and the hydrogen state throughout the reactor as a function of time. The several numbers that are of particular importance are as follows:

1. Nozzle cooling inlet pressure.
2. Total hydrogen reactivity.
3. Hydrogen temperature at the core inlet plenum.
4. Temperature gradients in the core.

In writing the code the major obstacle was the lack of techniques and data needed to describe the two-phase heat transfer and fluid flow regimes. Some heat transfer data was correleated and a quasi-steady flow model was chosen in order to get a code started. The first code, STUP, was written to investigate models for two phase flow calculations and to calculate the behavior of the reflector alone as it is cooled by liquid hydrogen. Following this, HEX was written to incorporate similar heat transfer and flow relations into a complex systems code designed particularly to handle Kiwi-B type reactors. Both STUP and HEX, and a modification of STUP called TRIP, will be discussed in the balance of the paper.

Description of Model Used

All calculations discussed here employ the quasi-steady-state assumption, or what is sometimes called the "single mass velocity model". It assumes

that at any instant the mass-flow rate $W(t) = \rho vA$ is spatially constant. Both STUP and HEX use time-dependent equations for the thermal behavior of the tube walls, and both are single-tube models.

In STUP, a mean temperature is applied at the center section of the tube. The radial temperature distribution is assumed uniform, and an arbitrary longitudinal temperature gradient is imposed. The overall temperature level is then determined by the cooling rate.

TRIP modifies STUP by applying the same calculations to three thermally insulated tubes in parallel, representing three sections of the reflector: reflector segment, control rod, and reflector cylinder. Flow is balanced to yield agreement on exit pressure.

In HEX, a single flow passage from each section of the reactor is considered, all joined in series. Energy is introduced into the channel walls at a pre-programmed rate and with an arbitrary spatial distribution. The wall temperatures are determined by solving a time-dependent diffusion problem with a convective boundary condition at the flow-passage wall and an outer boundary condition appropriate to the section of the reactor represented. Axial heat conduction in the channel walls is neglected in comparison with the conduction radially into the coolant, and the calculation is thus one-dimensional.

Heat Transfer and Pressure Drop Correlations

The heat transfer and pressure loss correlations used in both STUP and HEX are displayed in Fig. 1. Equation (1) is a correlation of data on heat transfer to two-phase hydrogen by Core, et al.[1] This correlation has a standard deviation of 27% and an exceptionally strong dependence on Prandtl number. The correlation gave reasonable results in the STUP calculations to be described shortly. The strong Prandtl number dependence caused some difficulty with HEX in trying to calculate an experimental cool-down run; by setting the Prandtl number to a constant value of 0.714, good results were obtained.

The correlation of Hendrichs, et al,[2] has not been tested at this writing since it may require extensive revision in HEX. It appears promising and will probably be included in the code at some future date.

Frictional pressure losses for two-phase flow are computed according to the correlation of Lockhart and Martinelli, equations (3) through (6), and the friction factor for gaseous flow is computed from Colburn's correction to Reynold's analogy, equation (7).

Numerical Methods

STUP and HEX both employ finite-difference methods for the solution of the differential equations involved. The integration of the ordinary differential equations for steady compressible flow is accomplished by Euler's method on a mesh of cells imposed along the channel axis. Higher order methods proved to be of no significant benefit in this model, which deals only with subsonic flow. In HEX, wall temperatures are computed for each of a number of radial cells associated with each axial cell using a Crank-Nicholson form of differencing with the spatial derivatives evaluated only at the advanced time. This form of differencing was chosen to avoid difficulties with negative wall temperatures in beryllium, the c_p of which becomes very small at temperatures below 80°K. The wall calculation is coupled to the flow equations through an iterative scheme, whereby the flow equations are integrated using the heat flux from the previous iteration, and the hydrogen temperature so determined used as a boundary condition to improve the wall temperatures. This iteration is continued in a given axial cell until the temperatures stabilize.

Experimental Background

The STUP calculation has been checked against results from the experimental cool-down by liquid hydrogen of an aluminum block, which served as a model of the reflector (Fig. 2). The experiments are described in detail in Part 2 of this paper, "Cryogenic Cool-Down Experiments", by Watts, Lyle, and Balcomb. Three experimental runs with flow rates of 15.2, 31.2, and 41.0 gpm were selected for analysis. The calculations were started at time 10 seconds since the flow rate was uncertain at earlier times. Comparisons between STUP computations and observed conditions are shown in Figures 3 to 5. Similar calculations were undertaken with HEX, and, after the modification in the two-phase heat transfer coefficient described earlier, these gave results very similar to those of STUP.

Studies of the Kiwi-B reflector system by means of the TRIP code showed that because of the changing rates of cooling in the reflector segment, control rod and reflector cylinder, their relative impedance varies significantly during a startup. Comparing a TRIP calculation with a single tube representation of the reflector, which is used by HEX, indicates good agreement on mean exit propellant temperatures but disagreement on pressure drop across the reflector. For example, in a typical startup computation the two codes computed temperatures only 15 R° apart, but differed by 50% in pressure drop.

Conclusion

The work described in this paper has provided a tool which is capable of describing to some degree the sequence of events occurring in the startup of a nuclear rocket. The accuracy of this description appears to be satisfactory in describing the sequence of events occurring in the startup of a nuclear rocket. Quasi-steady-state equations do not appear to yield erroneous results in this system. The use of a single tube model for the reflector, which has three different subsections, gives good agreement on temperature, but poor agreement on pressure drop when compared to a three tube model. Modifications to improve this model by using better two-phase correlations are under consideration.

References

1. Core, Harkee, Misra, Sato: "Heat Transfer Studies", Aerojet General Corp., WADC Contract 0.AF 33(616)-5289, September, 1959.

2. Hendrichs, Graham, Hsu, and Mederro: "Correlations of Hydrogen Heat Transfer in the Boiling and Supercritical Pressure States", Lewis Research Center, NASA, Presented at the American Rocket Society Propellants, Combustion and Liquid Rockets Conference, April, 1961.

HEAT TRANSFER

TWO PHASE

$$\left(\frac{hD}{k}\right) = (.000709)(Re_f)^{.656}(Pr_f)^{-13}\left(\frac{\rho_f}{\rho}\right)^{.223}\left(\frac{T_w}{T}\right)^{.212} \quad ---(1)$$

where $Re_f = \frac{4\dot{w}}{\pi D \mu_f}$

GAS

$$\left(\frac{hD}{k}\right) = (.0217)(Re)^{.8}(Pr)^{.4}\left(\frac{T_w}{T}\right)^{-.34} \quad ----------(2)$$

PRESSURE DROP

TWO PHASE

$$\left(\frac{dP}{dX}\right) = \phi^2 \left(\frac{dP}{dX}\right)_L \quad ----------(3)$$

$$\left(\frac{dP}{dX}\right)_L = \frac{f_L V_L^2 \rho_L}{gD} \quad ----------(4)$$

$$X^{-1} = \left(\frac{1-Z}{Z}\right)^{.9}\left(\frac{\rho_g}{\rho_L}\right)^{.5}\left(\frac{\mu_L}{\mu_g}\right)^{.1} \quad ----------(5)$$

$$\left.\begin{aligned} \phi^2 &= 13.05(X)^{1.36} + 2.517, \quad X \geq 1.11 \\ \phi^2 &= 15.84(X)^{.659}, \quad X < 1.11 \end{aligned}\right\} \quad ----------(6)$$

GAS

$$f = \frac{2h(Pr)^{2/3}}{\rho v c_p} \quad ----------(7)$$

FIGURE 1

HEAT TRANSFER AND PRESSURE LOSS CORRELATIONS

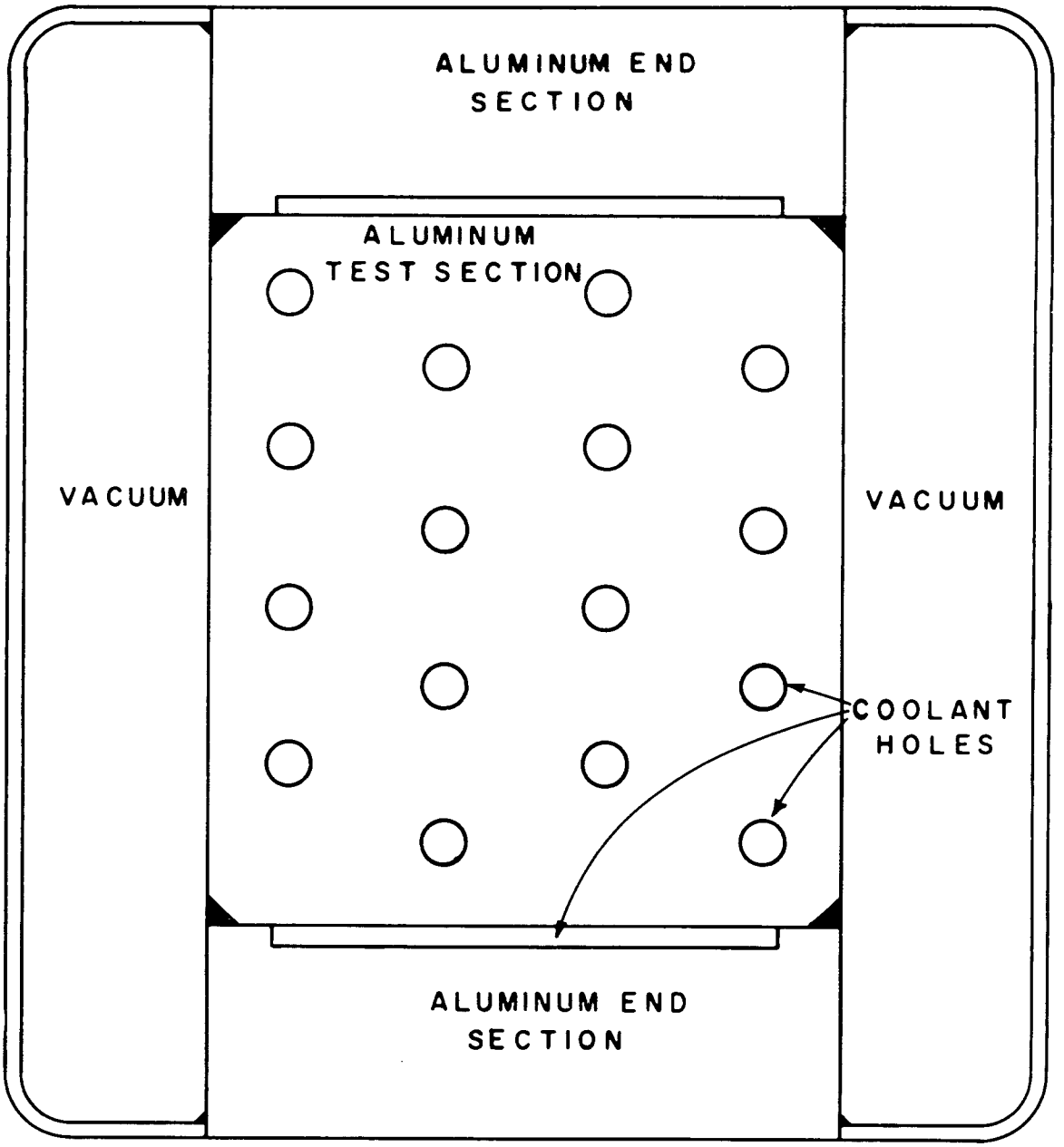

FIGURE 2.

CROSS SECTION OF THE REFLECTOR MOCKUP
EXPERIMENT TEST SECTION

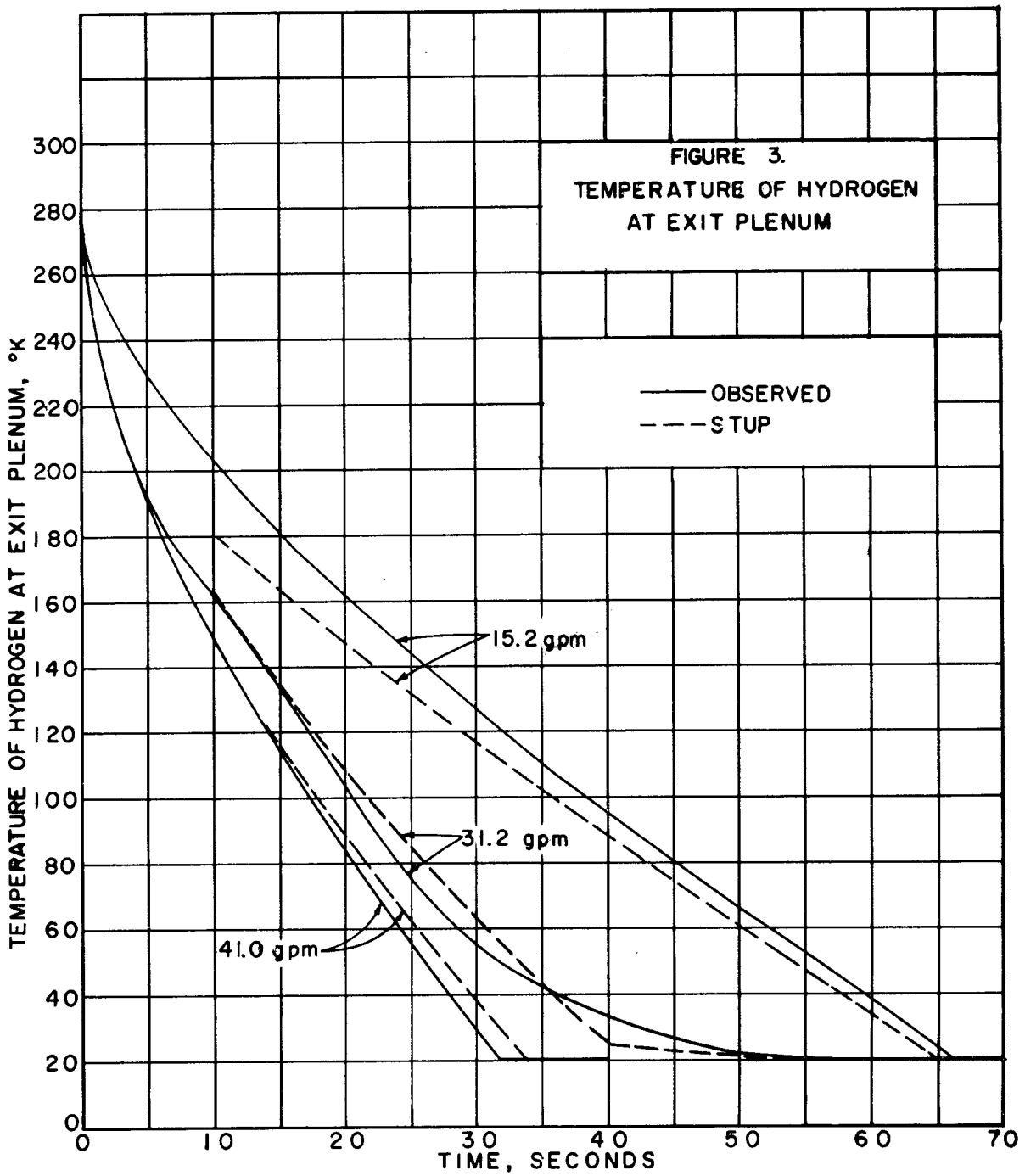
FIGURE 3.
TEMPERATURE OF HYDROGEN
AT EXIT PLENUM
OBSERVED
STUP
15.2 gpm
31.2 gpm
41.0 gpm
TEMPERATURE OF HYDROGEN AT EXIT PLENUM, °K
TIME, SECONDS
0
20
40
60
80
100
120
140
160
180
200
220
240
260
280
300
0
10
20
30
40
50
60
70

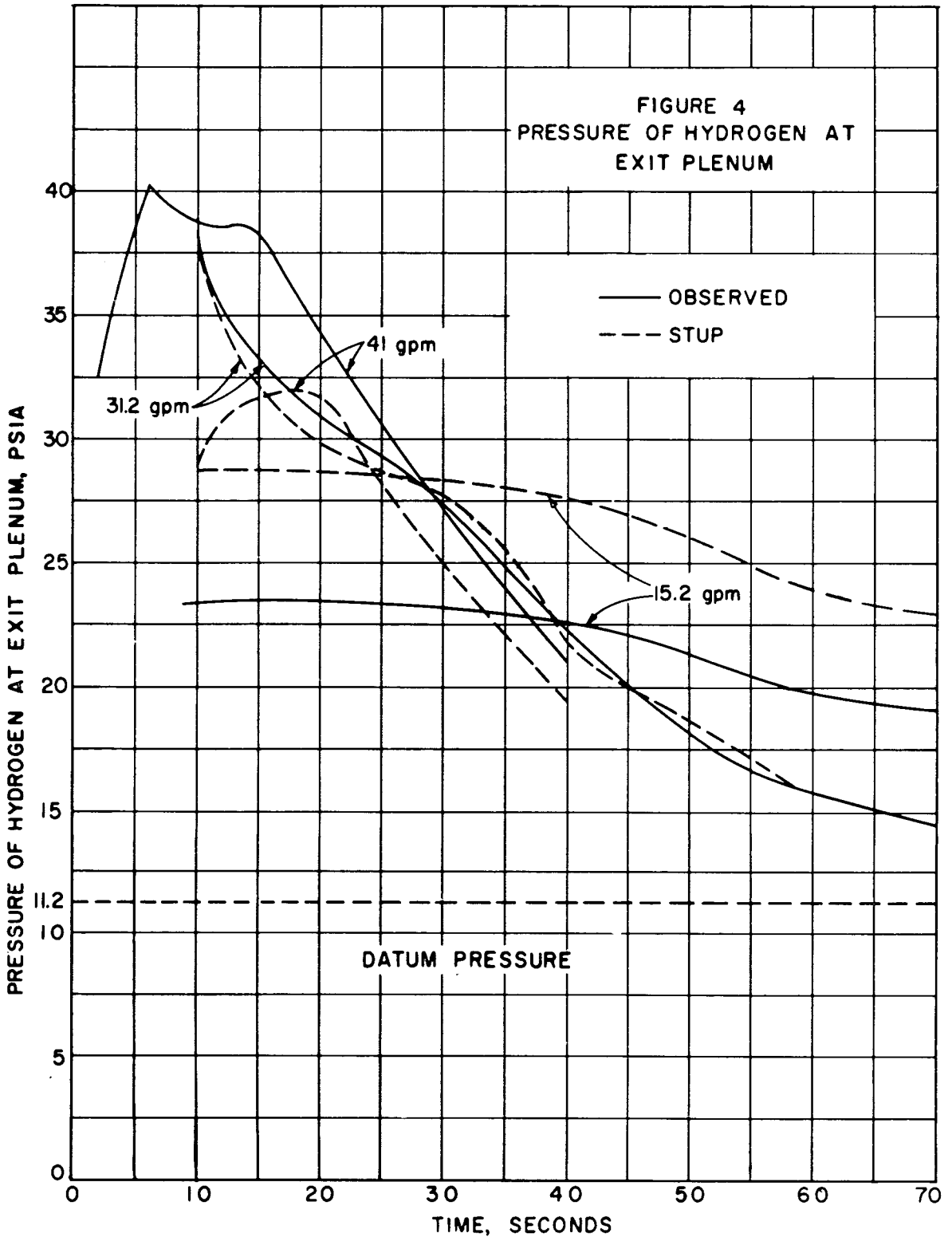
FIGURE 4
PRESSURE OF HYDROGEN AT EXIT PLENUM
OBSERVED
STUP
41 gpm
31.2 gpm
15.2 gpm
DATUM PRESSURE
PRESSURE OF HYDROGEN AT EXIT PLENUM, PSIA
TIME, SECONDS
0
5
10
11.2
15
20
25
30
35
40
0
10
20
30
40
50
60
70

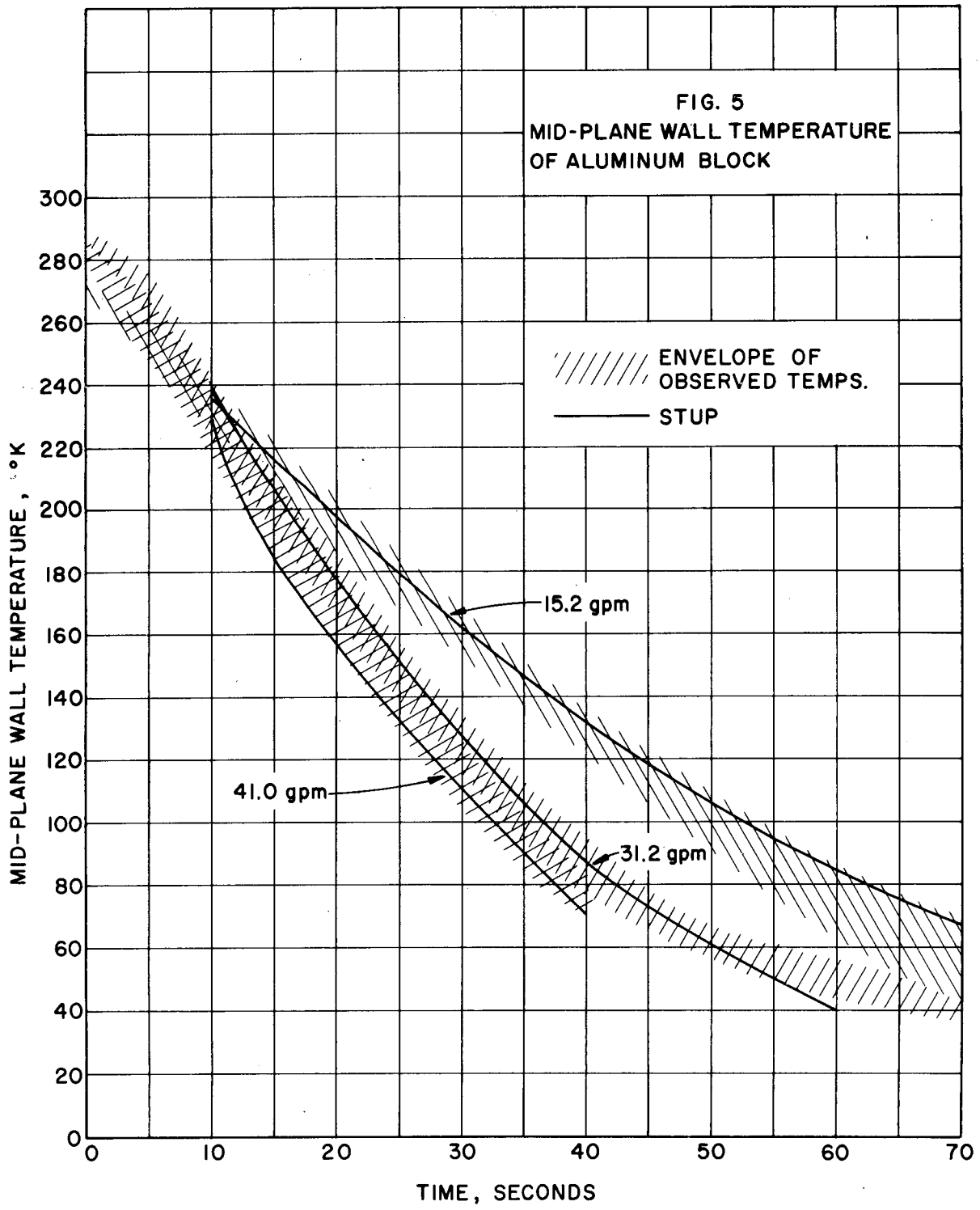
FIG. 5
MID-PLANE WALL TEMPERATURE
OF ALUMINUM BLOCK
ENVELOPE OF
OBSERVED TEMPS.
STUP
15.2 gpm
41.0 gpm
31.2 gpm
MID-PLANE WALL TEMPERATURE, °K
TIME, SECONDS
0
20
40
60
80
100
120
140
160
180
200
220
240
260
280
300
0
10
20
30
40
50
60
70

USE OF TANK MOUNTED BOOSTER PUMPS FOR PROVIDING NPSH FOR TURBO PUMPS OPERATING IN A RADIATION ENVIRONMENT

By John DiStefano
Manager Advanced Product Development

Pesco Products Division
Borg-Warner Corporation

SUMMARY

This paper outlines the results of a test program which was planned to demonstrate the feasibility of using a tank mounted, all-inducer, high speed liquid hydrogen booster pump to provide NPSH for the turbo pump in a reactor-powered vehicle. The cavitation problem associated with pumping liquid hydrogen, when used as a propellant, is further aggravated by localized heating caused by radiation from the reactor.

This heating occurs from gamma ray and neutron flux absorption in the bottom two or three feet of the liquid hydrogen tank. Depending upon the amount of sub-cooling available in the liquid hydrogen when the reactor is started, it is possible for the neutron slowdown to heat the hydrogen to the saturation point, or even superheat some localized regions.

Estimates of heating near the bottom of the tank have indicated that it can be equivalent to a power level of 1.0 watt/cm^2, which is equal to a heat flux of 53 BTU/sq.ft.-min. Figure I indicates how this heating takes place.

The question that the test program was planned to answer is this:

Can a tank mounted booster pump deliver saturated or violently boiling liquid hydrogen to the inlet of a downstream pump with sufficient NPSH to suppress any incident of cavitation?

INTRODUCTION

A test program to prove the feasibility of using a tank mounted booster pump to provide maximum NPSH for the turbo pump in a reactor powered vehicle must demonstrate hydraulic and thermal similarity.

Hydraulic Similarity

Hydraulic similarity must be established from a non-cavitation and cavitation performance standpoint. Before any hydraulic similarity between prototype (reactor installation) and model (test vehicle) can be established, the prototype flow rate must be determined. For a first generation reactor powered vehicle, a flow rate of 8,000 gpm (approximately 80 pps of liquid hydrogen) was assumed. To establish hydraulic similarity, it is also necessary to determine pump inlet and outlet pressures. For purposes of this program, tank pressures of 15 to 20 psia with a pump head rise of five to 10 psi were assumed. It is believed that these are valid numbers for a first attempt at solving the problem.

Non-Cavitation Similarity

Here the criterion is the parameter, Specific Speed, N_s, is defined as: where N = Pump rpm
Gpm = Pump flow
H = Pump head in feet.

$$N_s = \frac{N\sqrt{Gpm}}{(H)^{3/4}}$$

Inducers operate in the specific speed range of 5,000 to 9,000 rpm. Assuming an N_s = 7,000 and a head rise of 300 feet (almost 10 psi), one calculates a prototype operation speed of:

$$N = \frac{7,000\ (300)^{3/4}}{\sqrt{8,000}} = 5{,}450 \text{ rpm}$$

Hydraulic similarity will be obtained in pump developing the same head, if the ratio of pump speed is inversely proportional to the square root of the flow, thus:

$$n = N\sqrt{\frac{Q}{q}}$$ where caps refer to prototype or larger pump

For N = 5,450

and q = 1,000

$$n = 5{,}450\sqrt{\frac{8,000}{1,000}} = 15,300 \text{ rpm}$$

The test vehicle used in this program delivered 1,000 gpm with a head rise of 330 feet (10 psi) at its best efficiency point, while operating at 14,800 rpm. Test data obtained at 20,000 rpm demonstrated inlet hydraulic similarity to a 9,000 specific speed number.

Cavitation Similarity

When comparing similar installations (tank or line mounted pumps) pumping similar fluids, the parameter suction specific speed can be used

to compare and predict the cavitation performance of centrifugal pumps. Suction specific speed, SSS, is defined as follows:

$$SSS = \frac{N\sqrt{GPM}}{(H_{sv})^{3/4}}$$

Where N = Pump speed, rpm

GPM = Pump delivered flow in gallons per minute.

H_{sv} = Net positive suction head, which is the physical head of liquid above the pump inlet when pumping a boiling liquid.

Pesco tank mounted liquid hydrogen pumps have demonstrated the capability of consistently achieving suction specific speeds of over 200,000. An optimum tank-bottom installation utilizing a good inlet bell, has achieved SSS numbers of over 400,000.

To demonstrate the same capability of emptying a tank of boiling liquid; i.e., the ability to pump to the same H_{sv} value, the model pump speed calculates as follows:

$$n = N\sqrt{\frac{Q}{q}} = 5,450\sqrt{\frac{8,000}{1,000}}$$

$$= 15,300 \text{ rpm}$$

Thermal Similarity

Heat leak conditions and thermal similarity were established by measuring liquid hydrogen boil-off. The boil-off rate was determined by noting the change of liquid level in the tank per unit of time. Knowing latent heat for vaporization of liquid hydrogen, the exposed area of the tank and the tank pressure, it was possible to determine the heat leak per unit area. These calculations are somewhat conservative, since most of the heat leakage takes place at the pump mounting surface, which is in itself a heat short. Heat leak rates in excess of 80 BTU/min.-ft.^{2} were calculated greater by 50 per cent than the estimated rates expected in a nuclear reactor powered vehicle.

Pump Description

The inducer test pump, which was driven by a hydraulic motor is illustrated in Figure 2. An inducer-impeller pump was modified for this program. The modifications were:

A. The second stage pump impeller was removed and replaced with a stationary spool piece, which effectively guided the liquid flow into the volute.

B. The outside diameter of the inducer was reduced to 3.83 inches with an inlet angle of 10.7° and a discharge angle of 21.2°.

C. A straight inlet adapter was provided over the modified inducer.

TEST PROGRAM

1. Normal Speed Movie Observation

The boiling activity of liquid hydrogen at the inlet of a tank mounted booster pump was filmed with a Bolex camera at a speed of 18 frames per second. This was done in two stages; first, with the tank pressurized to 5 psig, and second, with the tank un-pressurized. The boiling was filmed while the tank was under constant pressure, and also while it was being de-pressurized.

2. High Speed Still Photography Observation

The above procedure was repeated and photographed with a Nikon F camera and an Edgerton microflash unit in order to observe the actual vapor formation around and within the inducer.

APPARATUS

Description of Test Installation No. 1 (See Figure 3)

For the moving picture test setup, the pump and drive assembly were mounted to the 7,000 gallon dewar sump, and were foam insulated at the mounting base. Sufficient heat leak (over 80 BTU/min.-ft.^{2}) was allowed through this area to simulate the radiation heat leak condition in the space.

Three banks of lights and reflectors were installed inside the dewar, one set being submerged in the liquid hydrogen. All lamps were lighted at a reduced voltage to protect their filament. The liquid hydrogen flow patterns were photographed through an eight inch diameter vacuum insulated view port located on top of the dewar cover. The pictures were taken with a Bolex movie camera equipped with an electric motor drive. The camera was set at f2.8 lense opening and operated at a speed of 18 frames per second.

Description of Test Installation No. 2 (See Figure 4)

For the high speed still photographic test setup, the pump installation was the same as for test installation No. 1. The light source, however, was obtained by using an electronic flash unit manufactured by Edgerton, Germeshausen, and Grier, Inc. The microflash unit, model No. 549 was housed inside a vacuum insulated container which was attached to a sight duct. The entire unit was lowered into the liquid hydrogen test dewar. The unit was so arranged that when a stroboscope was triggered, a mirror attached to the duct would reflect light onto the inducer inlet area. The flash duration from this unit was 0.5 microseconds with peak light intensity of 50×10^6 beam candle power. A still image of rotating elements was

photographed by a motor driven, remotely operated Nikon F camera equipped with a 200 mm f4 telephoto lense which was set at an opening of approximately f8. Kodak Tri X film was used.

RESULTS AND DISCUSSION

Normal Speed Photography

A seven minute film clip showing the boiling activity of liquid hydrogen in the vicinity of the pump inlet, under various test conditions, was shown at the oral presentation of this paper. Of particular interest is the active, deep foaming condition to which the boiling liquid flared during the de-pressurization testing.

High Speed Photography

Figures 5 and 6 are typical photographs of the liquid hydrogen surface during saturation. Photographic technique has not proceeded to a point where photographs can be taken of liquid and vapor entering the pump inlet and indirect passages below the surface of the liquid. This program will be continued during the next year to obtain this photographic data.

Test Data

Figure 7 is a plot of "static" boiling test data obtained with the test vehicle without an inlet bell. Note the fall-off in flow and pressure, and an intermediate liquid level, from 20 to 17-1/2 inches. This is followed by a gradual deterioration in performance with decreasing liquid level. Suction specific speeds in excess of 350,000, before any appreciable fall-off in performance, were obtained with the test vehicle. This represents exceptionally good cavitation performance.

Figure 8 is a plot of "dynamic" boiling tests run in this program. "Dynamic" boiling tests differ from "static" boiling as follows:

Static boiling is the condition existing when the liquid hydrogen is at saturation. Dynamic boiling conditions occur when tank pressure is rapidly decreased from saturation conditions. Depressurization rates of 1 psi per second were used for this program. Note that the test data in Figure 8, shows that the pump was started after tank de-pressurization was initiated. Even under these extreme boiling conditions, the test vehicle delivered single phase liquid with adequate net positive suction head.

CONCLUSIONS

The test program reported on herein, demonstrates that a tank mounted booster pump can be used to deliver boiling liquid hydrogen to the turbo pump of a reactor-powered vehicle with adequate NPSH to prevent cavitation. It further demonstrates that tank-mounted, high speed, all inducer type booster pumps exhibit extreme improvements in the commonly

accepted cavitation parameters. These improvements are attributed to special design features, thermal properties of liquid hydrogen, and certain physical phenomena associated with tank mounted pumps.

The phenomena are:

1. High vapor-handling capability of a properly designed inducer pump.

2. A tank installation having an inlet bell to the pump will prevent the formation and coalescence of vapor from choking the inlet to the pumping mechanism.

The cavitation performance of a pump depends not only upon the net positive suction head or state of the liquid entering the pump, but also on the ratio of vapor and liquid in the flowing stream and the distribution of vapor and liquid therein.

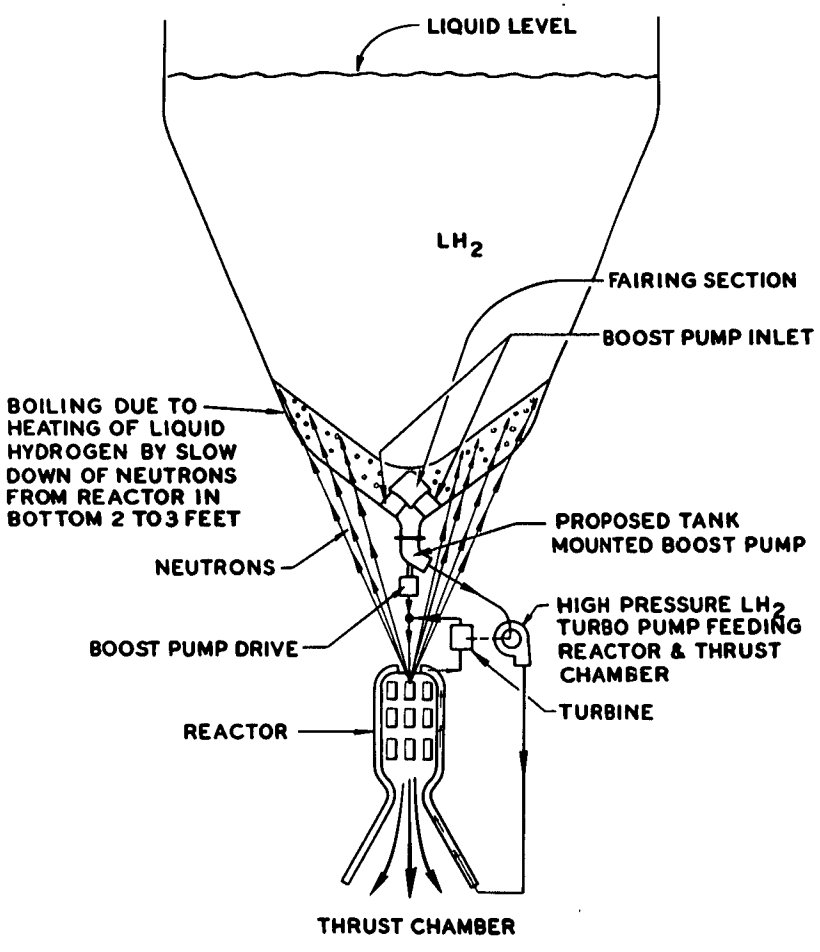

FIGURE 1

SCHEMATIC SHOWING BOILING AT TANK BOTTOM
IN REACTOR POWERED VEHICLE

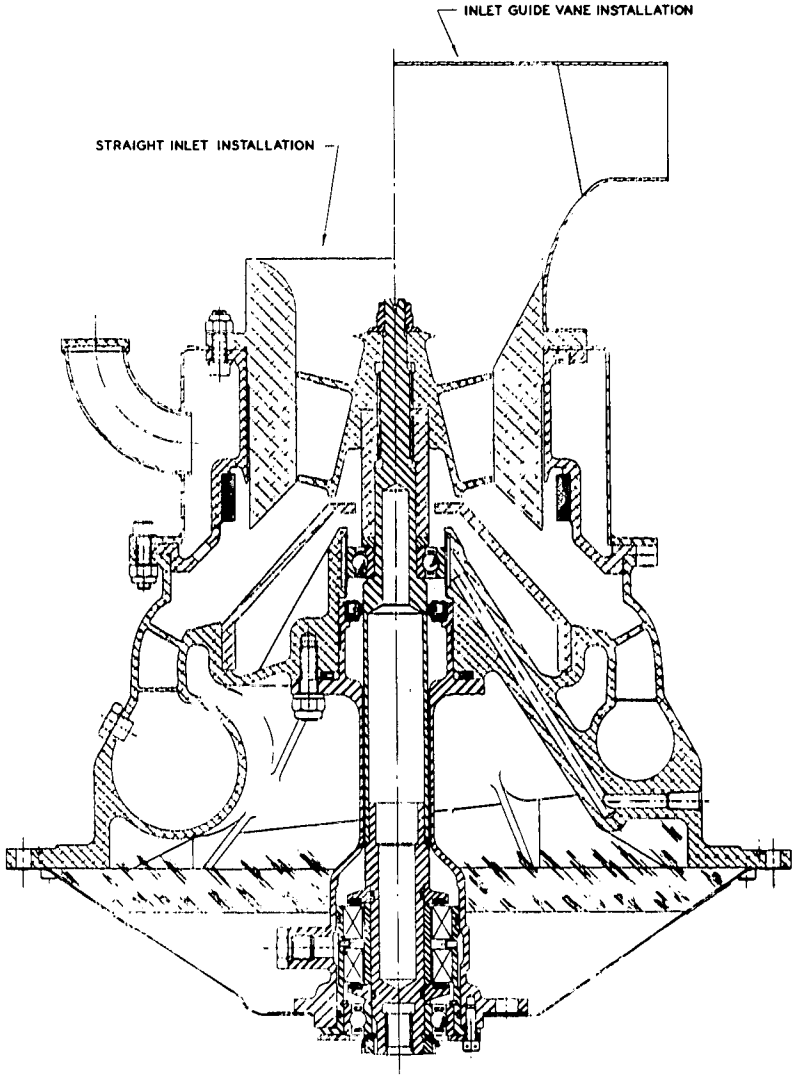

CROSS SECTION
OF
HIGH SPEED INDUCER TEST PUMP

FIGURE 2

CROSS SECTION OF HIGH SPEED INDUCER TEST PUMP

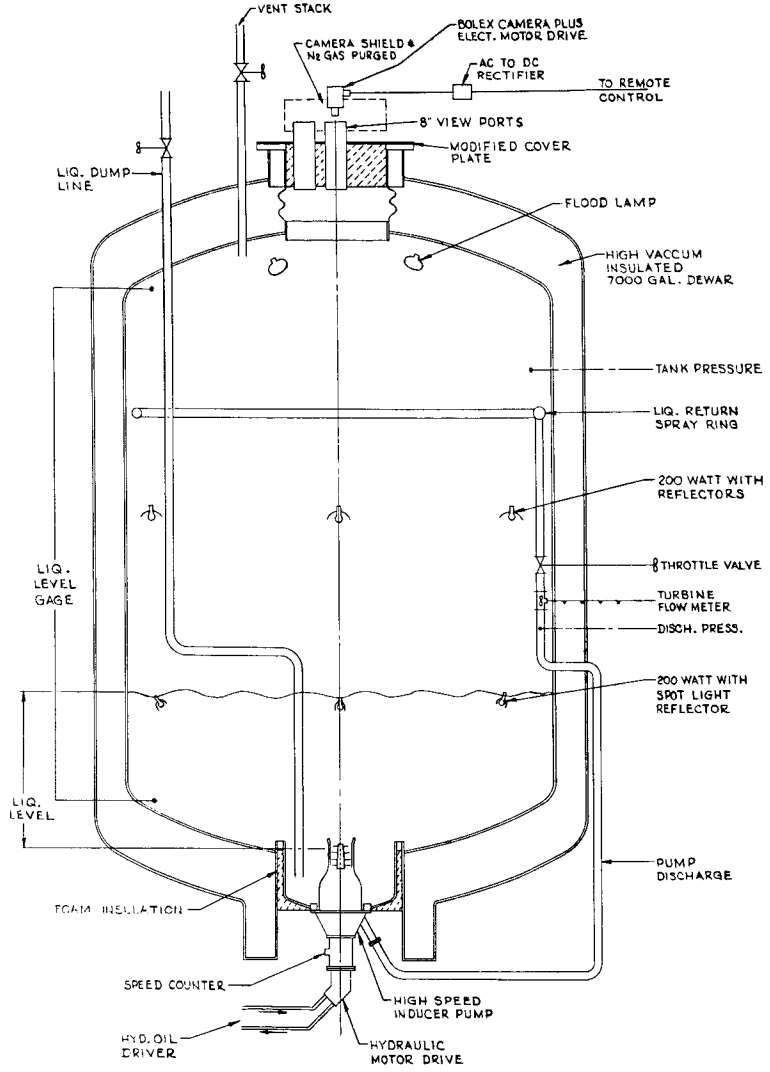

SCHEMATIC
OF
TEST INSTALLATION Nº 1

FIGURE 3

SCHEMATIC OF TEST INSTALLATION NO. 1

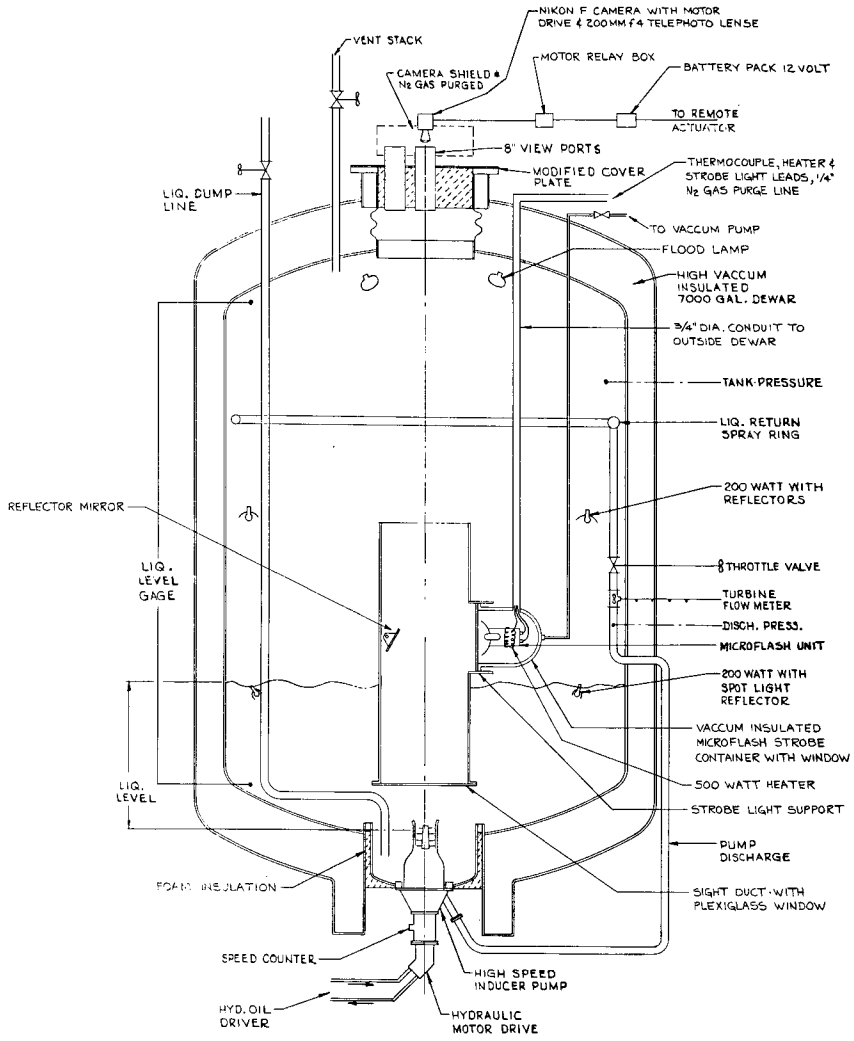

SCHEMATIC
OF
TEST INSTALLATION Nº 2

FIGURE 4

SCHEMATIC OF TEST INSTALLATION NO. 2

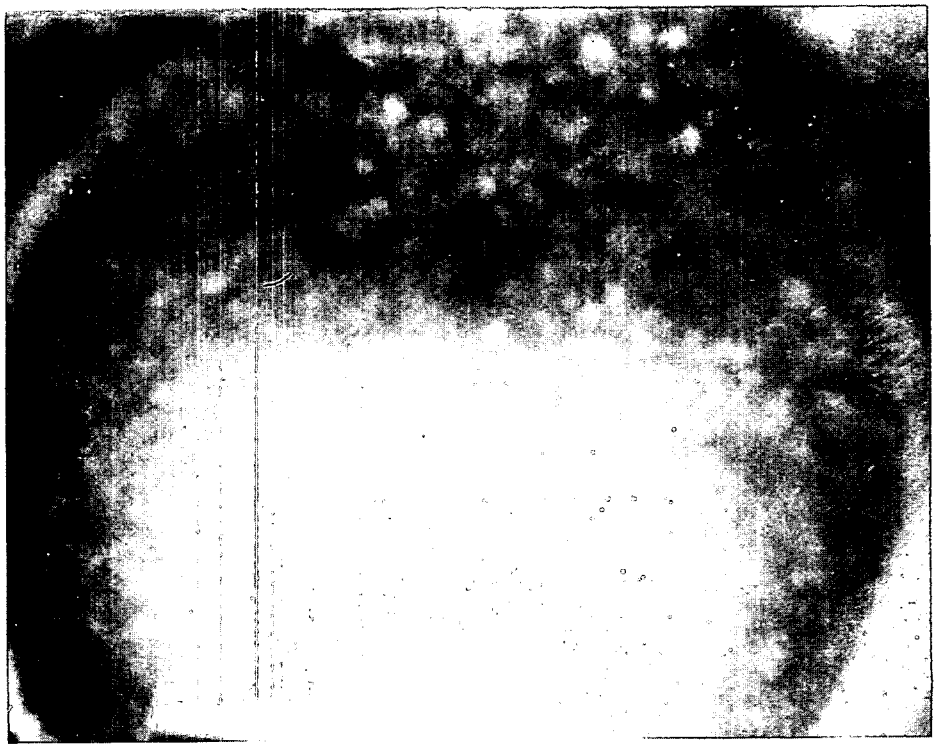

FIGURE 5

SURFACE OF LIQUID HYDROGEN DURING SATURATION
WITH PUMP SPEED OF 15,000 RPM

FIGURE 6

SURFACE OF LIQUID HYDROGEN DURING SATURATION
WITH PUMP SPEED OF 9,000 RPM

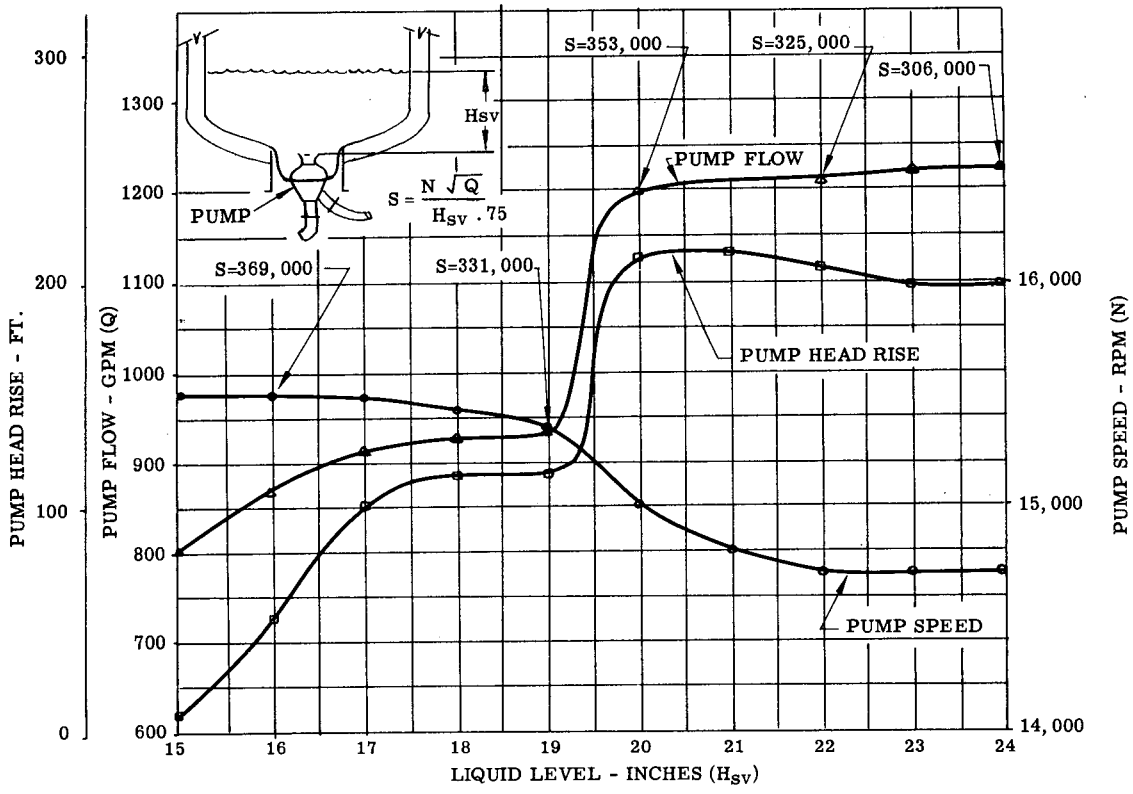

FIGURE 7 PUMP DOWN PERFORMANCE IN BOILING LIQUID HYDROGEN

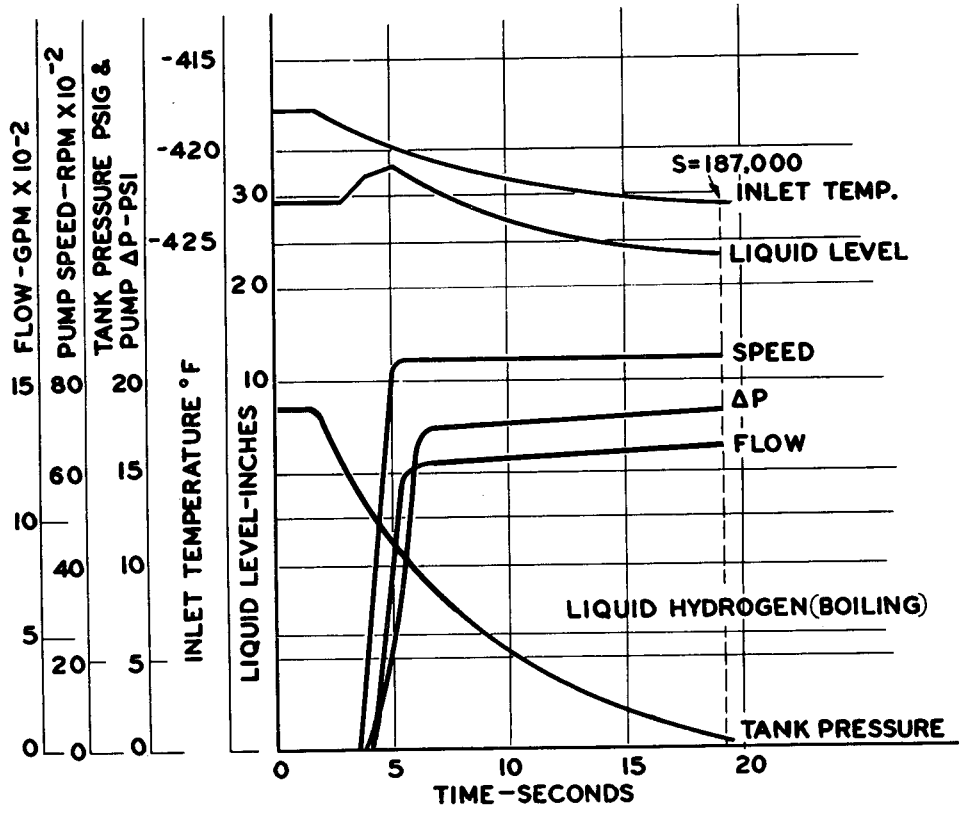

FIGURE 8 PLOT OF DYNAMIC BOILING TEST

THE WELDING OF 7000 SERIES ALUMINUM FOR NUCLEAR ROCKET APPLICATIONS

A. J. KISH, Senior Metallurgical Engineer
Applied Research and Development
ACF Industries, Incorporated
Albuquerque Division

INTRODUCTION: The 7000 series aluminum alloys are of considerable interest for a variety of applications because of the high strength levels attainable in this alloy series. After heat treatment, they exhibit strength levels approaching 80 KSI ultimate and 70 KSI yield and strength/density ratios of 750,000 plus. Where strength-weight ratio is a major factor, 7000 series aluminum is generally considered equivalent to 250,000 psi steels.

The use of 7000 series aluminum, although very extensive, has been limited in many applications because of the questionable welding characteristics normally associated with this alloy series. Relatively little information is available on the procedures and application of welding processes on 7000 series alloys. A research program has been in existence at the Albuquerque Division since 1957 involving weldability studies in this area. Some of these results are discussed and it is hoped that further interest will be stimulated in filler alloy improvement, optimization of welding technique, and application of welded 7000 series aluminum.

GENERAL COMPOSITION EFFECTS: The nominal composition of these alloys include the elements zinc, magnesium, and copper, each of which contribute to the heat treated strength properties but are not especially desirable for optimum welding characteristics. The effects resulting from presence of these elements can best be described in terms of the as-cast microstructure of a 7000 series alloy. During cooling from the melt, various constituents with varying compositions are formed in discrete temperature ranges (Figure 1). The temperatures at which these constituents solidify, vary, depending on the composition of the still molten area. Naturally, subsequent heating of the solidified material, whether by high heat treating temperature or welding heat input, will remelt these localized areas. The result is a localized molten area in a solid matrix. Depending on time and temperature conditions, diffusion in the incipient melted area can occur. When this structure is cooled, tiny areas of incipient porosity can result with drastic detrimental effects on elongation and strength of the material. Such an effect can occur either in the weld metal area or base metal material. The minimum temperature at which this effect occurs is normally lower in cast material than wrought material since the wrought material is more homogenous and severe composition gradients have been diffused.

The structure of deposited weld metal is much finer in constituent size and arrangement than the as-cast structure of a casting, since the weld cooling rate is much more rapid. Composition difference and constituent content, however, are similar. The formation of eutectic does not appear detrimental provided that it is diffused into solid solution at temperatures below that which result in melting of the structure and resultant incipient porosity.

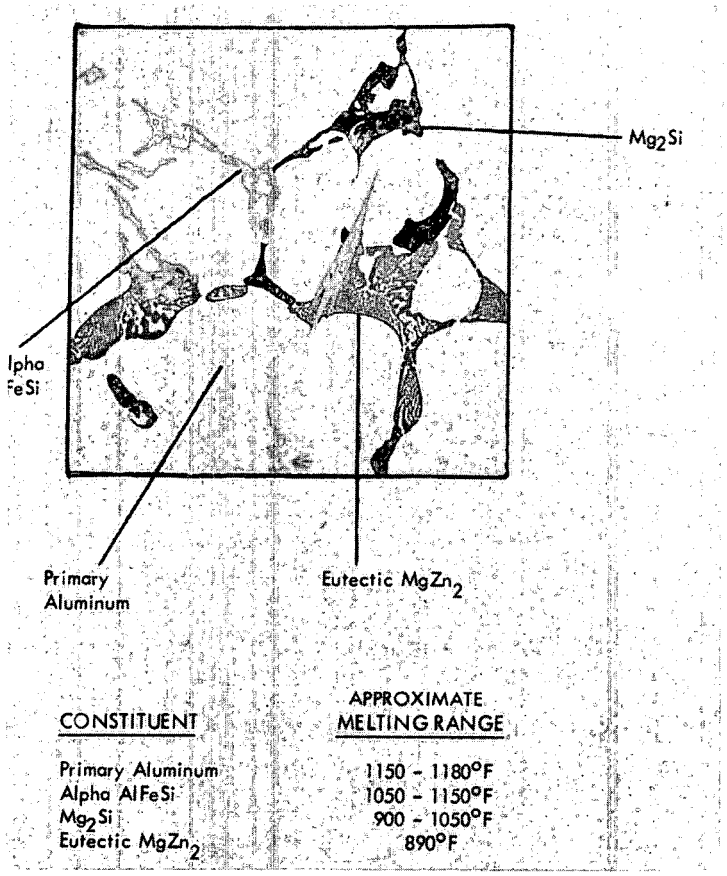

FIGURE 1. Typical constituents in the as-cast 7075 aluminum and approximate melting range.
500X Dilute Kellers Etch

WELD PROBLEMS - BASE METAL: Two major areas of concern must be evaluated when 7000 series alloys are subjected to the influence of a welding arc. These areas are: (1) The effect of welding heat input on the base metal heat affected zones. (2) The effect of welding heat input on the structure of the weld metal and previously deposited weld passes.

The weld area is heated to the melting point of aluminum or higher. Areas in the base metal are thus subjected to varying temperature gradients. Localized areas in the base metal that contain concentrations of alloying element melt under the influence of this heat input and form a eutectic structure (Figure 2). Base metal heat affected zones are thus characterized by formation of eutectic at grain boundaries or in conjunction with constituent previously present.

The weld metal so deposited exhibits a structure that depends on the type of welding process and the current conditions used in welding. Since the cooling rate of the weld puddle is normally very rapid, constituent formation is extremely small, and generally uniformly dispersed. Welding conditions that produce excessive heat input, high interpass temperature, or excessive base metal preheat temperature generally result in a stringer type eutectic or constituent formation at grain boundaries. The influence of subsequent weld passes or rapid solution treatment on this type structure can result in incipient melting of these areas and resultant weld cracking (Figure 3). The use of homogenization treatments at temperatures below normal solution temperature is extremely beneficial in avoiding this type cracking characteristic. It is advantageous to avoid the initial stringer or grain boundary formation through use of modified filler alloy composition or adjustment of welding process and technique.

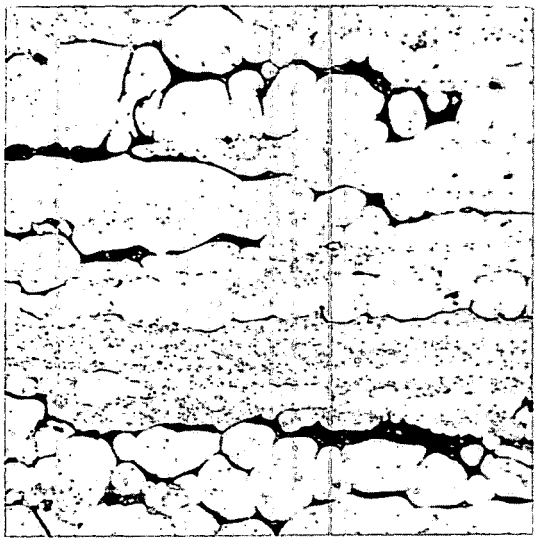

FIGURE 2. Eutectic formation at grain boundary and constituent area in 7079 base metal subjected to welding heat input.

500X Dilute Kellers Etch

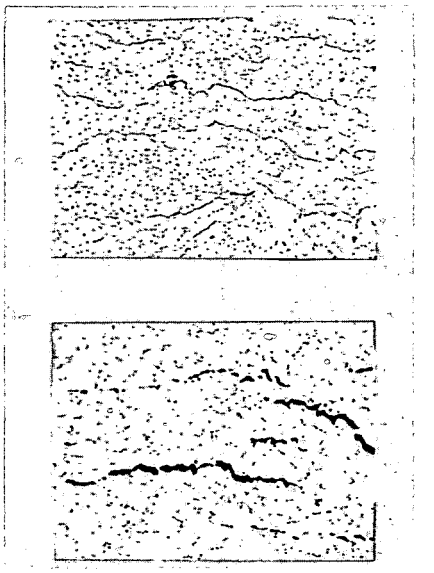

FIGURE 3. (TOP) As-Welded weld area showing stringer eutectic formation. (BOTTOM) Same area after rapid solution treatment and water quench.

250X (reduced 50%) Dilute Kellers Etch

If 7000 series alloys are not used as filler material, then the joint configuration and filler alloy must be adjusted such that weld dilution produces a weld composition responsive to 7000 series heat treatment cycles.

HEAT TREATMENT CONSIDERATIONS: Heat treatment after welding should consist of a homogenization cycle to refine or diffuse the eutectic formation present in the weld and heat affected zones. After homogenization is complete, normal solution treatment can be conducted.

Aging cycles should be performed to produce optimum ductility in the weld area. Best results have been obtained through use of a progressive age cycle or slight over-aging treatment.

WELDING CONSIDERATIONS: This welding research program was initiated with possible future application in joining of a 7000 series alloy Rover Case Section. Considerations that were established as applicable included: (1) The welding process should be reproducible and not overly complex, it should be adaptable to joining of 1 to 1-1/2 inch aluminum with circumferential welding of approximate 50 inch diameter. (2) Full heat treatment would be performed after welding since optimum across-weld strength was desired. (3) Mechanical properties across the weld joint of 70 KSI ultimate, 60 KSI yield, and 3% elongation in 2 inches were desired. (4) Welding would be conducted on a Double-Vee type joint with welding performed from both sides. (5) Fatigue strength and corrosion resistance of the weld joint were not of major concern. (6) The weld joint must behave satisfactorily in a cryogenic environment of - 180°F to - 200°F. (7) The weld area should not be overly notch sensitive.

WELDING PROCESS: Four welding processes were evaluated in this program. Pertinent characteristics of each are shown in Figure 4.

TIG-Fusion welding was conducted utilizing the standard tungsten electrode and a

butt type joint on the material to be welded. Weld metal areas consisted of remelted areas of the base metal joined since no filler addition was added.

TIG-Faying Strip welding was conducted under essentially the same conditions utilized for fusion welding. A butt type joint was utilized with a 1/16 wide 5000 series aluminum faying strip, placed between the butting edges. This faying strip protrudes approximately 1/16 inch over the thickness of material to be welded. In this manner, the normal surface depression due to welding, is eliminated. The weld area consists of diluted base metal and alloy addition from the faying strip material.

MIG welding was conducted on conventional grooved 7000 series base material. In this process, the weld wire addition serves as the arc source since the arc occurs between the added filler wire and the base metal groove area. No tungsten electrode is used and the weld area consists of essentially filler alloy composition with normal welding element loss. This process is usually faster and results in larger weld passes. Over-all heat input levels tend to be higher than those characteristic of the TIG processes.

The TIG-Cold Wire Feed process also utilizes conventional type weld grooves in the material to be joined. The arc is furnished by a tungsten electrode and a filler addition is introduced in front of the arc area. Welding conditions approach those of the fusion, or faying strip process and normally result in small weld passes.

Results in 5/8 inch 7000 series aluminum welded by these processes are included in Table I.

The TIG-Fusion welds were characterized by high strength levels since the weld composition was sufficient for adequate responsive to heat treatment. Elongation, however, was extremely low and resulted from excessive melting at weld grain boundaries and constituent areas. Occasional difficulties resulted from incipient cracking in the base metal heat affected zones.

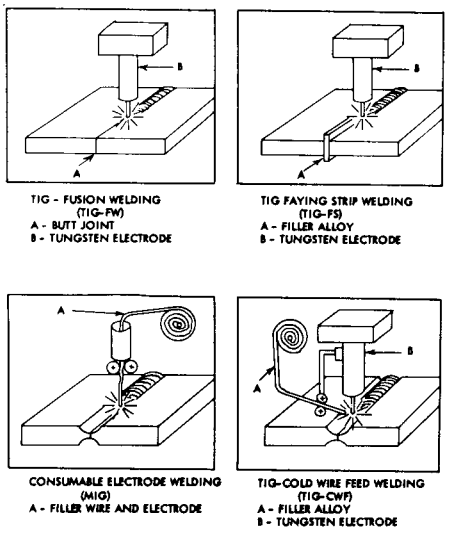

FIGURE 4. Welding Processes used in joining of 7000 series aluminum.

PROCESS	UTS KSI	YS KSI	%E	NO. SPEC.
TIG - FW	73.4	70.4	0.0	20
MIG	64.1	–	0.3	80
TIG - FS	74.5	67.4	4.1	114
TIG - CWF (5000 FILLER)	80.0	72.9	4.2	50
TIG - CWF (7000 FILLER)	71.2	63.9	3.8	214

TABLE 1. Strength results of 7075 and 7079 aluminum joined by four welding processes.

The MIG welds were also characterized by extremely low elongation values and somewhat lower across-weld strength. Detrimental effects in the base metal heat affected zones were much more severe. With heat input levels that did not detrimentally effect base metal, the weld quality and properties were poor. Additional investigation should be conducted with MIG drop transfer or short-arc techniques where heat input levels would be lowered. TIG-Faying strip welds were characterized by good strengths and elongation. Weld dilution was adequate for good heat treatment response and the heat input effects on

base metal were negligible. This process, however, is limited to applications for which a faying strip can be fabricated and to material thicknesses up to one inch. Welding must be conducted in a maximum of two passes, one from each side of plate.

TIG-CWF welds with 5000 series filler alloys also produced high strength - high elongation welds, but this process is limited to a base metal thickness and a joint configuration that produces adequate weld dilution with the 7000 series base metal. In material thickness over 3/4 inch with a single U joint, proper base metal dilution is not obtained. The across-weld strength is then a function of the 5000 series filler alloy strength.

TIG-CWF welds with 7000 series filler also produce desired strength levels with good elongations. In material thickness over 3/4 inch some element weld loss occurs, however, weld composition is still adequate for proper heat treatment response.

Better welding characteristics and elongation levels were obtained through use of a modified filler composition containing lower nominal magnesium and slightly higher copper content that the conventional 7079 filler. This special filler alloy, designated "Alloy 1." was developed from studies of weld compositions that were optimum in TIG-Faying Strip welds. Beneficial results in weld metal microstructure and as-welded ductility were significant. Results in 7079 alloy up to 1-1/2 inches thick welded with the modified "Alloy 1" filler have been consistently good.

GENERAL WELDING VARIABLES: The most successful welding process investigated has been the Tungsten Inert Gas - Cold Wire Feed Process with Alloy 1 filler. Some general comments regarding the weld variables involved follow: (1) Current levels should be maintained as low as possible, consistent with good quality. Most successful results have been obtained with current levels of:

Thickness	Amperes	Thickness	Amperes
1/4	195-205	5/8	250-270
3/8	210-220	1-1/2	260-280

The first pass in thick sections should deposited at low current levels since burn through of the land area is not desired. (2) The welding operation should be conducted at a rate of 6 to 10 inches per minute depending on welding behavior. Slower travel should not be used; faster travel generally results in entrapped dross, porosity, and poor weld quality. (3) Voltage should be between 11 to 14 volts and is a function of other weld variables. (4) Wire feed should be introduced at 30 to 45 inches per minute for 1/16 inch diameter wire. The rate will vary depending on weld behavior, head travel, type, and size of weld pass desired. (5) Double U joints with 45° to 60° included angle appear best in thick sections. Weld material should be balanced on both sides of thickness centerline if possible. In section sizes of 5/8 inch or less, Single-U or Single-Vee joints are satisfactory. TIG-CWF welding of 7000 series alloys above 1-3/4 inches is not recommended. (6) Each weld pass should be arranged such that fusion with adjacent passes is obtained and welding over sharp laps or narrow areas is not performed. Continuous welding in multipass circumferential welds is not recommended. (7) The filler alloy should be such that adequate heat treatment response is obtained. Most successful results have been obtained with the Alloy 1 filler, however, investigation of other modified filler alloys should be conducted. (8) Best results are obtained with 100% helium shield. (9) Tungsten electrodes of 1/16 inch diameter are advisable with either blunt or angled nose depending on weld pass appearance desired. (10) Although manual welds can be performed, they generally exhibit lower strength levels. Automatic welding is recommended. (11) Small defects can be readily repaired without detriment to weld strength levels. Chipping of defective areas can introduce difficulties if the chipped surface is rough. (12) The most common type weld defects are linear entrapped dross or linear porosity. They are most often caused by improper weld pass fusion or arrangement. (13) The influence of

linear weld defects are most pronounced on across-weld ultimate strength and elongation. Detrimental strength effects are generally more severe in across-weld tensile tests than in longitudinal all-weld test specimens. (14) Most welding is conducted with base metal in the -W or -T4 condition since maximum solution of alloying elements is present. Material in the -T6 condition has been successfully welded.

CHARACTERISTICS OF THE AS-WELDED AND AGED CONDITIONED: In applications where weldments receive only a subsequent aging treatment, the base metal over-aged zone caused by welding and heat input, influences the final strength of the joint. Weldments that are to receive only an aging treatment must be joined in a maximum of two passes or the subsequent weld passes will over-age the weld to low strength levels. If welding heat input is excessive, the over-aged zone in the base metal will exhibit low strength levels typical of annealed material.

7075-T6 Aluminum in 5/8 inch thickness joined by the TIG-CWF process with 5183 filler and welded with one pass each side exhibited exceptionally good strength results. Subsequent aging for 4 hours at 200°F, 4 hours at 250°F, and 4 hours at 315°F produced average across-weld strengths of 63.3 KSI ultimate, 53.6 KSI yield, and 6.0% elongation in 1.4 inches. Considerable elongation occurred in both the weld and base metal over-aged zones, with failure occurring randomly either in the weld or base metal. The 5/8 inch 7075-T6 alloy was joined in two passes at 270 amperes current and 10 IPM travel.

CHARACTERISTICS OF THE SOLUTION TREATED AND OVER-AGED CONDITION: In applications where high across-weld elongation is of greater interest than maximum strength levels, over-aging after solution treatment can be performed to advantage. Yield strength levels become more consistent when these over-aging cycles are used. Over-aging cycles investigated included variation of the final four hour portion of the progressive age cycle (4 hrs 200°F, 4 hrs 250°F, 4 hrs 315°F). Typical results are summarized in Figure 5.

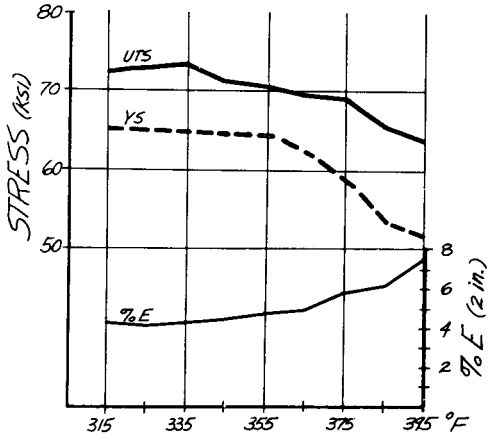

FIGURE 5. Across Weld mechanical properties of welded 7075 aluminum as influenced by final four hour progressive age temperature.

	UTS KSI	YS KSI	%E 2 IN.	N-UTS KSI	N.R.
FHT-A	68.0	63.1	3.0	64.7	.95
FHT-B	69.5	63.6	3.8	65.6	.94
FHT-C	69.5	61.7	4.2	62.3	.90
AGE A	55.5	43.5	2.5	47.0	.85
AS W.	50.4	37.0	3.0	41.7	.81
BM-T	75.0	65.1	11.5	68.8	.92

TABLE II. Notch-Unnotch properties across-weld in welded 7079 aluminum. Standard NASA .001R Specimens.
FHT = Full Heat Treat
AGE A = Age Only
AS W = As Welded
BM-T = Base Metal Transverse

NOTCH CHARACTERISTICS: The notch characteristics of 7000 series weld metal were evaluated at room temperature with the standard NASA type notch tensile specimen (Table II). Notch-Unnotch strengths were evaluated in conditions representing weldments given three variations in age cycle as well as age only and as-welded conditions. These included variation in the final four hour portion of the progressive age cycle at temperatures of 315°F, 330°F, and 345°F respectively. The weld material is not excessively notch sensitive regardless of heat treated condition.

CRYOGENIC BEHAVIOR: Weldment application in the Rover Program would involve use of weld material in a cryogenic environment of -180° to 200°F.

Tensile tests were conducted on unnotched and notched across-weld specimens at room temperature, -100°F, -300°F, and -423°F. A series of 7075 weldments were evaluated in terms of .177 inch diameter round specimens, both unnotched and with .001 notch radius. Results of these across-weld tests are included in Table III. As temperature decreases, across-weld strength increases, while elongation and notch strength decrease. This effect is most significant between -200°F and -423°F.

Base metal cryogenic tests were conducted on 7079 unnotched and notched (.010 radius) 1/4 inch flat specimens. The results show increase in strength as the temperature decreases (Table IV). The elongation tends to decrease but notch strength remains substantial. The base metal notch ratio decreases to a low of .84 at -423°F.

Similar across weld specimens in welded 7079 aluminum show a comparable behavior (TABLE V) with the lowest notch ratio of .79 obtained at -423°F.

TEMP. °F	UTS KSI	YS KSI	%E 2 IN.	N-UTS KSI	N.R.
R.T.	75.1	65.2	3.3	91.8	1.22
-100	78.6	68.4	2.4	93.1	1.18
-300	85.8	80.3	0.8	66.0	.77
-423	91.9	82.6	NIL	61.4	.67

TABLE III. Cryogenic across-weld notch-unnotch properties in welded 7075 aluminum. Round .177 diameter .001 R notch specimens fully heat heat treated.

TEMP. °F	UTS KSI	YS KSI	%E 2 IN.	N-UTS KSI	N.R.
R.T.	72.8	63.0	12.0	76.8	1.05
-100	80.6	69.3	9.5	82.6	1.02
-300	90.1	77.2	6.5	82.4	.91
-423	94.0		5.0	79.1	.84

TABLE IV. Cryogenic base metal notch-unnotch properties in 7079 aluminum base metal. Flat 1/4 inch .010 R notch specimens fully heat treated.

PRESSURE VESSEL BEHAVIOR: The behavior of a number of 7000 series welds was evaluated under the stress conditions involved in testing of a pressure vessel configuration. Six 4.5 inch ID spherical vessels were fabricated by circumferential welding of two hemispherical shapes. Each sphere was of nominal .100 wall thickness with a 1/8 inch build-up in the weld area. Hydrostatic pressure test results are included in VI.

Even with a substantial weld defect present (Sphere No. 6), the pressure vessel behavior was good. In all spheres, pressurized to burst, (except No. 6), yielding was

TEMP. °F	UTS KSI	YS KSI	%E 2 IN.	N-UTS KSI	N.R.
R.T.	67.9	58.3	4.0	66.5	.98
-100	69.7	58.9	3.5	69.5	.99
-300	76.3	69.1	2.5	71.3	.93
-423	80.3		3.0	64.0	.79

TABLE V. Cryogenic across-weld notch-unnotch properties of welded 7079 aluminum. Flat 1/4 inch - .010 notch specimens fully heat treated.

NO.	PSIG	TEST	CALC. STRESS KSI	WT. LBS.
2	6500	BURST	73.5	.75
3	7000	BURST	79.2	.74
4	6500	PROOF	73.5	.74
5	6500	PROOF	73.5	.73
6	6000	BURST DEFECT)	67.9	.77

TABLE VI. Hydrostatic pressure test results of welded .100 inch wall 7075 aluminum spheres - fully heat treated.

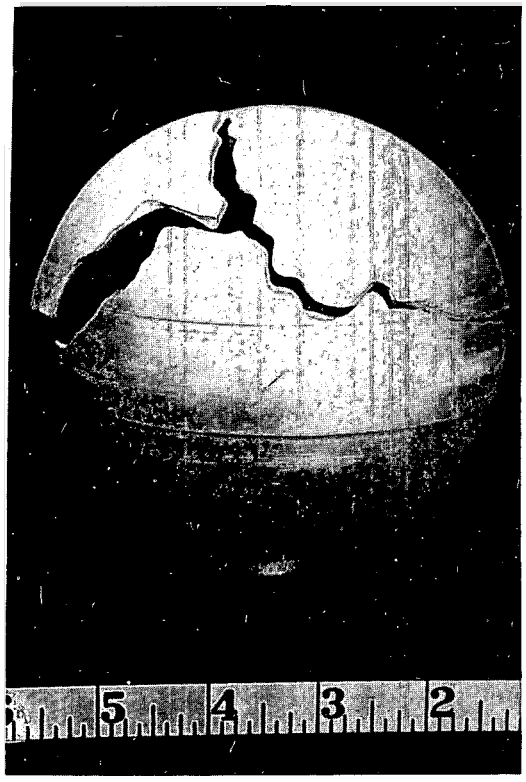

FIGURE 6. Typical burst failure of welded 7075 aluminum sphere.

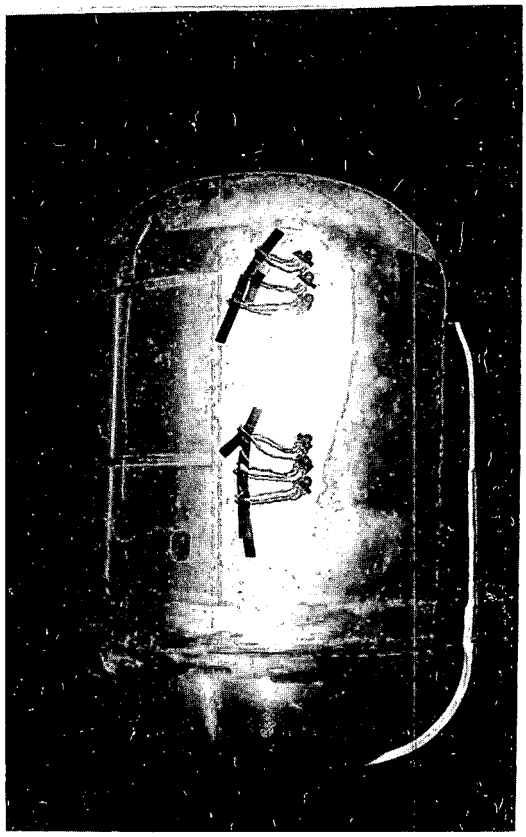

FIGURE 7. Typical burst failure of welded pressure vessel. KIWI B thickness to diameter 1/2 scale model.

observed approximately 200-300 PSIG before burst. A typical burst failure is shown in Figure 6.

Two one-half scale cylindrical pressure vessels were fabricated with identical thickness-diameter ratios in the weld area as the KIWI B case vessels. After full heat treatment both were pressurized to failure. Vessel No. 1 failed at 2350 PSIG with a maximum weld strain of 10,000 micro inches per inch and a maximum weld stress of 72,500 psi (measured at 2200 PSIG). The second vessel failed at 2150 PSIG with maximum weld strain of 5850 micro inches per inch and a maximum weld stress of 67,000 psi (measured at 2000 PSIG). A typical burst failure (Vessel No. 1) is shown in Figure 7.

TEST RESULTS FROM SIMULATED CIRCUMFERENTIAL JOINT IN THE ROVER REACTOR VESSEL: In order to verify the results of 7000 series test plates prior to actual fabrication of a KIWI vessel, a series of full scale cylindrical 7079 test rings were fabricated. These rings were of identical diameter and thickness as that to be used in the Rover case section (Figure 8). In fact, the ring material was removed from 4-1/2 inch thick 7079 pressings fabricated for KIWI B reactor vessel applications. Optimum welding conditions, as determined from previous testing, were used in welding of the test rings.

Across-weld tensile specimens were removed from 45° segments around the circumference of each weldment. Average results are included in Table VII.

Statistical analysis showed that with 95% confidence, 99% of the specimens could be expected to exhibit strength levels of 73.4 KSI ultimate, 64.5 KSI yield, and 3.0% elongation or higher.

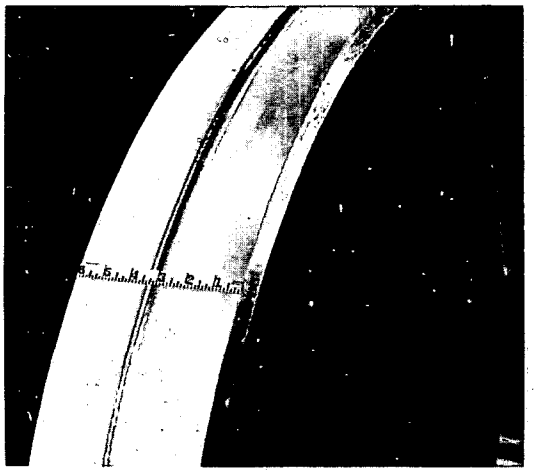

FIGURE 8. Simulated Rover reactor vessel circumferential joint of welded 7079 aluminum.

SEGMENT	UTS KSI	YS KSI	%E 2 IN.
1	75.2	66.3	5.3
2	74.4	65.6	4.0
3	75.1	65.8	5.5
4	75.2	65.5	7.0
5	74.3	65.1	5.0
6	74.9	65.9	6.0
7	74.8	66.2	5.5
8	75.2	65.8	6.0

TABLE VII. Average mechanical properties at 45° segments in simulated vessel joint. Average of five .505 diameter specimens.

WELDING THE KIWI B REACTOR VESSEL: The KIWI B reactor vessel is fabricated by pressing a dome shape from a 4-1/2 inch thick 7079 circular blank. The operation is conducted at 750°F and is completed in one stage. A cylindrical section of 4-1/2 inch thickness is then machined from a second pressing and welded to the dome shape.

Welding of 7079 aluminum above 1-1/2 inches thick was not desired in this application, so the weld area was machined to a one inch thickness approximately 4 inches each side of the weld groove. The weld groove configuration was a double-U type with the ID portion machined to the centerline of thickness. Nine weld passes were first deposited in the ID groove by the TIG-CWF process. The OD groove was then back machined to sound weld metal and the remaining weld passes alternated in groups of four to minimize dis-

tortion and stress build-up.

The welding operation employed the TIG-CWF process with Alloy 1 filler. Each weld pass was separate, that is, involved a weld start and stop. Weld starts were staggered around the weld circumference and welding was not conducted if interpass temperature exceeded 200°F.

Welding conditions were:

Current	250-280 amperes	Tungsten Extension	9/16 inches
Volts	14 volts	Shield	100 CHF Helium
Traverse	6.5 - 7.5 IPM	Wire	1/16 diameter Alloy 1
Weld Feed	28 - 45 IPM		
Tungsten Diam.	1/16 inches	Interpass Temperature	125° - 150°F

The welding operation on the OD groove portion is shown in Figure 9. This unit, after final processing, was pressurized through 75 cycles to 1000 PSIG. An additional 4 KIWI B 7079 welded case sections have been successfully fabricated.

FIGURE 9. Welding of the KIWI B reactor vessel by the tungsten Inert Gas - Cold Wire Feed Process.

CONCLUSIONS: The weldability of 7000 series aluminum alloy has been investigated by the evaluation of 158 weldments in material 1/4 inch to 3 inches in thickness. In addition, twenty 7000 series pressure vessels and cylindrical weldments have been successfully fabricated.

Welding of the 7000 series aluminum alloys is particularly sensitive to equipment reliability and operator skill. The welding technique and procedure must be developed and verified utilizing test weldments and scale model configurations.

Based upon the results of the development program described, it may be concluded that 7075 and 7079 aluminum structures can be successfully welded.

THE IMPORTANCE OF ENGINE DESIGN ON REMOTE HANDLING OF NUCLEAR ROCKET ENGINES

by William W. Barton*

This paper details the types of equipment that have been designed to remotely handle the NERVA engine at the Nuclear Rocket Development Station, Jackass Flats, Nevada. The author stresses throughout the report the necessity for close coordination of nuclear engine-remote handling equipment design early in the program and examines some of the problems associated with NERVA engine remote handling that have been considered. Several criteria are provided as guidelines to be followed on design initiation. Their application to subsequent phases of the design program and to the types of equipment that have resulted are illustrated through discussion of equipment capability.

INTRODUCTION

Nuclear rocket engine test programs completed to date and planning for those to be conducted in the future have made it apparent that the remote handling equipment used for subsequent disassembly and re-assembly of the irradiated power plant and its associated subassemblies must be considered an integral part of the total engine design and development program. Because of the limitations imposed on engine handling procedures through the necessity of conducting all operations in a radioactive "hot cell" facility, close coordination of the design of both the engine and the equipment that will handle it should be established early and continue through the design completion.

This concern for remote handling tools and equipment may seem alien to the task of engine development, as such. But careful consideration of the unique problems investigated in current practice that are associated with engine assembly/disassembly readily illustrate the interrelatedness of design requirements for both engine and handling equipment that ensures maximum performance capability of the power plant.

SIGNIFICANT DIFFERENCES BETWEEN DIRECT AND REMOTE OPERATIONS

Direct assembly and disassembly of a conventional rocket engine is not a simple matter. Since a rocket engine does not have a through shaft, its assembly and disassembly is in some ways simpler than that of a large turbojet engine; but, nevertheless, many special tools and handling fixtures and many manhours of skilled labor are required for its assembly and disassembly. Accurate positioning and alignmnet of components is required, nuts must be properly torqued down and safety wired, etc.

In the case of a nuclear rocket engine, initial assembly may be performed directly since there will be no radiation problem at this time. However, in the case of a tested nuclear rocket engine (or, for that matter, a new engine with activated or contaminated parts) remote assembly and disassembly are re-

*NERVA Project Manager, AMF Atomics, A Division of American Machine and Foundry Co., Greenwich, Connecticut

quired if the radiation level precludes direct access by personnel.

As was the case with direct operations, special tools and handling fixtures can be used in remote operations. But now the skilled labor can contact the engine only by remote means such as master-slave or electro-mechanical manipulators.

It is true that an experienced operator can perform surprising feats with a master-slave manipulator. However, the load and reach capabilities of such a manipulator severely limit its use during gross assembly or disassembly of a nuclear rocket engine in a large hot cell. It is not until we come to remote assembly, disassembly or post mortem of an engine subsystem or component that the use of master-slave manipulators becomes desirable.

Electromechanical manipulators, with their greater power and travel, are usually required for the gross assembly or disassembly of an engine. These general-purpose manipulators may be installed in a large hot cell either overhead or on the walls.

For more specific operation, such as clamping, gripping or providing a precise motion, single-purpose remotely actuated mechanisms are used. These are usually mounted on the engine handling fixtures or stands.

In addition to manipulators, the operators of a remote facility normally have at their disposal remotely operated cranes, small tools and viewing equipment.

It is in its use that the remote handling equipment mentioned above most significantly differs from its counterpart in direct assembly and disassembly operations. Some points for consideration are:

Load Capacity

Cranes, handling fixtures and stands and special-purpose mechanisms can be selected or designed to handle the weight of any anticipated nuclear rocket engine. General-purpose electromechanical manipulators, however, are sorely pressed to maneuver the weights involved and to provide the necessary torques without themselves becoming unwieldy.

"Feel"

Electromechanical manipulators presently used and those actively contemplated for use on nuclear rocket engines do not provide feedback to their operators. This is a serious drawback when it comes to inserting or withdrawing a fragile component or to tightening a clamp or tubing connection which later must prove to be leak tight. Similarly, the act of lowering an engine or a subsystem onto a stand without benefit of sensitive guiding hands can at times present problems.

Accessibility

If an engine is to be remotely assembled or disassembled, the manipulators (or the tools they hold) must have access to every disconnect point. Since manipulators are not always as small as desired and do have a limited number of motions, accessibility of nuts, electrical disconnects and pipe joints is often a problem. And it is here, perhaps more than anywhere else, that the early and continued coordination of the design of the engine and its remote handling equipment pays off handsomely.

Viewing

Viewing through a shielding window perhaps five or six feet thick to perform a remote disassembly procedure which might be taking place ten or twenty ft. from the inside surface of the window leaves much to be desired, particularly when you are trying to perform a delicate operation. Closed-circuit television helps in many instances for close up viewing and for alternate viewing angles.

Speed of Operation

It is not surprising in view of the points considered above that remote assembly and disassembly operations are agonizingly slow when compared with similar operations that are performed directly. In a test program where reliability of a nuclear engine is to be demonstrated by many tests, remote assembly and disassembly could become a "bottleneck" if not adequately implemented within the schedule. Even with a more leisurely test schedule, fast teardown of a tested engine is very important since early access to the fuel elements for analysis is desired.

FACTORS GOVERNING SELECTION OF A REMOTE HANDLING SYSTEM

In most instances, there are several approaches to the accomplishment of a remote handling task. At one extreme, a remote handling system consisting of very simple equipment will perform the task for the least capital equipment expenditure but it may require an inordinately long operating time; whereas, at the other extreme, a special, automated machine will perform the same task in the least time, but it probably will be very expensive.

If at all possible, it is advisable at the outset of a program involving remote operations to investigate several intentionally different systems for accomplishing the desired task. The conceptual design of these remote handling systems should be carried forward to the point where an evaluation can be made. Also, detailed time analyses of remote handling procedures should be made of each system.

One method for evaluating different remote handling systems is to establish a list of points for consideration. In the case of the remote handling equipment for the NERVA program, for example, some forty points were considered. Since all points were not of equal importance, a weighting factor of one to four was assigned to each point.

A committee of qualified technical personnel of various disciplines was formed to evaluate objectively the various remote handling systems. Following a general review of the systems and a discussion of the meaning of the points considered, each member of the committee rated each of the points for each remote handling system. Weighting factor values were not available to committee members at the time of rating.

The results of such an evaluation, although not infallible, point out the anticipated strengths and weaknesses of the various approaches to a remote handling system. Often an examination of the results stimulates a more extensive investigation of some particular aspect of the system. Also, it is sometimes possible to blend the favorable features of more than one system, thereby further improving the selected approach.

NERVA REMOTE HANDLING SYSTEM

In the case of the remote handling system for the NERVA program, an evaluation of the requirements has led to the selection of the following equipment:

1. Engine Installation Vehicle (EIV)
2. Overhead Positioning Subsystem (OPS)
3. Floor-Mounted Handling Subsystem (FMHS)
4. Wall-Mounted Handling Subsystem (WMHS)

Items 2, 3 and 4 constitute the system used in the main hot bay of the Engine Maintenance, Assembly and Disassembly (E-MAD) Building for remote assembly and disassembly of the NERVA engine.

Engine Installation Vehicle (EIV)

The EIV (shown in Figure 1) is a special-purpose rail flat car used to transport a NERVA engine between an Engine Test Stand and a Maintenance, Assembly and Disassembly facility. It can also accommodate a non-nuclear engine experiment or a radiation-effects reactor.

The vehicle weighs approximately 75 tons and measures 52 feet from the centerline of the carriage to the opposite striker. It travels over a standard gauge track at a speed of three to five mph, propelled by a Prime Mover System. Power and control for all motions on the EIV originate on the Prime Mover System.

The rolling stock undercarriage of the vehicle is of steel construction. As far as possible, it incorporates standard car-building components, such as trucks, suspension systems, wheels, brake systems, coupler, draft gear and cushioning unit. Attached to the underframe are four power-driven jacks, which serve to level and stabilize the vehicle during engine transfer operations. An inching drive mechanism on the forward truck provides fine positioning of the vehicle for the final few feet of travel into the engine test stand.

A carriage mounted on the forward end of the flat car superstructure holds the engine. Vertical, fore-and-aft, transverse and azimuth motions are incorporated in the carriage. The engine is supported by a semi-circular member at the front of the carriage which fits beneath the upper flange of the engine pressure vessel. Four remotely operated clamps are used to secure the engine to the carriage.

In operation, the EIV (pushed by the Prime Mover System) carries the engine from its assembly area to the Engine Test Stand area. Here the EIV is remotely decoupled from the Prime Mover System. Electrical connections between the two, however, are maintained through a flexible cable. The vehicle inches itself into position in the Engine Test Stand and the four jacks are lowered onto hard spots on the ramp. The flat car is then raised sufficiently to eliminate the effect of the truck springs and leveled with respect to the Engine Test Stand in tilt and roll. Fore-and-aft, transverse and azimuth motions of the carriage are then utilized to position the upper face of the engine directly beneath the attachment fixture on the stand. Vertical motion of the carriage then mates the engine with the stand. Once the engine is securred to the stand, the EIV is withdrawn from the area.

Following a test of the engine, the EIV is again brought into the stand and positioned. The engine is gripped, released from the stand, and transported back to the hot bay of the Maintenance, Assembly and Disassembly facility.

Overhead Positioning Subsystem (OPS)

Remote assembly and disassembly of the NERVA engine is performed in the main hot bay of the E-MAD Building by the OPS working in conjuction with the

Floor-Mounted Handling Subsystem and the Wall-Mounted Handling Subsystem.

The OPS consists of a bridge, trolley, telescoping mast, azimuth drive, auxiliary manipulator, a family of six positioning heads, and a control system. As shown in Figure 2, the bridge of $67\frac{1}{2}$ feet length spans the width of the hot bay. The 196 feet travel of the bridge is shown in Figure 3. Elevation of the bridge runway rails is 51 feet above the floor of the main bay.

Mounted through an opening in the bridge trolley is the telescoping mast. Concurrent vertical motion of the three movable sections of the mast is obtained from a single drive. Total stroke of the mast is $39\frac{1}{2}$ feet. In the fully extended position, the positioning head at the bottom of the mast reaches within six feet of the floor and the auxiliary manipulator (when extended) easily reaches to the floor. With the mast fully retracted, the OPS can move into the crane maintenance area and still provide manipulator coverage.

An azimuth drive at the bottom of the mast provides a total of 720^{o} of rotation to the auxiliary manipulator carriage and positioning head grippers.

The auxiliary manipulator is attached to a carriage located within the bottom telescoping section of the mast. The manipulator is of electromechanical type with a capability of supporting and positioning a load of 600 pounds in any attitude or position when fully extended. Vertical travel of the manipulator carriage within the mast permits extension of the manipulator (so that the upper pivot point of the manipulator can be brought below the positioning head) and retraction (so that the manipulator can be brought fully within the mast structure).

Any one of six positioning heads can be remotely attached to the azimuth drive ring at the bottom of the mast. A separate positioning head is used for the engine test stand adapter, the upper thrust structure, the lower thrust structure, the pressure vessel, the top shield and the turbopump assembly of the NERVA engine.

Control of all OPS operations is accomplished remotely from consoles located in the galleries adjacent to the main hot bay. In addition, position of the bridge, trolley, mast and azimuth drive and vertical load measurement on the mast are indicated on the consoles. All power and control connections from the facility to the bridge are via bus bars.

The OPS is used to grasp, transport, elevate and position the NERVA engine or its major subsystems in the main hot bay of the E-MAD Building. For example, when a tested engine is delivered into the building on the EIV, the mast is positioned directly over the engine and is then lowered until the upper thrust structure of the engine can be grasped. The engine is then released from the EIV carriage and moved to another area in the hot bay where disassembly of the engine is initiated.

The auxiliary manipulator on the OPS provides heavy manipulator capability throughout the main hot bay and crane maintenance area whenever the positioning head attached to the mast is unloaded. This freedom of movement of the auxiliary manipulator is particularly helpful when working in conjunction with one or two wall-mounted manipulators on a complicated handling and viewing operation.

Floor-Mounted Handling Subsystem (FMHS)

Some 36 simple stands and fixtures constitute the FMHS. These stands and fixtures are used to hold and store the engine and engine subsystems during remote assembly and disassembly and to transport engine subsystems to other cells in the facility.

A typical arrangement of the FMHS in the main hot bay of the E-MAD Building is shown in Figure 4. Ample flexibility for varied assembly and disassembly procedures is provided since the stands can be moved anywhere in the bay by the OPS, the Wall-Mounted Handling Subsystem, or the facility crane.

Two remotely operated carriages operate on the standard gauge track running through the main hot bay. An engine subsystem, such as the reactor core, may be transported in a stand temporarily mounted on one of these carriages from the main hot bay to another disassembly cell in the facility. Power and control are brought to the carriages through bus bars installed in a trough between the rails in the floor.

In Figure 5, a carriage is shown in conjunction with the Engine Checkout Stand. This stand is used to hold the completely assembled engine during its final checkout. The framework of the stand is designed to support the engine without unduly restricting access to critical engine components. As in the case of the EIV, the engine is supported by a semi-circular member on the stand which fits beneath the upper flange of the engine pressure vessel. Retractable clamps are used to secure the engine to the stand. Four independent jacks are used to raise the stand clear of the carriage and, if required, to level the stand.

Two other stands are shown in Figure 6. The upper of these two stands, the Subsystem stand, is used to hold the non-nuclear engine (i.e., the pressure vessel head and all engine subsystems above it with the exception of the major external ducts and wiring harnesses). Remotely operated clamps are used to secure the pressure vessel head to the stand. If the engine pressure vessel is attached to the pressure vessel head, then the High-Position Support Stand is also employed to elevate the pressure veseel clear of the floor.

When it is necessary to lift and transport the Subsystem Stand in the main hot bay, a handling yoke is attached to the stand in order to provide a centrally located lifting eye. Remotely operated mechanical locking devices are provided for locking the yoke onto the stand.

The same handling yoke can be used to lift other stands. In Figure 7, it is shown attached to the Pressure Vessel Stand. This stand uses remotely operated arms to hold the engine pressure vessel. Rollers on the stand bear against the upper flange of the pressure vessel, thereby providing freedom of rotation of the engine about its own axis. Such indexing motion is necessary for certain remote assembly/disassembly operations.

A final example of the FMHS stands is the Lower Thrust Structure Stand shown in Figure 8. This stand provides a total of 270° rotation about a horizontal axis in order to provide optimum access to the engine turbopump assembly, which is located inside the thrust structure.

Wall-Mounted Handling Subsystem (WMHS)

The third member of the remote handling system in the E-MAD Building is the WMHS. As illustrated in Figure 9, this subsystem has four electromechanical manipulators mounted on traveling booms. Each traveling boom consists of a trolley, a carriage, and a boom assembly. The trolley rides the length of the main hot bay between upper and lower rails. The carriage travels vertically approximately 25 feet on the column of the trolley. It also pivots through 180° in a horizontal plane relative to the column. The boom assembly is pivoted from the carriage. A telescoping section and a universal joint in the boom assembly provides further flexibility of movement to the travelling boom.

Since the variety of tasks required of the manipulators covers a wide range, two different capacities of manipulators have been considered. They are desig-

nated as heavy-duty manipulators and medium-duty manipulators. Without delving into the detailed motion and load requirements, suffice it to say that the heavy-duty manipulator must position and support a 600-pound load in any position or attitude when extended to its maximum length, whereas the medium-duty manipulator need only handle a 250-pound load under similar conditions.

The manipulators are attached to the mounting plates on the booms in a standard manner such that remote connection and disconnection are possible. This feature provides interchangeability of manipulators to ease the maintenance problem and to further augment the flexibility of the overall remote handling system. It also permits future upgrading of the WMHS to incorporate the latest in manipulator hardware and to provide for a wider spectrum of manipulators if the need arises.

The WMHS performs a wide variety of tasks, such as the lifting, supporting and transporting of tools, fixtures, and components, and the basic manipulating motions necessary for engine assembly and disassembly over almost the entire working area of the main hot bay. When any two travelling booms are positioned directly across the bay from each other, their manipulators are capable of passing at floor level an item from one manipulator to the other.

ACKNOWLEDGEMENT

Under Subcontract NP-3 to Aerojet-General Corporation, Azusa, California, AMF Atomics is presently designing the NERVA Engine Installation Vehicle, Overhead Positioning Subsystem and Floor-Mounted Handling Subsystem described above. Their permission to publish this material is gratefully acknowledged.

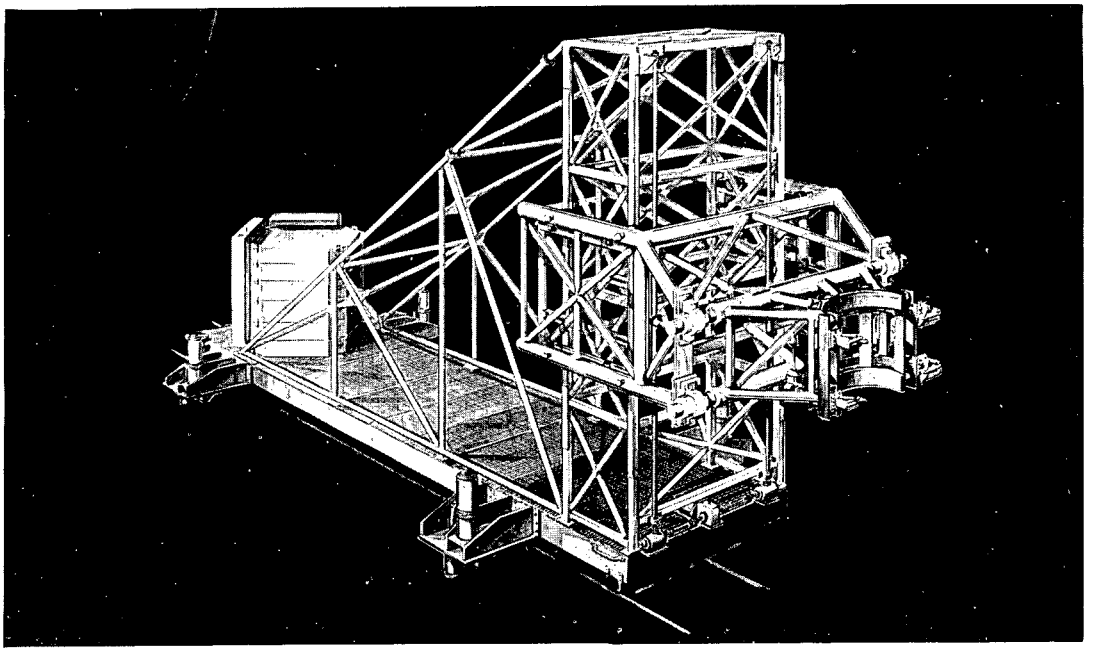

Figure 1. Engine Installation Vehicle

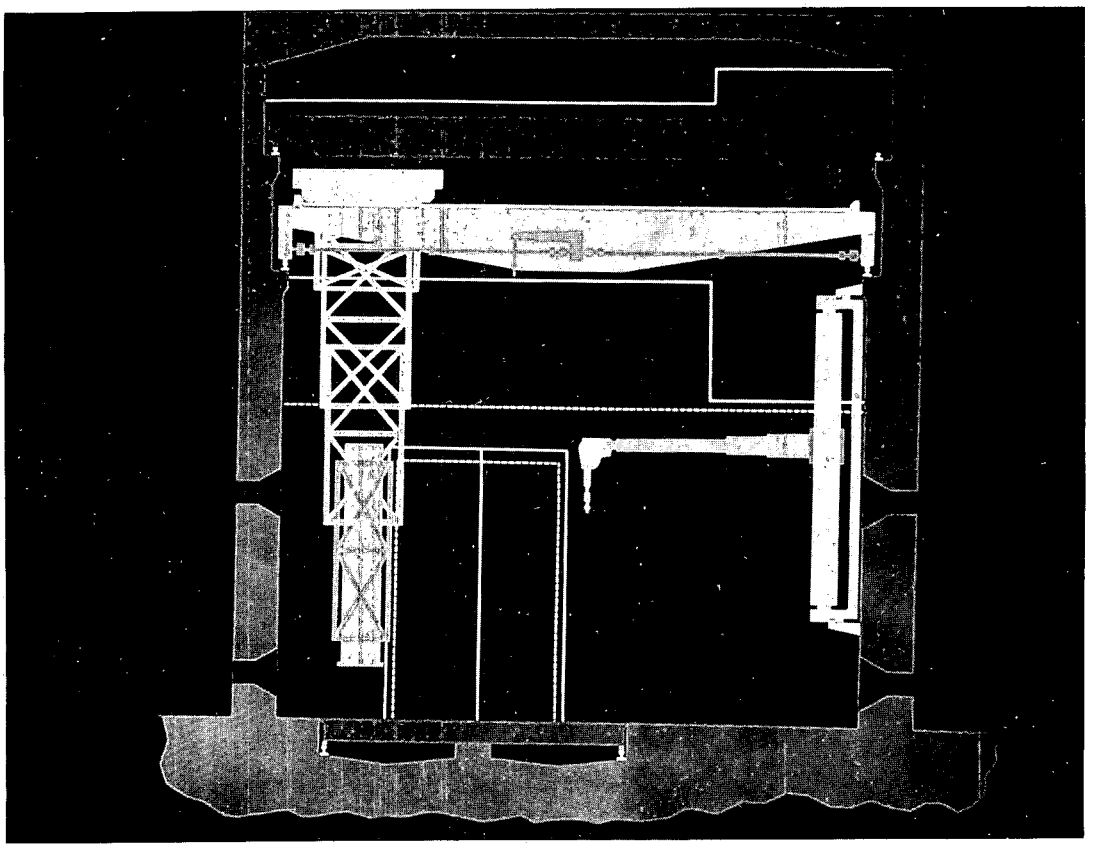

Figure 2. E-MAD Remote Handling System - End Elevation

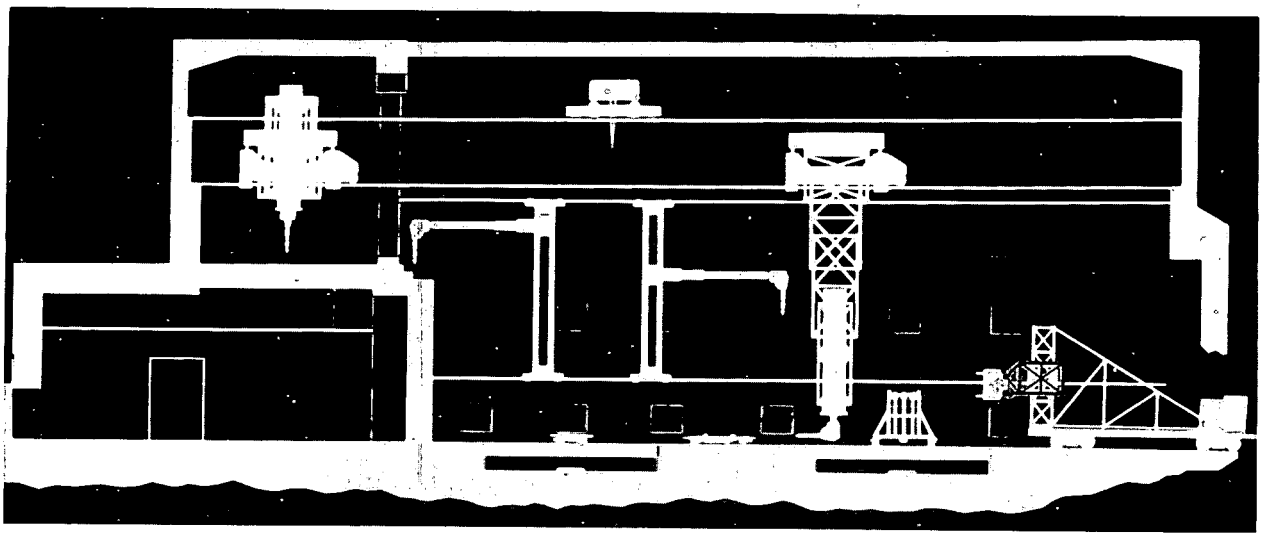

Figure 3. E-MAD Remote Handling System - Side Elevation

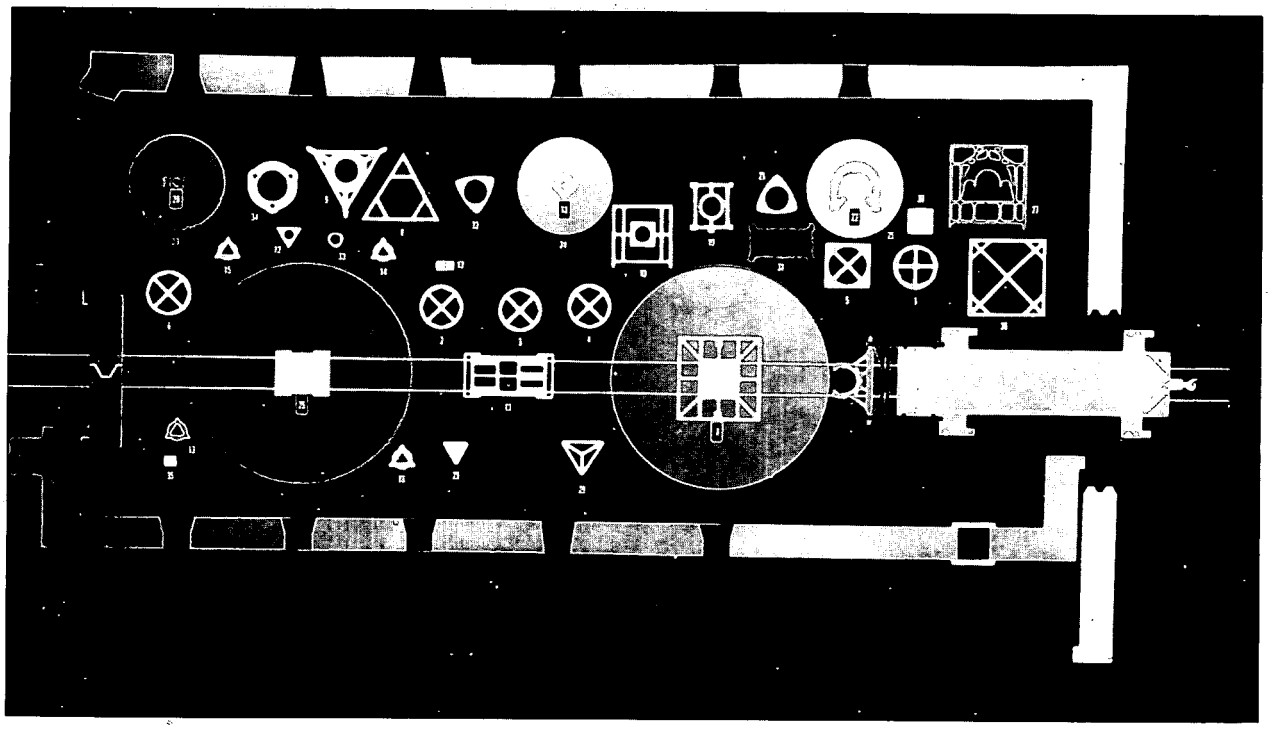

Figure 4. E-MAD Remote Handling System - Plan

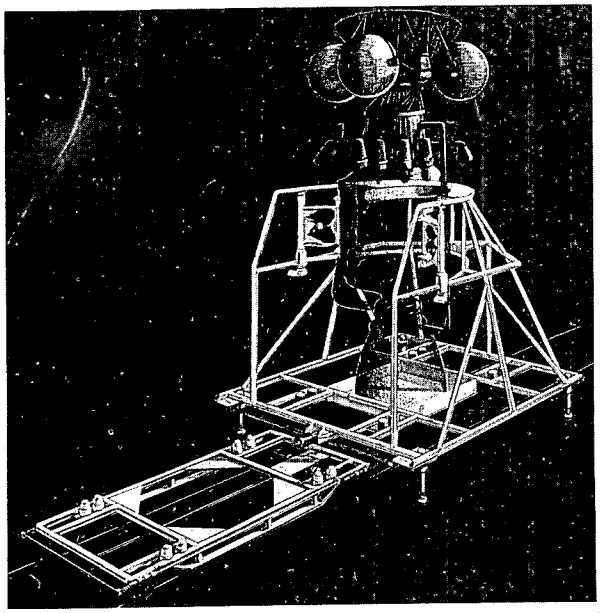

Figure 5. Engine Checkout Stand and Carriage

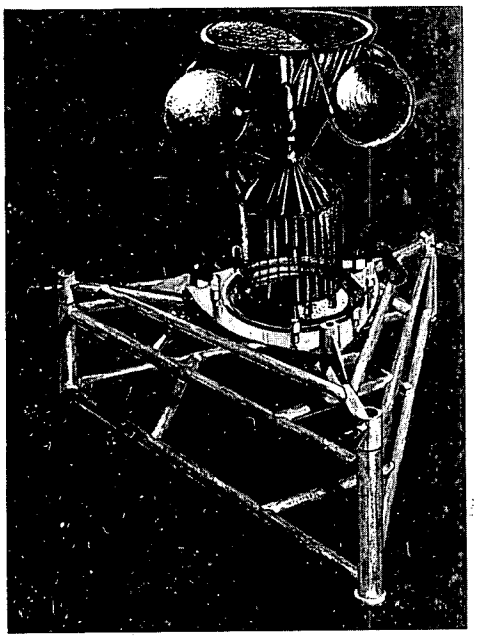

Figure 6. Subsystem Stand and High-Position Support Stand

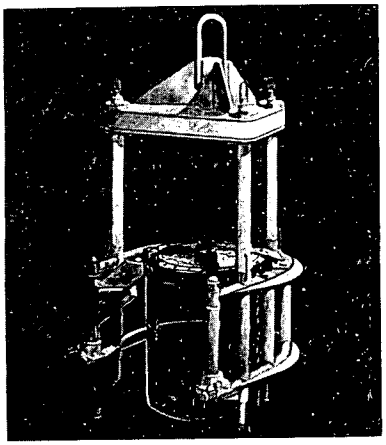

Figure 7. Pressure Vessel Stand and Handling Yoke

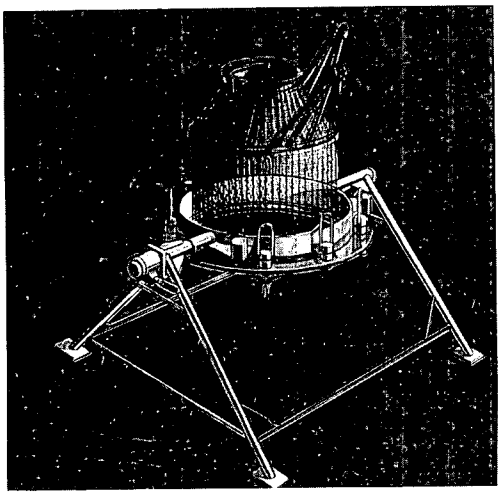

Figure 8. Lower Thrust Structure Stand

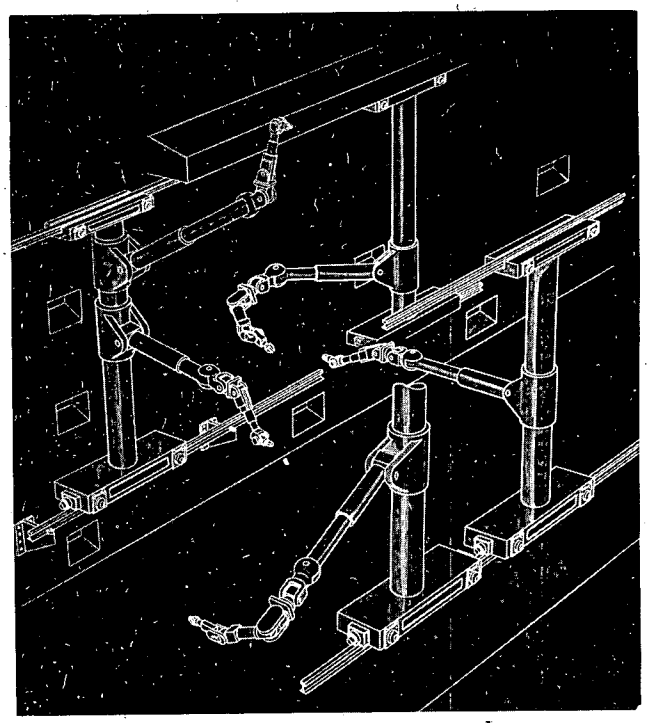

Figure 9. Wall-Mounted Handling Subsystem

SOME STRUCTURAL ASPECTS OF GAMMA HEATING IN NUCLEAR ROCKETS

John O. Mingle

Department of Nuclear Engineering

Kansas State University

In the normal structural design of rockets, temperature effects are generally of major importance especially for components associated with the combustion chamber and with cryogenic liquids. However, once a strong gamma radiation field is present, as in a nuclear rocket, all structural members are subject to temperature effects produced by the gamma heating. This situation leads to two main areas of concern: (a) the effect of temperature on the physical properties, such as the tensile strength, and (b) the associated thermal stresses caused by the temperature gradients. Both of these effects are common problems but the interaction of thickness and temperature leads to an interesting "diminishing returns" situation.

Temperature Distributions and Thermal Stresses

The temperature distribution within a material due to gamma heating can be approximately handled by utilization of a modified linear energy absorption coefficient, at least in one dimensional problems. This coefficient, μ_B, represents the build-up effect (1) due to multiple Compton scattering of gamma photons as well as regeneration as the result of pair production. The attenuation law then is

$$I = I_o \exp(-\mu_B X) \tag{1}$$

where I represents the gamma flux intensity and X the linear distance. The volumetric rate of energy absorption becomes the product of the cross section and the flux, i.e.

$$H = \mu_B I = \mu_B I_o \exp(-\mu_B X) \tag{2}$$

since μ_B also represents a cross section for energy absorption per unit volume. The total rate of energy absorption within a finite thickness, L, of slab then becomes

$$q = \int H dV = A I_o (1 - \exp(\mu_B L)) \tag{3}$$

where A is the area involved (in Y, Z directions).

In many instances this q/A represents the heat flux out of the slab since usually one boundary is assumed to be thermally insulated. If a convection coefficient, h, is employed then

$$q/A = hT_L = I_o (1 - \exp(-\mu_B L)) \tag{4}$$

where now T_L is the excess of the surface temperature over the coolant temperature. In most rocket applications the only cooling mechanism will be the thermal radiation from the areas physically away from the combustion or associated areas of the rocket. This gives an equivalent radiation coefficient

to black space as

$$h_r = \sigma_r \varepsilon T_L^3 \tag{5}$$

where σ_r is the Stefan-Boltzmann constant and ε the emmissivity of the surface. The surface temperature then becomes

$$T_L = \left\{ I_o (\sigma_r \varepsilon)^{-1} (1 - \exp(-\mu_B L)) \right\} \tag{6}$$

The temperature distribution within the slab is determined from the solution to the heat conduction differential equation

$$\frac{d^2T}{dX^2} + \frac{H}{k} = 0 \tag{7}$$

where the thermal conductivity, k, is assumed constant at an average value. Using Eq. (2) with a source side insulated boundary and a constant outside surface temperature, i.e.

$$X = 0, \quad \frac{dT}{dX} = 0; \quad X = L, \quad T = T_L \tag{8}$$

produces

$$T = T_L + (I_o/k) \left\{ L - X + \mu_B^{-1} (\exp(-\mu_B L) - \exp(\mu_B X)) \right\} \tag{9}$$

The average temperature, $\bar{T}$, for the slab then is

$$\bar{T} = \frac{1}{L} \int_o^L T dX = T_L + (I_o/\mu_B^2 Lk) \left\{ \frac{1}{2} (\mu_B L)^2 + (1 + \mu_B L) \exp(-\mu_B L) - 1 \right\} \tag{10}$$

In the case of small $\mu_B L$ (<0.2) this reduces to

$$\bar{T} - T_L = I_o \mu_B L^2 / 3k \tag{11}$$

This difference between the surface and the average slab temperature is used to determine the thermal stresses, σ, associated with this temperature gradient as (2)

$$\sigma = \frac{\alpha E}{1-\nu} (\bar{T} - T_L) \tag{12}$$

where α is the coefficient of thermal expansion, E is the modulus of elasticity, and ν is Poisson's ratio. This expression is only approximate but usually is satisfactory since the thermal stresses are generally small compared with the strength of the material. The temperature $\bar{T}$ is also used for evaluation of physical properties.

The tensile strength of the material evaluated at this average temperature and corrected for the thermal stresses leads to an effective tensile strength, S_{eff}, for the particular thickness of the slab. For use through the actual load, W, utilizes the product of this effective tensile strength and the thickness thus producing a curve containing a maximum. That is

$$W = LS_{eff} = L\,(S - \sigma) \qquad (13)$$

where as L increases, then S_{eff} decreases. This condition shows that the maximum load per unit width is obtained with a definite thickness for any constant surface gamma flux. For a thickness greater than this value, the allowable load is reduced. This would indicate that from a design viewpoint this thickness, L_{max}, is the maximum feasible. The associated load is referred to as W_{max}.

Example Determinations

The evaluation of this maximum condition for a particular material involves data on the variation of physical properties with temperature (3) and in addition the value for the build-up attenuation coefficient. This μ_B is a function on the energy of the gamma photons as well as the type of material and the depth within the material. However, for gamma photons of an average energy of two Mev, such as is usually obtained from a nuclear reactor, this factor is approximately a constant when converted to a mass basis of μ_B/ρ where ρ is the density of the material. This value is 0.02 cm^2/gm (4) and represents a cross section for interaction based upon a per unit mass basis. So that for many purposes

$$\mu_B = 0.02\,\rho\ (cm^{-1}) \qquad (14)$$

where naturally ρ is in gm/cc.

Calculations performed for typical materials of 4130 carbon steel and 6063 aluminum alloy give the curves shown in Figures 1 to 4. All physical properties except the tensile strength were assumed to vary linearly with temperature. In addition a value of 0.80 was used for the emmissivity of steel while 0.25 was employed for aluminum. Absolute temperatures were used for the initial computations.

Because of the high thermal conductivity of aluminum, the surface and average temperatures are essentially the same, thus resulting in practically no thermal stresses. Hence the decreased strength results from the effect of temperature upon the tensile strength entirely. Figure 1 shows a typical set of calculations for an aluminum type alloy. The distinct maximum in the load curve readily shows the "diminishing returns" of increased thickness. However, for steel, the thermal stresses are important, and the effective tensile strength becomes essentially zero at approximately a slab thickness of 4.8 centimeters for a surface gamma flux of 10^5 Btu/hr, ft^2.

The resultant maximum values for steel and aluminum shown in Figures 2 and 3 can be correlated by a log-log type expression. These become

$$W_{max} = 8.70\,(L_{max})^{0.936} \qquad \text{(aluminum)} \qquad (15)$$

$$W_{max} = 19.0\,(L_{max})^{0.967} \qquad \text{(steel)} \qquad (16)$$

Here the units of thickness, L, are centimeters while for the load, W, they are 1000 lb/inch width. A more useful expression can be obtained if these quantities are correlated with the gamma flux intensity such as in Figure 4. The resultant equations then become for aluminum

$$L_{max} = 1.99\ (I_o/1000)^{-1.102} \qquad (17)$$

$$W_{max} = 16.6\ (I_o/1000)^{-1.031} \qquad (18)$$

while for steel the values are

$$L_{max} = 214\ (I_o/1000)^{-0.979} \qquad (19)$$

$$W_{max} = 2890\ (I_o/1000)^{-0.911} \qquad (20)$$

The units of I_o here are Btu/hr, ft^2 while the range of values employed represents the intensities in the immediate vicinity of a 1000 megawatt nuclear reactor which is of nominal size for a nuclear rocket. In this respect a useful conversion factor is

$$1\ \text{Mev/sec, cm}^2 = 5.08\ (10)^{-10}\ \text{Btu/hr, ft}^2 \qquad (21)$$

since the former is the commonly given units of gamma photon fluxes.

For all these equations a least squares analysis was performed when sufficient data was present to warrant such a treatment, such as is shown in Figure 4 for aluminum.

CONCLUSIONS

This paper shows the "law of diminishing returns" as it applies to structural considerations in nuclear rockets in the presence of an intense gamma field. In many cases this analysis leads to the requirement of auxiliary cooling, particularly since the best possible situation of black space has been assumed. Although the actual values for the maximum load as given by Equations (16), (18), and (20) is highly sensitive to the value of the emmissivity chosen, the values given by Equation (17) and (19) for the maximum thickness are believed to be approximately correct regardless of the emmissivity. In this respect they would represent a practical design limit.

Although considerations are given only for slab geometry, in actual situations an equivalent thickness can be estimated. An expression for a rod is $D/(\pi-2)$ where D is the diameter. This represents an average straight-line constant X-direction distance through the rod obtained with a weighting factor of the Y-distance. This weighting factor is employed to compensate for the variable distance of heat conduction.

In general, the gamma heating is present both during and after reactor operation since the source is the result of fission products as well as prompt gammas. In this respect the structural degradation will continue even after reactor shut-down, so that gamma heating might be a particularly cognizant problem for nuclear rockets having restart capabilities.

REFERENCES

1. Bonilla, C. F., Nuclear Engineering, 255, McGraw-Hill, New York, 1957.

2. Ibid, 538.

3. Besserer, C. W., Missile Engineering Handbook, Section 4, Van Nostrand, Princeton, N. J., 1958.

4. Murray, R. L., Introduction to Nuclear Engineering, 2 ed., 258, Prentice-Hall, Englewood Cliffs, N.J., 1961.

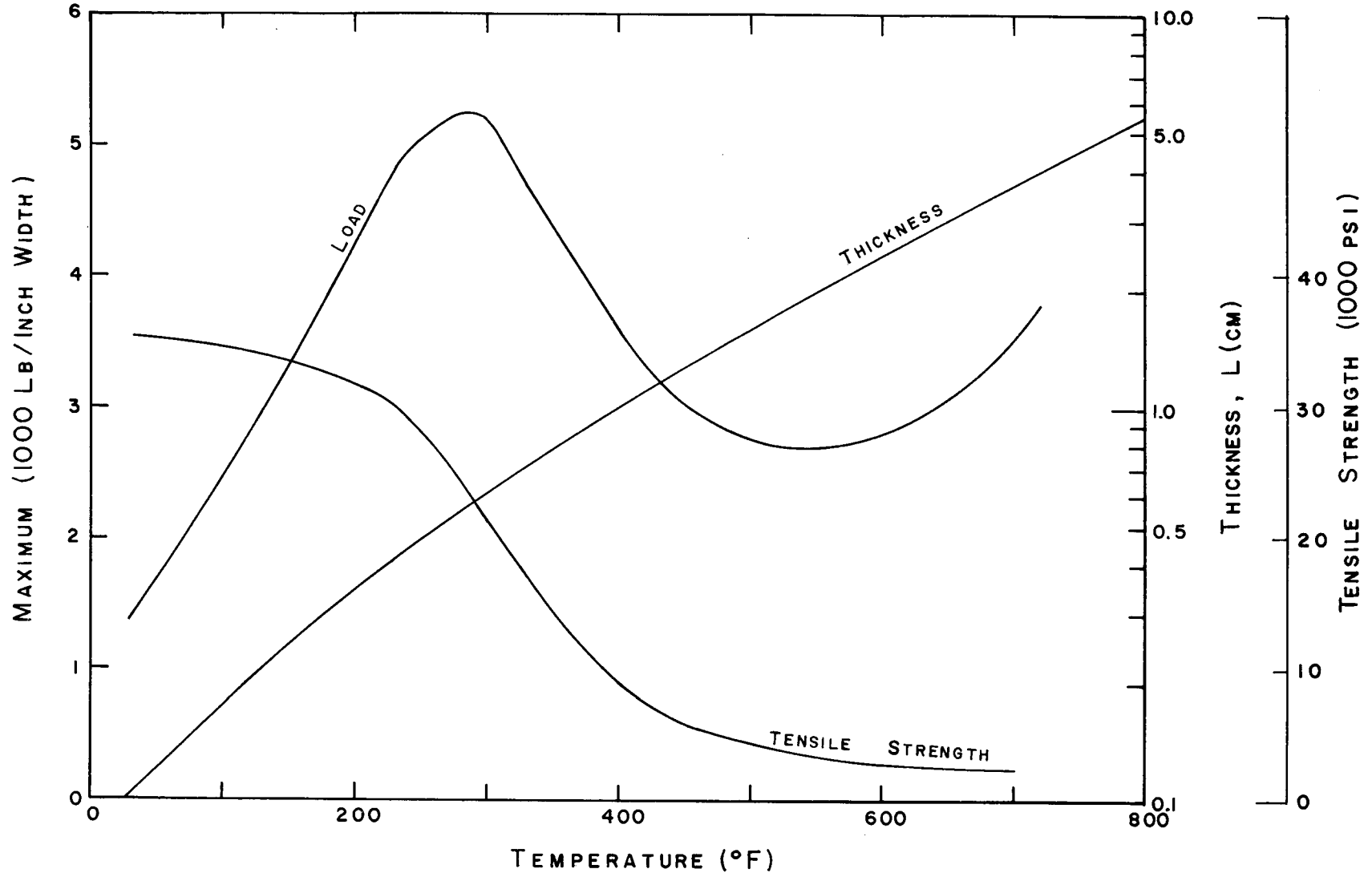

FIGURE 1.

LOAD — TEMPERATURE — THICKNESS RELATIONSHIP FOR A TYPICAL ALUMINUM – TYPE ALLOY

(I =3050 BTU / HR, FT.^{2}; ϵ =0.25)

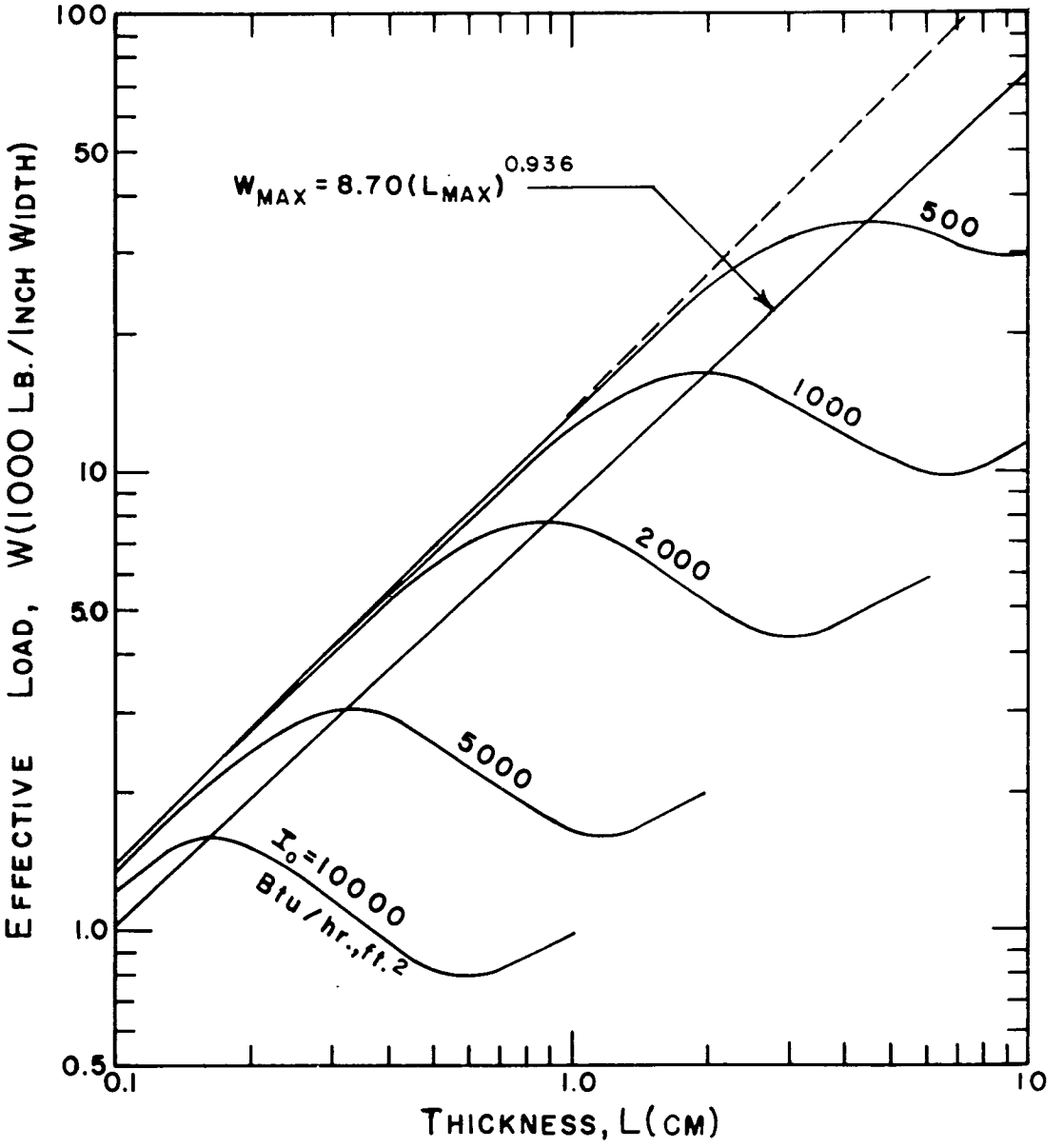

FIGURE 2: EFFECTIVE LOAD FOR 6063 ALUMINUM ALLOY

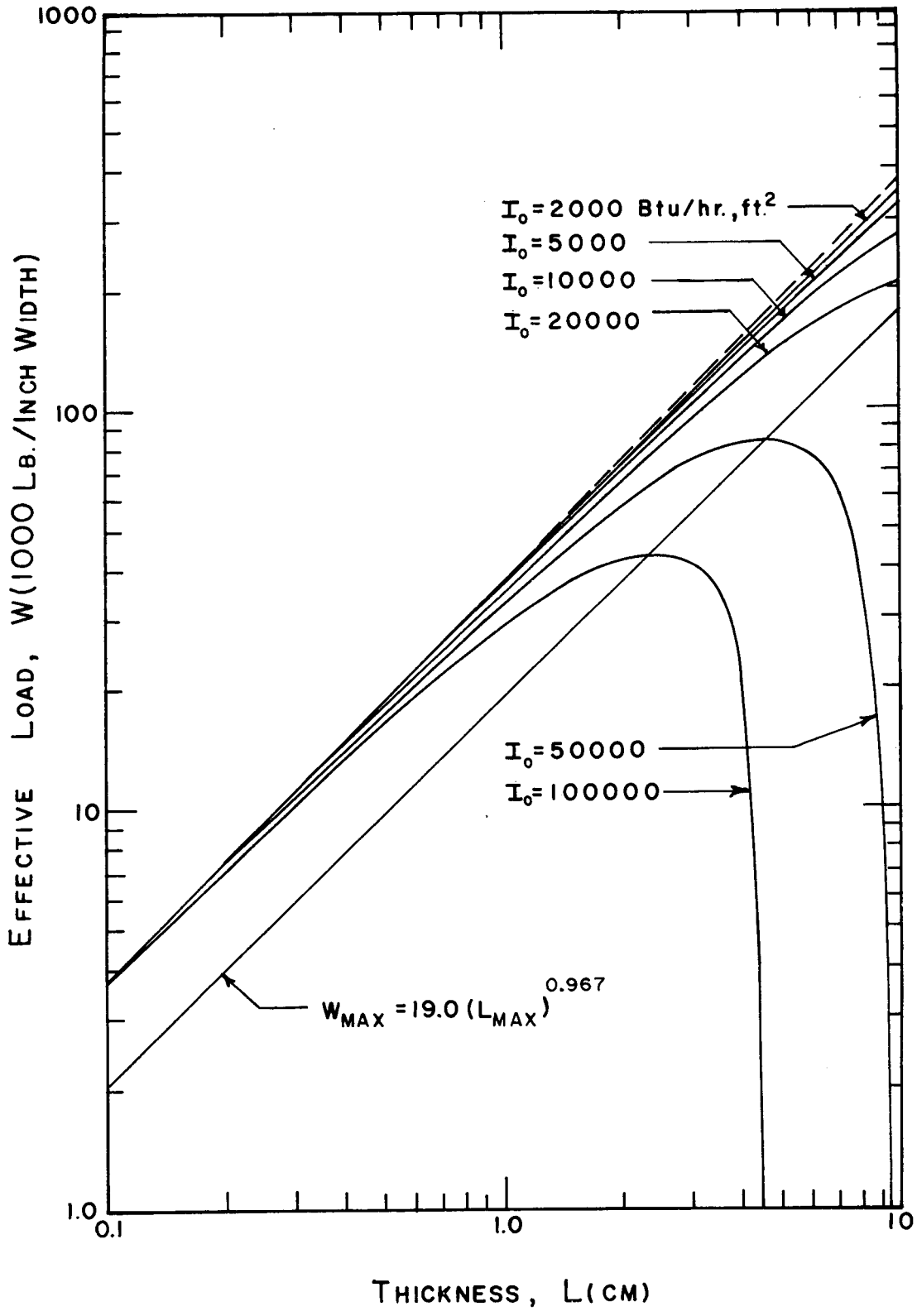

FIGURE 3. EFFECTIVE LOAD FOR 4130 STEEL

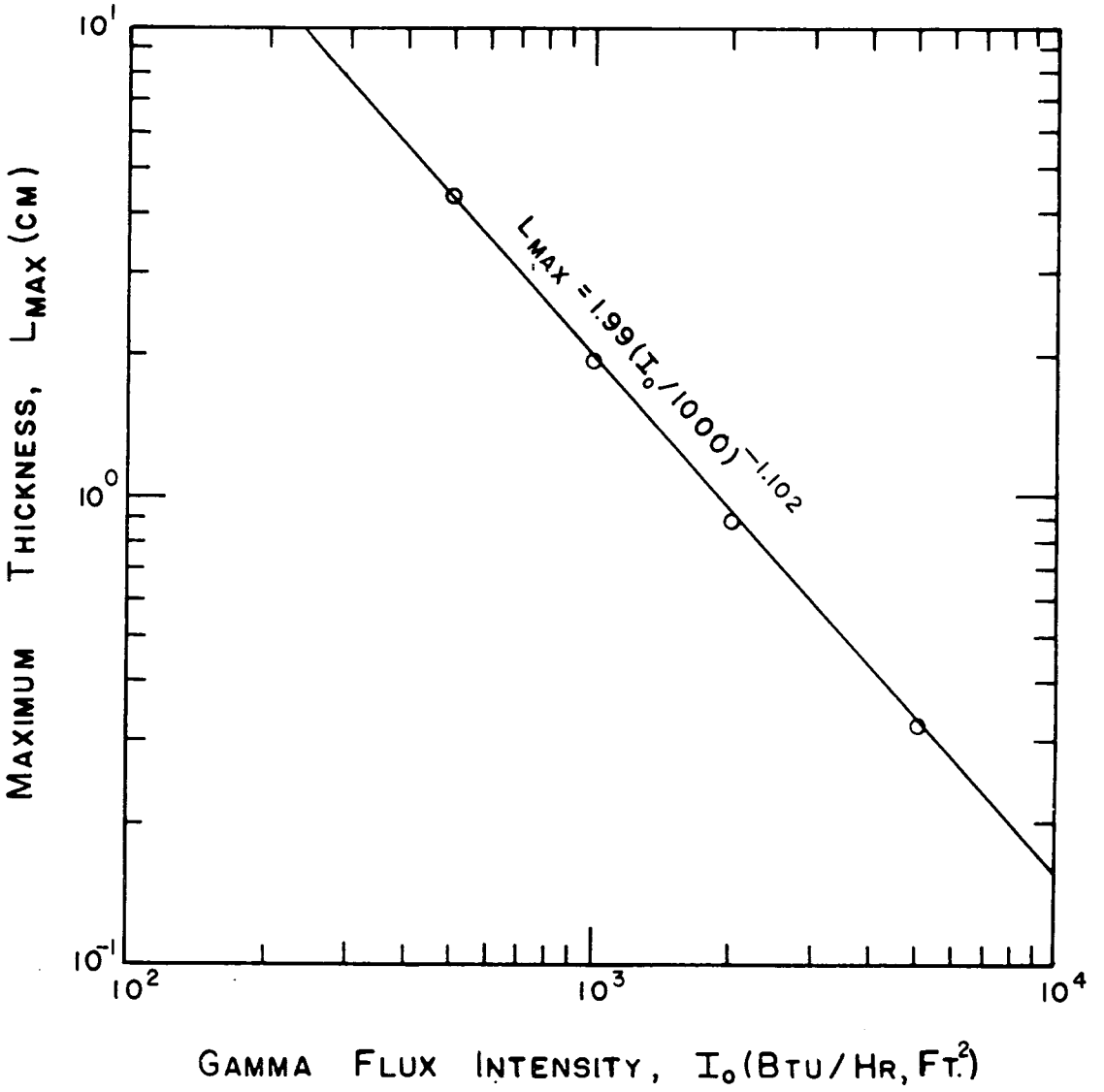

FIGURE 4: GAMMA FLUX INTENSITY EFFECT ON MAXIMUM SLAB THICKNESS FOR 6063 ALUMINUM ALLOY